



TECHNISCHE
UNIVERSITÄT
WIEN

Dissertation

ION-AGGREGATION AND ITS IMPACT FOR ASYMMETRIC CATALYSIS

Ausgeführt zum Zwecke der Erlangung des akademischen Grades eines Doktors
am Institut für Angewandte Synthesechemie unter der Leitung von

Assoc. Prof. Dipl.-Ing. Dr. techn. Katharina Schröder

Eingereicht an der Technischen Universität Wien

von

Msc. **Ádám Márk Pálvölgyi**

Matrikelnummer: 11728990

Hietzinger Kai 143/270, 1130 Wien

Wien, im März 2021

| | |
|---|------------|
| Acknowledgements | III |
| Abstract | IV |
| Kurzfassung | V |
| List of abbreviations | VI |
| 1. Introduction | 1 |
| 1.1 Chirality and its importance in our life | 1 |
| 1.2 Asymmetric catalysis | 2 |
| 1.3 Transition-metal-catalyzed asymmetric hydrogenations..... | 3 |
| 1.4 Transition-metal-catalyzed asymmetric transfer hydrogenations..... | 5 |
| 1.4.1 Ligand types..... | 6 |
| 1.4.2 Hydrogen sources..... | 7 |
| 1.4.3 Alternative solvents for asymmetric transfer hydrogenations – Towards ATH in aqueous media..... | 7 |
| 1.5 Organocatalysis | 9 |
| 1.5.1 Iminium and enamine catalysis | 10 |
| 1.5.2 Organocatalytic asymmetric transfer hydrogenation | 13 |
| 1.6 Asymmetric allylic alkylation | 19 |
| 1.6.1 Catalytic cycle | 19 |
| 1.6.2 Nature of the leaving group | 19 |
| 1.6.3 Nature of the nucleophile | 20 |
| 1.6.4 Regioselectivity considerations | 21 |
| 1.6.5 Enantioselectivity considerations..... | 21 |
| 1.6.6 Chiral ligands for asymmetric allylic alkylations..... | 24 |
| 1.6.7 Allylic alcohols as electrophiles for allylic alkylations | 25 |
| 1.6.8 Pd/enamine catalysis..... | 28 |
| 1.7 Bibliography..... | 32 |
| 2. Transition metal-catalyzed asymmetric transfer hydrogenations in alternative reaction media. | 39 |
| 3. Counterion-enhanced organocatalysis: A novel approach for the asymmetric transfer hydrogenation of enones | 62 |
| 4. Asymmetric allylic alkylations | 90 |
| 5. Conclusions | 111 |
| Appendix A | 115 |
| Appendix B | 141 |
| Appendix C | 147 |
| Appendix D | 187 |

Acknowledgements

In the first place, I would like to thank my supervisor, Prof. Dr. Katharina Bica-Schröder, offering me the opportunity to carry out my work in her research group. I am thankful for her support and for the valuable advices during my PhD.

I am also grateful to Prof. Dr. Michael Schnürch for the co-supervision and for his support in the last year of my PhD.

I would like to say thanks to all my current and former lab colleagues: Alice Cognigni, Mahtab Hejazifar, Olga “Alina” Lanaridi, Aitor Sainz Martinez, Philipp Miksovsky, Kristóf Stágel, Lisa Eisele, Blete Hulaj and Michaela Zuckerhut for the professional and collaborative, yet relaxing and friendly atmosphere in the Lab. I would like to give special thanks to my enthusiastic former master and bachelor students Fabian Scharinger and Jakob Smith for their valuable work.

Thanks to Max Kaiser and Nicolas Kratena for the fruitful scientific discussions.

I am very thankful to Dr. Christian Hametner and to Dr. Christian Stanetty for valuable NMR advices as well as to Dr. Laszlo Czollner for his help with the HR-MS measurements. Special thanks to Florian Untersteiner for all his practical help but also for the nice non-scientific discussions.

I would like to acknowledge all the non-scientific staff of the institution who helped me somehow during my PhD work.

Last but not least, I would like to thank my entire family and all my friend. Special thanks to my Fiancée, supporting me during my entire PhD.

Abstract

In light of the growing awareness for economic and sustainable chemical transformations, the field of catalysis is of special interest. Given the high demand for enantiomerically pure products for pharmaceutical and agricultural applications, catalytic reactions involving chiral catalysts became particularly attractive in the last decades.

This thesis is dedicated to the synthesis and application of new chiral catalysts for asymmetric transformations. In total, four different sub-projects were carried out.

- (1) The first part of this work concentrates on the application of ion-tagged chiral ligands for ruthenium-catalyzed asymmetric transfer hydrogenations in aqueous media. The fine tuning of the ligand structure together with the choice of anion resulted in water-soluble chiral ligands, which showed high catalytic activity and high enantioselectivity under environmentally benign, aqueous conditions.
- (2) The second part focuses on the development of a novel strategy for organocatalytic asymmetric transfer hydrogenations. The concept of counterion enhanced catalysis relies on the ion-pairing of natural L-amino acids as source of chirality with racemic, atropisomeric phosphoric acids. These chiral frameworks, in combination with Hantzsch esters as biomimetic hydrogen source were found to be a powerful tool for the asymmetric transfer hydrogenation of cyclic enones while providing a simpler alternative to current state-of-art catalyst systems.
- (3) The third project concentrates on the synthesis and application of Trost Modular Ligands with *P,O*-binding motif. A small set of easily prepared carbamate-monophosphate ligands was applied for asymmetric allylic alkylations using activated allylic electrophiles. High catalytic activity and good to excellent enantioselectivity was observed both for the allylation of carbonucleophiles and amines.
- (4) The last project focuses on the direct α -allylation of α -branched aldehydes with allylic alcohols. The three-component catalyst system comprising of a chiral amine, an atropisomeric phosphoric acid and a palladium source enabled the smooth quaternization of aldehydes with poorly electrophilic allylic alcohols *via* Pd/enamine dual activation, yielding high isolated yields and excellent enantioselectivity.

Kurzfassung

Angesichts des wachsenden Bewusstseins für wirtschaftliche und nachhaltige chemische Umwandlungen ist das Gebiet der Katalyse von besonderem Interesse. Mit der hohen Nachfrage nach enantiomerenreinen Produkten für pharmazeutische und landwirtschaftliche Anwendungen wurden katalytische Reaktionen mit chiralen Katalysatoren in den letzten Jahrzehnten besonders attraktiv.

Diese Arbeit befasst sich mit der Synthese und Anwendung neuer chiraler Katalysatoren für asymmetrische Transformationen. Insgesamt wurden vier verschiedene Teilprojekte durchgeführt.

- (1) Der erste Teil dieser Arbeit konzentriert sich auf die Anwendung von ionisch modifizierten chiralen Liganden für Ruthenium-katalysierte asymmetrische Transferhydrierungen in wässrigen Medien. Die Feinabstimmung der Ligandenstruktur zusammen mit der Wahl des Anions führte zu wasserlöslichen chiralen Liganden, die unter umweltfreundlichen, wässrigen Bedingungen eine hohe katalytische Aktivität und eine hohe Enantioselektivität zeigten.
- (2) Der zweite Teil befasst sich mit der Entwicklung einer neuen Strategie für organokatalytische asymmetrische Transferhydrierungen. Das Konzept der gegenionenverstärkten Katalyse beruht auf der Ionenpaarung natürlicher L-Aminosäuren als Quelle der Chiralität mit racemischen atropisomeren Phosphorsäuren. Diese chiralen Gerüste erwiesen sich in Kombination mit Hantzschestern als biomimetische Wasserstoffquelle als leistungsstarkes Werkzeug für die asymmetrische Transferhydrierung cyclischer Enone und bieten gleichzeitig eine einfachere Alternative zu aktuellen Katalysatorsystemen.
- (3) Das dritte Projekt konzentriert sich auf die Synthese und Anwendung von modularen Trost-Liganden mit *P,O*-Bindungsmotiv. Ein kleines Set einfach hergestellter Carbamat-Monophosphat-Liganden wurde für asymmetrische allylische Alkylierung unter Verwendung aktivierter Allylelektrophilen angewendet. Eine hohe katalytische Aktivität und eine gute bis ausgezeichnete Enantioselektivität wurden sowohl für die Allylierung von Carbonucleophilen als auch von Aminen beobachtet.
- (4) Das letzte Projekt konzentriert sich auf die direkte α -Allylierung von α -verzweigten Aldehyden mit Allylalkoholen. Das katalytische Drei-Komponenten-System bestehend aus einem chiralen Amin, einer atropisomeren Phosphorsäure und einer Palladiumquelle ermöglichte die reibungslose Quaternisierung von Aldehyden mit schwach elektrophilen Allylalkoholen über Pd/Enamin-Doppelaktivierung, was zu hohen isolierten Ausbeuten und ausgezeichneter Enantioselektivität führte.

List of abbreviations

| | |
|-----------------|--|
| AAA | Asymmetric allylic alkylation |
| ACDC | Asymmetric Counteranion-Directed Catalysis |
| AdCOOH | 1-Adamantanecarboxylic acid |
| ATH | Asymmetric transfer hydrogenation |
| BF ₄ | Tetrafluoroborate |
| BINAP | 2,2'-Bis(diphenylphosphino)-1,1'-binaphthyl |
| BIPHEP | Bis(diphenylphosphino)biphenyl |
| COD | 1,5-Cyclooctadiene |
| CPA | Chiral phosphoric acid |
| CsDPEN | <i>N</i> -Champhorsulfonyl-1,2-diphenylethylenediamine |
| DACH | 1,2-Diaminocyclohexane |
| DEAD | Diethyl azodicarboxylate |
| DIOP | <i>O</i> -Isopropylidene-2,3-dihydroxy-1,4bis(diphenylphosphino)butane |
| DIPAMP | 1,2-Bis[(2-methoxyphenyl)(phenylphosphino)]ethane |
| L-DOPA | L-Dihydroxyphenylalanine |
| DPEN | 1,2-Diphenyl-1,2-ethylenediamine |
| DPPBA | (2-Diphenylphosphino)benzoic acid |
| dppf | 1,1'-Bis(diphenylphosphino)ferrocene |
| EDG | Electron donating group |
| ee | Enantiomeric excess |
| EWG | Electron withdrawing group |
| FLP | Frustrated Lewis pair |
| HOMO | Highest occupied molecule orbital |
| LUMO | Lowest unoccupied molecule orbital |
| NADH | Nicotinamide adenine dinucleotide |
| PMP | <i>p</i> -Methoxyphenyl |
| TMG | 1,1,3,3-Tetramethylguanidine |
| TML | Trost modular ligand |
| tppts | Trisodium 3,3',3''-phosphinetriyltribenzenesulfonate |
| TRIP | 3,3'-Bis(2,4,6-triisopropylphenyl)-1,1'-binaphthyl-2,2'-diyl hydrogenphosphate |
| TsDPEN | <i>N-p</i> -Tosyl-1,2-diphenylethylenediamine |
| Xanthphos | 4,6-Bis(diphenylphosphino)-10 <i>H</i> -phenoxazine |

1. Introduction

1.1 Chirality and its importance in our life

Chirality plays an overwhelming role in nature. At the molecular level our life is highly asymmetric as all living organisms are composed of chiral biomolecules like proteins, nucleic acids and polysaccharides.

Driven by the pharmaceutical and agricultural industries, the demand for chiral compounds has sharply increased in the last decades. Despite the highly increasing number of chiral pharmaceuticals, the importance of single enantiomeric products was recognized only in the late 1950s, as the incautious usage of *Thalidomide* resulted in devastating effects.¹ Since then scientists are aware that living organisms can show drastically different biological response to enantiomers of chiral drugs. With more than 80% of the pharmaceutical drugs being chiral and more than 50% of these being sold in enantiomerically pure form, chirality is still one of the major concerns in modern pharmaceutical chemistry.²

The introduction of chirality into a molecule can be achieved by three main methodologies: (I) by using a chiral starting material, (II) by the resolution of racemic products and (III) by asymmetric synthesis. A general overview of the different pathways is depicted in Figure 1.

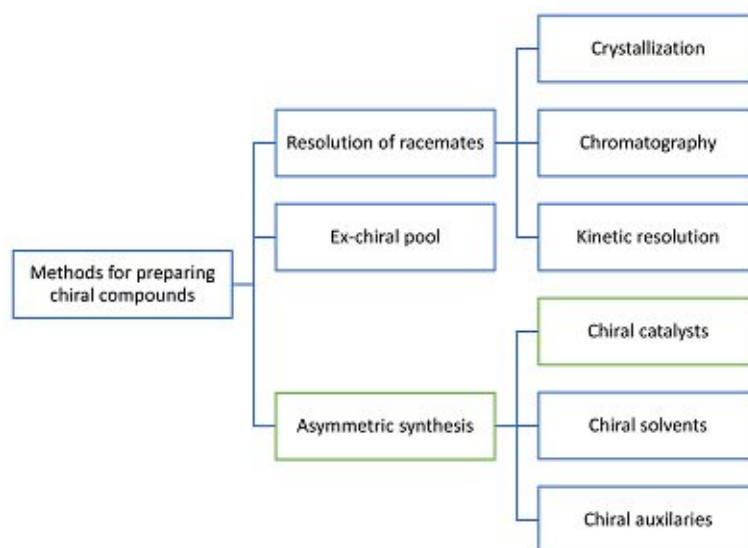


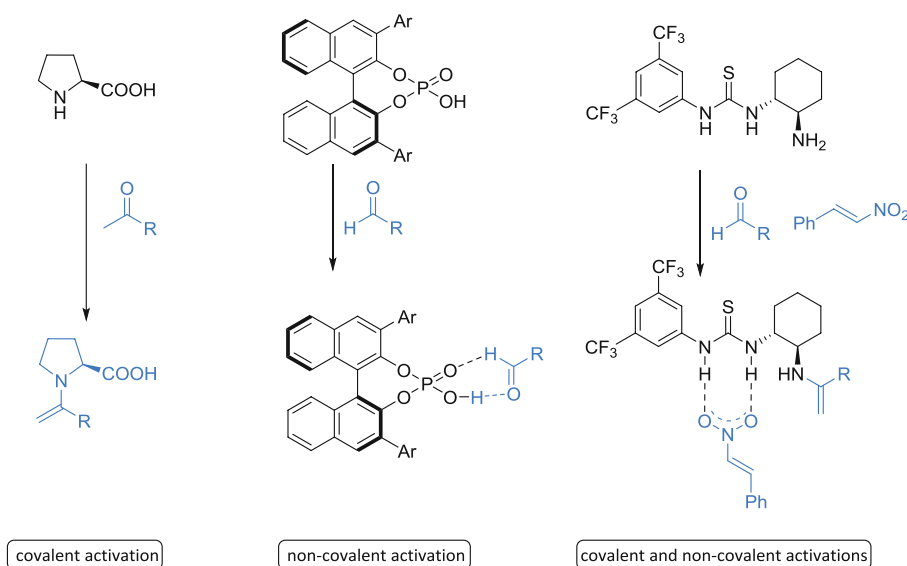
Figure 1. Different methods to introduce chirality.

Among all these methods, the field of asymmetric catalysis (Figure 1, green pathway) is of particular interest. As each molecule of the chiral catalyst can yield many molecules of chiral product by means

of continuous regeneration, this strategy is the most atom-efficient and therefore it is the most suitable to agree with the Green Chemistry Principles.³

1.2 Asymmetric catalysis

Covalent or non-covalent interaction(s) between a chiral catalyst and an achiral (or chiral racemic) substrate leads to the formation of substrate-catalyst complexes (Scheme 1).



Scheme 1. Covalent and non-covalent activation of different substrates on the example of different organocatalysts.

Since such complexes as well as their transition states are in diastereomeric relation; they differ in activation energy, which results in asymmetric induction. The relationship between the competing diastereomeric transition states and the enantioselectivity can be therefore described by normal Boltzmann-distributions as depicted on Figure 2.

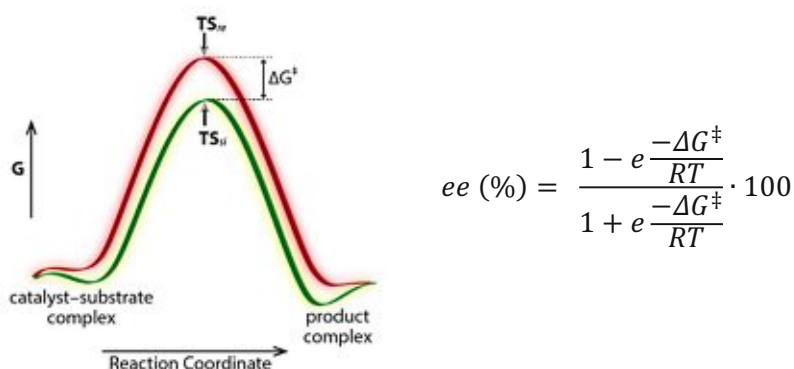


Figure 2. Relationship between reaction kinetics and enantioselectivity by using a chiral catalyst. ΔG^\ddagger represents the energy difference of the diastereomeric transition states.⁴

1.3 Transition-metal-catalyzed asymmetric hydrogenations

The hydrogenation of unsaturated compounds is one of the most fundamental transformations in organic chemistry.

As a pioneer on this field, in 1966 Sir Geoffrey Wilkinson reported that $[\text{RhCl}(\text{PPh}_3)_3]$ can be successfully used for the hydrogenation of unhindered primary alkenes under relatively mild conditions.⁵ The initially rather limited substrate scope was extended to tri- and tetrasubstituted alkenes by the subsequent work of Crabtree in 1979 (Figure 3).⁶

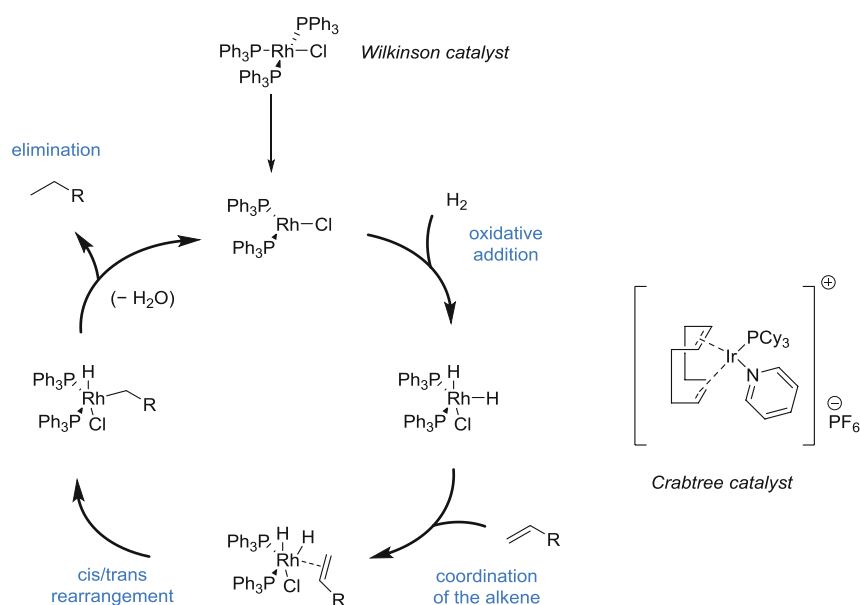
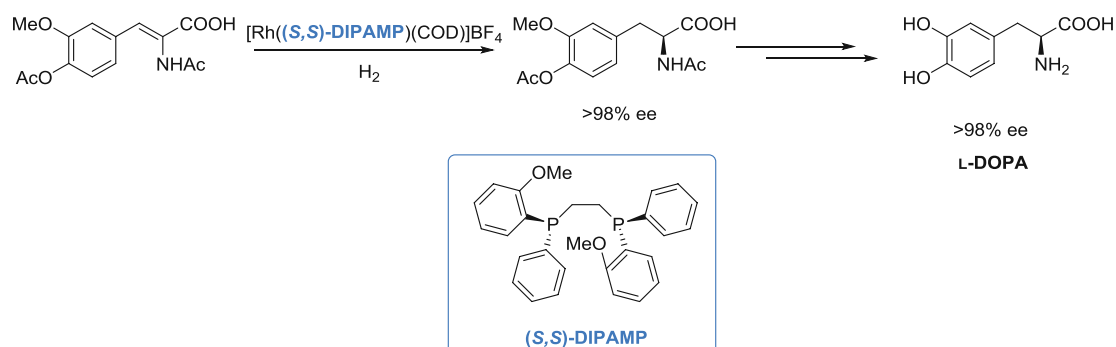


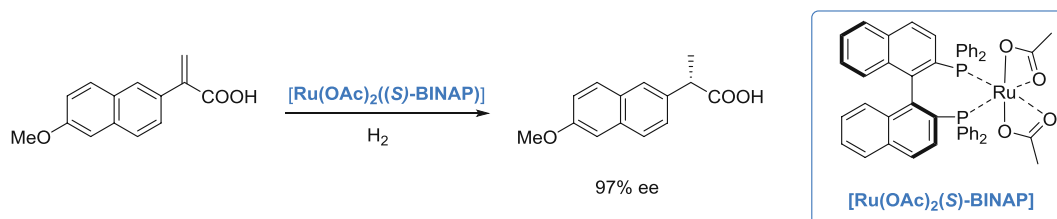
Figure 3. Wilkinson-hydrogenation of unhindered olefins with $[\text{RhCl}(\text{PPh}_3)_3]$ (left) and its extension by the Ir-based Crabtree's catalyst (right).

By replacing the PPh_3 units of the *Wilkinson catalyst* with *P*-chiral monodentate ligands, Knowles discovered the ligand (*S,S*)-DIPAMP, which was proven to be very efficient for the hydrogenation of enamides, and later resulted in the first synthetic route for the asymmetric synthesis of L-DOPA, an anti-Parkinson drug (Scheme 2).⁷



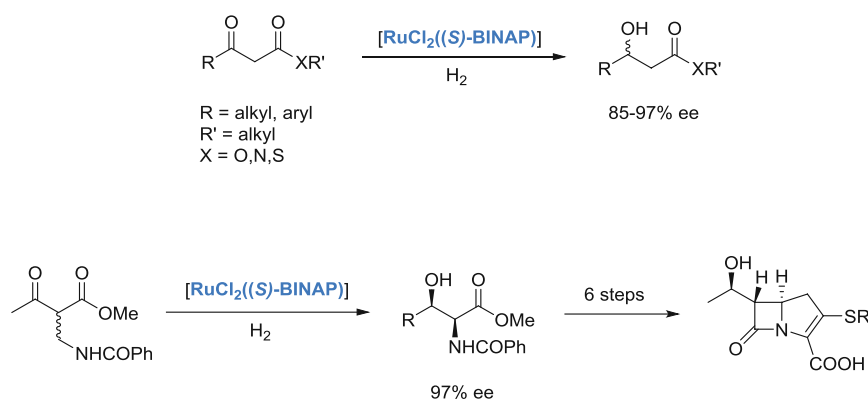
Scheme 2. The first highly asymmetric synthesis of L-DOPA.

The discovery of chiral ruthenium-based catalysts could significantly expand the scope of asymmetric hydrogenations. Noyori and co-workers reported that $[\text{Ru}(\text{OAc})_2(\text{S-BINAP})]$ can be successfully used for the asymmetric hydrogenation of acrylic acids. This method could be later used for the enantioselective synthesis of the anti-inflammatory drug (*S*)-Naproxen (Scheme 3).⁸



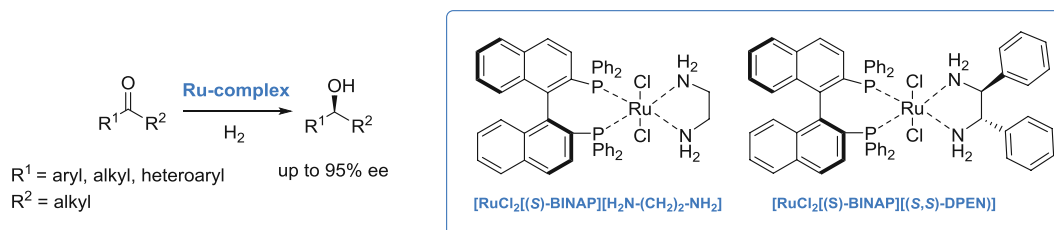
Scheme 3. Enantioselective synthesis of Naproxen.

While the aforementioned catalyst system was limited to the reduction of olefins, the use of $[\text{RuX}_2((\text{S-BINAP}))]$ provided a powerful alternative for the asymmetric hydrogenation of various β -keto ester derivatives.⁹ Later on, this method could be used for the stereoselective total synthesis of different carbapenem antibiotics (Scheme 4).¹⁰



Scheme 4. Enantioselective hydrogenation of β -keto esters (top) and its use for the synthesis of Carbapenems (bottom).

As another milestone in the field of asymmetric hydrogenation, the discovery of diamine-containing catalysts allowed to further expand the reaction scope to unfunctionalized ketone substrates as well. By using either BINAP-ethylenediamine or BINAP-DPEN ligands, a wide range of aromatic and aliphatic ketones could be reduced with excellent enantioselectivity (Scheme 5).¹¹



Scheme 5. Asymmetric hydrogenation of unfunctionalized ketones with diamine-containing ligands.

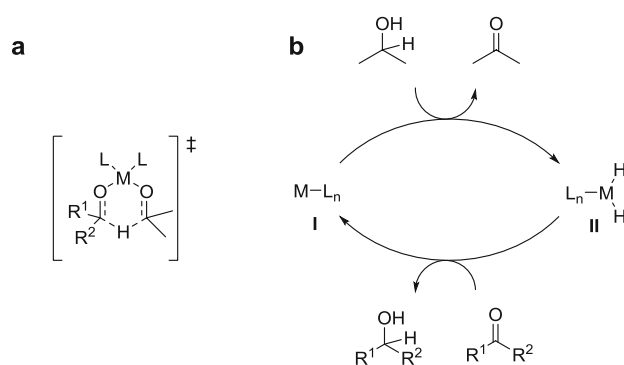
1.4 Transition-metal-catalyzed asymmetric transfer hydrogenations

Even though gaseous hydrogen is a cheap and easily accessible reagent, its handling is accompanied with major drawbacks: it is explosive and its use requires pressurized reaction conditions.

Transfer hydrogenation (TH) can be defined as the reduction of multiple bonds with the aid of a hydrogen source other than H₂ in the presence of a catalyst.¹² Given the above-mentioned issues associated with the use of molecular hydrogen, transfer hydrogenation provides an attractive alternative: the use of inexpensive and non-hazardous molecules as hydrogen source results in operational simplicity and safety. Moreover, such reactions are generally carried out at ambient temperatures and atmospheric pressure, so no special equipment is required.

Based on the type of hydrogen-transfer, two mechanisms were proposed, as depicted on Scheme 6.

- Direct transfer of hydrogen *via* a concerted pathway through a six-membered cyclic transition state. This mechanism is very similar to the one proposed for the Meerwein-Ponndorf-Verley reduction in 1925 (Scheme 6, a).¹³
- Reduction *via* hydridic route: A stepwise procedure, in which at first the metal catalyst I reacts with the hydrogen source resulting in the catalytically active metal-hydride II, which is followed by the hydride transfer between II and the hydrogen acceptor (Scheme 6, b). Most of the transition-metal-catalyzed TH reactions follow this pathway.



Scheme 6. Mechanism of a transfer hydrogenation. a) Transition state for the reduction *via* direct hydrogen transfer. b) Reduction *via* hydridic route.

In 1980, the first asymmetric transfer hydrogenation was reported by Menchi *et al.*, as they achieved very moderate enantioselectivity (<10% ee) by using H₄Ru₄(CO)₈[(-)-DIOP]₂.¹⁴ With the breakthrough from the Noyori group from 1995¹⁵, the field of asymmetric transfer hydrogenation (ATH) got tremendous attention.¹⁶ Apart from the first established transition-metal-catalyzed ATH, several advances were reported for organo- and biocatalytic ATH reactions as well.

Complexes of late transition-metal elements like Ru, Rh and Ir with ligands featuring nitrogen, oxygen, phosphorous and sulphur heteroatoms are extensively used for ATH reactions. In this chapter, the effect of ligands, hydrogen donors, and reaction media will be discussed.

1.4.1 Ligand types

For the purpose of asymmetric transfer hydrogenation, various bidentate ligands like diphosphines (**I-III**),^{17,18} bipyridines (**IV**),¹⁹ oxazolines (**V-VI**),^{20,21} β -amino alcohols (**VII-VIII**),^{22,23} diamines (**IX-X**),^{24,25} but also tri- and tetradentate ligand systems (**XI-XII**) were developed (Figure 4).^{26,27}

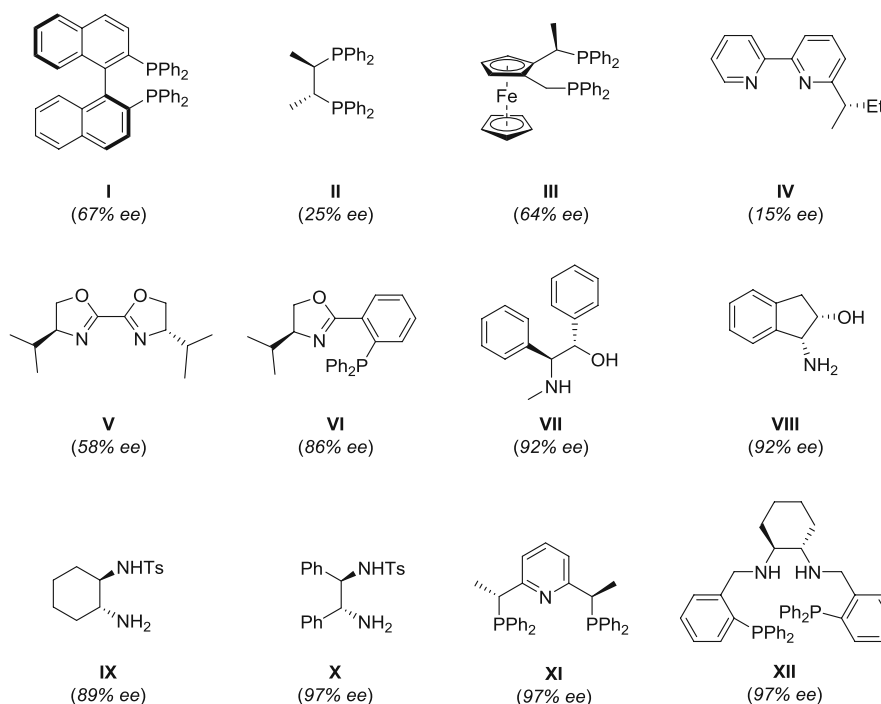
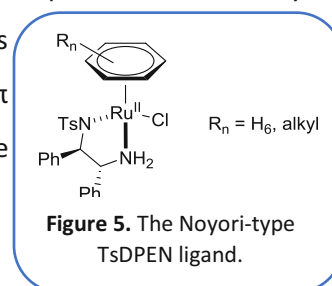


Figure 4. Different ligands for asymmetric transfer hydrogenation and their selectivity in the ATH of acetophenone.

Among all of those ligands, the Noyori-Ikariya catalyst (Figure 5) and its various modifications employing diamines like **X** became particularly popular. Because of their wide-range pH-stability, they are compatible not just with isopropanol, but also with formic acid-triethylamine hydrogen source, which made them suitable for both the ATH of ketones and imines. The unique enantioselectivity of such ligands originated from several factors. The attractive interactions between the spectator ligand and the π -cloud of the substrate, the SO₂- π repulsive forces between the substrate and the tosyl group, and the activation of the substrate *via* N-H \cdots O hydrogen bonding (NH-effect) play a synergistic role, resulting in exceptional enantioselectivity.



1.4.2 Hydrogen sources

Secondary alcohols, especially isopropanol in the presence of an additional inorganic base, are frequently used as hydrogen source for ATH reactions. Even though it provides a cheap and straightforward method, its reactivity is hampered by the isopropanol/acetone equilibrium, as the oxidation of the hydrogen donor results in the formation of acetone, which might act as competitive substrate for the reduction.

In order to overcome this problem, the mixture of formic acid and triethylamine (generally as a 5/2 azeotrope) can be used. As the dehydrogenation of the reagent results in the formation of CO₂, this is an irreversible process. However, the stability of the ligand should be taken into account because of the acidic environment.

Apart from these alternatives, salts of formic acid like sodium formate became also quite popular as cheap, non-toxic and easily accessible H₂-sources. Just like the mixture of formic acid and triethylamine, it also renders the ATH reaction irreversible. As it provides slightly basic conditions, its use can also solve the previously mentioned ligand-stability issues. Moreover, sodium formate as a water-soluble hydrogen source makes aqueous ATH reactions easily feasible.

1.4.3 Alternative solvents for asymmetric transfer hydrogenations – Towards ATH in aqueous media

Asymmetric transfer hydrogenations are generally carried out either in classical organic solvents or in the excess of reagent as reaction media (*in substantia* reaction), which results in additional waste formation. The possible reduction of waste-generation and the use of innocuous solvents are amongst the main goals of green and sustainable chemistry. The use of water has clear environmental and economic benefits as it is a cheap, non-toxic and easily accessible solvent.

Apart from the above-mentioned advantages, water also enables the use of sodium formate as benign hydrogen source. As the majority of substrates and products are water-insoluble, its use leads to a liquid-liquid biphasic catalytic system facilitating product separation, catalyst immobilization and catalyst recycling (Figure 6).

Eventually, water can also lead to a dramatic reaction rate increase for ATH reactions: because its high polarity and tendency for hydrogen-bond formation it can stabilize both ionic intermediates and transition states and facilitate the formation of the active catalyst, resulting in higher catalytic activities.²⁸ Furthermore, the strong hydrogen-bond network can further increase the energy difference between the respective diastereomeric transition states, which leads to a higher enantioselectivity.²⁹

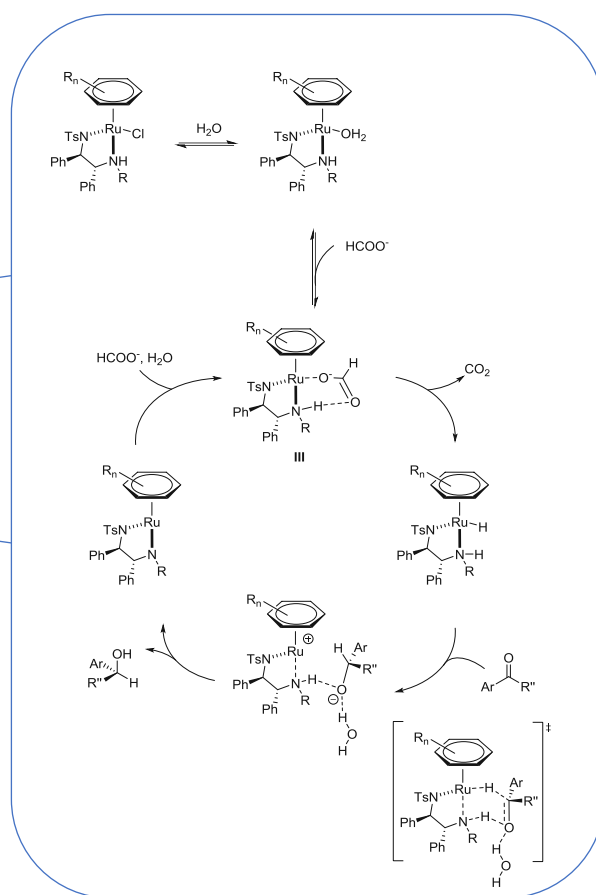
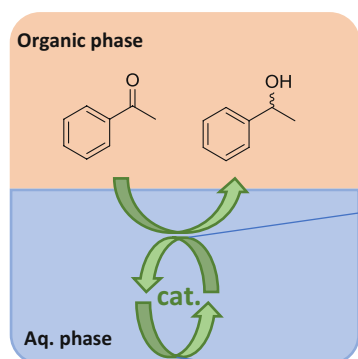


Figure 6. Concept of liquid-liquid biphasic catalysis for asymmetric transfer hydrogenation.

Over the last two decades, several different approaches have been established aiming to enhance the water-solubility of the TsDPEN ligand, thus making it suitable for aqueous ATH reactions. One common way to achieve this is by anchoring the ligand with polyethylene glycol units which results in improved water-solubility, albeit requires significant synthetic efforts.³⁰ The formation of sulphonate salts *via* aromatic sulphonation also leads to better solubility behavior; however, regioselectivity issues upon ligand synthesis should be taken into account.³¹ The polarity of the ligand can be also increased by the introduction of cationic groups. Such methods implementing alkylammonium or imidazolium units generally require less synthetic effort, meanwhile allowing a careful fine-tuning of the catalytic properties by the choice of cation, counterion or chain-length.^{32,33} Eventually, the introduction of cationic groups with long alkyl chains can also lead to the formation of metallomicelles, providing a good alternative for the ATH reaction of more challenging aliphatic substrates.³⁴ Alternatively, a better water-solubility can be rationalized by the addition of external surfactants or by using inherently water-soluble chiral ligands such as Ru-CsDPEN or Ir-CsDPEN.^{35,36} A brief overview of the different hydrophilic modifications is shown in Figure 7.

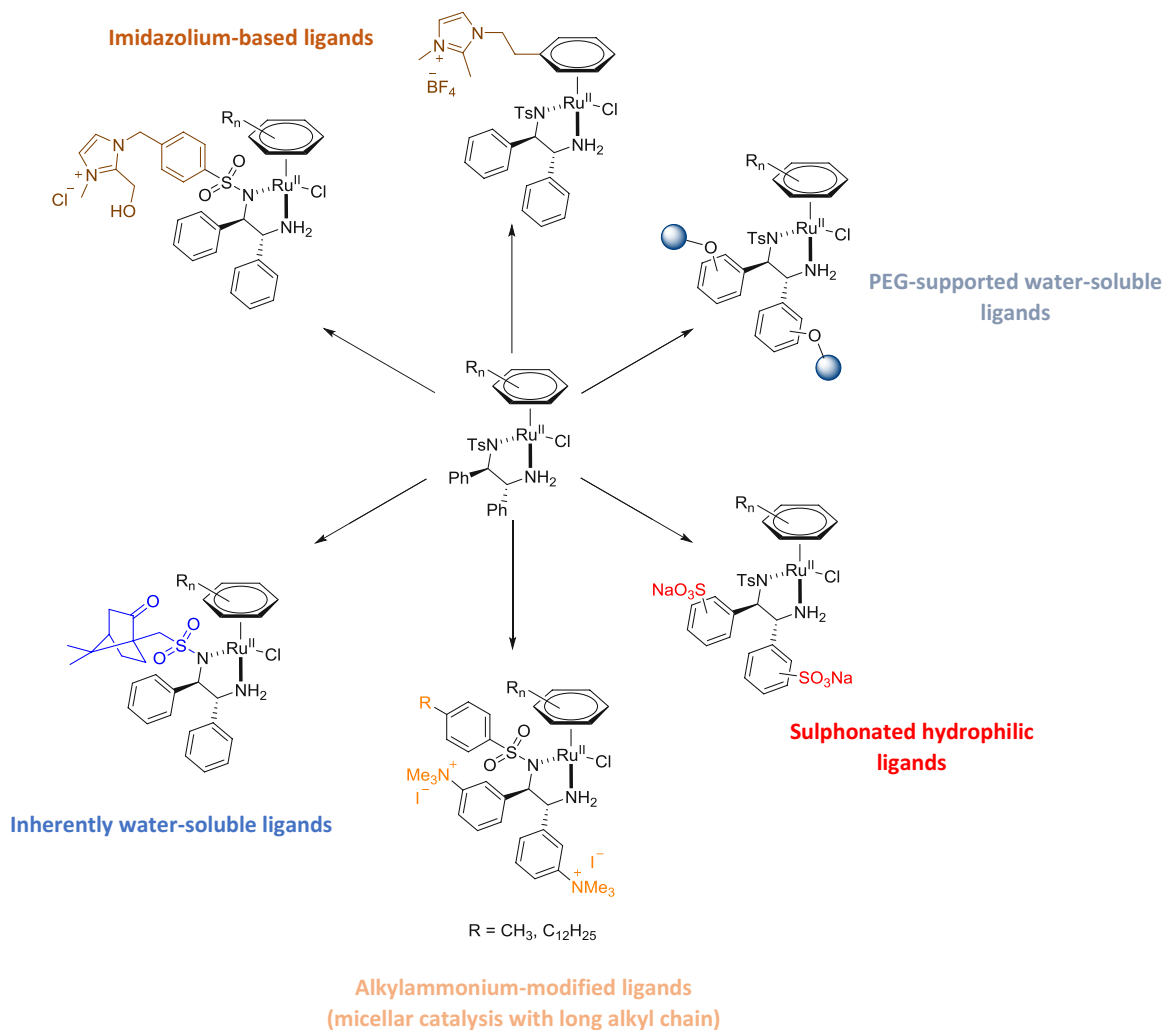


Figure 7. Hydrophilic modification of DPEN-ligands for aqueous ATH reactions.

1.5 Organocatalysis

Parallel to transition-metal catalysis, organocatalysis became particularly popular in the last twenty years. The term itself was first coined by MacMillan in 2000. Organocatalysis refers to a catalytic reaction, in which the rate of reaction is accelerated by using small organic molecules composing of carbon, hydrogen, oxygen, nitrogen, sulphur, phosphorous and other non-metallic elements. As no expensive and/or toxic metals are required and such catalysts generally do not show air or moisture sensitivity, organocatalysis is certainly superior over transition-metal catalysis in several aspects; however, its disadvantages like the significantly higher catalyst loadings and the more limited substrate scope should be also taken into account.

Many different activation modes exist for the interplay of the organocatalyst and the substrate. In general, we can distinguish two main sub-groups. In case of covalent activation, the catalyst binds covalently on the substrate for activation and asymmetric induction, while the non-covalent activation

results in only secondary bonding between the substrate and the chiral catalyst. An overview of the activation modes is depicted on Figure 8.

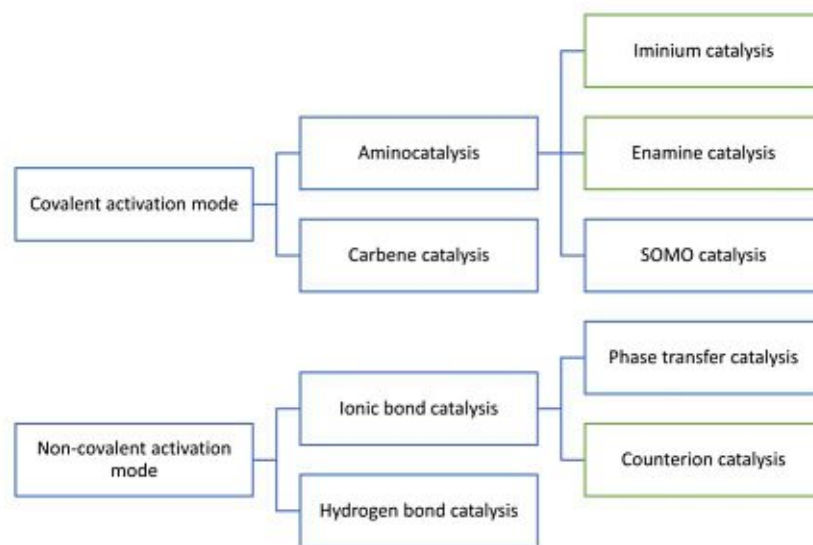


Figure 8. Different activation modes in organocatalysis.

1.5.1 Iminium and enamine catalysis

Iminium catalysis is widely used for the activation of α,β -unsaturated carbonyl compounds. The reversible condensation of a chiral amine and the substrate results in the formation of iminium ions. Similar to Lewis-acid activation the energy of the Lowest Unoccupied Molecular Orbital (LUMO) is significantly lowered, resulting in an enhanced electrophilicity which means that the iminium can be readily quenched by nucleophiles (Figure 9).

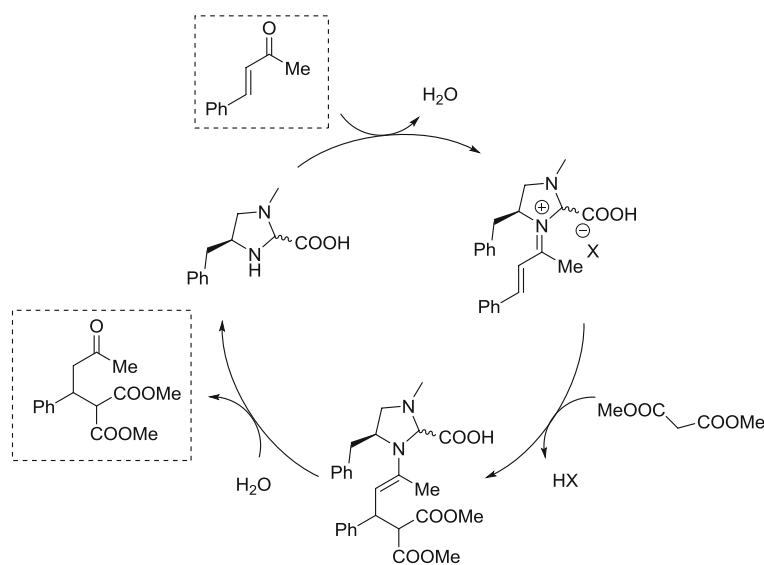


Figure 9. Iminium-catalyzed conjugate addition with a malonate nucleophile.

Generally, along with the aminocatalyst, an equimolar amount of acid co-catalyst is also required. This facilitates both the iminium formation and the hydrolysis; therefore, it is crucial for high catalytic activity.

The activation of aldehydes or ketones as enamines results in an increased Highest Occupied Molecular Orbital (HOMO) compared to that for the substrate, thus it can easily react with the LUMO of an electrophile (Figure 10).

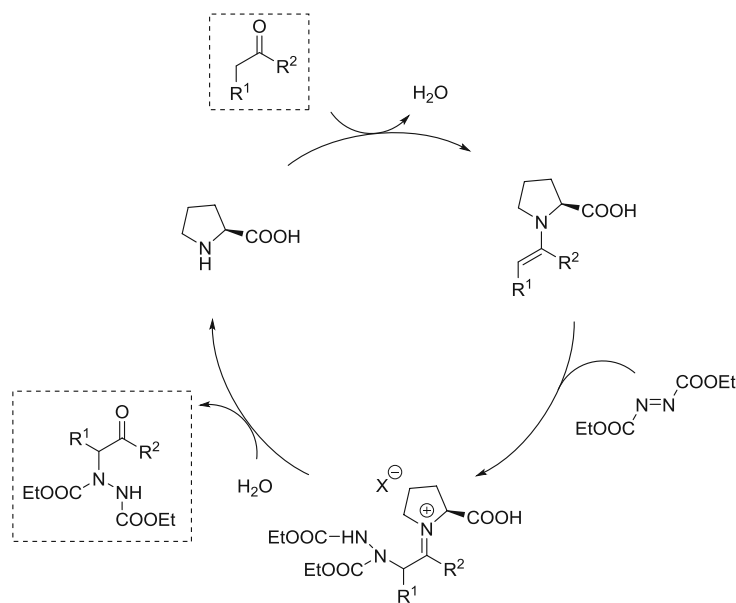


Figure 10. Enamine-catalyzed amination of ketones with DEAD.

The stereochemistry of an iminium or enamine-catalyzed reaction can be achieved either *via* directing or blocking groups on the amine. “Type A” amines featuring internal hydrogen donors orient the attack of the nucleophile or electrophile *via* hydrogen-bonding. On the other hand, “type B” amines with non-protic bulky group can efficiently block one side of the enamine or iminium, resulting in increased stereocontrol. Representative examples for both types and their mechanism of action are shown in Figure 11 and Figure 12, respectively.

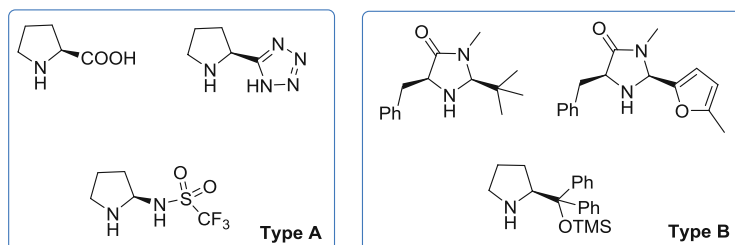


Figure 11. “Type A” and “Type B” aminocatalysts for iminium and enamine catalysis.

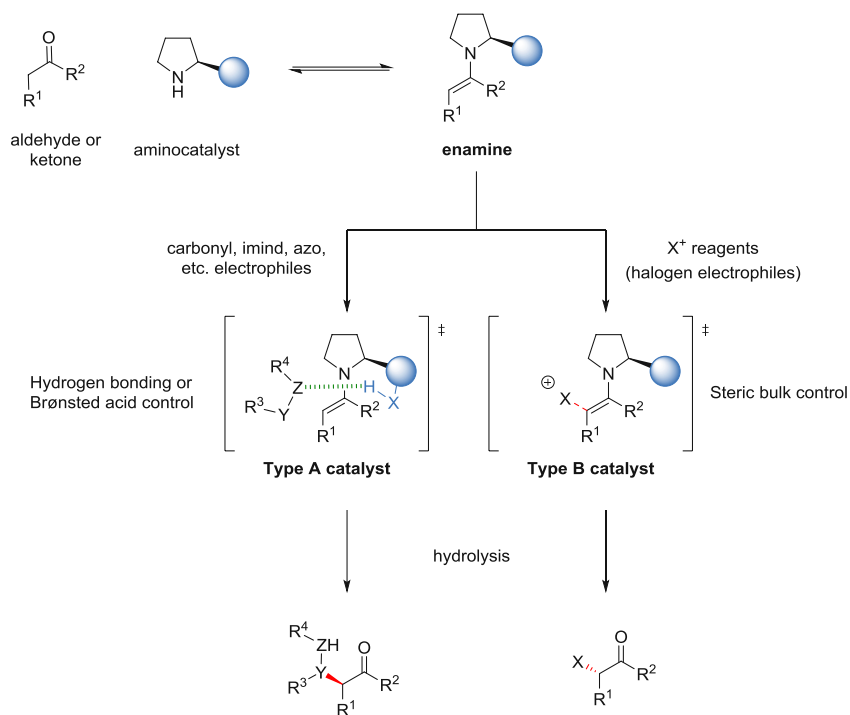


Figure 12. Controlling enantioselectivity with "Type A" and "Type B" amines (only enamine catalysis depicted).

Typical iminium catalyzed reactions are conjugate additions with malonates, cycloadditions, Friedel-Crafts reactions and transfer hydrogenations, while enamine catalysis was found to be a crucial tool for Aldol-condensations, α -functionalizations, Mannich-reactions and conjugate addition of nitroalkanes. A range of transformations enabled *via* iminium and enamine catalysis is shown in Figure 13.

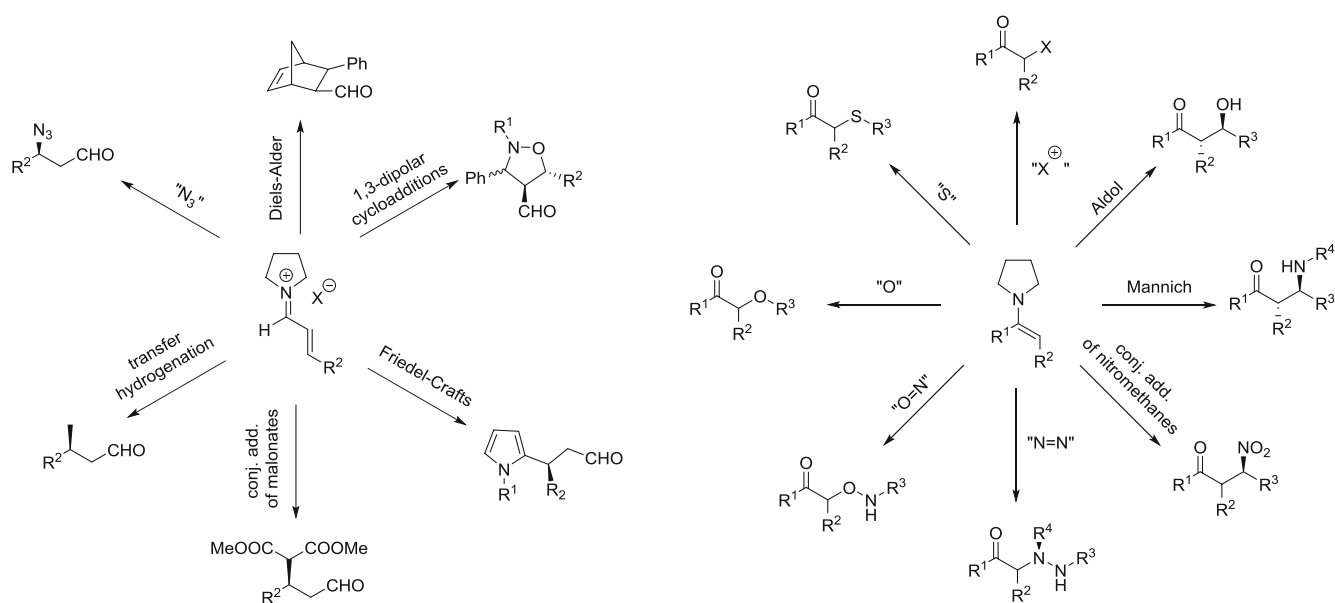
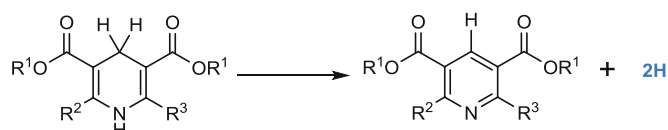


Figure 13. Typical transformations involving iminium (left) and enamine (right) catalysis.

1.5.2 Organocatalytic asymmetric transfer hydrogenation

Inspired by natural oxidoreductases like NADH, the introduction of 1,4-dihydropyridines (Hantzsch esters, **HEs**) as biomimetic hydrogen sources opened the era of organocatalytic asymmetric transfer hydrogenations. As neither gaseous H₂, nor expensive and/or toxic metal sources are required, such asymmetric transformations show great air and moisture tolerance which results in operational safety and simplicity. In these transformations, the aromatization of such dihydropyridines as driving force facilitates the hydride donation, as depicted in Scheme 7.

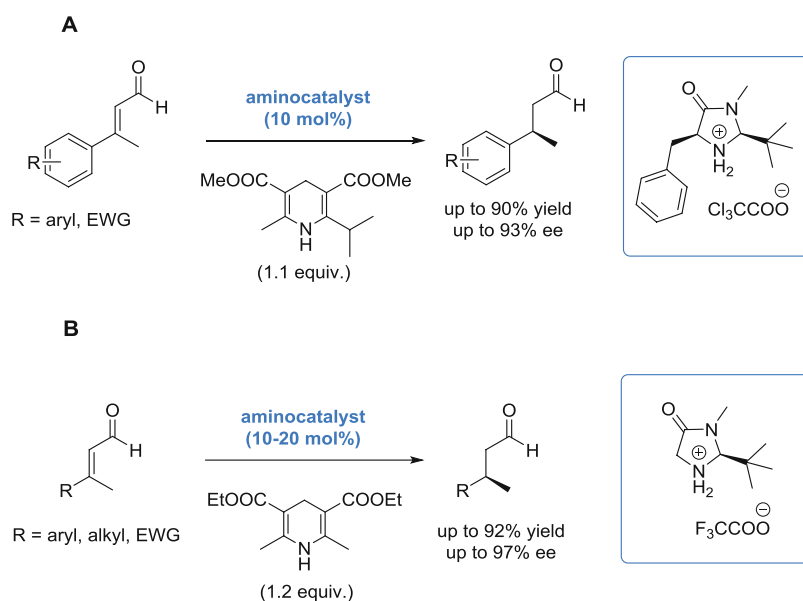


Scheme 7. The aromatization of Hantzsch ester as driving force for hydride-donation.

Apart from acting as hydrogen source, structural modification of the Hantzsch esters also allows a fine tuning of the overall catalytic activity and selectivity.

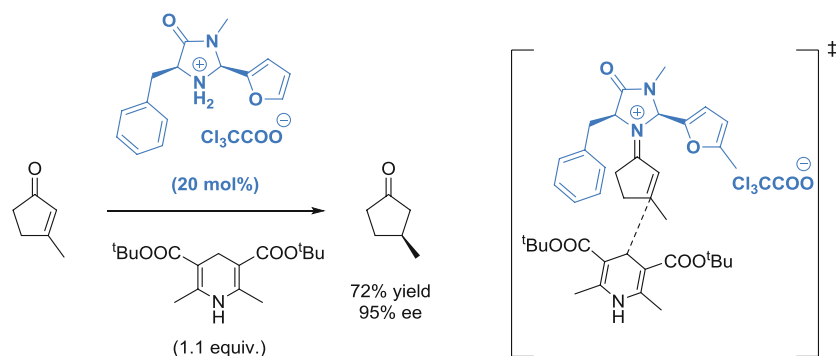
1.5.2.1 Iminium-catalyzed organocatalytic ATH reactions

In 2005, the groups of MacMillan and List independently reported the use of chiral imidazolidinones – later also known as the *MacMillan catalysts* – for the asymmetric transfer hydrogenation of enals. While both methods provided the optically active aldehyde product with >90% ee, the method of MacMillan (**B**) has the additional benefit of simpler catalyst preparation (Scheme 8).^{37,38}



Scheme 8. ATH of enals by List (**A**) and MacMillan (**B**).

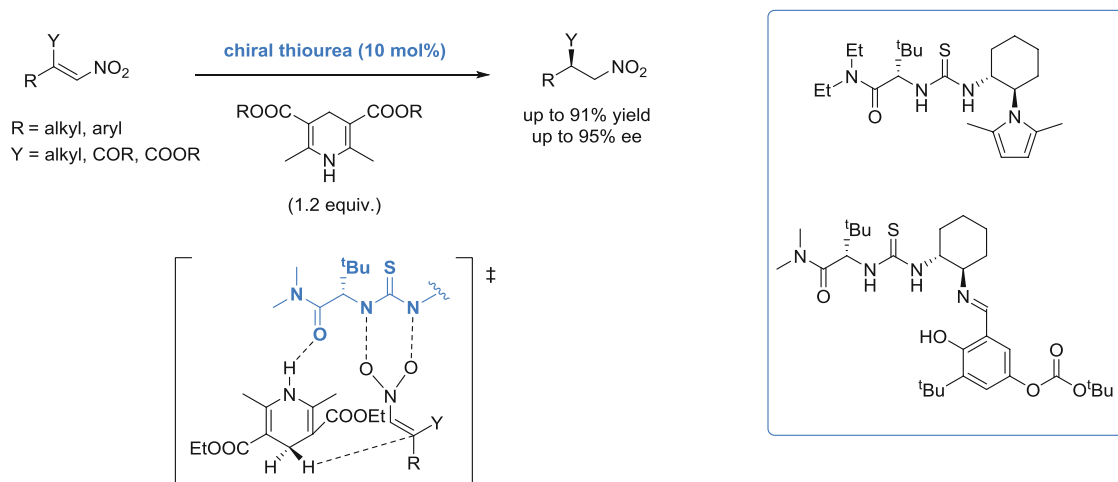
The aforementioned MacMillan-type catalysts; however, were unable to catalyze the ATH of ketones. After careful catalyst optimization, a second-generation imidazolidinone bearing a furyl substituent was found to be suitable to expand the reaction scope towards ketones when using a rather high catalyst loading. A modified Hantzsch ester featuring *tert*-butylester units was also necessary to achieve high yields and enantioselectivity (Scheme 9).³⁹



Scheme 9. ATH of cyclic enones with a second-generation *MacMillan catalyst*.

1.5.2.2 Chiral thioureas for ATH reactions

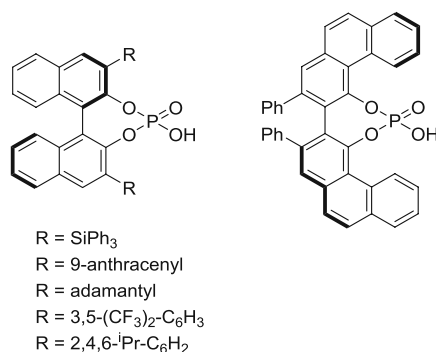
Chiral thioureas are widely used for the activation of nitroolefins in asymmetric catalysis. Among others, the Jacobsen-type thioureas in the presence of Hantzsch esters were proven to be efficient for the ATH reaction of various nitroolefin substrates, providing a good alternative for the synthesis of optically active nitroalkanes and β -amino acid-derivatives (Scheme 10).^{40,41}



Scheme 10. Asymmetric transfer hydrogenation of nitroolefins *via* chiral thiourea catalysis.

1.5.2.3 Chiral phosphoric acids as Brønsted-acids for ATH reactions

The class of BINOL-derived chiral phosphoric acids (CPA) became one of the most promising tools in the field of organocatalysis. Among others, chiral phosphoric acids (CPAs) were found to be suitable for various ATH reactions *via* simple Brønsted-acid catalysis. A series of different chiral phosphoric acids have been successfully used for the asymmetric reduction of imines and related compounds by using Hantzsch ester as biomimetic hydrogen source. A selection of CPAs and asymmetric transfer hydrogenations can be found in Table 1.



| Entry | Type of substrate | Substrate | Product | Reference |
|-------|---|-----------|---------|---|
| 1 | acyclic imines | | | Rueping, ⁴² List ⁴³ |
| 2 | quinolines | | | Rueping ⁴⁴ |
| 3 | α -iminoesters | | | Antilla ⁴⁵ |
| 4 | enamines | | | Antilla ⁴⁶ |
| 5 | <i>O</i> -hydroxyaryl imines | | | Wang ⁴⁷ |
| 6 | <i>N,O</i> -acetals (as imine precursor) | | | Zhou ⁴⁸ |
| 7 | aromatic ketones (reductive amination) | | | MacMillan ⁴⁹ |

Table 1. A selection of chiral phosphoric acids and their application in organocatalytic ATH reactions as Brønsted-acid.

Mechanistic studies proved that the phosphoric acid acts as bifunctional catalyst in such reactions: it is simultaneously responsible for the activation of the substrates *via* simple protonation (LUMO-lowering for increased electrophilicity) and for the activation of the Hantzsch ester (Figure 14, left). However, this general mechanism can be overruled when using substrates bearing protic hydrogen-containing substituents (Figure 14, middle and right).⁴⁷

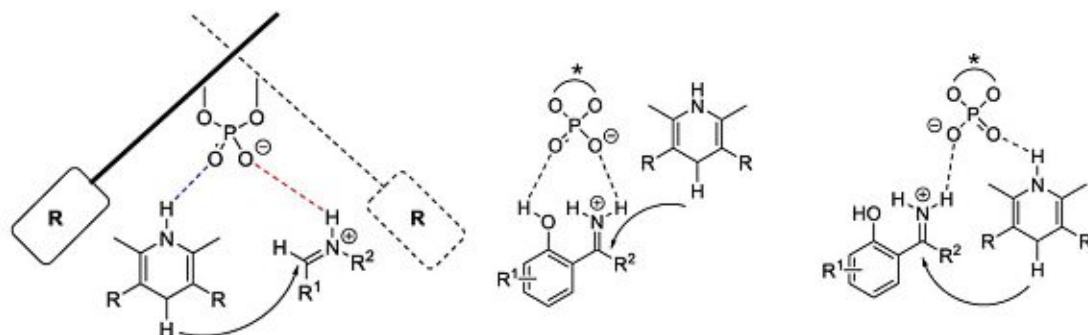
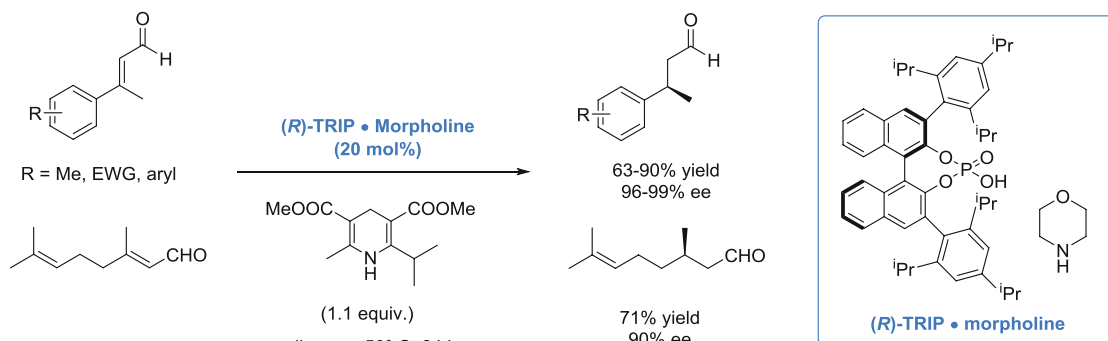


Figure 14. Bifunctional mechanism for the ATH of imines in general (left) and in the presence of a substrate featuring substituents with protic hydrogen (middle and right).⁴⁰

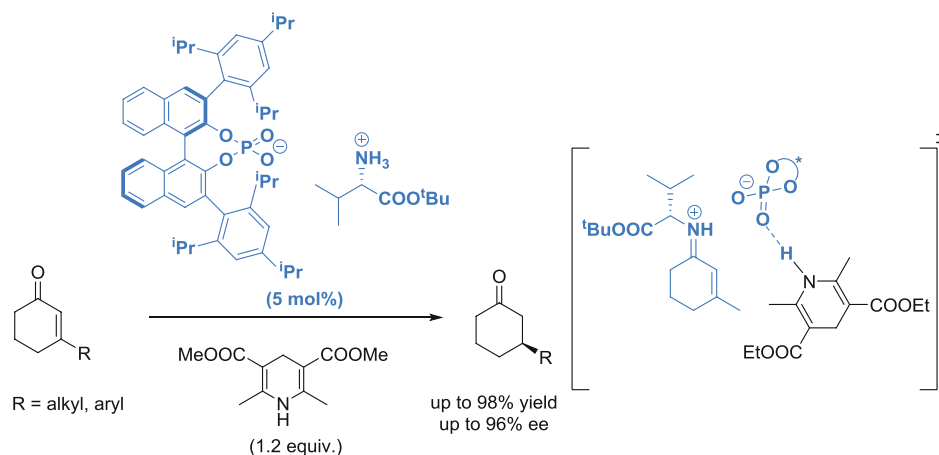
1.5.2.4 Chiral phosphoric acids as counteranions – Asymmetric counteranion-directed catalysis for ATH reactions

The concept of Asymmetric Counteranion-Directed Catalysis (ACDC) was coined by the group of List in 2006. It refers to the induction of enantioselectivity in a reaction proceeding through a cationic intermediate by means of tight ion-pairing with an enantiomerically pure counteranion. The ion-pairing between ammonium cations and chiral phosphate counterions is particularly prominent.⁵⁰ The ion-pairing of simple achiral secondary amines like morpholine with the bulky phosphoric acid (*R*)-TRIP provided a highly active and enantioselective catalyst for the organocatalytic ATH of aromatic and a few aliphatic enals (Scheme 11).⁵¹



Scheme 11. Asymmetric transfer hydrogenation of enals *via* ACDC.

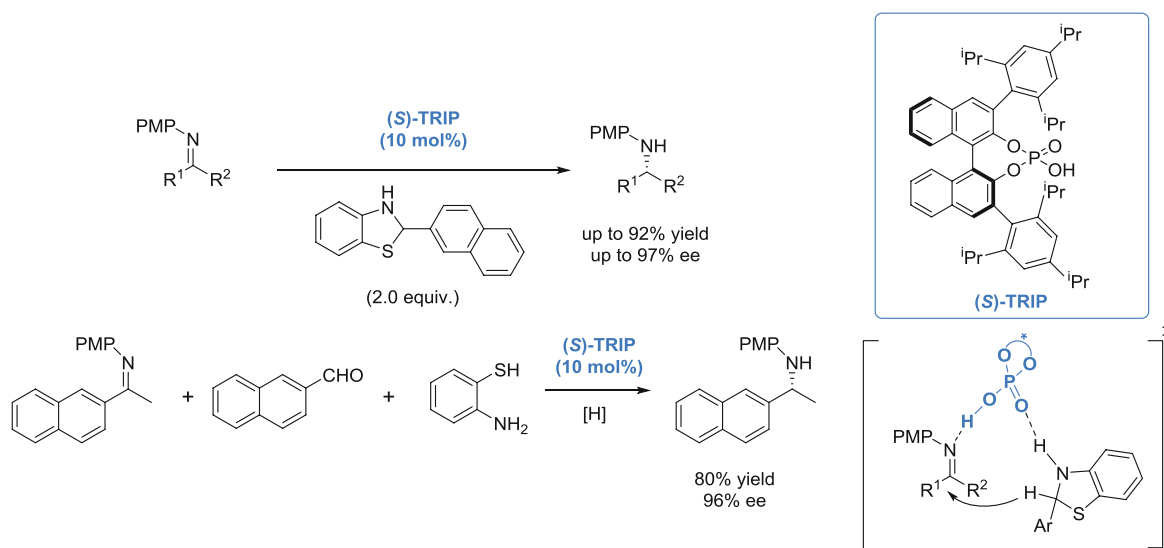
As a considerable advantage of ACDC over simple iminium catalysis, the scope could be successfully extended toward ketone substrates, as (*R*)-TRIP together with L-valine *tert*-butyl ester provided a powerful catalyst for the ATH of cyclic enones (Scheme 12).⁵²



Scheme 12. Asymmetric transfer hydrogenation of cyclic enones *via* ACDC.

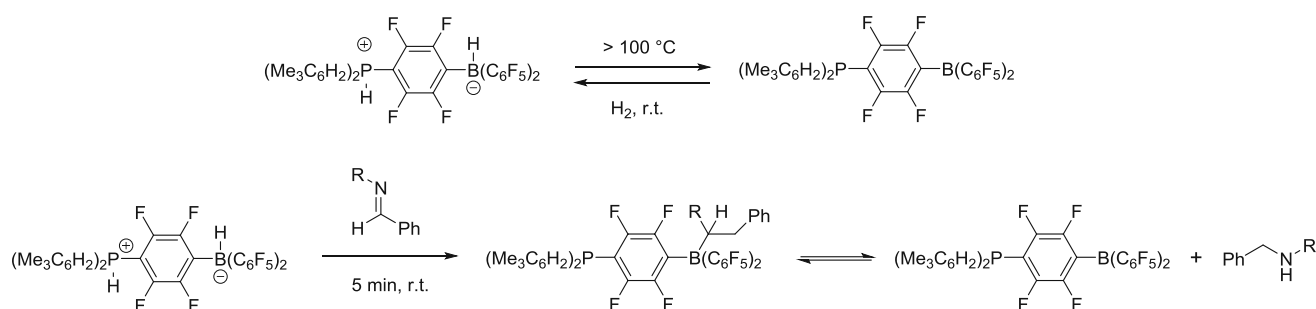
1.5.2.5 Organocatalytic ATH reactions with alternative hydrogen sources

While Hantzsch dihydropyridines are indeed the most frequently used hydrogen sources for organocatalytic ATH reactions, a few alternative methods employing other type of hydrogen donors have been developed as well. The group of Akiyama first achieved a CPA-catalyzed asymmetric transfer hydrogenation of ketoimines by using benzothiazolines as hydride donors.⁵³ Similarly to Hantzsch esters, the aromatization of the reductant as driving force facilitates the hydride donation. As the synthesis of the benzothiazolines requires similar reaction conditions to the subsequent ATH reaction, it was also possible to prepare the reductant *in situ* from the corresponding aldehyde and α -aminothiophenol (Scheme 13).⁵³



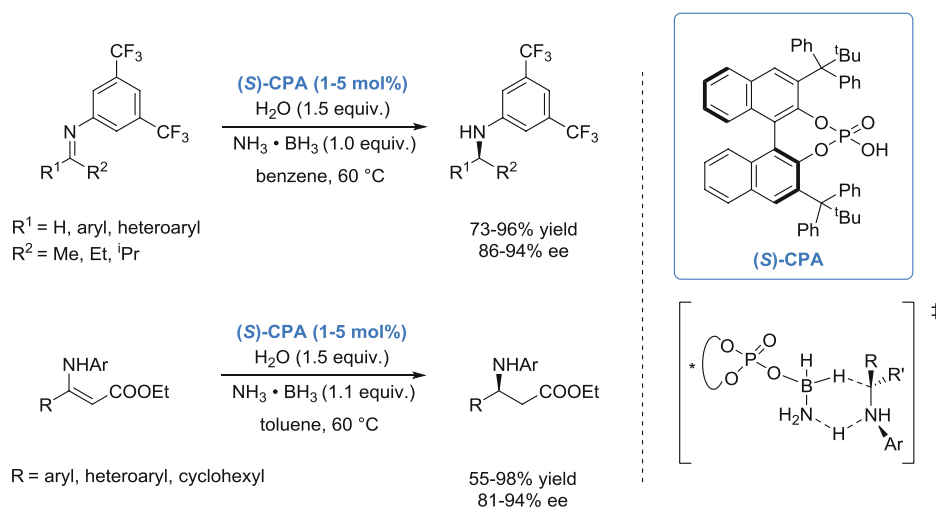
Scheme 13. ATH of ketoimines with benzothiazolines.

Eventually, frustrated Lewis pairs (FLPs) were also successfully applied for metal-free ATH reactions. In such special Lewis acid-base pairs, the large steric hindrance precludes the formation of traditional donor-acceptor complexes (Scheme 14, top).⁵⁴ In 2006 Welch *et al.* reported a zwitterionic FLP salt, featuring a sterically demanding phosphine and borane unit. As it contains both a protic and a hydridic hydrogen, it could heterolytically cleave H₂, forming phosphino-boranes. Because of the steric hindrance, these remains in monomeric form, and can readily take H₂ to reform the zwitterionic salt. Based on this pioneering work, Stephan and co-workers first achieved the transfer hydrogenation of imines relying on the aforementioned zwitterionic FLP system (Scheme 15, bottom).^{55,56}



Scheme 15. H-donation and uptake of FLPs (top) and their first application for transfer hydrogenations (bottom).

In 2010, the first highly stereoselective FLP-based asymmetric hydrogenation was published by Klankermayer; however, a H₂-pressure of 25 bar was required to reform the FLP catalyst.⁵⁷ The introduction of chiral phosphoric acids into FLP chemistry also allowed to carry out real transfer hydrogenations. For instance, β -enamino esters and ketimines can be efficiently reduced in the presence of a CPA-based chiral ammonia borane (Scheme 16). The phosphoric acid acts as a simple Brønsted acid to form the reactive species, and it is continuously regenerated with the assistance of water and excess of ammonia borane, allowing to lower the CPA loading below 1 mol%.⁵⁸



Scheme 16. Chiral phosphoric acid-catalyzed, ammonia borane mediated ATH of ketimines and β -enamino esters.

1.6 Asymmetric allylic alkylation

In 1965, J. Tsuji mentioned the first palladium-catalyzed allylic substitution by using stoichiometric amount of $[\text{Pd}(\text{allyl})\text{Cl}]_2$. In 1973, Trost *et al.* reported first a stoichiometric, and later a catalytic variant of such a reaction.^{59,60} Since then, palladium-catalyzed asymmetric allylic alkylation (AAA) became one of the most important tools for the synthesis of optically active allylic compounds, and also plays a key role in the synthesis of biologically active allylic molecules.^{61,62,63} As it requires mild reaction conditions – reactions are generally carried out at room temperature and atmospheric pressure – and provides operational simplicity, no special equipment is necessary; moreover, AAA shows remarkable functional group tolerance and can be performed with various allylic electrophiles and nucleophiles.

1.6.1 Catalytic cycle

The generally accepted mechanism of a palladium-catalyzed asymmetric substitution is depicted in Figure 15. Coordination (A) of the allylic substrate with the $\text{Pd}(0)$ species leads to the formation of a η^2 -complex, which is then followed by oxidative addition/ionization (B) to generate the active η^3 - π -allylpalladium intermediate. This soft electrophilic complex can be then attacked by either a soft or a hard nucleophile (C). Finally, decomplexation of the previously formed η^2 -complex leads to the substituted allylic product (D).

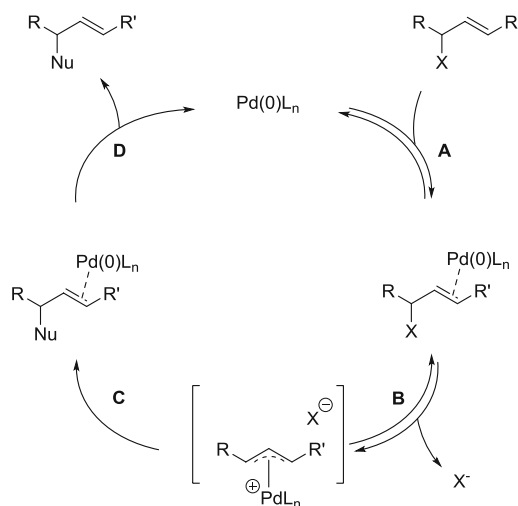
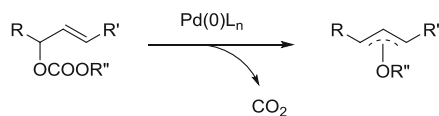


Figure 15. General mechanism of allylic substitution.

1.6.2 Nature of the leaving group

The most frequently applied leaving groups are acetates, carbonates, carbamates and halides, but also carboxylates, phosphates and sulfonates were successfully used in allylic substitutions. Given the relative stability of the η^3 - π -allylpalladium species and the reversibility of the oxidative addition, the

counteranion (X^-) may also act as nucleophile, preventing the formation of the desired product. To overcome this problem, the poor nucleophilicity of the leaving group should be taken into account. Allylic carbonate substrates can render the oxidative addition irreversible by means of decarboxylation, while the alkoxide formed can also help in the deprotonation of the nucleophile (Scheme 17).⁶⁴

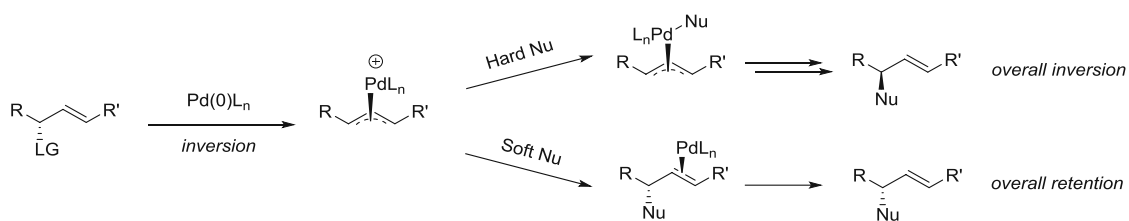


Scheme 17. Formation of π -allylpalladium alkoxides using allylic carbonate substrates.

As the introduction of these good leaving groups requires pre-functionalization(s) and results in additional waste formation, significant synthetic efforts have been done towards the use of non-activated allylic substrates. This will be discussed in more details in the chapter 1.6.7.

1.6.3 Nature of the nucleophile

The exact mode of attack of nucleophile on the η^3 - π -allylpalladium intermediate, thus the overall stereochemical outcome of an allylic substitution largely depends on the nature of the nucleophile. Stabilized or “soft” nucleophiles derived from conjugate acids whose $pK_a < 25$ attack directly on the π -allyl motif *via* S_N2 mechanism. Together with the inversion upon oxidative addition this leads to an overall retention in configuration. On the other hand, “hard” or unstabilized nucleophiles as Grignard and organozinc reagents attack first on the metal center *via* transmetalation, followed by reductive elimination, resulting in a net configurational inversion (Scheme 18).



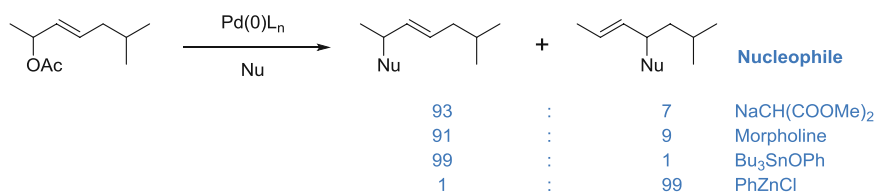
Scheme 18. Influence of the nucleophile on the stereochemistry.

“Soft” nucleophiles like malonates, amines, phthalimides, phenols and sulfonamides were found to be particularly well suitable for allylic substitutions, resulting in various C–C, C–N, C–O and C–S bond formations.^{61,65,66}

1.6.4 Regioselectivity considerations

Steric effect of substrates

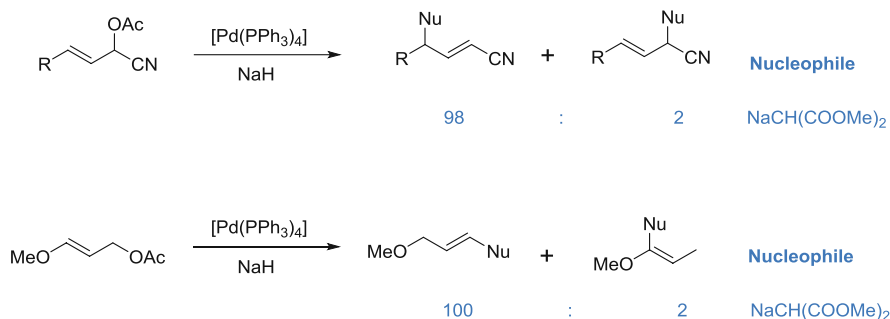
In order to minimize the steric repulsion between the nucleophile and the η^3 - π -allylpalladium species, the attack of a “soft” nucleophile takes place preferentially on the less substituted side of the allylic motif. However – as it was mentioned before – “hard” nucleophiles result in initial transmetalation and consequently also lead to the sterically more hindered regioisomer (Scheme 19).⁶⁷



Scheme 19. Influence of the substrate on the regioselectivity using “soft” and “hard” nucleophiles.

Electronic effect of substrates

It was also reported that EWGs generally promote the nucleophilic attack on the distal position in relation to the EWG itself, while EDG groups give rise to the substitution on the proximal position (Scheme 20).^{68,69}



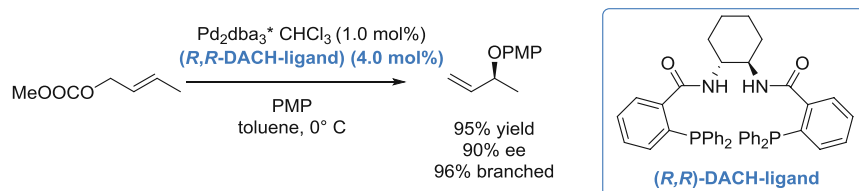
Scheme 20. Influence of extra functionalities on the regioselectivity.

1.6.5 Enantioselectivity considerations

For the majority of asymmetric reactions, enantioselectivity can be realized through the differentiation of the enantiotopic π faces of an unsaturated system. Contrarily, several different mechanisms can be described for AAA reactions, as each catalytic step – except of the decomplexation – provides an opportunity for asymmetric induction.

Preferential ionization via enantioselective olefin complexation

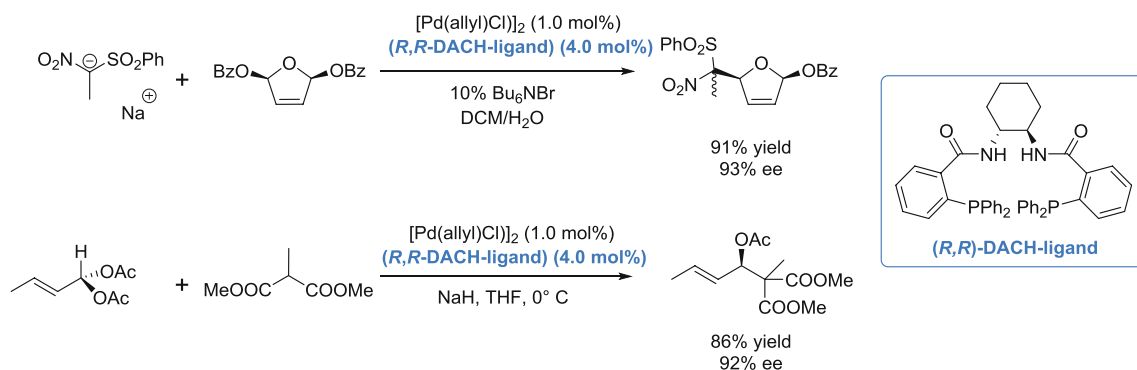
When using a non-symmetrically substituted olefin, the transition-metal complex should differentiate between its prochiral faces upon complexation. When one complex leads to a much faster ionization than the other and the subsequent nucleophilic attack is faster than the π - σ - π isomerization equilibrium, the enantiotopic olefin face complexation is the enantiodiscriminating step (Scheme 21).⁷⁰



Scheme 21. Metal-olefin complexation as enantiodiscriminating step.

Enantiotopic ionization of prochiral leaving groups

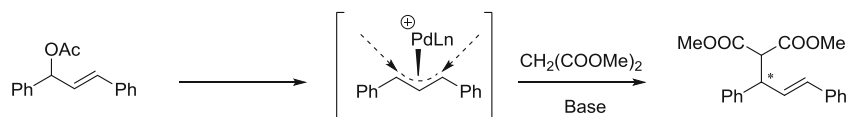
In case of the asymmetric allylation of *meso* or achiral *geminal* disubstituted allylic substrates, the catalyst differentiates between the enantiotopic leaving groups upon ionization. In order to reach high enantioselectivity, it is again crucial that the nucleophilic attack takes place much faster than the equilibrium between the diastereomeric η^3 - π -allylpalladium intermediates (Scheme 22).^{71,72}



Scheme 22. Enantiotopic ionization of a *meso* diester and a *geminal* diacetate.

Attack at enantiotopic termini of the allyl complex

When a chiral allylic substrate generates *meso- π -allyl intermediates upon ionization, the two allylic termini are enantiotopic and the regioselective addition of the nucleophile is the enantiodiscriminating step. A typical example is the AAA reaction of (\pm)-diphenylallyl-acetate with malonate nucleophiles (Scheme 23): nucleophilic attack from either side of the allylic intermediate (depicted with dashed arrows) results in the formation of enantiomers.*

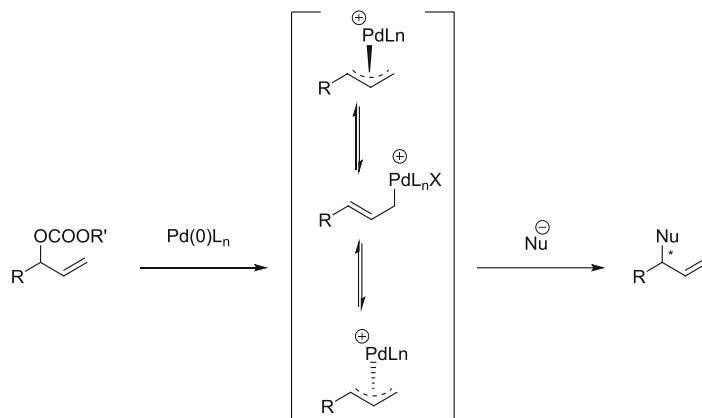


Scheme 23. Enantiotopic differentiation on the allylic termini as source of asymmetric induction.

Enantioface exchange in the η^3 - π -allylpalladium complex

In case the interconversion between the π -allylpalladium intermediates is faster than the nucleophilic attack or the initial coordination of the olefin is reversible, the enantioselectivity cannot be determined neither by the olefin face coordination, nor by enantiotopic ionization.

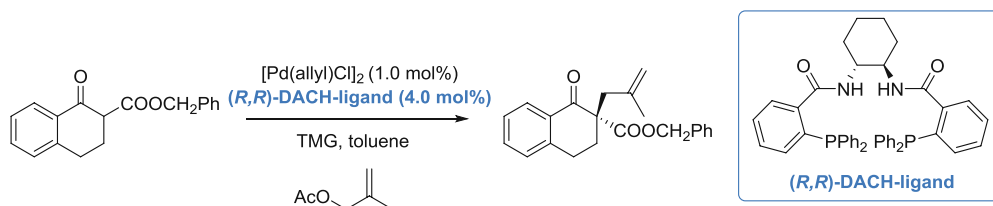
For example, the ionization of the allylic carbonate depicted in Scheme 24 results in two diastereomeric complexes which can interconvert *via* π - σ - π isomerization on the terminal carbon, and the reactivity difference between those will determine the degree of asymmetric induction.



Scheme 24. Asymmetric induction *via* differentiation of the π -allyl intermediates.

Differentiation of prochiral nucleophile faces

Enantioselectivity can be realized as well as the π -allyl system differentiates between the prochiral faces of the nucleophile. Such way for asymmetric induction is particularly challenging as the nucleophile approaches the complex opposite to the chiral ligand. Therefore, it is crucial that the chiral ligand must influence the approach of the nucleophile in its chiral environment. Typically, AAA reactions involving ketone enolate nucleophiles proceed *via* this mechanism (Scheme 25).⁷³



Scheme 25. Enantioselective AAA reaction with tetralone nucleophiles.

1.6.6 Chiral ligands for asymmetric allylic alkylations

Because of the strong binding nature of nitrogen and phosphines to palladium, a wide range of ligands featuring diamines (**I**),⁷⁴ diphosphines (**II**, **VII**),⁷⁵ phosphoramidites (**VIII**),^{76,77} bisoxazolines (**IV-V**)⁷⁸ and unsymmetric oxazolines (**VI**)⁷⁹ have been successfully applied in AAA reactions. A brief selection of chiral ligands is depicted in Figure 16.

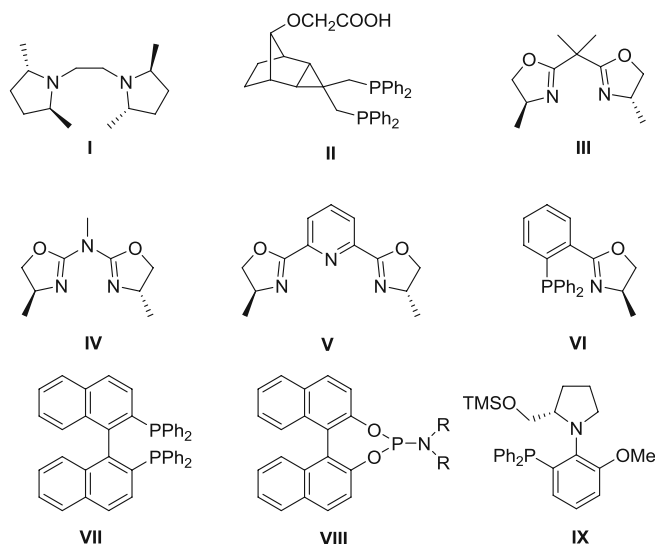


Figure 16. Some privileged ligands for AAA reactions.

The class of C_2 -symmetric diamine-based diphosphines are undoubtedly the most successful chiral ligands for asymmetric allylic alkylations (Figure 17). Since their development in 1992, the Trost Modular Ligands (TMLs), specially the DPPBA-based (DPPBA = 2-(diphenylphosphino)benzoic acid) ones are extensively used in this field, as they can be readily synthesized and provide excellent enantioselectivity.⁸⁰

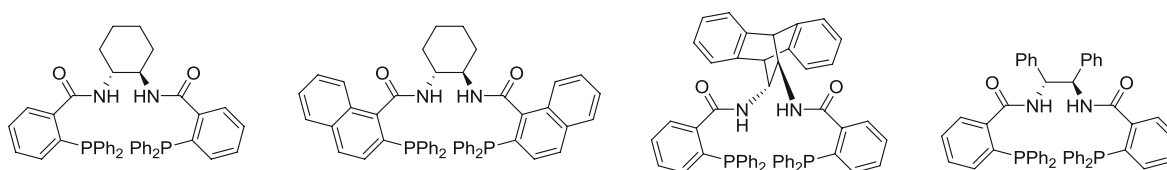


Figure 17. Typical DPPBA-based chiral ligands.

The first mechanistic interpretations with such DPPBA-based ligands used the so-called empirical cartoon-model. To minimize the steric repulsion upon forming the π -allylpalladium complex, the phenyl rings have a propeller-like arrangement. Two phenyl “walls” are perpendicular to the allylic plane, while two “flaps” are parallel to it. This generates a defined chiral pocket with two of the quadrants being blocked and results in asymmetric induction. For instance, as the leaving group is ionized to form the π -allylpalladium complex, it will preferentially depart from “right front quadrant”

(pathway B) to minimize steric repulsions. As a consequence, the nucleophile will also attack on the same place, determining the enantioselectivity of the reaction. (Figure 18).⁶⁵

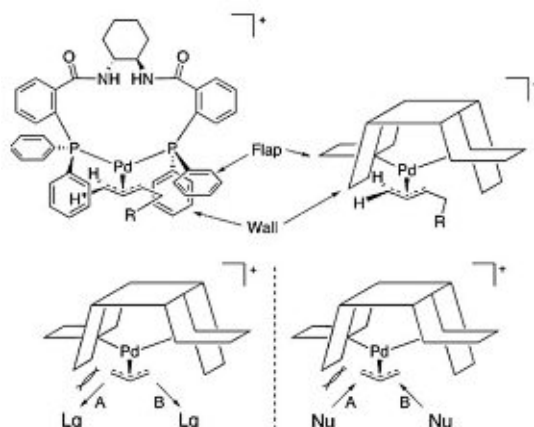


Figure 18. Simple cartoon-model of DPPBA-based ligands (top right) and a representative way for enantiodiscrimination (bottom).⁶⁵

Even though this model is widely used to rationalize the way of asymmetric induction in AAA reactions, the assumption that only time-averaged monomeric species are present in the reaction mixture is not realistic as multiple chelation modes are accessible and the monomeric π -allylpalladium species are in equilibrium with oligomeric complexes.⁸¹

1.6.7 Allylic alcohols as electrophiles for allylic alkylations

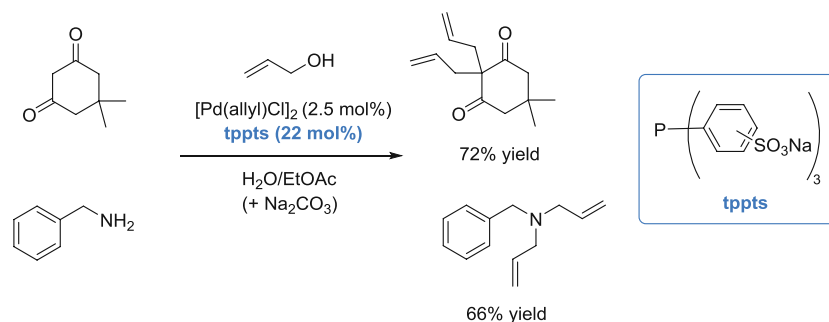
The traditional Tsuji-Trost reaction requires an allylic electrophile with a good leaving group. In order for the reaction to take place the hydroxyl group of the allylic alcohol is generally converted into an ester, carbonate or halide to increase its leaving-group ability. This pre-functionalization; however, means an additional reaction step and it also generates extra waste and therefore increasing the overall environmental impact of the reaction. In light of the growing importance of economic and sustainable processes, the implementation of non-functionalized allylic substrates in allylic alkylations is of special interest.

In order to increase the leaving-group ability of the hydroxyl group without pre-functionalization, it should be activated *in situ*.

Protic solvents as activators

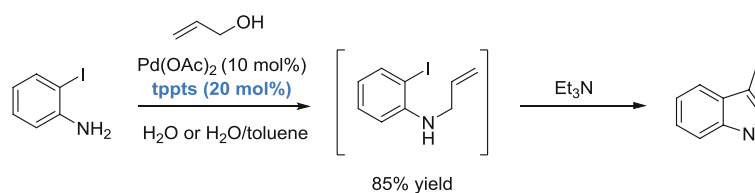
Protic solvents, especially water can play a crucial role in the activation of allylic alcohol electrophiles. The group of Oshima reported that the extensive hydrogen-bonding between water and the substrates plays a significant role in decreasing the activation barrier. Furthermore, excessive hydration of the OH-group can trigger the hydroxide elimination, while it also helps to stabilize the hydroxide anion.⁸²

Using a water-soluble catalyst a series of 1,3-diketones, β -keto esters and amines could be allylated with simple allylic alcohols in a liquid-liquid biphasic system (Scheme 26).



Scheme 26. Water-soluble Pd-complex for allylation of C- and N-nucleophiles with allyl alcohol.

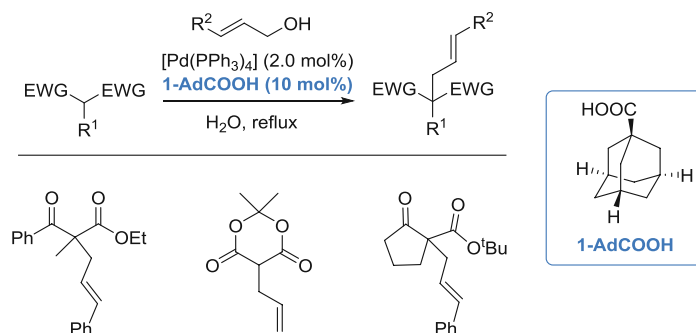
The same concept was used by Yokoyama *et al.* for the allylation of α -haloanilines. After the aqueous allylation, the intermediate was cyclized *via* intramolecular Heck-coupling, providing a straightforward synthesis to indoles (Scheme 27).⁸³



Scheme 27. Allylation of anilines with allyl alcohols for the one-pot synthesis of indoles.

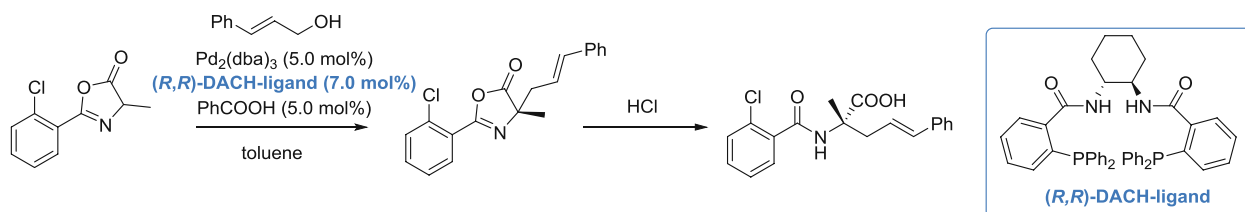
Brønsted-acid activation

In 2003, Kobayashi reported a procedure for carboxylic acid-assisted direct alkylation of various carbon nucleophiles in aqueous media. Even though the reaction was working *via* simple protic solvent activation, they observed dramatic reaction rate acceleration in the presence of carboxylic acids as co-catalysts (Scheme 28).⁸⁴



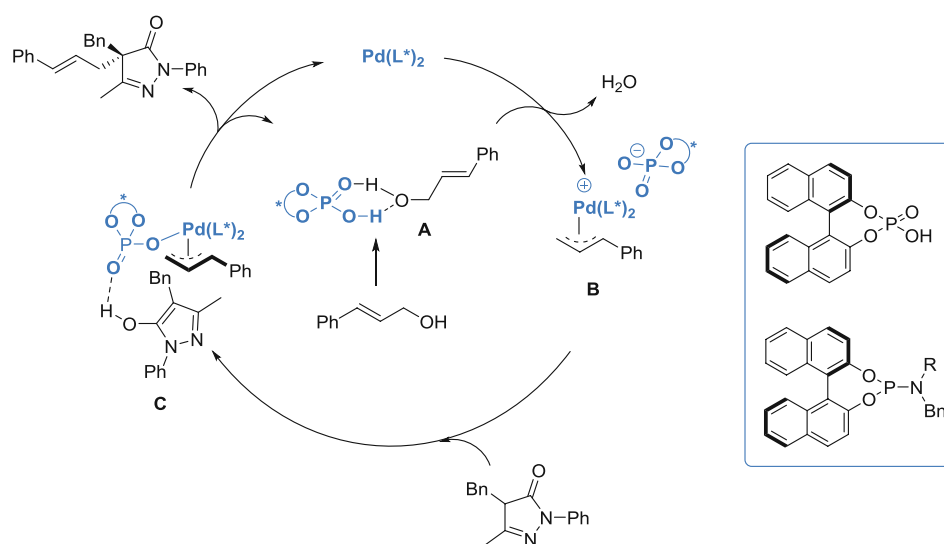
Scheme 28. Carboxylic acid-assisted allylations with allylic alcohols.

Recently, Jiang and Xia disclosed a simple, benzoic acid-accelerated AAA reaction of azlactones. The reaction provided a rapid excess to all-carbon quaternary allylic amino acids (Scheme 29).⁸⁵



Scheme 29. carboxylic acid-assisted allylation of azlactones.

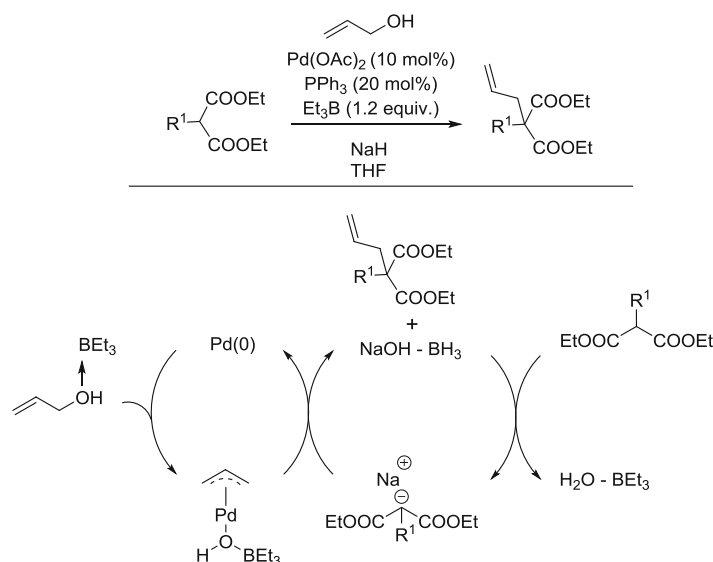
Gong and co-workers used BINOL-derived chiral phosphoramidite ligands together with BINOL-derived chiral phosphoric acids for the asymmetric allylic alkylation of pyrazol-5-ones. The chiral phosphoric acid plays a dual role in the reaction: it activates the allylic alcohol (**A**) and it also controls the stereochemistry of the intermediate **C** by means of hydrogen-bonding (Scheme 30).⁸⁶



Scheme 30. Carboxylic acid-assisted asymmetric allylation of azlactones.

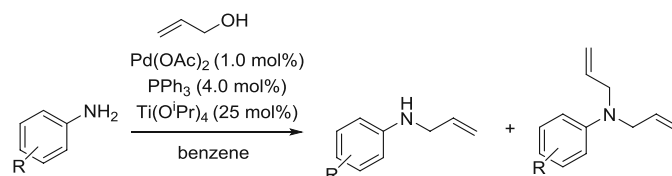
Lewis-acid activation

Lewis acid activation, like the use of boron reagents provides another way to activate an allylic alcohol. However, because of the strong interactions with the alcohol OH, these reactions initially required stoichiometric amount of Lewis acid, which could be only decreased by increasing the amount of triphenylphosphine loading. The Tamaru group reported the Et₃B-mediated allylation of carbonucleophiles. The boron presumably coordinates with the OH oxygen facilitating the oxidative addition (Scheme 31).^{87,88}



Scheme 31. Et₃B-promoted allylic alkylation (top) and its plausible mechanism (bottom).

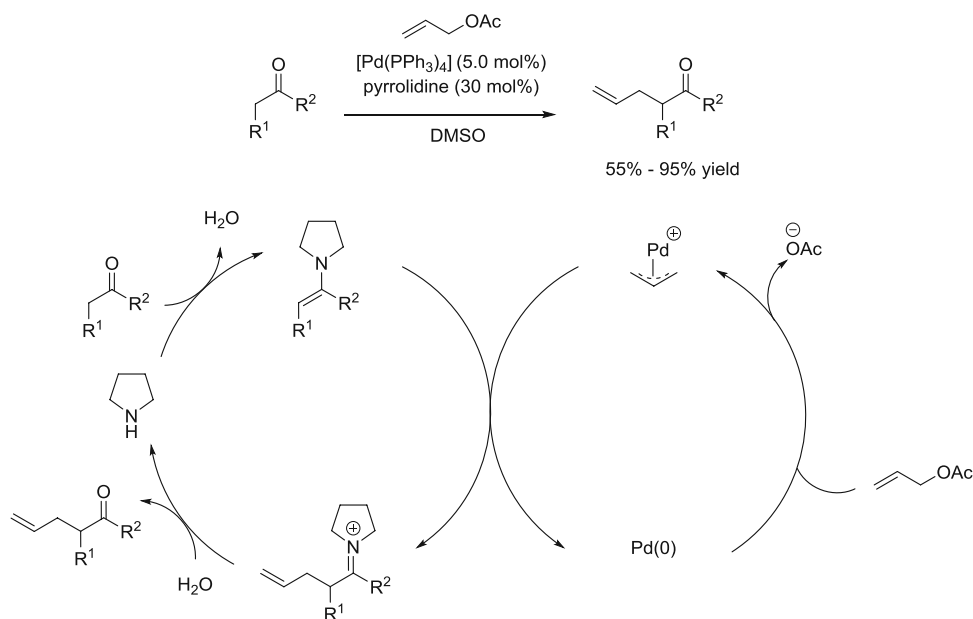
The addition of titanium-based Lewis-acids was also found to be a powerful strategy for the *in situ* activation of allylic alcohols, as several studies showed its useful application for the allylation of *C*- and *N*-nucleophiles by using either stoichiometric or catalytic amount of Ti(OⁱPr)₄, as depicted in Scheme 32.^{89, 90}



Scheme 32. Ti-mediated allylation of aniline derivatives with allyl alcohol.

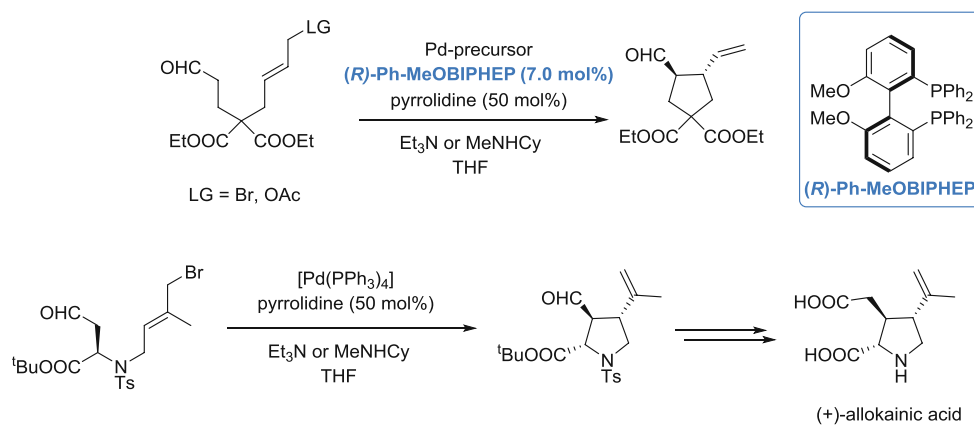
1.6.8 Pd/enamine catalysis

The idea of merging enamine or iminium activation and transition-metal catalysis led to a new era in chemistry, as it could achieve chemical transformations that are not accessible by individual catalysis. The combination of an aminocatalyst and a transition-metal catalyst was first achieved by the group of Córdova in 2006 as they investigated the direct α -allylation of ketones with activated electrophiles *via* the synergistic use of [Pd(PPh₃)₄] and pyrrolidine (Scheme 33, top).⁹¹ The authors proposed that the reaction mechanism comprises two catalytic cycles. The carbonyl compound is activated *in situ* *via* enamine formation providing a soft nucleophilic species, meanwhile the soft electrophilic allylpalladium- π complex is generated in the second catalytic cycle (Scheme 33, bottom).



Scheme 33. Pd/enamine catalyzed direct allylation of carbonyls with activated electrophiles.

Using a similar approach, Saicic *et al.* reported the enantioselective cyclization of aldehydes *via* intramolecular α -allylation (Scheme 34, top). Importantly, the chirality should be introduced in the Pd-cycle, as the use of traditional chiral aminocatalysts (e.g. *MacMillan catalyst*) resulted in either catalyst deactivation or in the formation of a racemic product.⁹² They also demonstrated the synthetic utility of such cyclic aldehydes for the stereoselective synthesis of (+)-allokainic acid (Scheme 34, bottom).⁹³

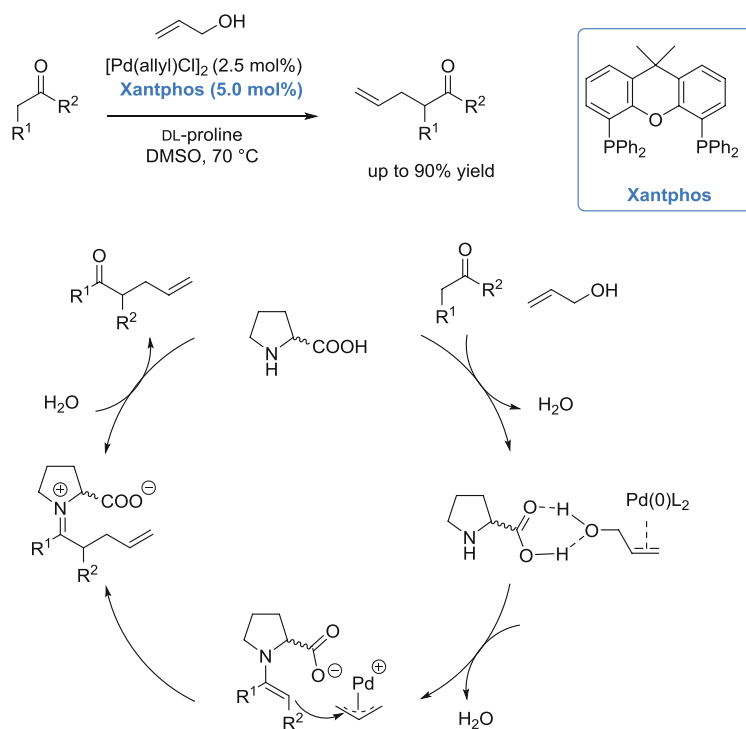


Scheme 34. Cyclization of aldehydes *via* enantioselective α -allylation (top) and its use for natural product synthesis (bottom).

While the aforementioned protocols could indeed provide a useful tool for the direct allylation of ketones and aldehydes, they necessarily involve a good leaving group. As mentioned before, the use of non-functionalized allylic alcohols has both economic and environmental benefits.

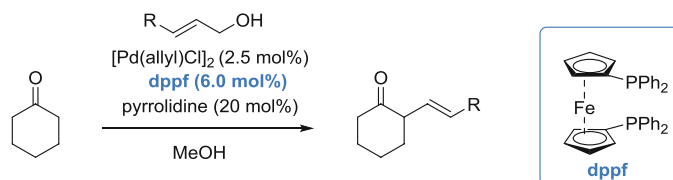
In 2009, the group of Breit first achieved the direct allylation of carbonyl compounds by using simple allylic alcohol reagents *via* Pd/proline dual activation (Scheme 35). For high catalytic activity, a phosphine ligand with a large bite angle – Xantphos – was required. The authors claimed that proline

acts as a dual activator: it forms the reactive enamine species, meanwhile its carboxyl groups might facilitate the leaving of the allylic alcohol hydroxyl and the formation of a tighter ion pair intermediate, resulting in higher reaction rates. Even though the authors screened chiral aminocatalysts as well, only racemic products could be obtained.⁹⁴



Scheme 35. Pd/proline dual activation for the direct allylation of ketones with allylic alcohols.

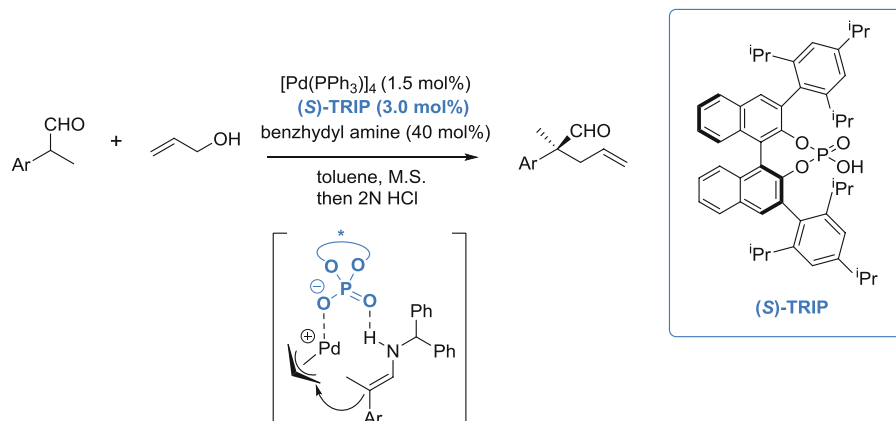
Addressing the same problem, Huo *et al.* reported a slightly different approach. Instead of using DL-proline as additive, they carried out the reactions *via* Pd/pyrrolidine catalysis in protic solvents (Scheme 36). The authors reported that the cleavage of the C-O bond of the allylic alcohols can be readily achieved in methanol through the strong hydrogen-bonding with the solvent molecules.⁹⁵



Scheme 36. Pd/pyrrolidine dual activation in protic solvents.

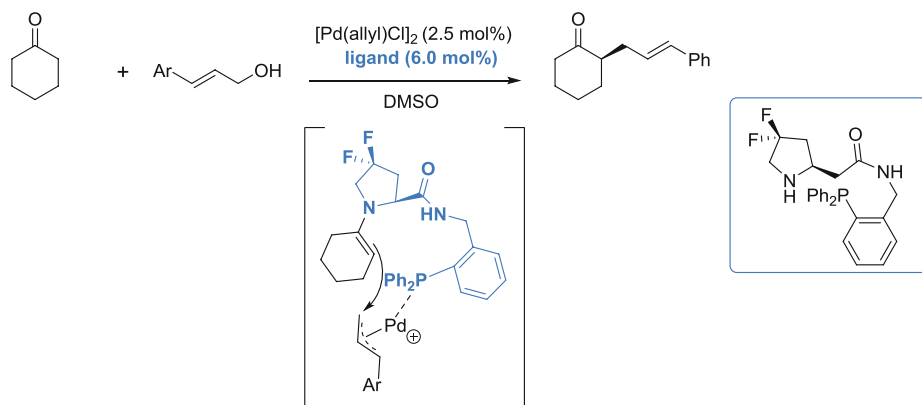
The first example for the asymmetric direct allylation of carbonyl compounds with non-activated allylic reagents was done by the List group in 2011. High catalytic activity and selectivity was achieved through the synergistic action of $[Pd(PPh_3)_4]$, benzhydryl amine and (*S*)-TRIP. The high enantioselectivity could be rationalized through the formation of a key intermediate involving all three

catalyst components. Even though the procedure was excellent for aromatic α -branched aldehydes, inferior results were obtained for the quaternization of aliphatic analogues (Scheme 37).⁹⁶



Scheme 37. List's strategy for the direct allylation of α -branched aldehydes (top) and the key intermediate of the reaction (bottom).

Recently, the Shibasaki group reported a procedure for the direct α -allylation of ketones with allylic alcohols. The chiral bifunctional, phosphine-substituted proline catalyst could enable such transformations for the first time; however, only moderate enantioselectivity could be achieved (Scheme 38).⁹⁷



Scheme 38. Direct allylation of ketones with allylic alcohols (top) and its key intermediate (bottom).

1.7 Bibliography

- (1) Hammami, R.; Nouira, I.; Frein, Y. Effects of Customers' Environmental Awareness and Environmental Regulations on the Emission Intensity and Price of a Product. *Decis. Sci.* **2018**, *49* (6), 1116–1155. <https://doi.org/10.1111/deci.12302>.
- (2) Urquhart, L. Top Companies and Drugs by Sales in 2019. *Nat. Rev. Drug Discov.* **2020**, *19* (4), 228–228. <https://doi.org/10.1038/d41573-020-00047-7>.
- (3) Halpern, J.; Trost, B. M. Asymmetric Catalysis. *Proc. Natl. Acad. Sci. U. S. A.* **2004**, *101* (15), 5347. <https://doi.org/10.1073/pnas.0401811101>.
- (4) Sunoj, R. B. Transition State Models for Understanding the Origin of Chiral Induction in Asymmetric Catalysis. *Acc. Chem. Res.* **2016**, *49* (5), 1019–1028. <https://doi.org/10.1021/acs.accounts.6b00053>.
- (5) Osborn, J. A.; Jardine, F. H.; Young, J. F.; Wilkinson, G. The Preparation and Properties of Tris(Triphenylphosphine)Halogenorhodium(I) and Some Reactions Thereof Including Catalytic Homogeneous Hydrogenation of Olefins and Acetylenes and Their Derivatives. *J. Chem. Soc. A Inorganic, Phys. Theor.* **1966**, 1711. <https://doi.org/10.1039/j19660001711>.
- (6) Crabtree, R. Iridium Compounds in Catalysis. *Acc. Chem. Res.* **1979**, *12* (9), 331–337. <https://doi.org/10.1021/ar50141a005>.
- (7) Vineyard, B. D.; Knowles, W. S.; Sabacky, M. J.; Bachman, G. L.; Weinkauff, D. J. Asymmetric Hydrogenation. Rhodium Chiral Bisphosphine Catalyst. *J. Am. Chem. Soc.* **1977**, *99* (18), 5946–5952. <https://doi.org/10.1021/ja00460a018>.
- (8) Miyashita, A.; Takaya, H.; Souchi, T.; Noyori, R. 2, 2'-Bis(Diphenylphosphino)-1, 1'-Binaphthyl(Binap). *Tetrahedron* **1984**, *40* (8), 1245–1253. [https://doi.org/10.1016/S0040-4020\(01\)82411-X](https://doi.org/10.1016/S0040-4020(01)82411-X).
- (9) Noyori, R.; Ohkuma, T.; Kitamura, M.; Takaya, H.; Sayo, N.; Kumobayashi, H.; Akutagawa, S. Asymmetric Hydrogenation of .Beta.-Keto Carboxylic Esters. A Practical, Purely Chemical Access to .Beta.-Hydroxy Esters in High Enantiomeric Purity. *J. Am. Chem. Soc.* **1987**, *109* (19), 5856–5858. <https://doi.org/10.1021/ja00253a051>.
- (10) Kumobayashi, H. Industrial Application of Asymmetric Reactions Catalyzed by BINAP-Metal Complexes. *Recl. des Trav. Chim. des Pays-Bas* **1996**, *115* (4), 201–210. <https://doi.org/10.1002/recl.19961150403>.
- (11) Noyori, R.; Ohkuma, T. Asymmetric Catalysis by Architectural and Functional Molecular Engineering: Practical Chemo- and Stereoselective Hydrogenation of Ketones. *Angew. Chemie Int. Ed.* **2001**, *40* (1), 40–73. [https://doi.org/10.1002/1521-3773\(20010105\)40:1<40::AID-ANIE40>3.0.CO;2-5](https://doi.org/10.1002/1521-3773(20010105)40:1<40::AID-ANIE40>3.0.CO;2-5).
- (12) Zassinovich, G.; Mestroni, G.; Giadiali, S. Asymmetric Hydrogen Transfer Reactions Promoted by Homogeneous Transition Metal Catalysts. *Chem. Rev.* **1992**, *92* (5), 1051–1069. <https://doi.org/10.1021/cr00013a015>.
- (13) Laue, T.; Plagens, A. Meerwein-Ponndorf-Verley-Reduktion; 1994; pp 221–223. https://doi.org/10.1007/978-3-322-94726-0_70.
- (14) Bianchi, M.; Matteoli, U.; Menchi, G.; Frediani, P.; Pratesi, S.; Piacenti, F.; Botteghi, C. Asymmetric Synthesis by Chiral Ruthenium Complexes. *J. Organomet. Chem.* **1980**, *198* (1), 73–80. <https://doi.org/10.1016/S0022->

328X(00)84665-3.

- (15) Hashiguchi, S.; Fujii, A.; Takehara, J.; Ikariya, T.; Noyori, R. Asymmetric Transfer Hydrogenation of Aromatic Ketones Catalyzed by Chiral Ruthenium(II) Complexes. *J. Am. Chem. Soc.* **1995**, *117* (28), 7562–7563. <https://doi.org/10.1021/ja00133a037>.
- (16) Wang, D.; Astruc, D. The Golden Age of Transfer Hydrogenation. *Chem. Rev.* **2015**, *115* (13), 6621–6686. <https://doi.org/10.1021/acs.chemrev.5b00203>.
- (17) Genêt, J.-P.; Ratovelomanana-Vidal, V.; Pinel, C. Asymmetric Hydrogen Transfer Reaction of Aryl Ketones with Chiral Diphosphine-Ruthenium(II) Catalysts. *Synlett* **1993**, *1993* (07), 478–480. <https://doi.org/10.1055/s-1993-22497>.
- (18) Cabou, J.; Brocard, J.; Péliniski, L. Chiral Ferrocenyl Diphosphines for Asymmetric Transfer Hydrogenation of Acetophenone. *Tetrahedron Lett.* **2005**, *46* (7), 1185–1188. <https://doi.org/10.1016/j.tetlet.2004.12.059>.
- (19) Botteghi, C.; Chelucci, C.; Chessa, G.; Delogu, G.; Gladiali, S.; Soccolini, F. Optically Active Nitrogen Ligands. *J. Organomet. Chem.* **1986**, *304* (1–2), 217–225. [https://doi.org/10.1016/S0022-328X\(00\)99687-6](https://doi.org/10.1016/S0022-328X(00)99687-6).
- (20) Müller, D.; Umbricht, G.; Weber, B.; Pfaltz, A. C₂-Symmetric 4,4',5,5'-Tetrahydrobi(Oxazoles) and 4,4',5,5'-Tetrahydro-2,2'-Methylenebis(Oxazoles) as Chiral Ligands for Enantioselective Catalysis Preliminary Communication. *Helv. Chim. Acta* **1991**, *74* (1), 232–240. <https://doi.org/10.1002/hlca.19910740123>.
- (21) Langer, T.; Helmchen, G. Highly Efficient New Catalysts for Enantioselective Transfer Hydrogenation of Ketones. *Tetrahedron Lett.* **1996**, *37* (9), 1381–1384. [https://doi.org/10.1016/0040-4039\(96\)00011-1](https://doi.org/10.1016/0040-4039(96)00011-1).
- (22) Takehara, J.; Hashiguchi, S.; Fujii, A.; Inoue, S.; Ikariya, T.; Noyori, R. Amino Alcohol Effects on the Ruthenium(II)-Catalyzed Asymmetric Transfer Hydrogenation of Ketones in Propan-2-ol. *Chem. Commun.* **1996**, No. 2, 233. <https://doi.org/10.1039/cc9960000233>.
- (23) Palmer, M.; Walsgrove, T.; Wills, M. (1R,2S)-(+)-Cis-1-Amino-2-Indanol: An Effective Ligand for Asymmetric Catalysis of Transfer Hydrogenations of Ketones. *J. Org. Chem.* **1997**, *62* (15), 5226–5228. <https://doi.org/10.1021/jo970405a>.
- (24) Matsumura, K.; Hashiguchi, S.; Ikariya, T.; Noyori, R. Asymmetric Transfer Hydrogenation of α , β -Acetylenic Ketones. *J. Am. Chem. Soc.* **1997**, *119* (37), 8738–8739. <https://doi.org/10.1021/ja971570a>.
- (25) Püntener, K.; Schwink, L.; Knochel, P. New Efficient Catalysts for Enantioselective Transfer Hydrogenations. *Tetrahedron Lett.* **1996**, *37* (45), 8165–8168. [https://doi.org/10.1016/0040-4039\(96\)01853-9](https://doi.org/10.1016/0040-4039(96)01853-9).
- (26) Jiang, Q.; Van Plew, D.; Murtuza, S.; Zhang, X. Synthesis of (1,1')-2,6-Bis[1-(Diphenylphosphino)Ethyl]Pyridine and Its Application in Asymmetric Transfer Hydrogenation. *Tetrahedron Lett.* **1996**, *37* (6), 797–800. [https://doi.org/10.1016/0040-4039\(95\)02298-8](https://doi.org/10.1016/0040-4039(95)02298-8).
- (27) Gao, J.-X.; Ikariya, T.; Noyori, R. A Ruthenium(II) Complex with a C₂-Symmetric Diphosphine/Diamine Tetradentate Ligand for Asymmetric Transfer Hydrogenation of Aromatic Ketones †. *Organometallics* **1996**, *15* (4), 1087–1089. <https://doi.org/10.1021/om950833b>.
- (28) Wu, X.; Li, X.; Hems, W.; King, F.; Xiao, J. Accelerated Asymmetric Transfer Hydrogenation of Aromatic Ketones in Water. *Org. Biomol. Chem.* **2004**, *2* (13), 1818–1821. <https://doi.org/10.1039/b403627a>.

- (29) Wu, X.; Liu, J.; Di Tommaso, D.; Iggo, J. A.; Catlow, C. R. A.; Bacsá, J.; Xiao, J. A Multilateral Mechanistic Study into Asymmetric Transfer Hydrogenation in Water. *Chem. - A Eur. J.* **2008**, *14* (25), 7699–7715. <https://doi.org/10.1002/chem.200800559>.
- (30) Li, X.; Wu, X.; Chen, W.; Hancock, F. E.; King, F.; Xiao, J. Asymmetric Transfer Hydrogenation in Water with a Supported Noyori-Ikariya Catalyst. *Org. Lett.* **2004**, *6* (19), 3321–3324. <https://doi.org/10.1021/ol0487175>.
- (31) Ma, Y.; Liu, H.; Chen, L.; Cui, X.; Zhu, J.; Deng, J. Asymmetric Transfer Hydrogenation of Prochiral Ketones in Aqueous Media with New Water-Soluble Chiral Vicinal Diamine as Ligand. *Org. Lett.* **2003**, *5* (12), 2103–2106. <https://doi.org/10.1021/ol0345125>.
- (32) Kang, G.; Lin, S.; Shiwakoti, A.; Ni, B. Imidazolium Ion Tethered TsDPENs as Efficient Water-Soluble Ligands for Rhodium Catalyzed Asymmetric Transfer Hydrogenation of Aromatic Ketones. *Catal. Commun.* **2014**, *57*, 111–114. <https://doi.org/10.1016/j.catcom.2014.08.006>.
- (33) Geldbach, T. J.; Dyson, P. J. A Versatile Ruthenium Precursor for Biphasic Catalysis and Its Application in Ionic Liquid Biphasic Transfer Hydrogenation: Conventional vs Task-Specific Catalysts. *J. Am. Chem. Soc.* **2004**, *126* (26), 8114–8115. <https://doi.org/10.1021/ja048886k>.
- (34) Li, J.; Tang, Y.; Wang, Q.; Li, X.; Cun, L.; Zhang, X.; Zhu, J.; Li, L.; Deng, J. Chiral Surfactant-Type Catalyst for Asymmetric Reduction of Aliphatic Ketones in Water. *J. Am. Chem. Soc.* **2012**, *134* (45), 18522–18525. <https://doi.org/10.1021/ja308357y>.
- (35) Wang, W.; Li, Z.; Mu, W.; Su, L.; Wang, Q. Highly Efficient Asymmetric Transfer Hydrogenation of Ketones in Emulsions. *Catal. Commun.* **2010**, *11* (5), 480–483. <https://doi.org/10.1016/j.catcom.2009.12.002>.
- (36) Li, X.; Blacker, J.; Houson, I.; Wu, X.; Xiao, J. An Efficient Ir(III) Catalyst for the Asymmetric Transfer Hydrogenation of Ketones in Neat Water. *Synlett* **2006**, *2006* (08), 1155–1160. <https://doi.org/10.1055/s-2006-932490>.
- (37) Yang, J. W.; Hechavarria Fonseca, M. T.; Vignola, N.; List, B. Metal-Free, Organocatalytic Asymmetric Transfer Hydrogenation of α,β -Unsaturated Aldehydes. *Angew. Chemie* **2005**, *117* (1), 110–112. <https://doi.org/10.1002/ange.200462432>.
- (38) Ouellet, S. G.; Tuttle, J. B.; MacMillan, D. W. C. Enantioselective Organocatalytic Hydride Reduction. *J. Am. Chem. Soc.* **2005**, *127* (1), 32–33. <https://doi.org/10.1021/ja043834g>.
- (39) Tuttle, J. B.; Ouellet, S. G.; MacMillan, D. W. C. Organocatalytic Transfer Hydrogenation of Cyclic Enones. *J. Am. Chem. Soc.* **2006**, *128* (39), 12662–12663. <https://doi.org/10.1021/ja0653066>.
- (40) Martin, N. J. A.; Cheng, X.; List, B. Organocatalytic Asymmetric Transferhydrogenation of β -Nitroacrylates: Accessing β 2 -Amino Acids. *J. Am. Chem. Soc.* **2008**, *130* (42), 13862–13863. <https://doi.org/10.1021/ja8069852>.
- (41) Ferraro, A.; Bernardi, L.; Fochi, M. Organocatalytic Enantioselective Transfer Hydrogenation of β -Amino Nitroolefins. *Adv. Synth. Catal.* **2016**, *358* (10), 1561–1565. <https://doi.org/10.1002/adsc.201600061>.
- (42) Rueping, M.; Sugiono, E.; Azap, C.; Theissmann, T.; Bolte, M. Enantioselective Brønsted Acid Catalyzed Transfer Hydrogenation: Organocatalytic Reduction of Imines. *Org. Lett.* **2005**, *7* (17), 3781–3783. <https://doi.org/10.1021/ol0515964>.
- (43) Hoffmann, S.; Seayad, A. M.; List, B. A Powerful Brønsted Acid Catalyst for the Organocatalytic Asymmetric Transfer

Hydrogenation of Imines. *Angew. Chemie Int. Ed.* **2005**, *44* (45), 7424–7427.

<https://doi.org/10.1002/anie.200503062>.

- (44) Rueping, M.; Antonchick, A. P.; Theissmann, T. A Highly Enantioselective Brønsted Acid Catalyzed Cascade Reaction: Organocatalytic Transfer Hydrogenation of Quinolines and Their Application in the Synthesis of Alkaloids. *Angew. Chemie Int. Ed.* **2006**, *45* (22), 3683–3686. <https://doi.org/10.1002/anie.200600191>.
- (45) Li, G.; Liang, Y.; Antilla, J. C. A Vaulted Biaryl Phosphoric Acid-Catalyzed Reduction of α -Imino Esters: The Highly Enantioselective Preparation of α -Amino Esters. *J. Am. Chem. Soc.* **2007**, *129* (18), 5830–5831. <https://doi.org/10.1021/ja070519w>.
- (46) Li, G.; Antilla, J. C. Highly Enantioselective Hydrogenation of Enamides Catalyzed by Chiral Phosphoric Acids. *Org. Lett.* **2009**, *11* (5), 1075–1078. <https://doi.org/10.1021/ol802860u>.
- (47) Nguyen, T. B.; Bousserouel, H.; Wang, Q.; Guéritte, F. Phosphoric Acid-Catalyzed Enantioselective Transfer Hydrogenation of N-Aryl-Ortho-Hydroxybenzophenone Ketimines. *Adv. Synth. Catal.* **2011**, *353* (2–3), 257–262. <https://doi.org/10.1002/adsc.201000754>.
- (48) Chen, M.-W.; Chen, Q.-A.; Duan, Y.; Ye, Z.-S.; Zhou, Y.-G. Asymmetric Hydrogenolysis of Racemic Tertiary Alcohols, 3-Substituted 3-Hydroxyisoindolin-1-Ones. *Chem. Commun.* **2012**, *48* (11), 1698–1700. <https://doi.org/10.1039/C2CC16832D>.
- (49) Storer, R. I.; Carrera, D. E.; Ni, Y.; MacMillan, D. W. C. Enantioselective Organocatalytic Reductive Amination. *J. Am. Chem. Soc.* **2006**, *128* (1), 84–86. <https://doi.org/10.1021/ja057222n>.
- (50) Qian, D.; Sun, J. Recent Progress in Asymmetric Ion-Pairing Catalysis with Ammonium Salts. *Chem. – A Eur. J.* **2019**, *25* (15), 3740–3751. <https://doi.org/10.1002/chem.201803752>.
- (51) Mayer, S.; List, B. Asymmetric Counteranion-Directed Catalysis. *Angew. Chemie Int. Ed.* **2006**, *45* (25), 4193–4195. <https://doi.org/10.1002/anie.200600512>.
- (52) Martin, N. J. A.; List, B. Highly Enantioselective Transfer Hydrogenation of α,β -Unsaturated Ketones. *J. Am. Chem. Soc.* **2006**, *128* (41), 13368–13369. <https://doi.org/10.1021/ja065708d>.
- (53) Zhu, C.; Akiyama, T. Benzothiazoline: Highly Efficient Reducing Agent for the Enantioselective Organocatalytic Transfer Hydrogenation of Ketimines. *Org. Lett.* **2009**, *11* (18), 4180–4183. <https://doi.org/10.1021/ol901762g>.
- (54) Stephan, D. W. Activation of Dihydrogen by Non-Metal Systems. *Chem. Commun.* **2010**, *46* (45), 8526. <https://doi.org/10.1039/c0cc03313h>.
- (55) Welch, G. C.; Juan, R. R. S.; Masuda, J. D.; Stephan, D. W. Reversible, Metal-Free Hydrogen Activation. *Science* (80-). **2006**, *314* (5802), 1124–1126. <https://doi.org/10.1126/science.1134230>.
- (56) Stephan, D. W.; Erker, G. Frustrated Lewis Pairs: Metal-Free Hydrogen Activation and More. *Angew. Chemie Int. Ed.* **2010**, *49* (1), 46–76. <https://doi.org/10.1002/anie.200903708>.
- (57) Chen, D.; Wang, Y.; Klankermayer, J. Enantioselective Hydrogenation with Chiral Frustrated Lewis Pairs. *Angew. Chemie Int. Ed.* **2010**, *49* (49), 9475–9478. <https://doi.org/10.1002/anie.201004525>.
- (58) Zhou, Q.; Meng, W.; Yang, J.; Du, H. A Continuously Regenerable Chiral Ammonia Borane for Asymmetric Transfer

Hydrogenations. *Angew. Chemie - Int. Ed.* **2018**, *57* (37), 12111–12115. <https://doi.org/10.1002/anie.201806877>.

- (59) Trost, B. M.; Dietsch, T. J. New Synthetic Reactions. Asymmetric Induction in Allylic Alkylations. *J. Am. Chem. Soc.* **1973**, *95* (24), 8200–8201. <https://doi.org/10.1021/ja00805a056>.
- (60) Trost, B. M.; Strege, P. E. Asymmetric Induction in Catalytic Allylic Alkylation. *J. Am. Chem. Soc.* **1977**, *99* (5), 1649–1651. <https://doi.org/10.1021/ja00447a064>.
- (61) Trost, B. M.; Van Vranken, D. L. Asymmetric Transition Metal-Catalyzed Allylic Alkylations. *Chem. Rev.* **1996**, *96* (1), 395–422. <https://doi.org/10.1021/cr9409804>.
- (62) Lu, Z.; Ma, S. Metal-Catalyzed Enantioselective Allylation in Asymmetric Synthesis. *Angew. Chemie Int. Ed.* **2008**, *47* (2), 258–297. <https://doi.org/10.1002/anie.200605113>.
- (63) Watson, I. D. G.; Styler, S. A.; Yudin, A. K. Unusual Selectivity of Unprotected Aziridines in Palladium-Catalyzed Allylic Amination Enables Facile Preparation of Branched Aziridines. *J. Am. Chem. Soc.* **2004**, *126* (16), 5086–5087. <https://doi.org/10.1021/ja049242f>.
- (64) Tsuji, J. New Synthetic Reactions Catalyzed by Palladium Complexes. *Pure Appl. Chem.* **1986**, *58* (6), 869–878. <https://doi.org/10.1351/pac198658060869>.
- (65) Trost, B. M.; Machacek, M. R.; Aponick, A. Predicting the Stereochemistry of Diphenylphosphino Benzoic Acid (DPPBA)-Based Palladium-Catalyzed Asymmetric Allylic Alkylation Reactions: A Working Model. *Acc. Chem. Res.* **2006**, *39* (10), 747–760. <https://doi.org/10.1021/ar040063c>.
- (66) Trost, B. M.; Toste, F. D. Regio- and Enantioselective Allylic Alkylation of an Unsymmetrical Substrate: A Working Model. *J. Am. Chem. Soc.* **1999**, *121* (19), 4545–4554. <https://doi.org/10.1021/ja9828713>.
- (67) Keinan, E.; Sahai, M. Regioselectivity in Organo-Transition-Metal Chemistry. A Remarkable Steric Effect in π -Allyl Palladium Chemistry. *J. Chem. Soc., Chem. Commun.* **1984**, No. 10, 648–650. <https://doi.org/10.1039/C39840000648>.
- (68) Tsuji, J.; Ueno, H.; Kobayashi, Y.; Okumoto, H. Palladium-Catalyzed Regioselective Reactions of α -Acetoxy- β,γ -Unsaturated Nitriles and γ -Acetoxy- α,β -Unsaturated Ester with Nucleophiles. *Tetrahedron Lett.* **1981**, *22* (27), 2573–2574. [https://doi.org/10.1016/S0040-4039\(01\)90523-4](https://doi.org/10.1016/S0040-4039(01)90523-4).
- (69) Vicart, N.; Cazes, B.; Goré, J. Reactivity of 1-Alkoxy π -Allylpalladium Complexes. *Tetrahedron Lett.* **1995**, *36* (4), 535–538. [https://doi.org/10.1016/0040-4039\(94\)02334-8](https://doi.org/10.1016/0040-4039(94)02334-8).
- (70) Trost, B. M.; Crawley, M. L. A “Chiral Aldehyde” Equivalent as a Building Block Towards Biologically Active Targets. *Chem. - A Eur. J.* **2004**, *10* (9), 2237–2252. <https://doi.org/10.1002/chem.200305634>.
- (71) Trost, B. M.; Dudash, Jr., J.; Dirat, O. Application of the AAA Reaction to the Synthesis of the Furanoside OfC-2-Epi-Hygrocin A: A Total Synthesis OfC-2-Epi-Hygrocin A. *Chem. - A Eur. J.* **2002**, *8* (1), 259–268. [https://doi.org/10.1002/1521-3765\(20020104\)8:1<259::AID-CHEM259>3.0.CO;2-D](https://doi.org/10.1002/1521-3765(20020104)8:1<259::AID-CHEM259>3.0.CO;2-D).
- (72) Trost, B. M.; Lee, C. B. Geminal Dicarboxylates as Carbonyl Surrogates for Asymmetric Synthesis. Part II. Scope and Applications. *J. Am. Chem. Soc.* **2001**, *123* (16), 3687–3696. <https://doi.org/10.1021/ja003775g>.
- (73) Trost, B. M.; Schroeder, G. M. Palladium-Catalyzed Asymmetric Alkylation of Ketone Enolates. *J. Am. Chem. Soc.*

1999, 121 (28), 6759–6760. <https://doi.org/10.1021/ja991135b>.

- (74) Gamez, P.; Dunjic, B.; Fache, F.; Lemaire, M. C 2 Diamine, Pseudo-C 2 Poly(Amide) and Poly(Urea) as Chiral Inductors in Asymmetric Catalysis. *J. Chem. Soc. Chem. Commun.* **1994**, No. 12, 1417. <https://doi.org/10.1039/c39940001417>.
- (75) Yamazaki, A.; Morimoto, T.; Achiwa, K. Synthesis and Application of Chiral Bisphosphine Ligands Containing a Hetero-Functional Group. *Tetrahedron: Asymmetry* **1993**, 4 (11), 2287–2290. [https://doi.org/10.1016/S0957-4166\(00\)80084-1](https://doi.org/10.1016/S0957-4166(00)80084-1).
- (76) Leitner, A.; Shu, C.; Hartwig, J. F. Effects of Catalyst Activation and Ligand Steric Properties on the Enantioselective Allylation of Amines and Phenoxides. *Org. Lett.* **2005**, 7 (6), 1093–1096. <https://doi.org/10.1021/ol050029d>.
- (77) Graening, T.; Hartwig, J. F. Iridium-Catalyzed Regio- and Enantioselective Allylation of Ketone Enolates. *J. Am. Chem. Soc.* **2005**, 127 (49), 17192–17193. <https://doi.org/10.1021/ja0566275>.
- (78) Desimoni, G.; Faita, G.; Jørgensen, K. A. C 2 -Symmetric Chiral Bis(Oxazoline) Ligands in Asymmetric Catalysis. *Chem. Rev.* **2006**, 106 (9), 3561–3651. <https://doi.org/10.1021/cr0505324>.
- (79) Carroll, M. P.; Guiry, P. J. P,N Ligands in Asymmetric Catalysis. *Chem. Soc. Rev.* **2014**, 43 (3), 819–833. <https://doi.org/10.1039/C3CS60302D>.
- (80) Trost, B. M.; Van Vranken, D. L. Asymmetric Ligands for Transition-Metal-Catalyzed Reactions: 2-Diphenylphosphinobenzoyl Derivatives of C2-Symmetric Diols and Diamines. *Angew. Chemie Int. Ed. English* **1992**, 31 (2), 228–230. <https://doi.org/10.1002/anie.199202281>.
- (81) Lloyd-Jones, G. C.; Stephen, S. C.; Fairlamb, I. J. S.; Martorell, A.; Dominguez, B.; Tomlin, P. M.; Murray, M.; Fernandez, J. M.; Jeffery, J. C.; Riis-Johannessen, T.; Guereziz, T. Coordination of the Trost Modular Ligand to Palladium Allyl Fragments: Oligomers, Monomers and Memory Effects in Catalysis. *Pure Appl. Chem.* **2004**, 76 (3), 589–601. <https://doi.org/10.1351/pac200476030589>.
- (82) Kinoshita, H.; Shinokubo, H.; Oshima, K. Water Enables Direct Use of Allyl Alcohol for Tsuji–Trost Reaction without Activators. *Org. Lett.* **2004**, 6 (22), 4085–4088. <https://doi.org/10.1021/ol048207a>.
- (83) Yokoyama, Y.; Hikawa, H.; Mitsuhashi, M.; Uyama, A.; Hiroki, Y.; Murakami, Y. Total Synthesis without Protection: Three-Step Synthesis of Optically Active Clavicipitic Acids by a Biomimetic Route. *European J. Org. Chem.* **2004**, 2004 (6), 1244–1253. <https://doi.org/10.1002/ejoc.200300603>.
- (84) Manabe, K.; Kobayashi, S. Palladium-Catalyzed, Carboxylic Acid-Assisted Allylic Substitution of Carbon Nucleophiles with Allyl Alcohols as Allylating Agents in Water. *Org. Lett.* **2003**, 5 (18), 3241–3244. <https://doi.org/10.1021/ol035126q>.
- (85) Zhou, H.; Yang, H.; Liu, M.; Xia, C.; Jiang, G. Brønsted Acid Accelerated Pd-Catalyzed Direct Asymmetric Allylic Alkylation of Azlactones with Simple Allylic Alcohols: A Practical Access to Quaternary Allylic Amino Acid Derivatives. *Org. Lett.* **2014**, 16 (20), 5350–5353. <https://doi.org/10.1021/ol502535z>.
- (86) Tao, Z.-L.; Zhang, W.-Q.; Chen, D.-F.; Adele, A.; Gong, L.-Z. Pd-Catalyzed Asymmetric Allylic Alkylation of Pyrazol-5-Ones with Allylic Alcohols: The Role of the Chiral Phosphoric Acid in C–O Bond Cleavage and Stereocontrol. *J. Am. Chem. Soc.* **2013**, 135 (25), 9255–9258. <https://doi.org/10.1021/ja402740q>.

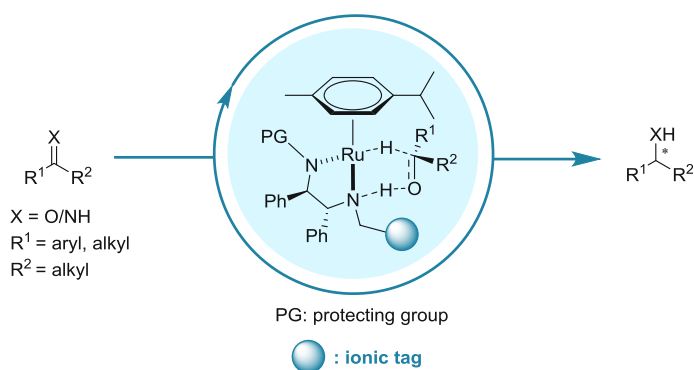
- (87) Tamaru, Y.; Horino, Y.; Araki, M.; Tanaka, S.; Kimura, M. Et₃B-Promoted, Pd(0)-Catalyzed Allylation of Active Methylene Compounds with Allylic Alcohols. *Tetrahedron Lett.* **2000**, *41* (30), 5705–5709. [https://doi.org/10.1016/S0040-4039\(00\)00934-5](https://doi.org/10.1016/S0040-4039(00)00934-5).
- (88) Kimura, M.; Mukai, R.; Tanigawa, N.; Tanaka, S.; Tamaru, Y. Triethylborane as an Efficient Promoter for Palladium-Catalyzed Allylation of Active Methylene Compounds with Allyl Alcohols. *Tetrahedron* **2003**, *59* (39), 7767–7777. [https://doi.org/10.1016/S0040-4020\(03\)01234-1](https://doi.org/10.1016/S0040-4020(03)01234-1).
- (89) Itoh, K.; Hamaguchi, N.; Miura, M.; Nomura, M. Palladium-Catalysed Reaction of Aryl-Substituted Allylic Alcohols with Zinc Enolates of β -Dicarbonyl Compounds in the Presence of Titanium(IV) Isopropoxide. *J. Chem. Soc., Perkin Trans. 1* **1992**, No. 21, 2833–2835. <https://doi.org/10.1039/P19920002833>.
- (90) Yang, S.-C.; Chung, W.-H. Palladium-Catalyzed N-Allylation of Anilines by Direct Use of Allyl Alcohols in the Presence of Titanium(IV) Isopropoxide. *Tetrahedron Lett.* **1999**, *40* (5), 953–956. [https://doi.org/10.1016/S0040-4039\(98\)02456-3](https://doi.org/10.1016/S0040-4039(98)02456-3).
- (91) Ibrahem, I.; Córdova, A. Direct Catalytic Intermolecular α -Allylic Alkylation of Aldehydes by Combination of Transition-Metal and Organocatalysis. *Angew. Chemie Int. Ed.* **2006**, *45* (12), 1952–1956. <https://doi.org/10.1002/anie.200504021>.
- (92) Vulovic, B.; Bihelovic, F.; Matovic, R.; Saicic, R. N. Organocatalyzed Tsuji–Trost Reaction: A New Method for the Closure of Five- and Six-Membered Rings. *Tetrahedron* **2009**, *65* (50), 10485–10494. <https://doi.org/10.1016/j.tet.2009.10.006>.
- (93) Vulovic, B.; Gruden-Pavlovic, M.; Matovic, R.; Saicic, R. N. Substrate Stereocontrol in the Intramolecular Organocatalyzed Tsuji–Trost Reaction: Enantioselective Synthesis of Allokainates. *Org. Lett.* **2014**, *16* (1), 34–37. <https://doi.org/10.1021/ol4028557>.
- (94) Usui, I.; Schmidt, S.; Breit, B. Dual Palladium- and Proline-Catalyzed Allylic Alkylation of Enolizable Ketones and Aldehydes with Allylic Alcohols. *Org. Lett.* **2009**, *11* (6), 1453–1456. <https://doi.org/10.1021/ol9001812>.
- (95) Huo, X.; Yang, G.; Liu, D.; Liu, Y.; Gridnev, I. D.; Zhang, W. Palladium-Catalyzed Allylic Alkylation of Simple Ketones with Allylic Alcohols and Its Mechanistic Study. *Angew. Chemie Int. Ed.* **2014**, *53* (26), 6776–6780. <https://doi.org/10.1002/anie.201403410>.
- (96) Jiang, G.; List, B. Direct Asymmetric α -Allylation of Aldehydes with Simple Allylic Alcohols Enabled by the Concerted Action of Three Different Catalysts. *Angew. Chemie Int. Ed.* **2011**, *50* (40), 9471–9474. <https://doi.org/10.1002/anie.201103263>.
- (97) Shibasaki, M.; Kumagai, N.; Yasuda, S. Direct Asymmetric α -Allylation of Ketones with Allylic Alcohols via Pd/Enamine Cooperative Function. *Heterocycles* **2012**, *86* (1), 745. [https://doi.org/10.3987/COM-12-S\(N\)34](https://doi.org/10.3987/COM-12-S(N)34).

2. Transition metal-catalyzed asymmetric transfer hydrogenations in alternative reaction media

The asymmetric reduction of prochiral ketones and imines represents a well-established method for the synthesis of optically active secondary alcohols and amines. Thanks to its operational simplicity and safety, the concept of asymmetric transfer hydrogenation (ATH) represents an attractive tool in this field.¹⁶ Since the pioneering work of R. Noyori in 1995, ruthenium-complexes featuring 1,2-diamine or β -amino alcohol ligands are particularly often used for such transformations.¹⁵ While numerous elegant methods were reported for highly active and enantioselective ATH reactions; because of the poor water-solubility of the ligands, the use of an organic solvent as reaction media was frequently required. Apart from being a cheap, abundant and environmentally friendly solvent, water as reaction medium can also result in a dramatic increase in reactivity and enantioselectivity for ATH reactions.^{28,29} Furthermore; as a practical aspect, it can “immobilize” the complex in the aqueous layer, facilitating the product separation and the catalyst reuse. However; in order to make the transition metal complex water-soluble and thus suitable for aqueous ATH, an alternative ligand design featuring very polar and/or ionic groups is required.

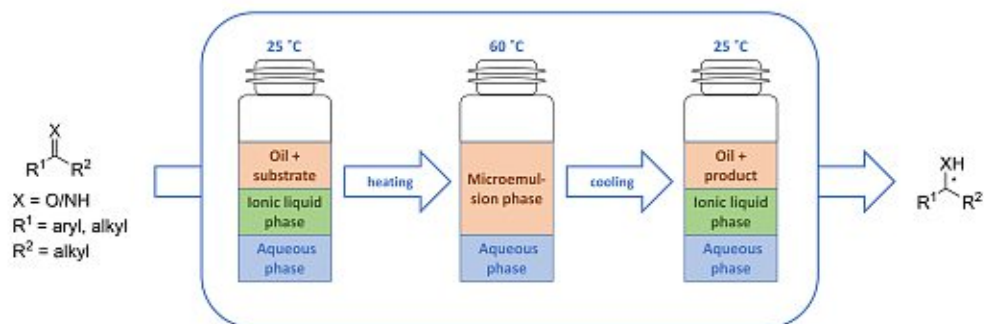
In this particular chapter, the use of ion-tagged chiral ligands for ruthenium-catalyzed asymmetric transfer hydrogenations (ATH) in aqueous media and in thermomorphic microemulsions will be presented, respectively.

- 1.) The main objective of the first sub-project was the design and the synthesis of a small set of DPEN-based chiral ionic ligands by tuning its steric and electronic properties. Eventually, their application for the ATH of ketones and imines in aqueous media should be investigated (Scheme 39).



Scheme 39. Ion-tagged chiral ligands for aqueous ATH reactions.

- 2.) The goal of the second sub-project was the use of hydrophilic, sulphonated DPEN-ligands for the ATH of ketones and imines in thermomorphic ionic liquid-based microemulsions, which could potentially offer another alternative for catalyst immobilization (Scheme 40).



Scheme 40. Ionic liquid-based microemulsions for ATH reactions.

The following manuscripts will be presented in this chapter:

- 1.) Pálvölgyi, Á. M.; Bitai, J.; Zeindlhofer, V.; Schröder, C.; Bica, K. Ion-Tagged Chiral Ligands for Asymmetric Transfer Hydrogenations in Aqueous Medium. *ACS Sustain. Chem. Eng.* **2019**, *7* (3), 3414–3423.

As a first author, I planned and performed a major part in the experimental work and I also had major contribution to writing the manuscript.

- 2.) Hejazifar, M.; Pálvölgyi, Á. M.; Bitai, J.; Lanaridi, O.; Bica-Schröder, K. Asymmetric Transfer Hydrogenation in Thermomorphic Microemulsions Based on Ionic Liquids. *Org. Process Res. Dev.* **2019**, *23* (9), 1841–1851.

As a co-author, I contributed in the final stage of the experimental work and in the manuscript preparation.

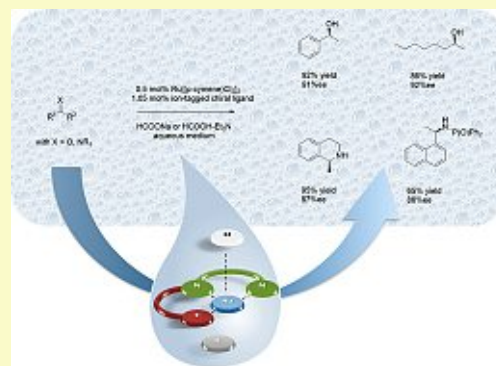
Ion-Tagged Chiral Ligands for Asymmetric Transfer Hydrogenations in Aqueous Medium

Ádám Márk Pálvölgyi,[†] Jacqueline Bitai,[†] Veronika Zeindlhofer,[‡] Christian Schröder,[‡] and Katharina Bica^{*,†}[†]Institute of Applied Synthetic Chemistry, Vienna University of Technology, Getreidemarkt 9/163, A-1060 Vienna, Austria[‡]Department of Computational Biological Chemistry, University of Vienna, Währinger Str. 17, 1090 Vienna, Austria

Supporting Information

ABSTRACT: We report the design and synthesis of novel ion-tagged chiral ligands for asymmetric transfer hydrogenation (ATH) in aqueous medium. Based on (*R,R*)-1,2-diphenylethylene diamine (DPEN) as structural motif, a straightforward three-step protocol was developed that gave access to novel chiral ligands with carbamate-substructure and pyridinium headgroup. The careful optimization of steric and electronic properties in combination with the adaption of solubility via choice of the anion gave a set of chiral and water-soluble ligands for use in ruthenium-catalyzed asymmetric transfer hydrogenations in aqueous medium. Eventually, a pool of aliphatic and aromatic ketones as well as two imine substrates were reduced with excellent isolated yields up to 95% and enantioselectivities >90% ee under environmentally benign conditions in the absence of additional surfactants.

KEYWORDS: Chiral ligands, Transfer hydrogenation, Asymmetric synthesis, Water, Ruthenium



INTRODUCTION

Optically active secondary alcohols and amines are important building blocks and key intermediates for the production of numerous active compounds for the agricultural and pharmaceutical industries.¹ The catalytic asymmetric reduction of prochiral ketones and imines is a versatile and well-established tool for their preparation, and a variety of catalytic systems have been investigated to balance conversion, selectivity and atom efficiency of the reaction.²

In light of the growing awareness for safe and sustainable strategies, the concept of transfer hydrogenation has received tremendous attention.^{3–5} Because of the use of small and nonhazardous organic molecules as hydrogen donor and the operational simplicity, asymmetric transfer hydrogenations have emerged as a particularly powerful methodology and as an alternative to conventional hydrogenations relying on hydrogen gas. Apart from well-established hydrogen sources such as isopropyl alcohol and formic acid-Et₃N mixtures, sodium formate has become a popular hydrogen donor as it is cheap, nontoxic and easy to handle. Moreover, the evolution of CO₂ as byproduct formed from sodium formate or formic acid-Et₃N mixtures renders the reaction irreversible. As an additional bonus, sodium formate as water-soluble hydrogen source opens the possibility to perform the reaction in aqueous medium.⁶

The use of water instead of conventional organic solvents as reaction medium is certainly advantageous in terms of a greener and more sustainable methodology, as it can be considered safe, economical, nontoxic and benign compared to typical organic solvents.^{7–11} It has been already shown that the ATH reaction of

ketones in water proceeds with significantly increased reaction rates compared with the conventional isopropanol-based systems.¹² This might be attributed to the high inherent hydrogen bonding ability of water, which stabilizes the transition state and facilitates the hydride delivery compared to other solvents. Additionally, water may also lower the activation energy of the decarboxylation step, thereby increasing the reaction rates in the catalytic cycle.¹² However, it also causes several challenges, as many transition metal catalysts including the state-of-the-art Ru(II) catalysts for asymmetric transfer hydrogenation relying on the 1,2-diphenylethylene diamine (DPEN) or *N*-(*p*-toluenesulfonyl)-1,2-diphenylethylene diamine (TsDPEN) motif have very low solubility in water.¹³ Hence, synthetic efforts in recent years have been aiming at modifying well-established ligands and catalysts toward water-soluble analogues to improve catalyst solubility and facilitate product separation. One common approach to overcome the limited water solubility of many ligands relies on the introduction of hydrophilic groups such as polyethylene glycol chains, although considerable synthetic effort is often required to obtain these modified ligands.^{14,15} Alternatively, sulfonation of typical arene ligands is employed to form water-soluble sodium sulfonate salts, a strategy which has been applied in several industrially relevant processes such as the Rhône-Poulenc Ruhrchemie process for hydroformylation in aqueous

Received: October 30, 2018

Revised: December 13, 2018

Published: January 7, 2019

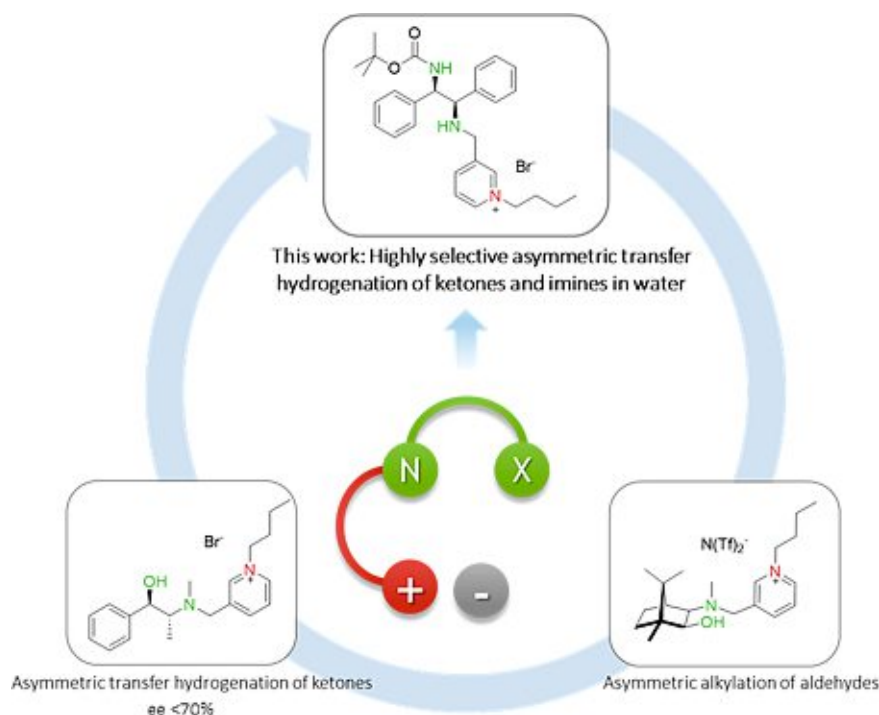
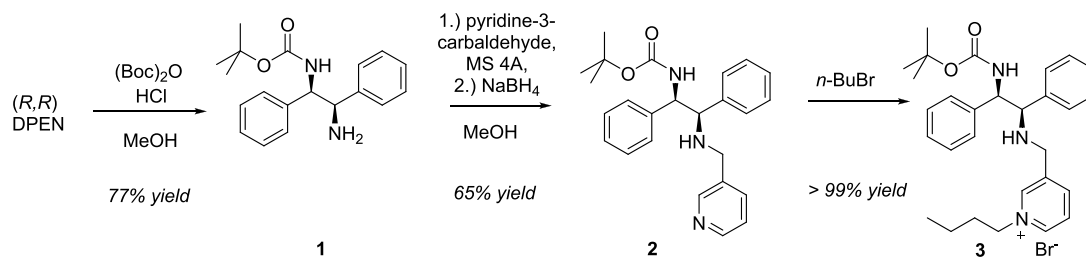


Figure 1. Lead structure of coordinating chiral ionic liquids as key motif for ion-tagged carbamate ligands and their use in asymmetric transfer hydrogenations in water.

Scheme 1. Route for the Synthesis of Ion-Tagged Chiral Carbamate Ligands on the Example of Pyridinium Bromide 3



biphasic medium.^{16,17} This strategy was also used to improve water solubility of TsDPEN-based ligands, although harsh reagents were required for sulfonation resulting in mixtures of *ortho*, *meta* or *para*-sulfonated ligands that must be separated in tedious chromatographic procedures before use.¹⁸

The implementation of cationic groups inspired by ionic liquids based on ammonium, imidazolium or pyridinium cations has the advantage of facile ligand modification. The variation of alkyl chain length or counterion allows to fine-tune properties to the given reaction conditions while simultaneously solubilizing the ligand in polar reaction media such as water or ionic liquids.^{19–21} Several studies reported increased water solubility of the TsDPEN structural motif after functionalization with cationic groups, including modification with heterocyclic or trialkylammonium cations.^{22,23} This approach, featuring cationic surfactant-type catalysts, becomes especially attractive concerning the enantioselective transfer hydrogenation of aliphatic ketones, which has been challenging, with only few successful examples in the literature.²⁴ Inspired by these works and based on the results previously obtained with amino alcohol based chiral ionic ligand structures in our group, we herein report the extension of this modular ligand design to diamine based scaffolds (Figure 1).²⁵

Because of their coordinating nature, chiral ionic liquids with *N,O* substructure as shown in Figure 1 (bottom) were successfully applied in the asymmetric alkylation of aldehydes in biphasic conditions.²⁶ Moreover, as a result of their tunable structure and adaptable solubility, the hydrophilic bromide was applied in Ruthenium-catalyzed asymmetric transfer hydrogenations of aromatic ketones under aqueous conditions.^{25,26} However, the observed enantioselectivities were limited to <70% ee, indicating that the amino alcohol backbone is inefficient and that further optimization is required for a truly enantioselective transfer hydrogenation with a broader substrate scope.

Herein, we expand our concept toward the design of chiral ion-tagged ligands with carbamate substructure and variable alkyl chain length. Through the careful optimization of electronic and steric properties of the cationic core structure in combination with tunable solubility resulting from the choice of a suitable counterion, these novel ligands could be successfully applied for highly asymmetric transfer hydrogenations of ketones and imines under aqueous conditions.

RESULTS AND DISCUSSION

In our previous work on the design of chiral ionic liquids, we developed a straightforward synthesis for coordinating chiral

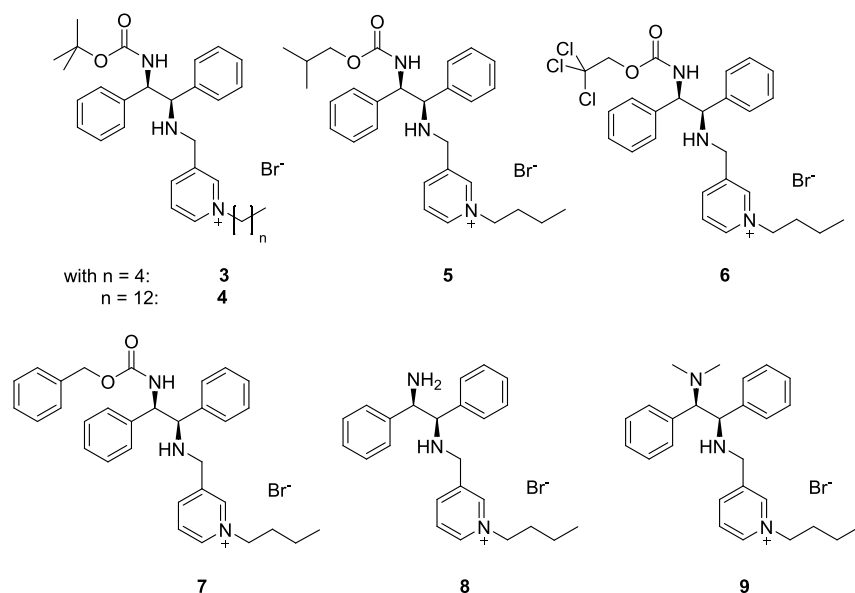


Figure 2. (*R,R*)-Diphenylethylenediamine-based ion-tagged chiral ligands 3–9 used in this study.

ionic liquids with *N,O* structural motif based on commercially available and chiral-pool derived amino alcohols (Figure 1). A key step in the synthesis is the formation and selective alkylation of a *N,N,O*-tridentate ligand, resulting in the formation of chiral ionic liquids with pyridinium headgroup and amino alcohol core structure.²⁷ This protocol was adapted toward the design of ion-tagged carbamate ligands with (*R,R*)-diphenylethylenediamine (*R,R*-DPEN), a common structural element in many ATH ligands, as core structure (Scheme 1).

After monoprotection of (*R,R*)-diphenylethylenediamine with (Boc)₂O, the intermediate carbamate was reacted with pyridine-2-carbaldehyde in the presence of activated molecular sieve, and it was subsequently reduced with sodium borohydride to obtain tridentate ligand 2. As already established in previous papers, careful alkylation with 4-bromobutane at 50 °C resulted in the selective alkylation of the pyridine headgroup and provided the desired hydrophilic ion-tagged chiral ligand 3 in three steps with good overall yield (Scheme 1).

In the case of the *tert*-butyloxycarbonyl (Boc)-substituted ligand 3, the *n*-butyl chain was optionally replaced with a *n*-dodecyl group (4), as previous studies have shown considerable impact of amphiphilic structures on asymmetric transfer hydrogenations in water. For a further exploitation of the substitution patterns, the carbamate group was varied to include different substituents that are routinely used as amine protecting groups, including *iso*-butyloxycarbonyl-, 2,2,2-trichloroethoxycarbonyl (Troc)- or benzyloxycarbonyl (Cbz)-substituted ligands (5–7). For reasons of comparison, the corresponding diamine-based ligands 8–9 with a primary or tertiary amine substituent instead of the carbamate group were also synthesized. Eventually, a small set of water-soluble chiral ligands 3–9 was obtained for the further evaluation in asymmetric transfer hydrogenation (Figure 2).

In order to characterize the influence of the ion tag on the *N,N*-backbone for compounds 1–3 DFT computational studies in Gaussian 09 on the B3LYP/6-311++G(2d,2p) level of theory including solvation in water via a polarizable continuum model (PCM) were performed.^{28–30} The obtained minimum structures in Figure 3 show a significant distance of the pyridine moiety to the chiral backbone. Hence little interference of the

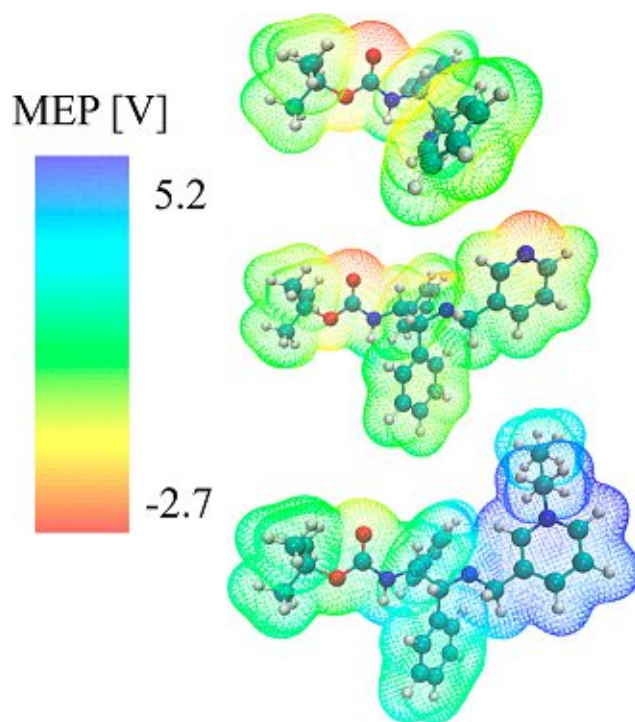


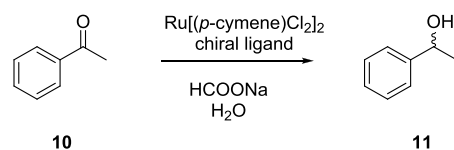
Figure 3. Molecular electrostatic potential of Boc-modified chiral carbamate ligand without pyridinium moiety (1, top), with pyridine moiety (2, middle) and ion-tagged ligand after alkylation (3, bottom) mapped to the electron density surface at 0.003 e/Å³.

ion tag with the coordination of the *N,N*-substructure in the carbamate ligand and no strong intramolecular interaction between these groups is expected. The molecular electrostatic potential (MEP) of ion-tagged ligand 3 reveals that the positive charge remains located on the pyridinium ring (blue area in Figure 3). The negative MEP of the Boc group is increased slightly in the full ligand compared to the neutral form. However, partial charges of the respective oxygens of the Boc group change only marginally from -0.679 e to -0.663 e using the Merz–Singh–Kollman scheme and even less using the CHELPG

scheme for charge assignment, indicating only a small influence of the cationic moiety on the electronic properties of the chiral *N,N*-backbone.^{31,32} However, additional computations considering the full complex are required to verify our findings and will be the topic of future studies.

With this set of novel chiral ligands in hand, we initially investigated the asymmetric transfer hydrogenation of acetophenone (**10**) as benchmark reaction in water with sodium formate as hydrogen donor (Scheme 2).

Scheme 2. Asymmetric Transfer Hydrogenation of Acetophenone in Water



Reactions were initially studied for 24 h at 25 °C using [Ru(*p*-cymene)Cl₂]₂ as precatalyst. Due to the ionic nature of the ligands **3–9**, the preformed chiral Ru-complex was readily soluble in water. Considerable differences were observed in the reactivity, emphasizing the importance of careful substituent choice for obtaining a highly active and selective catalyst (Table 1).

Table 1. Ligand Screening in the Asymmetric Transfer Hydrogenation of Acetophenone in Water

| entry ^a | chiral ligand | time [h] | temperature [°C] | conversion ^{b,c} [%] | ee ^{d,e} [%] |
|--------------------|---------------|----------|------------------|-------------------------------|-----------------------|
| 1 | 3 | 24 | 25 | >99 (92) | 91 (<i>R</i>) |
| 2 | 4 | 24 | 25 | 63 (58) | 91 (<i>R</i>) |
| 3 | 5 | 24 | 25 | 92 (90) | 80 (<i>R</i>) |
| 4 | 6 | 24 | 25 | 74 (70) | 71 (<i>R</i>) |
| 5 | 7 | 24 | 25 | 78 (76) | 67 (<i>R</i>) |
| 6 | 8 | 24 | 25 | 20 | 46 (<i>R</i>) |
| 7 | 8 | 48 | 25 | 30 | 31 (<i>R</i>) |
| 8 | 9 | 24 | 25 | 19 | 8 (<i>S</i>) |
| 9 | 9 | 48 | 25 | 21 | <5 (<i>S</i>) |

^aPerformed with 2 mmol acetophenone using 0.021 mmol (1.05 mol %) chiral ligand, 0.01 mmol (0.5 mol %) Ru[(*p*-cymene)Cl₂]₂ and 10 mmol HCOONa in 4 mL H₂O at 25 °C. ^bDetermined by ¹H NMR of the crude product. ^cIsolated yields in parentheses. ^dDetermined by chiral HPLC using a DAICEL Chiralcel IB column. ^eAbsolute configuration determined by comparison of the optical rotation with literature data.

As immediately visible from the screening of ligands, the presence of an electron-withdrawing, bulky substituent as the Boc group on the diamine ligand is mandatory for the application in asymmetric transfer hydrogenation of aromatic ketones (Table 1). Even for a reaction time of 48 h, conversions and enantioselectivities remained low for ligands without carbamate substituent (Table 1, entries 6–9). This is particularly pronounced in case of the dimethylated diamine derivative **9** (Table 1, entries 8–9), which lacks the ability for attractive N–H⋯O hydrogen bonding to coordinate and activate the substrate for subsequent hydrogen transfer from the metal center to the carbonyl C atom. Without this precoordination, the otherwise enantiodiscriminating C–H⋯π interaction between the arene ligand and the aromatic ring of the substrate is also rendered ineffective. Moreover, the dimethyl-

lation in ligand **9** compared to **8** seems to distort the catalyst geometry in a way that the opposite diastereomer becomes favored, resulting in the preferred formation of the (*S*)-enantiomer. This inversion of enantioselectivity due to full alkylation has already been reported in the literature by Dub and Gordon.³³

The superior performance of carbamate ligands **3–7** can be explained by a similar effect as reported in the literature for the TsDPEN ligand, whose improved performance compared to chiral amino alcohols stems from the interaction of oxygen lone pairs in the SO₂ group with the π cloud of the approaching aromatic ketone.^{3,4} A comparable situation may be present with carbamate ligands **3–7**, resulting in a higher energy difference between favored and disfavored diastereomeric transition states, and consequently, a higher enantiomeric excess. Among all carbamate ligands, the Boc derivatives **3** and **4** were the most suitable, since the highest selectivities of >90% ee were obtained (Table 1, entries 1 and 2). However, the amphiphilic character resulting from the dodecyl chain in ligand **4** is not beneficial, as a lower conversion for the aromatic ketone acetophenone was observed in this case. The superior performance of ligands **3** and **4** in terms of enantioselectivity might be explained by the considerable steric demand of the *t*-butyl group.

Further optimization of the reaction conditions with the carbamate-derived ligands **3** and **5–7** revealed that the catalytic system was able to retain its high selectivity and activity over a wide temperature range (Figure 4). While the conversion was typically increasing hardly any losses in enantioselectivity were observed, particularly for ligand Boc-modified ligand **3**. With this chiral ligand full conversion was observed within only 60 min at 60 °C while maintaining a high enantioselectivity of 89% ee. Encouraged by these results on enantioselectivity, we further investigated the effect of the temperature on the selectivity (Figure 4, right). Even at 80 °C an acceptable enantioselectivity of 85% was found; however, a drop occurred when increasing the temperature to 100 °C. This extraordinary thermal stability of asymmetric transfer hydrogenations in water is not unprecedented: A similar behavior was reported by Aupoix et al., whose work on *N*-heterocyclic carbene-derived ligands resulted in almost stable enantioselectivities up to 80 °C, although significantly lower conversion was obtained.³⁵

The impact and extraordinary performance of water as reaction medium should be highlighted with regard to the high activity and selectivity obtained with chiral ligand **3**. Comparative runs were done with different solvents and various hydrogen donors that are typically used for this reaction (Table 2). Apart from potential environmental benefits and advantages in reaction processing, water as in combination with sodium formate as hydrogen donor outshines all other conditions. Low conversion and moderate selectivity was observed with isopropanol as solvent, either in pure form, or with an azeotropic mixture of formic acid and Et₃N in a 5/2 molar ratio or sodium formate as additional hydrogen donor (Table 2, entries 1–3). While methanol was more suitable and gave quite similar results with both hydrogen donors, the addition of water improved both conversion and enantioselectivity (Table 2, entries 4–7). Eventually, the best result was obtained using pure water and sodium formate, which might be caused by the outstanding hydrogen bond network of water that can stabilize the transition state and lower the activation barrier for the rate limiting hydride transfer. At the same time, the rigid network may lock the substrate in its position, which results in the significantly improved selectivity obtained in water with chiral ligand **3**.

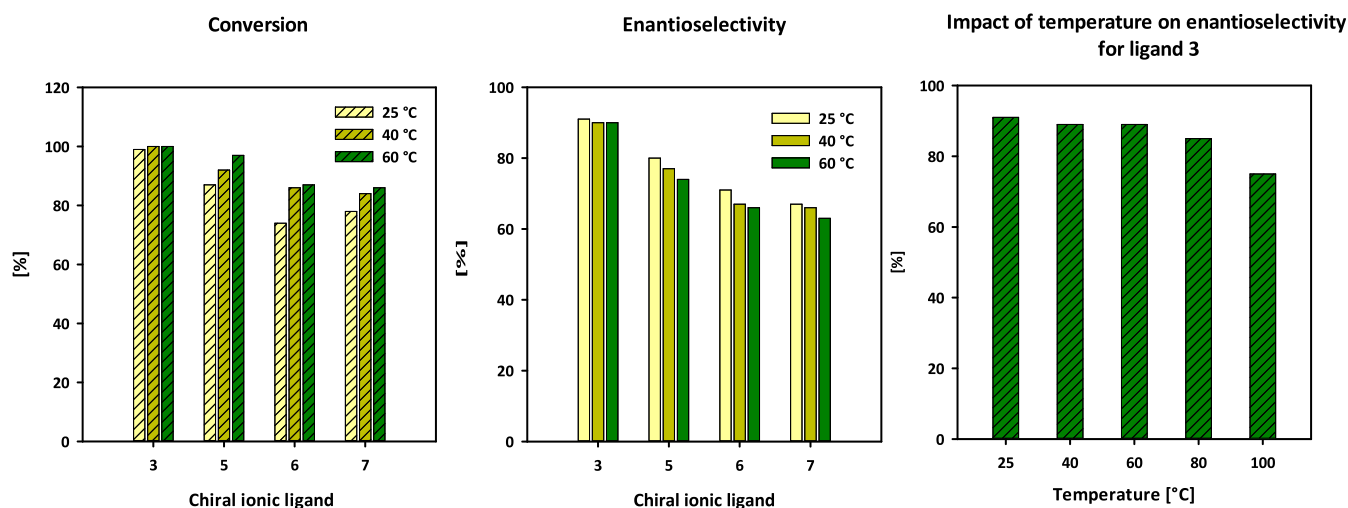


Figure 4. Impact of temperature on conversion (left) and enantioselectivity (middle) with carbamate-based ligands 3 and 5–7 as well as thermal stability with ligand 3 (right) in the asymmetric transfer hydrogenation of acetophenone.

Table 2. Screening of Solvents and Hydrogen Donors in the Asymmetric Transfer Hydrogenation of Acetophenone Using Chiral Ligand 3

| entry ^a | solvent | hydrogen donor | conversion ^b [%] | ee ^{c,d} [%] |
|--------------------|---------------------------|-------------------------------|-----------------------------|-----------------------|
| 1 ^e | isopropyl alcohol | – | 36 | 72 (R) |
| 2 | isopropyl alcohol | HCOOH-Et ₃ N (5/2) | 45 | 75 (R) |
| 3 ^f | isopropyl alcohol | HCOONa | 38 | 71 (R) |
| 4 | MeOH | HCOOH-Et ₃ N (5/2) | 80 | 80 (R) |
| 5 ^f | MeOH | HCOONa | 82 | 79 (R) |
| 6 | MeOH/H ₂ O 1/1 | HCOOH-Et ₃ N (5/2) | 92 | 83 (R) |
| 7 | MeOH/H ₂ O 1/1 | HCOONa | >99 | 89 (R) |
| 8 | H ₂ O | HCOOH-Et ₃ N (5/2) | >99 | 87 (R) |
| 9 | H ₂ O | HCOONa | >99 | 91 (R) |

^aPerformed with 2 mmol acetophenone using 0.021 mmol (1.05 mol %) chiral ligand 3, 0.01 mmol (0.5 mol %) Ru[(*p*-cymene)Cl₂]₂ and 10 mmol HCOONa or 1 mL HCOOH-Et₃N (molar ratio 5/2) in a total volume of 4 mL at 25 °C. ^bDetermined by ¹H NMR of the crude product. ^cDetermined by chiral HPLC using a DAICEL Chiralcel IB column. ^dAbsolute configuration determined by comparison of the optical rotation with literature data. ^ePerformed with 0.04 mmol KOH at 40 °C. ^f5% (v/v) H₂O was added to solubilize sodium formate.

With the optimized conditions in hand, the substrate scope was further investigated with a number of aromatic and aliphatic ketones employing chiral ligand 3 and 4. Because of the lack of C–H... π interactions between the active catalyst and the substrate, the asymmetric transfer hydrogenation of aliphatic ketones is challenging with just a few literature examples, which typically suffer from low yields and enantioselectivities.^{36,37} The suitability of chiral ligands 3 and 4 strongly depends on the substrates (Table 3). In the case of aromatic substrates comparable enantioselectivities were found with both ligands, while yields were significantly higher with *N*-butylpyridinium salt 3 compared to the *N*-dodecylpyridinium analogue 4. It seems that micellation, and ultimately incooperation of the aromatic substrate in the core of the aggregate reduces catalytic activity. However, a different behavior is observed in the case of aliphatic ketones (Table 3, entries 17–26). With increasing

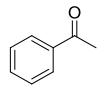
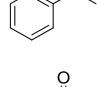
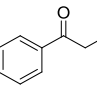
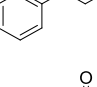
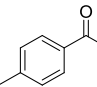
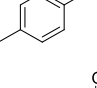
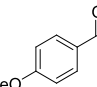
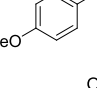
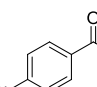
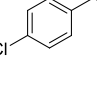
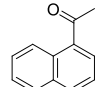
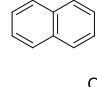
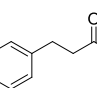
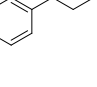
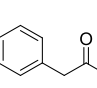
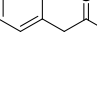
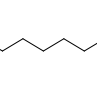
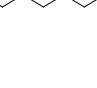
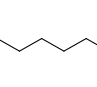
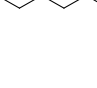
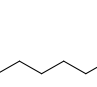
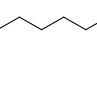
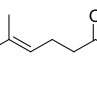
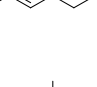
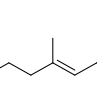
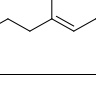
aliphatic character of the substrates, the importance of the amphiphilic character of ligand 4 becomes eminent as we have previously observed with long-chain chiral pyrrolidinium salts in asymmetric Aldol reactions.³⁸ This effect is particularly pronounced for 2-octanone (Table 3, entries 17 and 18), where the enantioselectivity could be drastically improved from 25% ee to 92% ee, together with an increase in yield from 69% to 86% when changing from chiral ligand 3 to 4. Overall, the results shown in Table 3 highlight the benefit of an increased alkyl chain length for the stereoselective reduction of aliphatic ketones, indicating that hydrophobic interactions between the alkyl chains of the ligand and the ketone play a dominant role in the absence of π -interactions between substrate and catalyst. A similar effect was reported by Deng et al., whose elegant work on chiral surfactant derived metallomicelles with TsDPEN core enabled excellent conversions and remarkable stereoselectivities for a number of aliphatic ketones and keto esters.^{24,39}

Eventually, we expanded the scope toward the considerably more challenging asymmetric transfer hydrogenation of imines. For this purpose, two representing substrates, 1-methyl-3,4-dihydroisoquinoline (12) and *N,N*-diphenylphosphinoketamine 13 were chosen (Figure 5).

While there are still open questions regarding the mechanism of imine reduction, literature data suggests an ionic mechanism rather than a concerted one for the asymmetric transfer hydrogenation after acidic activation.^{40–42} Moreover, Shende et al. reported a strong pH-dependency for the asymmetric transfer hydrogenation of imines in aqueous media.⁴³ Among all potential hydrogen sources, the azeotropic mixture of formic acid and Et₃N in a 5/2 molar ratio is most frequently used in the transfer hydrogenation of imine substrates, offering a wide substrate range and a irreversible reaction due to the formation of CO₂.⁴⁴

At first, the previously optimized reaction conditions were modified to accommodate the reduction of imines. While the reaction is extremely slow with HCOONa as only 3% conversion was observed after 24 h, a change to formic acid-Et₃N as hydrogen donor drastically improved the reactivity. Moreover, better results were observed in methanol/water mixtures as solvent, and results with formic acid-Et₃N in a 1.1/1 molar ratio were superior compared to the use of the azeotropic mixture (Table 4, entries 3 vs 4 and 5). Subsequently, screening of

Table 3. Substrate Scope: Asymmetric Transfer Hydrogenation of Various Aromatic and Aliphatic Ketones in Water

| Entry ^a | Substrate | Ligand | Isolated yield [%] ^b | ee [%] ^{c,d} |
|--------------------|---|--------|---------------------------------|-----------------------|
| 1 |  | 3 | 92 | 91 (R) |
| 2 |  | 4 | 58 | 91 (R) |
| 3 |  | 3 | 68 | 82 (R) |
| 4 |  | 4 | 54 | 85 (R) |
| 5 |  | 3 | 82 | 97 (R) |
| 6 |  | 4 | 62 | 98 (R) |
| 7 |  | 3 | 74 | 83 (R) |
| 8 |  | 4 | 54 | 86 (R) |
| 9 |  | 3 | 76 | 81 (R) |
| 10 |  | 4 | 58 | 85 (R) |
| 11 |  | 3 | 73 | 93 (R) |
| 12 |  | 4 | 44 | 96 (R) |
| 13 |  | 3 | 79 | 15 (S) |
| 14 |  | 4 | 86 | 17 (S) |
| 15 |  | 3 | 86 | 26 (S) |
| 16 |  | 4 | 71 | 34 (S) |
| 17 |  | 3 | 69 | 25 ^e (R) |
| 18 |  | 4 | 86 | 92 ^e (R) |
| 19 |  | 3 | 27 | 42 ^e (R) |
| 20 |  | 4 | 37 | 90 ^e (R) |
| 21 |  | 3 | 31 | 40 ^e (R) |
| 22 |  | 4 | 44 | 78 ^e (R) |
| 23 |  | 3 | 58 | 45 ^f (S) |
| 24 |  | 4 | 67 | 78 ^f (S) |
| 25 |  | 3 | 21 | 16 ^g (S) |
| 26 |  | 4 | 28 | 24 ^g (S) |

^aPerformed with ketone (2 mmol) using 0.021 mmol (1.05 mol %) chiral ligand, 0.01 mmol (0.5 mol %) Ru[(*p*-cymene)Cl₂]₂ and 10 mmol HCOONa in 4 mL H₂O at 25 °C for 24 h. ^bIsolated yield after purification via column chromatography. ^cDetermined by HPLC analysis using a DAICEL Chiralcel IB or AS-H columns. ^dAbsolute configuration determined by measurement of optical rotation data and comparison with literature values. ^eDetermined by ¹⁹F{¹H} NMR after derivatization with (*S*)-Mosher's acid chloride. ^fDetermined by GC analysis as acetate derivative. Only the *E*-isomer could be detected after the reactions.

carbamate ligands 3–7 revealed that they were equally suitable for the asymmetric reduction of imines 12 and 13. Among all

ligands, the Boc-substituted ion-tagged carbamate ligand 3 was the most successful, and the desired amine (1-methyl-1,2,3,4-

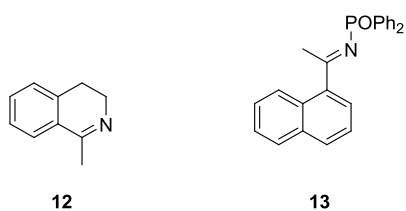


Figure 5. Selected imines substrates for the asymmetric transfer hydrogenation.

tetrahydroisoquinoline) could be isolated with 95% yield and 87% ee (Table 4, entry 4). Comparable selectivities were found for the reduction of *N,N*-diphenylphosphinoketimine 13 (Table 4, entries 9–13). However, because of solubility issues a methanol/water ratio of 1:2 was more suitable as the solvent system.

For further investigations on the robustness and recyclability of the novel catalytic system, a cumulative recycling study was carried out. The reaction was performed using acetophenone (2 mmol) as substrate and chiral ligand 3 under the previously optimized reaction conditions. After 60 min reaction time, a sample was taken to determine the conversion and enantioselectivity; meanwhile, another batch of acetophenone and fresh sodium formate was added. As can be seen in Figure 6, excellent catalytic activity with conversions $\geq 90\%$ was maintained for 7 runs, and only a marginal decrease of enantioselectivity was observed.

Further studies on the hydrolytic stability confirmed the robustness of the Boc-modified chiral ligand 3 for the application in aqueous medium. For this purpose, the ligand was heated in deuterium oxide at 25, 60 and 100 °C, respectively, while samples were taken at intervals to check the structural integrity via NMR spectroscopy. No changes were observed at 25 or 60 °C after 48 h, indicating excellent hydrolytic stability under the operating conditions asymmetric transfer hydrogenations in aqueous medium. Even at 100 °C only a minor change in purity was observed after 48 h, which results most likely from the migration of the *n*-butyl chain from the pyridine nitrogen to the benzylic nitrogen. The detailed procedure of the stability tests and the NMR spectra can be

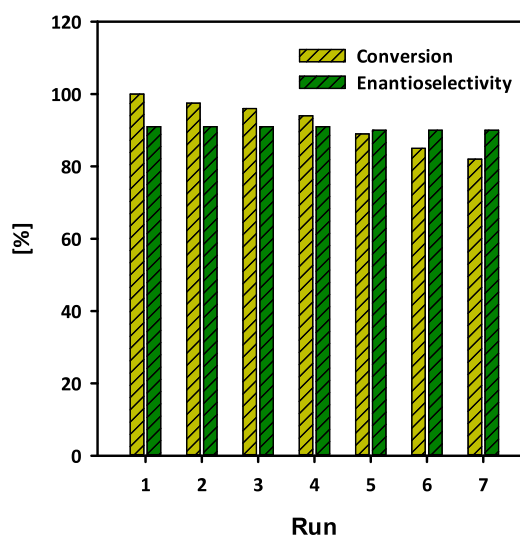


Figure 6. Cumulative recycling experiment. The reaction was performed using 2.0 mmol acetophenone, 0.021 mmol (1.05 mol %) chiral ligand 3, 0.01 mmol (0.5 mol %) $\text{Ru}[(p\text{-cymene})\text{Cl}_2]_2$ and 10.0 mmol sodium formate for 60 min at 60 °C. After every run, additional 2.0 mmol acetophenone, and 2.0 mmol sodium formate were added.

found in the Supporting Information (ESI pages S53 and S54, Figures S57–S59).

CONCLUSION

Herein, we reported the design and synthesis of novel ion-tagged chiral ligands for the asymmetric transfer hydrogenation of ketones and imines in aqueous medium. Based on the lead structure of previously established coordinating chiral ionic liquids as key motif, novel carbamate ligands with a pyridinium headgroup were synthesized in only three steps starting from commercially available chiral diamines. Because of the ionic nature of the ligands, the preformed chiral ruthenium-complex was readily soluble in water, allowing the asymmetric transfer hydrogenation of ketones to be performed in water as the sole solvent. The best performance was obtained with *tert*-butyloxycarbonyl (Boc)-substituted ligands 3 and 4 for a broad range of aromatic and aliphatic ketones under optimized

Table 4. Ligand Screening in the Asymmetric Transfer Hydrogenation of Imines 12 and 13

| entry ^a | chiral ligand | substrate | hydrogen donor | solvent | conversion ^{b,c} [%] | ee ^{d,e} [%] |
|--------------------|---------------|-----------|---------------------------------|---------------------------------|-------------------------------|-----------------------|
| 1 | 3 | 12 | HCOONa | H ₂ O | 3 | n.d. |
| 2 | 3 | 12 | HCOOH-Et ₃ N (1.1/1) | H ₂ O | 72 | 86 (R) |
| 3 | 3 | 12 | HCOOH-Et ₃ N (5/2) | H ₂ O/MeOH (V/V 1:1) | 60 | 62 (R) |
| 4 | 3 | 12 | HCOOH-Et ₃ N (1.1/1) | H ₂ O/MeOH (V/V 1:1) | >99 (95) | 87 (R) |
| 5 | 4 | 12 | HCOOH-Et ₃ N (1.1/1) | H ₂ O/MeOH (V/V 1:1) | 99 (96) | 86 (R) |
| 6 | 5 | 12 | HCOOH-Et ₃ N (1.1/1) | H ₂ O/MeOH (V/V 1:1) | 99 (90) | 50 (R) |
| 7 | 6 | 12 | HCOOH-Et ₃ N (1.1/1) | H ₂ O/MeOH (V/V 1:1) | 58 (55) | 30 (R) |
| 8 | 7 | 12 | HCOOH-Et ₃ N (1.1/1) | H ₂ O/MeOH (V/V 1:1) | 88 (82) | 42 (R) |
| 9 | 3 | 13 | HCOOH-Et ₃ N (1.1/1) | H ₂ O/MeOH (V/V 1:2) | 65 (60) | 86 (R) ^f |
| 10 | 4 | 13 | HCOOH-Et ₃ N (1.1/1) | H ₂ O/MeOH (V/V 1:2) | 54 (51) | 86 (R) ^f |
| 11 | 5 | 13 | HCOOH-Et ₃ N (1.1/1) | H ₂ O/MeOH (V/V 1:2) | 61 (57) | 73 (R) ^f |
| 12 | 6 | 13 | HCOOH-Et ₃ N (1.1/1) | H ₂ O/MeOH (V/V 1:2) | 55 (53) | 64 (R) ^f |
| 13 | 7 | 13 | HCOOH-Et ₃ N (1.1/1) | H ₂ O/MeOH (V/V 1:2) | 38 (34) | 55 (R) ^e |

^aPerformed with 1 mmol imine using 0.0105 mmol (1.05 mol %) chiral ligand, 0.00525 mmol (0.5 mol %) $\text{Ru}[(p\text{-cymene})\text{Cl}_2]_2$ and 0.5 mL HCOOH-Et₃N (n/n 1.1/1) in 1.5 mL solvent at 40 °C for 24 h. ^bDetermined by ¹H NMR from the crude product. ^cIsolated yields in parentheses. ^dDetermined by ¹⁹F{¹H} NMR after derivatization with (*S*)-Mosher's acid chloride. ^eAbsolute configuration determined by comparison of the optical rotation with literature data. ^fDetermined by chiral HPLC using a DAICEL Chiralcel AS-H column.

conditions, resulting in isolated yields up to 95% and enantioselectivities >90% ee. While best results for aromatic ketones were obtained with the *N*-butylpyridinium salt **3**, an increase in alkyl chain length to the *N*-dodecyl salt **4** resulted in drastically improved results for challenging aliphatic ketones. Moreover, a change of reaction conditions and hydrogen donor also enabled the asymmetric reduction of two different imine substrates using the same catalysts. Eventually, studies on recyclability showed that the catalytic system could be reused for at least seven runs with hardly any loss in performance, thereby demonstrating the robustness of the novel ligands for asymmetric transfer hydrogenations. Based on the promising results obtained in asymmetric transfer hydrogenation, we are currently expanding the application range of the novel ion-tagged chiral ligands toward a broad implementation in asymmetric catalysis in aqueous medium.

MATERIALS AND METHODS

All reagents were purchased from commercial suppliers and used without further purification, unless noted otherwise. Dichloromethane and methanol anhydrous solvents were predistilled and desiccated on Al₂O₃ columns (PURESOLV, Innovative Technology). Anhydrous acetonitrile was purchased from Acros Organics (extra dry solvent, AcroSeal technology).

Chromatography solvents were distilled prior to use. Column chromatographic purifications were performed on standard glass columns, using silica gel (40–63 μm, Merck) with the eluates stated. Preparative HPLC was performed on a Reveleris Prep Purification System using a Maisch ReproSil 100 C18 column (250 mm × 4.6 mm ID, 5 μm) and H₂O/acetonitrile as eluent at a flow rate of 15 mL/min. Determination of enantiomeric excess via HPLC measurements was performed on a Thermo Scientific/Dionex Ultimate 3000 instrument using a Chiralpack Chiracel Daicel IB column (250 mm × 4.6 mm ID, 5 μm) or AS-H column (250 mm × 4.6 mm ID, 5 μm).

¹H, ¹³C, ¹⁹F and ³¹P NMR spectra were recorded in CDCl₃ or MeOD solutions on a Bruker Advance UltraShield 400 (400 MHz) spectrometer. Chemical shifts (δ) are reported in ppm using tetramethylsilane (TMS) as internal standard. Coupling constants (J) are reported in Hertz (Hz). In order to explain the multiplicities, the following abbreviations were used: s = singlet, d = doublet, t = triplet, q = quartet, quin. = quintet, sex = sextet, m = multiplet, brs = broad singlet.

Infrared spectra were recorded on a PerkinElmer Spectrum 65 FT IR spectrometer equipped with a specac MK II Golden Gate Single Reflection ATR unit. HR-MS analysis was carried out in methanol solutions (c = 10 ppm) by using an HTCPL system auto sampler (CTC Analytics AG), an Agilent 1100/1200 HPLC with binary pumps, degasser and column thermostat (Agilent Technologies) and Agilent 6230 AJS ESI-TOF mass spectrometer. Optical rotation was measured on an Anton Paar MCP500 polarimeter at the specified conditions and the concentrations are stated in g/100 mL.

Synthesis of Chiral Ligands on the Example of Boc-Substituted Ligand **3.** *tert*-Butyl ((1*R*,2*R*)-2-amino-1,2-diphenylethyl)carbamate (**1**). (1*R*,2*R*)-1,2-Diphenylethylenediamine (*R,R*-DPEN, 9.1 mmol, 1.93 g) was dissolved in 20 mL anhydrous MeOH, and it was cooled to 0 °C. A 1 M solution of HCl in MeOH (10.8 mmol, 10.5 mL) was added dropwise, and the mixture was subsequently stirred at room temperature for 15 min. The formed precipitate was redissolved by the addition of 1 mL H₂O. Di-*tert*-butyl dicarbonate (13.5 mmol, 2.93 g) in 5 mL anhydrous MeOH was added dropwise and subsequently stirred at room temperature for 4 h. After completion, the reaction mixture was diluted with 10 mL H₂O, and the organic solvent was removed under reduced pressure. The obtained suspension was washed with Et₂O, and the organic layer was extracted with H₂O. The aqueous layers were basified with 2 M NaOH solution and extracted with CH₂Cl₂. The combined organic phases were dried over Na₂SO₄ and the solvent removed under reduced pressure. The crude product was redissolved in ethyl-acetate, and the solid residue

removed over a patch of silica. The solvent was removed *in vacuo*, obtaining Boc-protected diphenylethyl diamine **1** as a pale white solid (1.71 g, 77%). The product was used for the next step without further purification.

M.p.: 103–105 °C. HRMS (ESI-TOF) *m/z* [M + H]⁺ calculated for C₁₉H₂₅N₂O₂: 313.1911. Found: 313.1912. [α]_D²⁰: +8.7 (c 1.0, CHCl₃). IR (ATR, cm⁻¹): 3378 (N–H ν), 2977 (C–H ν), 1684 (C=O ν), 1514 (N–H δ), 1455 (C–H δ), 756 (C–H arom δ), 696 (C–H arom δ). ¹H NMR (200 MHz, CDCl₃) δ: 7.26–7.25 (m, 10H, *H*-arom), 5.81 (d, *J* = 8.51 Hz, 1H, CH–NHCO), 4.77 (brs, 1H, NH), 4.25 (d, *J* = 3.79 Hz, 1H, CH–NH₂), 1.38 (s, 2H, NH₂), 1.23 (s, 9H, C–(CH₃)₃). ¹³C NMR (100 MHz, CDCl₃) δ: 155.70 (s, 1C, NH–CO), 142.28 (s, 1C, C-arom), 141.05 (s, 1C, C-arom), 128.51 (s, 1C, C-arom), 128.35 (d, 2C, C-arom), 127.42 (s, 2C, C-arom), 127.21 (s, 1C, C-arom), 126.83 (d, 2C, C-arom), 126.47 (s, 2C, C-arom), 79.26 (s, 1C, C–(CH₃)₃), 60.03 (s, 1C, CH–NHCO), 59.93 (s, 1C, CH–NH₂), 28.33 (s, 3C, C–(CH₃)₃).

tert-Butyl ((1*R*,2*R*)-1,2-diphenyl-2-((pyridin-3-ylmethyl)amino)ethyl)carbamate (**2**). Boc-protected diphenylethyl amine **1** (3.2 mmol, 1.0 g) was dissolved in 30 mL anhydrous MeOH. Freshly activated molecular sieve 4 Å (2.0 g), and freshly distilled pyridine-3-carbaldehyde (3.2 mmol, 300 μL, 343 mg) were added, and the reaction mixture was refluxed until complete conversion. The reaction mixture was cooled to room temperature, NaBH₄ (4.8 mmol, 182 mg) was added, and the reaction was stirred until complete conversion. The mixture was filtered over a batch of silica and subsequently hydrolyzed with H₂O. Methanol was removed under reduced pressure, and the remaining aqueous phase was extracted with CH₂Cl₂. The combined organic phases were dried over Na₂SO₄ and the solvent removed under reduced pressure. The crude product was purified by column chromatography (light petrol:ethyl acetate 1:1 + Et₃N) to obtain pure product **2** as a colorless solid (843 mg, 65%).

M.p.: 90–91 °C. HRMS (ESI-TOF) *m/z* [M + H]⁺ calculated for C₂₅H₃₀N₃O₂: 404.2333. Found: 404.2333. [α]_D²⁰: +10.3 (c 1.0, CHCl₃). IR (ATR, cm⁻¹): 3378 (N–H ν), 2976 (C–H ν), 1683 (C=O ν), 1510 (N–H δ), 1463 (C–H δ), 756 (C–H arom δ), 698 (C–H arom δ). ¹H NMR (400 MHz, CDCl₃) δ: 8.39 (d, *J* = 4.05 Hz, 1H, *H*-pyridine), 8.28 (s, 1H, *H*-pyridine), 7.36 (d, *J* = 6.88 Hz, 1H, *H*-pyridine), 7.27–7.04 (m, 11H, *H*-pyridine, *H*-arom), 5.51 (d, *J* = 7.69 Hz, 1H, CH–NHCO), 4.78 (brs, 1H, NH–CO), 3.86 (s, 1H, CH–NH), 3.57 (d, *J* = 13.48 Hz, 1H, NH–CH₂), 3.34 (d, *J* = 13.48 Hz, 1H, NH–CH₂), 1.75 (brs, 1H, NH–CH₂), 1.27 (s, 9H, C–(CH₃)₃). ¹³C NMR (100 MHz, CDCl₃) δ: 155.60 (s, 1C, NH–CO), 149.57 (s, 1C, C-pyridine), 148.51 (s, 1C, C-pyridine), 140.21 (s, 1C, C-arom), 139.62 (s, 1C, C-arom), 135.61 (s, 1C, C-pyridine), 135.29 (s, 1C, C-pyridine), 128.46 (d, 2C, C-arom), 127.85 (d, 2C, C-arom), 127.66 (d, 2C, C-arom), 127.34 (d, 2C, C-arom), 126.58 (d, 2C, C-arom), 123.35 (s, 1C, C-pyridine), 79.58 (s, 1C, C–(CH₃)₃), 66.65 (s, 1C, CH–NH), 59.85 (s, 1C, CH–NHCO), 48.49 (s, 1C, NH–CH₂), 28.32 (s, 3C, C–(CH₃)₃).

1-Butyl-3-(((1*R*,2*R*)-2-((*tert*-butoxycarbonyl)amino)-1,2-diphenylethyl)amino)methyl)pyridin-1-ium Bromide (**3**). Finely powdered **2** (1.8 mmol, 753 mg) was mixed with *n*-butyl bromide (2.2 mmol, 307 mg), and the solution was stirred at 80 °C for 20 h. Remaining volatile materials were removed under reduced pressure to obtain product **3** as a yellow foam (1.0 mg, >99%). The obtained chiral ligand **3** was used for catalysis as received, while an analytical sample was purified via preparative HPLC. HRMS (ESI-TOF) *m/z* [M]⁺ calculated for C₂₉H₃₈N₃O₂: 460.2959. Found: 460.2974. [α]_D²⁰: +12.2 (c 1.0, CHCl₃). IR (ATR, cm⁻¹): 3245 (N–H ν), 2965 (C–H ν), 1691 (C=O ν), 1498 (N–H ν), 1463 (C–H δ), 756 (C–H arom δ), 699 (C–H arom δ). ¹H NMR (400 MHz, MeOD) δ: 8.76 (d, *J* = 5.87 Hz, 1H, *H*-pyridine), 8.71 (s, 1H, *H*-pyridine), 8.31 (d, *J* = 7.94 Hz, 1H, *H*-pyridine), 7.89 (t, *J* = 6.91 Hz, 1H, *H*-pyridine), 7.20–7.12 (m, 10H, *H*-arom), 4.51 (t, *J* = 7.25 Hz, 2H, N–CH₂), 3.92 (d, *J* = 7.94 Hz, 1H, CH–NH), 3.89–3.80 (m, 2H, NH–CH₂), 2.01–1.89 (m, 2H, N–CH₂–CH₂), 1.44–1.36 (m, 11H, N–(CH₂)₂–CH₂, C–(CH₃)₃), 1.03 (t, *J* = 7.25 Hz, 3H, N–(CH₂)₃–CH₃). ¹³C NMR (100 MHz, MeOD) δ: 157.91 (s, 1C, NH–CO), 148.70 (s, 1C, C-pyridine), 145.88 (s, 1C, C-pyridine), 144.78 (s, 1C, C-pyridine),

143.71 (s, 1C, C-pyridine), 142.16 (s, 1C, C-arom), 141.30 (s, 1C, C-arom), 129.41 (d, 2C, C-arom), 129.28 (d, 2C, C-arom), 129.04 (d, 2C, C-arom), 128.55 (d, 2C, C-arom), 128.39 (d, 2C, C-arom), 128.04 (s, 1C, C-pyridine), 80.44 (s, 1C, C—(CH₃)₃), 68.68 (s, 1C, CH—NH), 62.64 (s, 1C, N—CH₂), 61.91 (s, 1C, CH—NHCO), 48.78 (s, 1C, NH—CH₂), 34.36 (s, 1C, N—CH₂—CH₂), 28.73 (s, 3C, C—(CH₃)₃), 20.38 (s, 1C, N—(CH₂)₂—CH₂), 13.79 (s, 1C, N—(CH₂)₃—CH₃).

Representative Procedures for Asymmetric Transfer Hydrogenations. Asymmetric transfer hydrogenations were carried out in flame-dried flasks using standard Schlenk techniques. Before the reactions, a 20 mg/mL stock solution of Ru[(*p*-cymene)₂Cl₂]₂ in anhydrous acetonitrile was freshly prepared in a glovebox. All liquids involved in the reactions were freshly degassed by using the freeze–dry–thaw method.

Asymmetric Transfer Hydrogenation of Ketones on the Example of Acetophenone (10). An aliquot of a freshly prepared stock solution of Ru[(*p*-cymene)₂Cl₂]₂ (0.01 mmol, 306 μL) was transferred into a Schlenk-flask, and the solvent was removed under vacuum. Chiral ligand **3** (0.021 mmol, 11.35 mg) was dissolved in 4 mL of H₂O. This solution was added to the catalyst precursor and stirred at 40 °C for 30 min to form the active catalyst. Sodium formate (10.0 mmol, 680 mg) was added, followed by the addition of acetophenone (2.0 mmol, 240 mg, 233 μL). The reaction mixture was stirred at 25 °C for 24 h. The aqueous phase was extracted with diethyl ether. The combined organic phases were dried over Na₂SO₄ and concentrated *in vacuo*. The product was isolated via column chromatography (light petrol:ethyl acetate 10:1). Remaining solvents were removed under vacuum to yield 1-phenylethanol (**11**) as colorless liquid (224 mg, 92%). ¹H NMR (200 MHz, CDCl₃) δ: 7.29–7.18 (m, 5H, *H*-arom), 4.81 (q, *J* = 6.42 Hz, 1H, CH—OH), 1.82 (s, 1H, CH—OH), 1.42 (d, *J* = 6.45 Hz, 3H, CH—CH₃).

Determination of enantiomeric excess: DAICEL Chiracel IB column, hexane: ³PrOH 98.5:1.5 V/V, 1.0 mL/min, 25 °C, UV 254 nm: *t*_R (*R*) = 13.0 min, *t*_R (*S*) = 15.0 min.

Asymmetric Transfer Hydrogenation of Imines on the Example of 1-Methyl-3,4-dihydroisoquinoline (12). An aliquot of a freshly prepared stock solution of Ru[(*p*-cymene)₂Cl₂]₂ (0.005 mmol, 153 μL) was transferred into a Schlenk-flask, and the solvent was removed under vacuum. Chiral ligand **3** (0.0105 mmol, 5.86 mg) was dissolved in 1.5 mL H₂O/MeOH (V/V = 1/1). This solution was added to the catalyst precursor and stirred at 40 °C for 30 min to form the active catalyst. Formic acid/Et₃N mixture (*n/n* = 1.1/1, 0.5 mL) was added, followed by the addition 1-methyl-3,4-dihydroisoquinoline **12** (1.0 mmol, 145 mg, 141 μL). The reaction mixture was stirred at 40 °C for 24 h. Methanol was removed under reduced pressure, and the aqueous phase was basified with 0.5 M Na₂CO₃ solution. The aqueous layer was extracted with CH₂Cl₂. The combined organic phases were dried over Na₂SO₄ and concentrated *in vacuo*. The product was isolated via column chromatography (CH₂Cl₂: MeOH 10:1 + Et₃N) to afford 1-methyl-1,2,3,4-tetrahydroisoquinoline as a pale yellow oil (138 mg, 94%).

¹H NMR (200 MHz, CDCl₃) δ: 7.08–7.02 (m, 4H, *H*-arom), 4.03 (q, *J* = 6.60 Hz, 1H, CH—NH), 3.17–3.16 (m, 1H, CH_{2a}—NH), 2.98–2.70 (m, 3H, CH_{2b}—NH, CH₂-arom), 1.67 (br s, 1H, CH—NH), 1.39 (d, *J* = 6.60 Hz, 3H, CH—CH₃).

Determination of enantiomeric excess: The crude amine (0.1 mmol, 29 mg) was dissolved in anhydrous CH₂Cl₂ (1 mL) in a flame-dried Schlenk-flask. Et₃N (0.15 mmol, 21 μL) and (*S*)-Mosher's acid chloride (22 μL, 0.12 mmol) were added and the reaction mixture was stirred at 25 °C. After completion, 5 mL of CH₂Cl₂ was added, and the organic phase was successively washed with 0.5 M Na₂CO₃ and water, dried over Na₂SO₄ and concentrated *in vacuo*. ¹⁹F NMR (100 MHz, CDCl₃) δ: –69.74, (minor diastereomer), –71.30 (major diastereomer).

■ ASSOCIATED CONTENT

Supporting Information

The Supporting Information is available free of charge on the ACS Publications website at DOI: 10.1021/acssuschemeng.8b05613.

Detailed experimental procedures for the synthesis of chiral ligands, detailed procedure for the asymmetric transfer hydrogenation, NMR spectra of all new and known products and additional graphs (PDF)

■ AUTHOR INFORMATION

Corresponding Author

*Katharina Schröder (née Katharina Bica). Email: katharina.schroeder@tuwien.ac.at; Fax: +43 1 58801 16360; Tel: +43 1 58801 163601.

ORCID

Christian Schröder: 0000-0002-2167-5096

Katharina Bica: 0000-0002-2515-9873

Notes

The authors declare no competing financial interest.

■ ACKNOWLEDGMENTS

Dedicated to the memory of Ken R. Seddon. MRS Financial support by the Austrian Science Fund (project P29146-N34) is gratefully acknowledged.

■ REFERENCES

- Brooks, W. H.; Guida, W. C.; Daniel, K. G. The significance of chirality in drug design and development. *Curr. Top. Med. Chem.* **2011**, *11*, 760–770 PMID: PMC5765859.
- Modern Reduction Methods*; Anderson, P. G., Mwunslow, I. J., Eds.; Wiley-VCH: Weinheim, Germany, 2008; DOI: 10.1002/9783527622115.fmatter.
- Wang, D.; Astruc, D. The golden age of transfer hydrogenation. *Chem. Rev.* **2015**, *115*, 6621–6686.
- Palmer, M. J.; Wills, M. Asymmetric transfer hydrogenation of C = O and C = N bonds. *Tetrahedron: Asymmetry* **1999**, *10*, 2045–2061.
- Wu, X.; Wang, C.; Xiao, J. Asymmetric transfer hydrogenation in water with platinum group metal catalysts. *Platinum Met. Rev.* **2010**, *54*, 3–19.
- Wu, X.; Xiao, J. Aqueous-phase asymmetric transfer hydrogenation of ketones – a greener approach to chiral alcohols. *Chem. Commun.* **2007**, 2449–2466.
- Li, C.-J.; Chan, T.-H. *Comprehensive Organic Reactions in Aqueous Media*; John Wiley: New York, 1997.
- Organic Synthesis in Water*; Greico, P. A., Ed.; Blackie Academic: London, 1998.
- Lindstroem, U. M. Stereoselective Organic Reactions in Water. *Chem. Rev.* **2002**, *102*, 2751–2772.
- Sinou, D. Asymmetric Organometallic-Catalysed Reactions in aqueous media. *Adv. Synth. Catal.* **2002**, *344*, 221–237.
- Li, C.-J. Organic Reactions in aqueous Media with a Focus on Carbon-Carbon bond formation: A Decade Update. *Chem. Rev.* **2005**, *105*, 3095–3166.
- Wu, X.; Liu, J.; Di Tommaso, D.; Iggo, J. A.; Catlow, C. R. A.; Bacsá, J.; Xiao, J. A Multilateral Mechanistic Study into Asymmetric Transfer Hydrogenation in Water. *Chem. - Eur. J.* **2008**, *14*, 7699–7715.
- Hashiguchi, S.; Fujii, A.; Takehara, J.; Ikariya, T.; Noyori, R. Asymmetric Transfer Hydrogenation of Aromatic Ketones Catalyzed by Chiral Ruthenium(II) Complexes. *J. Am. Chem. Soc.* **1995**, *117*, 7562–7563.
- Li, X.; Chen, W.; Hems, W.; King, F.; Xiao, J. Asymmetric transfer hydrogenation of ketones with a polymer-supported chiral diamine. *Tetrahedron Lett.* **2004**, *45*, 951–953.

- (15) Li, X.; Wu, X.; Chen, W.; Hancock, F. E.; King, F.; Xiao, J. Asymmetric Transfer Hydrogenation in Water with a Supported Noyori–Ikariya Catalyst. *Org. Lett.* **2004**, *6*, 3321–3324.
- (16) Cornils, B.; Herrmann, W. A.; Eckl, R. W. Industrial aspects of aqueous catalysis. *J. Mol. Catal. A: Chem.* **1997**, *116*, 27–33.
- (17) Cornils, B.; Herman, W. A. *Applied Homogeneous Catalysis by Organometallic Catalysts*; Wiley-VCH: Weinheim, Germany, 1998.
- (18) Li, J.; Li, X.; Ma, Y.; Wu, J.; Wang, F.; Xiang, J.; Zhu, J.; Wang, Q.; Deng, J. Surfactant-accelerated asymmetric transfer hydrogenation with recyclable water-soluble catalyst in aqueous media. *RSC Adv.* **2013**, *3*, 1825–1834.
- (19) Doherty, S.; Goodrich, P.; Hardacre, C.; Knight, J. G.; Nguyen, M. T.; Parvulescu, V. I.; Paun, C. Recyclable Copper Catalysts Based on Imidazolium-Tagged Bis(oxazolines): A Marked Enhancement in Rate and Enantioselectivity for Diels–Alder Reactions in Ionic Liquid. *Adv. Synth. Catal.* **2007**, *349*, 951–963.
- (20) Doherty, S.; Goodrich, P.; Hardacre, C.; Parvulescu, V. I.; Paun, C. Efficient Heterogeneous Asymmetric Catalysis of the Mukaiyama Aldol Reaction by Silica- and Ionic Liquid-Supported Lewis Acid Copper(II) Complexes of Bis(oxazolines). *Adv. Synth. Catal.* **2008**, *350*, 295–302.
- (21) Geldbach, T. J.; Dyson, P. J. A Versatile Ruthenium Precursor for Biphasic Catalysis and Its Application in Ionic Liquid Biphasic Transfer Hydrogenation: Conventional vs Task-Specific Catalysts. *J. Am. Chem. Soc.* **2004**, *126*, 8114–8115.
- (22) Kang, G.; Lin, S.; Shiwakoti, A.; Ni, B. Imidazolium ion tethered TsDPENs as efficient water-soluble ligands for rhodium catalyzed asymmetric transfer hydrogenation of aromatic ketones. *Catal. Commun.* **2014**, *57*, 111–114.
- (23) Kalsin, A. M.; Peganova, T. y. A.; Novikov, V. V.; Zhamoytina, A. I.; Gonsalvi, L.; Peruzzini, M. Transfer Hydrogenation of Ketones Catalyzed by Surface-Active Ruthenium and Rhodium Complexes in Water. *Chem. - Eur. J.* **2014**, *20*, 846–854.
- (24) Li, J.; Tang, Y.; Wang, Q.; Li, X.; Cun, L.; Zhang, X.; Zhu, J.; Li, L.; Deng, J. Chiral Surfactant-Type Catalyst for Asymmetric Reduction of Aliphatic Ketones in Water. *J. Am. Chem. Soc.* **2012**, *134*, 18522–18525.
- (25) Vasiliou, M.; Gaertner, P.; Zirbs, R.; Bica, K. Coordinating Chiral Ionic Liquids: Design, Synthesis, and Application in Asymmetric Transfer Hydrogenation under Aqueous Conditions. *Eur. J. Org. Chem.* **2015**, *2015*, 2374–2381.
- (26) Vasiliou, M.; Leder, S.; Gaertner, P.; Mereiter, K.; Bica, K. Coordinating chiral ionic liquids. *Org. Biomol. Chem.* **2013**, *11*, 8092–8102.
- (27) Bica, K.; Leder, S.; Mereiter, K.; Gaertner, P. Design, synthesis, and application of novel chiral ONN ligands for asymmetric alkylation. *Monatsh. Chem.* **2013**, *144*, 447–453.
- (28) Frisch, M. J.; Trucks, G. W.; Schlegel, H. B.; Scuseria, G. E.; Robb, M. A.; Cheeseman, J. R.; Scalmani, G.; Barone, V.; Mennucci, B.; Petersson, G. A.; Nakatsuji, H.; Caricato, M.; Li, X.; Hratchian, H. P.; Izmaylov, A. F.; Bloino, J.; Zheng, G.; Sonnenberg, J. L.; Hada, M.; Ehara, M.; Toyota, K.; Fukuda, R.; Hasegawa, J.; Ishida, M.; Nakajima, T.; Honda, Y.; Kitao, O.; Nakai, H.; Vreven, T.; Montgomery, J. A., Jr.; Peralta, J. E.; Ogliaro, F.; Bearpark, M.; Heyd, J. J.; Brothers, E.; Kudin, K. N.; Staroverov, V. N.; Kobayashi, R.; Normand, J.; Raghavachari, K.; Rendell, A.; Burant, J. C.; Iyengar, S. S.; Tomasi, J.; Cossi, M.; Rega, N.; Millam, J. M.; Klene, M.; Knox, J. E.; Cross, J. B.; Bakken, V.; Adamo, C.; Jaramillo, J.; Gomperts, R.; Stratmann, R. E.; Yazyev, O.; Austin, A. J.; Cammi, R.; Pomelli, C.; Ochterski, J. W.; Martin, R. L.; Morokuma, K.; Zakrzewski, V. G.; Voth, G. A.; Salvador, P.; Dannenberg, J. J.; Dapprich, S.; Daniels, A. D.; Farkas, Ö.; Foresman, J. B.; Ortiz, J. V.; Cioslowski, J.; Fox, D. J. *Gaussian 09*, Revision D.01; Gaussian, Inc.: Wallingford, CT, 2009.
- (29) Becke, A. D. Density functional thermochemistry. III. The role of exact exchange. *J. Chem. Phys.* **1993**, *98*, 5648–5652.
- (30) Tomasi, J.; Mennucci, B.; Cammi, R. Quantum mechanical continuum solvation models. *Chem. Rev.* **2005**, *105*, 2999–3093.
- (31) Singh, U. C.; Kollman, P. A. An approach to computing electrostatic charges formolecules. *J. Comput. Chem.* **1984**, *5*, 129–145.
- (32) Breneman, C. M.; Wiberg, K. B. Determining atom-centered monopoles from molecular electrostatic potentials – the need for high sampling density in formamide conformational analysis. *J. Comput. Chem.* **1990**, *11*, 361–373.
- (33) Dub, P. A.; Henson, N. J.; Martin, R. L.; Gordon, J. C. Unravelling the Mechanism of the Asymmetric Hydrogenation of Acetophenone by [RuX₂(diphosphine)(1,2-diamine)] Catalysts. *J. Am. Chem. Soc.* **2014**, *136*, 3505–3521.
- (34) Dub, P. A.; Ikariya, T. Quantum Chemical Calculations with the Inclusion of Nonspecific and Specific Solvation: Asymmetric Transfer Hydrogenation with Bifunctional Ruthenium Catalysts. *J. Am. Chem. Soc.* **2013**, *135*, 2604–2619.
- (35) Aupoix, A.; Bournaud, C.; Vo-Thanh, G. Asymmetric Transfer Hydrogenation of Aromatic Ketones Using Rhodium Complexes of Chiral N-Heterocyclic Carbenes Derived from (S)-Pyroglutamic Acid. *Eur. J. Org. Chem.* **2011**, *2011*, 2772–2776.
- (36) Ahlford, K.; Lind, J.; Mäler, L.; Adolffson, H. Rhodium-catalyzed asymmetric transfer hydrogenation of alkyl and aryl ketones in aqueous media. *Green Chem.* **2008**, *10*, 832–835.
- (37) Gladiali, S.; Alberico, E. Asymmetric transfer hydrogenation: chiral ligands and applications. *Chem. Soc. Rev.* **2006**, *35*, 226–236.
- (38) Vasiliou, M.; Rainer, D.; Gaertner, P.; Reichel, C.; Schroeder, C.; Bica, K. Basic chiral ionic liquids: A novel strategy for acid-free organocatalysis. *Catal. Today* **2013**, *200*, 80–86.
- (39) Lin, Z.; Li, J.; Huang, Q.; Wang, Q.; Tang, L.; Gong, D.; Yang, J.; Zhu, J.; Deng, J. Chiral surfactant-type catalyst: enantioselective reduction of long-chain aliphatic ketoesters in water. *J. Org. Chem.* **2015**, *80*, 4419–4429.
- (40) Aberg, J. B.; Samec, J. S.; Bäckvall, J.-E. Mechanistic investigation on the hydrogenation of imines by [p-(Me₂CH)C₆H₄Me]RuH-(NH₂CHPhCHPhNSO₂C₆H₄-p-CH₃). Experimental support for an ionic pathway. *Chem. Commun.* **2006**, No. 26, 2771–2773.
- (41) Václavík, J.; Kuzma, M.; Prech, J.; Kacer, P. Kačer Asymmetric Transfer Hydrogenation of Imines and Ketones Using Chiral RuII(Cl)(η⁶-p-cymene)[(S,S)-N-TsDPEN] as a Catalyst: A Computational Study. *Organometallics* **2011**, *30*, 4822–4829.
- (42) Magee, M. P.; Norton, J. R. Stoichiometric, Catalytic, and Enantioface-Selective Hydrogenation of C = N Bonds by an Ionic Mechanism. *J. Am. Chem. Soc.* **2001**, *123*, 1778–1779.
- (43) Shende, V. S.; Deshpande, S. H.; Shingote, S. K.; Joseph, A.; Kelkar, A. A. Asymmetric Transfer Hydrogenation of Imines in Water by Varying the Ratio of Formic Acid to Triethylamine. *Org. Lett.* **2015**, *17*, 2878–2881.
- (44) Uematsu, N.; Fujii, A.; Hashiguchi, S.; Ikariya, T.; Noyori, R. Asymmetric Transfer Hydrogenation of Imines. *J. Am. Chem. Soc.* **1996**, *118*, 4916–4917.

Asymmetric Transfer Hydrogenation in Thermomorphic Microemulsions Based on Ionic Liquids

Mahtab Hejazifar, Ádám Márk Pálvölgyi, Jacqueline Bitai, Olga Lanaridi, and Katharina Bica-Schröder*

Institute of Applied Synthetic Chemistry, TU Wien, Getreidemarkt 9/163, 1060 Vienna, Austria

Supporting Information

ABSTRACT: A thermomorphic ionic-liquid-based microemulsion system was successfully applied for the Ru-catalyzed asymmetric transfer hydrogenation of ketones. On the basis of the temperature-dependent multiphase behavior of the targeted microemulsion, simple product separation as well as catalyst recycling could be realized. The use of water-soluble ligands improved the immobilization of the catalyst in the microemulsion phase and significantly decreased the catalyst leaching into the organic layer upon extraction of the product. Eventually, the optimized microemulsion system could be applied to a wide range of aromatic ketones that were reduced with good isolated yields (up to 98%) and enantioselectivities (up to 97%), while aliphatic ketones were less successful.

KEYWORDS: microemulsion, ionic liquid, asymmetric transfer hydrogenation, multiphase catalysis

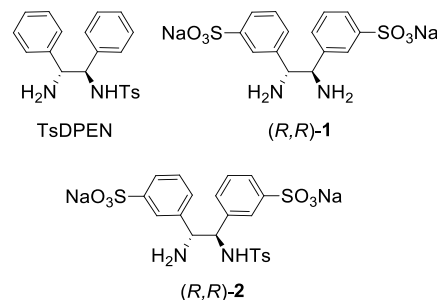
INTRODUCTION

Chiral secondary alcohols are important and invaluable intermediates for the preparation of pharmaceuticals and fine chemicals. One of the most versatile and powerful methods for their synthesis is the asymmetric reduction of ketones.¹ Among the wide field of asymmetric reduction methods, asymmetric transfer hydrogenation has emerged as a particularly powerful and practical tool because of its operational simplicity combined with high reaction rates and enantioselectivity.² The use of a simple organic compound as a hydrogen donor in transfer hydrogenation has several advantages over the use of molecular hydrogen since it avoids not only the risks and constraints associated with hydrogen gas but also the necessity for pressurized vessels and other specialized equipment.³ A number of different donor molecules can be employed as hydrogen source in transfer hydrogenations, including organic molecules such as formic acid and its salts, as well as primary and secondary alcohols.^{4–6}

Apart from the hydrogen donor, the appropriate choice of transition-metal catalyst and reaction conditions are crucial for achieving the desired chemo- or stereoselectivity under mild conditions in asymmetric transfer hydrogenations.³ Over the last three decades, considerable attention has been dedicated to the use of ruthenium-based complexes developed by Noyori and co-workers.^{4,7,8} Reported already in 1995, the highly active and selective (pre-)catalyst, a TsDPEN-coordinated (TsDPEN = *N*-(*p*-toluenesulfonyl)-1,2-diphenylethylenediamine) Ru(II) complex (Ru-TsDPEN) can be considered as a benchmark system for the asymmetric transfer hydrogenation of aromatic ketones (Scheme 1). This breakthrough has inspired intense research in the area of asymmetric transfer hydrogenations, which is growing steadily in the past years.^{2,7}

Recently, considerable effort has been dedicated to asymmetric transfer hydrogenations in aqueous reaction media. With the rising awareness for sustainable chemistry, water as solvents is often considered as safe, economical, nontoxic, and benign reaction medium compared with typical

Scheme 1. Structure of *N*-(*p*-Toluenesulfonyl)-1,2-diphenylethylenediamine (TsDPEN) and Water-Soluble Ligands (*R,R*-1) and (*R,R*-2) Used in This Work



organic solvents.^{1,2,9} The classical drawbacks of homogeneous catalysis, such as the difficult separation of product and catalyst or the tricky recycling of the catalyst can be overcome in an elegant liquid–liquid biphasic approach, relying on water as catalyst-carrying phase that can be easily separated from the insoluble products.¹⁰ Moreover, water is a particularly attractive and valuable solvent for transfer hydrogenations, since it enables the use of sodium formate as the most easily available, inexpensive, and nonreversible hydrogen source.^{9–12} However, the use of water as reaction medium in asymmetric transition-metal catalysis is still challenging, as many metal catalysts are unstable toward hydrolysis.¹ Moreover, the low solubility of many transition-metal catalysts in water is a limiting factor. To solve this issue, a number of water-soluble ligands and catalysts have been developed for asymmetric transfer hydrogenations of ketones in aqueous media, providing the desired secondary alcohols in high yield and enantioselectivity.^{1,2,7} Several strategies have been pursued to improve not only the water-solubility of the TsDPEN

Received: April 9, 2019

Published: July 2, 2019

structural motive, including the modification with anionic groups in case of aryl sulfonated systems (e.g.: (*R,R*)-1, (*R,R*)-2) and the functionalization with cationic groups such as trialkylammonium moieties, but also the development of polyethylene glycol-supported TsDPEN systems.^{13–17} Recently, we reported the synthesis of ion-tagged chiral ligands for asymmetric synthesis in water or ionic liquids, including the use for highly selective and efficient asymmetric transfer hydrogenation of aliphatic or aromatic ketones and imines in aqueous medium.^{18–20}

While ligand modifications with ionic groups or polymers can overcome the limited solubility of conventional transition-metal catalysts, the solubility of hydrophobic reactants such as higher ketones in water remains an issue in liquid–liquid biphasic catalysis.²¹ Microemulsions provide an attractive solution to overcome this problem, as they can simultaneously dissolve hydrophobic and hydrophilic reactants. In general, microemulsions are defined as thermodynamically stable, isotropic, and optically transparent solutions composed of two intrinsically immiscible solvents in the presence of one or more amphiphiles.^{22–24} The simultaneous dissolution of hydrophobic and hydrophilic solutes is a key advantage of microemulsions and resulted in a wide application range for catalytic reactions and processes.^{24,25} Moreover, the phase behavior and separation can be precisely tuned by temperature variation, which provides a particularly attractive tool for multiphase catalysis. A thermomorphic microemulsion (ME) system, as depicted in Figure 1, can overcome potential mass

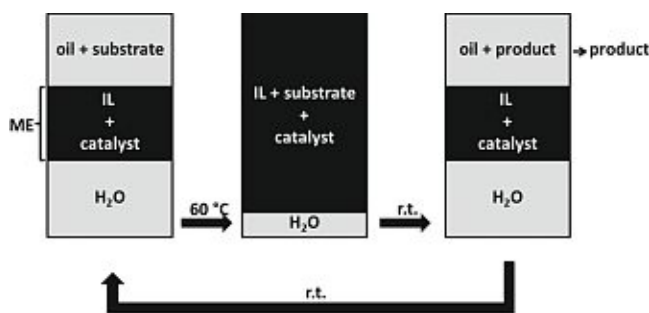


Figure 1. Thermomorphic asymmetric transfer hydrogenation in microemulsion.

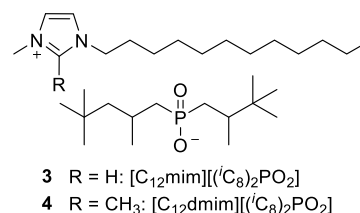
transfer limitations, since catalysis occurs in one homogeneous liquid phase, while simultaneously enabling an effective separation of catalyst and products due to temperature-induced phase separation.^{26,27}

So far, only few examples on transfer hydrogenation in microemulsions were reported.^{22,28} Batarseh et al. investigated the transfer hydrogenation of various unsaturated substrates by cyclohexene and similar water-insoluble hydrogen donors in aqueous microemulsion at 100–140 °C, relying mostly on fatty alcohol polyethylene glycol ethers as nonionic surfactants.²⁸ The influence of surfactant was also a key aspect in a study by Schwarze et al. in 2015, addressing the transfer hydrogenation of 4-acetylbiphenyl with 2-propanol as the hydrogen donor, Rh/TPPTS as catalyst, and K₂CO₃ as base.²² A strong influence of the surfactant on the catalytic activity was observed, as TX-100 showed about 10% higher conversions compared to fatty alcohol polyethylene glycol ethers in a three-phase *n*-heptane/water/surfactant/2-propanol microemulsion system, although higher concentrations of TX-100 led to a decrease in activity. As a consequence, the authors emphasized

that the initial selection of an appropriate surfactant that primarily supports the catalytic reaction and, in addition, gives the best performance in the separation step is of crucial importance. Considering that substrate, product, and their variable concentrations significantly influence the phase behavior and shift the phase boundaries to other temperatures, it is obvious that the selection and application of a reliable surfactant system in microemulsions is not an easy task.

Recently, we addressed the role of surface-active ionic liquids composed of both surface-active cations and anions for the formation of stable microemulsions with *n*-heptane and water, allowing for tunable surfactant structure with precise control over its composition.²⁴ Ionic liquids with long alkyl chains of typically eight carbon atoms or more show amphiphilic behavior, which renders them ideally suited for the development of microemulsions with potential advantages of conventional surfactants that are often sold as mixtures with variable composition. In our previous work, we reported the design of surface-active ionic liquids ([C₁₂mim][ⁱ(C₈)₂PO₂] (3) and [C₁₂dmim][ⁱ(C₈)₂PO₂] (4) (Scheme 2) that are able

Scheme 2. Surface Active Ionic Liquids Used for the Formation of Microemulsions



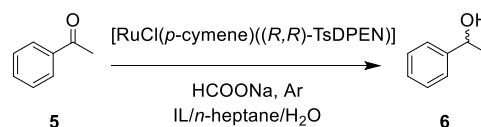
to form stable microemulsions with *n*-heptane and water as novel reaction media for thermomorphic palladium-catalyzed cross-coupling reactions. High reactivity was observed even at low catalyst loadings, while the temperature-dependent phase behavior allowed simple product separation and successful catalyst recycling through thermomorphic catalysis.²⁴

Herein, we expand our research toward ruthenium-catalyzed asymmetric transfer hydrogenation of ketones, aiming to overcome solubility issues of hydrophobic substrates and hydrophilic hydrogen donors in a targeted microemulsion system, while simultaneously facilitating product separation and catalyst recovery.

RESULTS AND DISCUSSION

Studies on Phase Behavior for the Reduction of Acetophenone. The reduction of acetophenone (5) to 1-phenylethanol (6) was selected as the model reaction to evaluate the application of ionic-liquid-based microemulsion systems as reaction media for asymmetric transfer hydrogenation (Scheme 3).

Scheme 3. Asymmetric Transfer Hydrogenation of Acetophenone (5) in Ionic-Liquid-Based Microemulsion Systems



As already stated by Schwarze et al. in 2015, the composition of the microemulsion system is of crucial importance for thermomorphic catalysis with microemulsion systems.²² Detailed investigations on the phase behavior of water/*n*-heptane/[C₁₂mim][(*i*-C₈)₂PO₂] (3) mixtures at 25 °C were reported in our previous paper, showing that all four types of Winsor microemulsion systems are present.²⁴ Specifically, Winsor type I systems are formed at small concentrations of surfactant as biphasic system (2Φ) of a oil-in-water (o/w) microemulsions with excess oil. Alternatively, the surfactant-rich water-in-oil (w/o) microemulsion may coexist with the surfactant-poor aqueous phase (2Φ, Winsor type II). Type III corresponds to a three-phase system (3Φ) where the ionic liquid-rich middle-phase coexists with both excess water and oil, while Winsor type IV is a single-phase (1Φ) isotropic solution which forms upon addition of higher surfactant concentrations.²⁹ However, the presence of additives and a variable substrate/product ratio inevitably affects the phase behavior, which is of particular importance for the chosen transfer hydrogenation, as the formed alcohol might act as a cosurfactant in the microemulsion. In order to identify a suitable composition of the ionic liquid-based microemulsion system that would allow separating the product in a three-phase system, phase diagrams were studied at different substrate/product ratios (see Figure 2 and SI Figures S1–

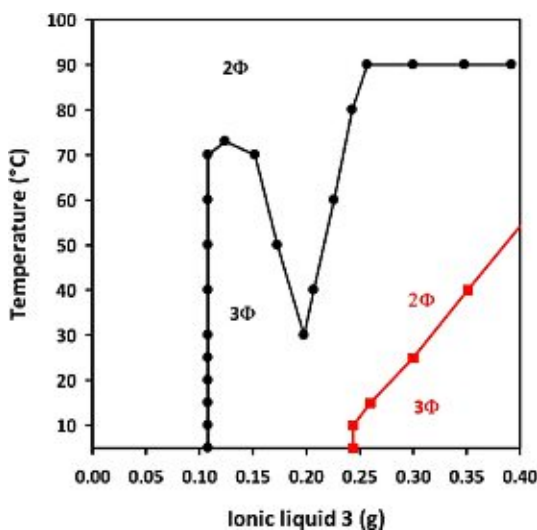


Figure 2. Phase diagram of (●) HCOONa (2 mmol), acetophenone (0.25 mmol), 1-phenylethanol (0.25 mmol), at equal mass fraction of water (2 g) and heptane (2 g) ($\alpha = 0.5$). (red ■) HCOONa (2 mmol), 1-phenylethanol (0.5 mmol), at an equal mass fraction of water and heptane ($\alpha = 0.5$).

S7). Consequently, the phase behavior of *n*-heptane/water mixtures at equal mass fraction ($\alpha = 0.5$) in the presence of HCOONa, acetophenone and 1-phenylethanol with variable ionic liquid [C₁₂mim][(*i*-C₈)₂PO₂] (3) content was studied at different temperatures. The composition of these microemulsions is typically characterized by parameters α and γ :

$$\alpha = \frac{m_{\text{oil}}}{(m_{\text{oil}} + m_{\text{water}})}$$

$$\gamma = \frac{m_{\text{IL}}}{(m_{\text{oil}} + m_{\text{water}} + m_{\text{IL}})}$$

The isotropic phase was determined by titration of the *n*-heptane/water mixture with $\alpha = 0.5$ and variable surfactant content γ for [C₁₂mim][(*i*-C₈)₂PO₂] (3) at different temperatures, according to the studies on phase behavior by Nowothnick et al.²⁵ After a defined amount of ionic liquid was added, the mixture was stirred and equilibrated at the indicated temperatures for an appropriate time until clear phases were observed. Figure 2 depicts the temperature-dependent phase diagram with acetophenone/1-phenylethanol in a ratio 1:1, corresponding to 50% conversion and with pure 1-phenylethanol to simulate complete conversion. In general, at lower temperatures and higher amount of ionic liquid a triphasic area (3Φ) with a surfactant-rich middle-phase (Winsor III) is observed, while at higher temperatures and lower amount of ionic liquid, two phases (2Φ) are formed where the microemulsion system coexists with excess water (Winsor II).²⁴ As expected, the increasing amount of 1-phenylethanol is affecting the phase behavior, resulting in a considerably smaller triphasic area. As can be seen from Figure 2, at least 0.3 g of ionic liquid 3 (corresponding to $\gamma = 0.15$) are required for the existence of a triphasic system at room temperature and hence for the isolation of the product via simple phase separation.

Optimization of the Asymmetric Transfer Hydrogenation of Acetophenone (5). After initially studying the phase behavior, the reduction of acetophenone (5) to 1-phenylethanol (6) was further evaluated at variable water/*n*-heptane/ionic liquid ratio and variable temperatures to optimize the reaction conditions (Table 1). In the attempt to minimize the volume of the organic solvent *n*-heptane as much as possible, we initially studied the effect of *n*-heptane on the asymmetric transfer hydrogenation, keeping the ionic liquid ratio fixed at 0.3 g as initially established in the phase-behavior studies. As can be seen from Table 1, a reduction of the *n*-heptane ratio from $\alpha = 0.56$ to $\alpha = 0$ was beneficial and yields increased from 47% to 98%, while the excellent enantioselectivity was maintained (entries 1–6). Main similar results are reported by Li et. al, who demonstrated that the presence of the organic solvents resulted in a much slower reaction.³⁰ However, keeping the consecutive workup in mind, we chose a *n*-heptane/water ratio of 0.5 g/2 g (corresponding to $\alpha = 0.2$) as optimum amount of organic solvent. A reduction of the ionic liquid ratio was not beneficial: apart from problems that would be occurring during phase separation, a decrease in ionic liquid reduced the yield to 86% (entries 5, 7–9).

Further studies on the effect of temperature showed that a lower yield can be compensated with increasing temperature (entries 10–14).^{28,29} The excellent enantioselectivity was maintained even at a temperature of 70 °C, which is in accordance with our previous observations.²⁰ The results for entries 15–18 suggest that the addition of an appropriate amount of water (i.e., decreasing γ while keeping the ionic liquid amount constant at 0.3 g) is beneficial to increase the yield of the reaction. A similar effect of water is reported by Wang et al.³¹ Eventually, at optimum reaction conditions (ionic liquid 3/*n*-heptane/water 0.3/0.5/2 g, 0.5 mmol acetophenone, 2 mmol HCOONa, 0.005 mmol (0.5 mol %) [RuCl(*p*-cymene)((*R,R*)-TsDPEN)], 20 h at 60 °C), excellent yield and enantiomeric excess $\geq 95\%$ were obtained. It is interesting to note that the asymmetric transfer hydrogenation proceeds also quite well without the presence of ionic liquid. Even in a biphasic system composed of water and *n*-heptane (2 g/0.5 g), high yields and enantioselectivity were obtained

Table 1. Optimization of the Asymmetric Transfer Hydrogenation of Acetophenone (5) Catalyzed by [RuCl(*p*-cymene)((*R,R*)-TsDPEN)], Performed with [C₁₂mim][C₈PO₂] (3)

| entry ^a | weight ratio IL/ <i>n</i> -heptane/H ₂ O | α | γ | temp [°C] | yield ^b [%] | ee ^{c,d} [%] |
|--------------------|---|----------|----------|-----------|------------------------|-----------------------|
| 1 | 0.3/2.5/2 | 0.56 | 0.06 | 40 | 47 | 92 (R) |
| 2 | 0.3/2/2 | 0.50 | 0.07 | 40 | 66 | 94 (R) |
| 3 | 0.3/1.5/2 | 0.43 | 0.08 | 40 | 72 | 94 (R) |
| 4 | 0.3/1/2 | 0.33 | 0.09 | 40 | 89 | 91 (R) |
| 5 | 0.3/0.5/2 | 0.20 | 0.11 | 40 | 95 | 92 (R) |
| 6 | 0.3/0/2 | 0 | 0.13 | 40 | 98 | 92 (R) |
| 7 | 0.25/0.5/2 | 0.20 | 0.09 | 40 | 91 | 93 (R) |
| 8 | 0.2/0.5/2 | 0.20 | 0.07 | 40 | 86 | 94 (R) |
| 9 | 0.15/0.5/2 | 0.20 | 0.06 | 40 | 86 | 94 (R) |
| 10 | 0.3/1.5/2 | 0.43 | 0.08 | 30 | 58 | 94 (R) |
| 11 | 0.3/1.5/2 | 0.43 | 0.08 | 40 | 74 | 95 (R) |
| 12 | 0.3/1.5/2 | 0.43 | 0.08 | 50 | 84 | 93 (R) |
| 13 | 0.3/1.5/2 | 0.43 | 0.08 | 60 | 97 | 93 (R) |
| 14 | 0.3/1.5/2 | 0.43 | 0.08 | 70 | 91 | 93 (R) |
| 15 | 0.3/0.5/0.5 | 0.50 | 0.23 | 60 | 83 | 94 (R) |
| 16 | 0.3/0.5/1 | 0.33 | 0.17 | 60 | 94 | 94 (R) |
| 17 | 0.3/0.5/1.5 | 0.25 | 0.13 | 60 | 98 | 93 (R) |
| 18 | 0.3/0.5/2 | 0.20 | 0.11 | 60 | 99 ^e | 95 (R) |
| 19 | 0.0/0.5/2 | 0.20 | 0.00 | 60 | 96 | 90 (R) |

^aPerformed with 0.5 mmol acetophenone, 2 mmol HCOONa, and 0.005 mmol (0.5 mol %) [RuCl(*p*-cymene)((*R,R*)-TsDPEN)] for 20 h, unless otherwise indicated. ^bYield determined via HPLC using phenol as internal standard. ^cThe enantiomeric excess was determined via HPLC using a DAICEL Chiracel IB column. ^dAbsolute configuration was determined via measurement of optical rotation values and comparison with literature data. ^eTurnover frequency was 370 h⁻¹.

(Table 1, entry 19). However, kinetic studies of the asymmetric transfer hydrogenation of acetophenone show that the reaction rate in the microemulsion formed upon addition of ionic liquid 3 is higher than in the conventional biphasic system (SI Figure S7), and a turnover frequency of 370 h⁻¹ could be achieved under optimized conditions. The nanometer-sized oil or water droplets in microemulsions provide highly dynamic nanoreactors, with the interface disintegrating and reforming on a time scale of milliseconds, which can promote favorable reaction kinetics.³²

While the variation of parameters could optimize yield and selectivity, several problems existed for workup and potential recycling of catalyst. After running the reaction at optimized conditions, the product was separated from the three-phase system formed. While the direct separation of product was possible, for convenience of handling on small scale, a mixture of *n*-heptane/diethyl ether (1:1, 2 mL) was added to facilitate phase separation and product extraction in the three-phase system. However, extensive leaching of the catalyst into the organic phase was observed by using [RuCl(*p*-cymene)((*R,R*)-TsDPEN)], which could be visually detected from the colorization of the organic phase (Figure 3, left).

To overcome the problems of catalyst leaching, which would inevitably result in product contamination and limited recyclability, we replaced the TsDPEN ligand with its water-soluble derivative (*R,R*)-2 (Scheme 1). The chiral water-soluble sulfonated product (*R,R*)-1 was prepared via treatment of commercially available (*R,R*)-DPEN with oleum according to the published methods, resulting in a mixture of different

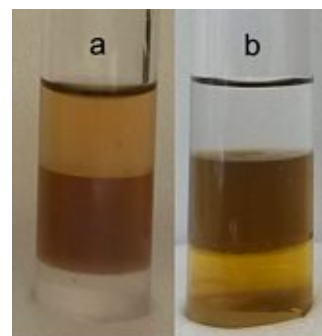


Figure 3. Phase distribution and leaching of catalyst into the oil phase in case of using (a) [RuCl(*p*-cymene)((*R,R*)-TsDPEN)], (b) [RuCl(*p*-cymene)((*R,R*)-2)]. Lower phase: aqueous layer, middle phase: catalyst containing surfactant-rich middle layer, upper phase: organic layer with product.

isomers.^{9,33} After purification of the crude sample by preparative HPLC, the major product, the bis-*meta*-sulfonated ligand, was isolated in 76% yield. The desired mono-*N*-tosylated derivative (*R,R*)-2 was obtained by subsequent tosylation in 62% yield.⁹ The water-soluble ruthenium catalyst [RuCl(*p*-cymene)((*R,R*)-2)] was prepared by reacting [RuCl₂(*p*-cymene)]₂ with (*R,R*)-2 at 40 °C for 1 h in aqueous media. As can be seen in Figure 3 (right), after running the reaction under similar conditions with [RuCl(*p*-cymene)((*R,R*)-2)], the organic phase remained colorless, suggesting that the ion-tagged ruthenium catalyst is efficiently immobilized in the surfactant-rich middle layer through additional interactions with the charged ionic liquid species and that there is no significant catalyst leaching into the organic layer.

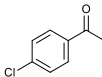
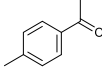
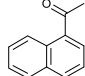
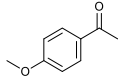
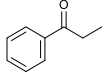
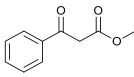
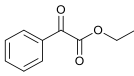
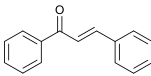
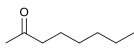
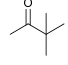
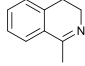
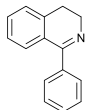
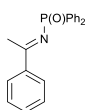
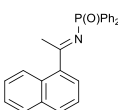
In order to quantify the effect of the ligand structure on the ruthenium leaching, ICP-OES measurements have been carried out from the corresponding *n*-heptane phases after the reaction. While 30 ppm of ruthenium were detected in the *n*-heptane phase in case of the unmodified [RuCl(*p*-cymene)((*R,R*)-TsDPEN)], only 2 ppm of ruthenium could be detected by switching to the ion-tagged and more hydrophilic [RuCl(*p*-cymene)((*R,R*)-2)], resulting in a significant improvement in the immobilization of the catalyst and confirming the previous qualitative results. Regarding the catalytic activity of the [RuCl(*p*-cymene)((*R,R*)-2)], as shown in Table 2, the obtained results were similar to those with the [RuCl(*p*-

Table 2. ATH of Acetophenone (5) in Different Microemulsion Systems

| entry ^a | ionic liquid | catalyst | con./yield ^{b,c} [%] | ee ^{d,e} [%] |
|--------------------|--------------|--|-------------------------------|-----------------------|
| 1 | 3 | [RuCl(<i>p</i> -cymene)((<i>R,R</i>)-TsDPEN)] | 99 (99) | 95 (R) |
| 2 | 3 | [RuCl(<i>p</i> -cymene)((<i>R,R</i>)-2)] | 99 (98) | 94 (R) |
| 3 | 4 | [RuCl(<i>p</i> -cymene)((<i>R,R</i>)-TsDPEN)] | 99 (99) | 93 (R) |
| 4 | 4 | [RuCl(<i>p</i> -cymene)((<i>R,R</i>)-2)] | 98 (96) | 94 (R) |

^aPerformed with ionic liquid/*n*-heptane/water 0.3/0.5/2 g, 0.5 mmol acetophenone, 2 mmol HCOONa, 0.005 mmol (0.5 mol %) catalyst at 60 °C for 24 h. ^bConversion determined via HPLC using phenol as internal standard. ^cIsolated yields after flash column chromatography given in brackets. ^dThe enantiomeric excess was determined via HPLC using a DAICEL Chiracel IB column. ^eAbsolute configuration was determined via measurement of optical rotation values and comparison with literature data.

Table 3. Scope and Limitations of ATH with a Variety of Ketones and Imines, Using Ionic-Liquid-Based Microemulsions

| Entry ^a | Substrate | Isolated yield ^b [%] | ee ^{c,d} [%] |
|--------------------|---|---------------------------------|------------------------------|
| 1 |  | 91 | 87 (<i>R</i>) |
| 2 |  | 85 | 97 (<i>R</i>) |
| 3 |  | 81 | 86 (<i>R</i>) |
| 4 |  | 68 | 88 (<i>R</i>) |
| 5 |  | 65 | 84 (<i>R</i>) |
| 6 |  | 73 | 94 (<i>R</i>) |
| 7 |  | 48 | 64 (<i>S</i>) |
| 8 |  | 64 | 55 (<i>R</i>) |
| 9 |  | 49 | 38 ^f (<i>S</i>) |
| 10 |  | < 1 ^c | n.d. |
| 11 |  | < 1 ^c | n.d. |
| 12 |  | 10 ^c | 26 (<i>R</i>) |
| 13 |  | 27 | 15 (<i>R</i>) |
| 14 |  | 15 | 42 (<i>R</i>) |

^aPerformed with IL 3/*n*-heptane/water 0.6/1/4 g, 1 mmol substrate, 4 mmol HCOONa, 0.01 mmol (0.5 mol %) [RuCl(*p*-cymene)((*R,R*)-2)] for 20 h at 60 °C. ^bIsolated yield after flash column chromatography. ^cYield determined by GC analysis. ^dThe enantiomeric excess was determined by chiral HPLC analysis. ^eAbsolute configuration was determined via measurement of optical rotation values and comparison with literature data. ^fDetermined by ¹⁹F{¹H} NMR after derivatization with (*S*)-Mosher's acid chloride.

cymene)((*R,R*)-TsDPEN)] under optimized conditions. However, a slightly longer reaction time of 24 h was required when using the hydrophilic ligand (*R,R*)-2 eventually giving the

product in excellent isolated yield and enantioselectivity. Almost identical behavior was found when using the ionic liquid [C₁₂dmim][(*i*-C₈)₂PO₂] (4) instead of [C₁₂mim]-

$[(C_8)_2PO_2]$ (3), indicating that the acidic proton in position 2 of the imidazolium is not involved in the process.

We subsequently investigated the substrate scope for a wider range of ketones and imines under the previously optimized conditions. While the ATH of 4'-methylacetophenone (Table 3, entry 2), gave similarly high ee of 97% compared to the reduction of acetophenone, other substituted aromatic ketones (Table 3, entries 1, 3–5) gave lower enantioselectivities (84–88% ee). High enantioselectivity was also observed for the ATH of a β -ketoester, whereas lower yield and selectivity was found for the corresponding α -analogue compound (Table 3, entries 6 and 7). This difference between the two types of ketoesters might be explained with the strong functional group chelation of the β -ester carbonyl with the chiral ligand, further stabilizing the diastereomeric transition states and thus leading to an overall higher enantiocontrol and higher reaction rate. In the case of (*E*)-chalcone, a double reduction was observed, resulting in 1,3-diphenylpropan-1-ol as the major product (Table 3, entry 8). These results are in good agreement with the previous reports.¹⁰

As expected from literature data, the reduction of aliphatic ketones is considerably more difficult and resulted in poor yield and enantioselectivity or no conversion at all (Table 3, entries 9 and 10).^{34–37} This can be based on the lack of π -CH interaction that plays a key role in the enantiocontrol when using ruthenium- or rhodium-arene catalysts for the reduction of aromatic ketones.³⁷

Apart from the reduction of ketones, Noyori-type complexes can be equally effective in the ATH of imines.^{38,39} Unlike the ATH reactions of ketones, this kind of transfer hydrogenation proceed via an ionic mechanism in which acidic activation of the imine starting materials is required.^{40,41} Therefore, the azeotropic mixture of formic acid and triethylamine (5:2 molar ratio) rather than sodium formate is used as a powerful and nonreversible hydrogen source.^{40,42} The microemulsion system shown here was also suitable for the reduction of imines (Table 3, entries 11–14). However, since the applied conditions were optimized for the reduction of ketones rather than imines, it is not surprising that yields remain low for all imines evaluated in the current work.

The recovery of the catalytic system was also tested by carrying out consecutive cycles with the water-soluble catalyst $[RuCl(p\text{-cymene})((R,R)\text{-}2)]$ in the optimized microemulsion system. After complete conversion of acetophenone, the product was carefully extracted from the microemulsion, while the catalyst remained immobilized in the intermediate phase. The vial was loaded with fresh acetophenone and 2.0 equiv of HCOOH to regenerate HCOONa. In general, catalytic activity with high enantioselectivity could be maintained for three cycles, although a decrease in conversion was observed in each recycling cycle (Table 4). The water-soluble ligand (*R,R*)-2 was more suitable for recycling with $[(C_{12}mim)[(C_8)_2PO_2]$ (3) and $[(C_{12}dmim)[(C_8)_2PO_2]$ (4), as higher conversions were observed compared with the result obtained from the TsDPEN-ligand reactions (e.g., Table 4, entries 1–3 vs 4–6). This can be associated with the prevention of leaching when the sulfonated ligand (*R,R*)-2 was used.

As we observed during the recycling experiments, the color of the solution changes from orange to dark brown, which indicates decomposition of the catalyst (Figure 3). In fact, recent studies by Hall et al. on the ruthenium-catalyzed transfer hydrogenation of acetophenone with isopropanol/

Table 4. Catalyst Recycling in the ATH of Acetophenone in the Presence of Ionic Liquids $[(C_8)_2PO_2]$ (3) and $[(C_{12}dmim)[(C_8)_2PO_2]$ (4)

| entry ^a | ionic liquid | catalyst | run | con. ^b [%] | ee ^{c,d} [%] |
|--------------------|--------------|--|-----|-----------------------|-----------------------|
| 1 | 3 | $[RuCl(p\text{-cymene})((R,R)\text{-}TsDPEN)]$ | 1 | 99 | 95 (R) |
| 2 | | | 2 | 62 | 92 (R) |
| 3 | | | 3 | 40 | 91 (R) |
| 4 | 3 | $[RuCl(p\text{-cymene})((R,R)\text{-}2)]$ | 1 | 99 | 94 (R) |
| 5 | | | 2 | 67 | 93 (R) |
| 6 | | | 3 | 46 | 92 (R) |
| 7 | 4 | $[RuCl(p\text{-cymene})((R,R)\text{-}TsDPEN)]$ | 1 | 99 | 94 (R) |
| 8 | | | 2 | 48 | 86 (R) |
| 9 | | | 3 | 16 | 59 (R) |
| 10 | 4 | $[RuCl(p\text{-cymene})((R,R)\text{-}2)]$ | 1 | 98 | 94 (R) |
| 11 | | | 2 | 62 | 88 (R) |
| 12 | | | 3 | 39 | 66 (R) |

^aPerformed with IL/*n*-heptane/water 0.6/1/4 g, 1 mmol acetophenone, 4 mmol HCOONa, 0.01 mmol (0.5 mol %) catalyst for 20 h at 60 °C. ^bConversion determined via HPLC using phenol as internal standard. ^cThe enantiomeric excess values were determined via chiral HPLC using a DAICEL Chiracel IB column. ^dAbsolute configuration was determined via measurement of optical rotation values and comparison with literature data.

KOH identified different pathways for the deactivation of the active hydride species, identifying the loss of the arene ligand as key step in the formation of ruthenium nanoparticles as ultimate degradation product.⁴³ Comparable results were also reported by several other research groups, indicating that the stability of the catalytic system rather than the immobilization of the complex is the limiting factor in these recycling experiments.^{12,44,45}

CONCLUSIONS

Herein, we showed that microemulsions based on the surface-active ionic liquids $[(C_{12}mim)[(C_8)_2PO_2]$ (3) and $[(C_{12}dmim)[(C_8)_2PO_2]$ (4) can be successfully applied for Ru-catalyzed asymmetric transfer hydrogenation of acetophenone. High yields and enantioselectivities were observed under optimized conditions in the case of aromatic ketones. Moreover, the temperature-dependent phase behavior of the microemulsion allowed for high reactivity in combination with facile product separation. The optimized microemulsion system could be applied to a wide range of aromatic ketones that were reduced with good isolated yields and selectivities, while aliphatic ketones were less successful.

Furthermore, it was shown that the use of a water-soluble ligand (*R,R*)-2 can improve immobilization of the catalyst in the intermediate phase and decrease the leaching in the organic phase, meanwhile the excellent conversion and enantioselectivity was also maintained in the case of reduction of acetophenone. However, only moderate results were obtained when studying recycling and reuse of the catalyst due to decomposition, indicating that there are still limitations when applying ionic-liquid-based microemulsion systems for asymmetric transfer hydrogenations.

EXPERIMENTAL SECTION

Materials and Methods. All reagents were purchased from commercial suppliers and used without further purification unless otherwise noted. Ionic liquids $[(C_{12}mim)\text{-}$

$[(C_8)_2PO_2]$ (3) and $[C_{12}dmim][[(C_8)_2PO_2]$ (4) were prepared according to previously reported procedures and dried for at least 24–48 h at room temperature or 50 °C and 0.01 mbar before use.^{46,24} Melting points were measured on an automated melting point system OPTI MELT of Stanford Research Systems. ¹H NMR, ¹³C NMR, and ¹⁹F NMR spectra were recorded on a Bruker Advance UltraShield 400 (400 MHz) spectrometer and chemical shifts (δ) are reported in ppm, using tetramethylsilane as internal standard. Coupling constants (J) are reported in Hertz (Hz). The following abbreviations were used to explain the multiplicities: s = singlet, d = doublet, t = triplet, q = quartet, quin. = quintet, sex. = sextet, m = multiplet, brs = broad singlet. HPLC analysis for determination of yield and conversion were performed on a Jasco HPLC unit equipped with a PDA detector and a C18 column (Maisch Reprosil 100, 250 \times 4.6 mm, 5 μ m) at 30 °C, using acetonitrile and water (ACN: H₂O 30:70 + 0.1% trifluoroacetic acid) as the mobile phase at a flow rate of 0.8 mL min⁻¹. The detection wavelength was at 210 nm. Phenol was used as internal standard, and calibration curves were prepared in the range from 2.0 to 0.01 mg mL⁻¹ for starting material and product. The enantiomeric excess values were determined via HPLC analysis on a DAIONEX UPLC that was equipped with a photodiode array (PDA) plus detector (190–360 nm), using a DAICEL IB or AS-H column (250 \times 4.60 mm, 5 μ m), mixtures of *n*-heptane/*i*-PrOH or *n*-hexane/EtOH as solvent, and flow rate of 0.7–1 mL min⁻¹. Reversed-phase flash chromatography was performed on a Grace Reveleris X2 preparative system using Phenomenex Luna C18 column (250 \times 21.2 mm, 10 μ m) at a flow rate of 15 mL min⁻¹. Optical rotation was measured on an Anton Paar MCP500 polarimeter at the specified conditions, and the concentrations are stated in g/100 mL. ICP-OES measurements were carried out on a radial ICP-OES spectrometer (Thermo iCAP 6500, Thermo Scientific, U.S.A.) by using a V-groove nebulizer (Thermo Scientific, U.S.A.) at 1400 W and argon as plasma gas. The flow of the nebulizer gas, cooling gas, and auxiliary gas were 0.5, 12, and 0.8 L min⁻¹, respectively. A solution of 5% *n*-octanol in conostan was used for the sample dilution. Signal intensities measured at the wavelength of 267.876 nm were used for the quantification of ruthenium, while emission lines 240.272 and 266.161 were used for monitoring and quality control during the measurements. Calibration curves for the quantification of ruthenium were prepared from a stock solution of Noyori catalyst $[RuCl(p\text{-cymene})((R,R)\text{-TsDPEN})]$ in 1-octanol in a range of 0.5–3.5 ppm. To correct for potential instrument drifts as well as nonspectral interferences, indium has been added to all standard and sample solutions; for quantification, the obtained ruthenium signals were normalized using the indium response measured at the wavelength of 230.606 nm.

Phase Diagrams. The phase behavior of water/*n*-heptane/ $[C_{12}mim][[(C_8)_2PO_2]$ (3) in the presence of HCOONa, acetophenone (5), and 1-phenylethanol (6) at different temperatures was determined by visual inspection titration of the mixture with $[C_{12}mim][[(C_8)_2PO_2]$ (3) at different temperatures. After adding a certain amount of ionic liquid, the mixture was stirred magnetically and left to equilibrate in a thermostated heating block. After visual assessment of phase behavior, new ionic liquid was added, and the procedure was repeated until clear phases were obtained.

Synthesis of (R,R)-2.^{9,33} A round-bottomed flask charged with 10 mL of oleum (65%) was cooled to 0 °C using an ice

bath. (R,R)-DPEN (1 g, 4.7 mmol) was added batchwise. The mixture was stirred for 24 h at 0 °C to room temperature. The viscous mixture was poured onto 100 g of crushed ice with vigorous stirring. After the pH value of the solution was adjusted to 9 with solid NaOH, the aqueous phase was washed with DCM. After removal of the water under reduced pressure, a yellow solid was obtained. The crude product was redissolved in 50 mL of CH₃OH, and the insoluble compound was removed by filtration. The product was purified by RP chromatography and 1.6 g (yield: 76%) of white solid (R,R)-1 was obtained. mp > 280 °C (decomposition); $[\alpha]_D^{20} +36.13$ ($c = 1.1$, H₂O); ¹H NMR (400 MHz; D₂O) δ : 5.15 (2H, s, 2 \times CHNH₂), 7.27 (2H, d, $J = 7.84$ Hz, *H*-arom), 7.39 (2H, t, $J = 7.86$ Hz, *H*-arom), 7.66 (2H, s, *H*-arom), 7.71 (2H, d, $J = 7.81$ Hz, *H*-arom).

Compound (R,R)-1 (1.5 g, 3.3 mmol) and Na₂CO₃ (1.4 g, 13.2 mmol) were dissolved in 20 mL of H₂O, then a THF solution (20 mL) of TsCl (759 mg, 3.9 mmol) was added to the aqueous solution dropwise with vigorously stirring at 0 °C. Once the addition was completed, the resulting mixture was warmed up to 40 °C and stirred for 24 h. This was followed by washing the aqueous layer with Et₂O and removal of the water under reduced pressure. The residue was redissolved in 50 mL of CH₃OH, followed by the removal of the insoluble compound by filtration. After concentration under reduced pressure, the resulting solid was purified by RP chromatography, and 1.2 g (yield: 62%) of colorless solid product (R,R)-2 was obtained. mp 240–249 °C; $[\alpha]_D^{20} +320.23$ ($c = 1.01$, H₂O); ¹H NMR (400 MHz; D₂O) δ : 1.95 (3H, s, CH₃), 4.57 (1H, d, $J = 8.9$ Hz, CHNH₂), 4.64 (1H, d, $J = 9.1$ Hz, CHNH), 6.58 (1H, d, $J = 7.8$ Hz, *H*-arom), 6.68 (1H, d, $J = 7.1$ Hz, *H*-arom), 6.75 (2H, d, $J = 8.3$ Hz, *H*-arom), 7.12–7.20 (6H, m, *H*-arom), 7.44–7.46 (1H, m, *H*-arom), 7.56 (1H, s, *H*-arom). ¹³C NMR (100 MHz; CDCl₃) δ : 20.4 (CH₃), 58.3 (CHNH₂), 60.6 (CHNH), 123.8 (C-arom), 124.2 (C-arom), 125.0 (C-arom), 126.1 (C-arom), 126.5 (C-arom), 126.6 (C-arom), 128.4 (C-arom), 129.0 (C-arom), 129.5 (C-arom), 129.8 (C-arom), 130.5 (C-arom), 131.1 (C-arom), 133.1 (C-arom), 134.4 (C-arom), 134.6 (C-arom), 142.7 (C-arom), 143.3 (C-arom), 144.8 (C-arom).

Synthesis of 1-Methyl-3,4-dihydroisoquinoline (Table 3, Entry 11).⁴⁷ Freshly distilled 2-phenylethylamine (1.49 g, 12.3 mmol) was dissolved in anhydrous pyridine (1.1 mL, 12.5 mmol), and acetic anhydride (1.22 mL, 12.8 mmol) was slowly added with a syringe. The reaction mixture was stirred at 90 °C for 2 h and subsequently allowed to cool to room temperature. Then the mixture was poured onto 25 g of ice and stirred for 5 min before 11 mL of HCl was added. The aqueous phase was extracted with EtOAc (3 \times 20 mL). The combined organic phases were subsequently washed with saturated NaHCO₃ solution, dried over Na₂SO₄, and the solvent was removed under reduced pressure. *N*-Phenethylacetamide was obtained as a light yellow solid (1.51 g, 75%) and could be used without further purification. In a round-bottom flask, P₂O₅ (2.90 g, 10.2 mmol) and POCl₃ (2.86 mL, 30.6 mmol) were mixed in 50 mL of *o*-xylene. *N*-Phenethylacetamide (1.33 g, 8.1 mmol) was added, and the mixture was refluxed for 20 h. After it was cooled to room temperature, the mixture was neutralized with 2 M NaOH. The phases were separated, and the aqueous phase was extracted with Et₂O. The combined organic phases were dried over Na₂SO₄, and the solvent was removed under reduced pressure. The crude product was purified via Kugelrohr distillation (0.4 mbar, 75 to 100 °C). 1-Methyl-

3,4-dihydroisoquinoline was obtained as a colorless liquid (948 mg, 54%). $^1\text{H NMR}$ (400 MHz; CDCl_3) δ : 2.33 (3H, s, CH_3), 2.62 (2H, t, $J = 7.1$ Hz, CCH), 3.60 (2H, t, $J = 6.1$ Hz, NCH_2), 7.08–7.24 (4H, m, H -arom).

Synthesis of 1-Phenyl-3,4-dihydroisoquinoline (Table 3, Entry 12).⁴⁸ 1-Phenyl-1,2,3,4-tetrahydroisoquinoline (628 mg, 3 mmol) was dissolved in 12.5 mL of DMF and stirred at 100 °C. After the reaction was completed, the solvent was removed from the crude reaction mixture under reduced pressure. The crude product was purified via column chromatography, and 1-phenyl-3,4-dihydroisoquinoline was obtained as colorless solid (94%). $^1\text{H NMR}$ (400 MHz; CDCl_3) δ : 2.80 (2H, t, $J = 7.1$ Hz, CCH), 3.85 (2H, t, $J = 7.4$ Hz, NCH_2), 7.28–7.63 (9H, m, H -arom).

General Procedure for the Preparation of *N*-Diphenylphosphinoyl Ketoimines (Table 3, Entries 13,14).⁴⁹ *N*-Diphenylphosphinoyl ketoimines were prepared according to the published method: To a stirred solution of $\text{NH}_2\text{OH}\cdot\text{HCl}$ (1.81 g, 26 mmol) and NaOAc (2.13 g, 26 mmol) in $\text{EtOH}/\text{H}_2\text{O}$ (1/1, 16 mL), ketone (18 mmol) was added and heated to reflux. After complete conversion, the mixture was cooled to –10 °C and left to crystallize for 24 h. The solid was filtered and washed with water. The product was dried and used directly for the next step. To a stirred solution of the corresponding oxime (9.6 mmol) and triethylamine (9.6 mmol) in petroleum ether/ CH_2Cl_2 (1/1, 30 mL), a solution of chlorodiphenylphosphine (10 mmol) in CH_2Cl_2 (5 mL) was added over 30 min at –45 °C. The mixture was stirred for 1 h at room temperature before the solvent was evaporated. The residue was dissolved in CH_2Cl_2 , washed with sat. NaHCO_3 brine, dried over Na_2SO_4 , and concentrated. The residue was purified by flash column chromatography using EtOAc /petroleum ether (1/1) as eluent. The product was further purified by recrystallization from $\text{CH}_2\text{Cl}_2/n$ -hexane.

P,P-Diphenyl-*N*-[(1*E*)-1-phenylethylidene]phosphinic Amide. $^1\text{H NMR}$ (400 MHz; CDCl_3) δ : 2.37 (3H, s, CH_3), 7.18–7.47 (11H, m, H -arom), 7.51–7.87 (4H, m, H -arom).

N-Diphenylphosphoryl-1-naphthalen-2-ylethanamine. $^1\text{H NMR}$ (400 MHz; CDCl_3) δ : 3.03 (3H, s, CH_3), 7.26–7.51 (10H, m, H -arom), 7.53–7.98 (7H, m, H -arom).

General Procedure for Parameter Optimization. A mixture of $[\text{RuCl}(p\text{-cymene})((R,R)\text{-TsDPEN})]$ (3.18 mg, 0.005 mmol), $[\text{C}_{12}\text{mim}][(\text{C}_8)_2\text{PO}_2]$ (0.3 g), sodium formate (136 mg, 2 mmol), degassed water (2 g), *n*-heptane (0.5 g), and acetophenone (60.08 mg, 0.5 mmol) was stirred in an oil bath at 60 °C under argon atmosphere for 20 h. The reaction mixture was diluted with MeOH to a total volume of 50 mL to obtain a homogeneous solution. A sample (200 μL) was taken, diluted with MeOH (800 μL), and an internal standard (200 μL of phenol in MeOH stock solution) was added. The sample was thoroughly mixed, filtered over a syringe filter (0.2 μm) and analyzed by Jasco HPLC. The enantiomeric excess values were determined via chiral HPLC. This strategy was also assessed to study kinetic behavior.

General Procedure for Product Isolation. A mixture of $[\text{Ru}(p\text{-cymene})\text{Cl}_2]_2$ (1.53 mg, 0.0025 mmol), (*R,R*)-2 (3.62 mg, 0.006 mmol), and degassed water (2 g) was stirred at 40 °C under argon atmosphere for 1 h. After it was cooled to room temperature, ionic liquid ($[\text{C}_{12}\text{mim}][(\text{C}_8)_2\text{PO}_2]$ (3) or $[\text{C}_{12}\text{dmim}][(\text{C}_8)_2\text{PO}_2]$ (4) (0.3 g), sodium formate (136 mg, 2 mmol), *n*-heptane (0.5 g) and ketone (0.5 mmol) were subsequently added, and the reaction mixture was reacted at 60 °C for 24 h. After it was cooled to room temperature, the

three-phase reaction mixture was extracted with degassed *n*-heptane/diethyl ether (1/1, 2 mL) four times. The combined extracts were concentrated in vacuum to afford the desired products that were further purified via flash column chromatography over silica.

Recycling Strategy for the Asymmetric Transfer Hydrogenation of Acetophenone. After the extraction of product, the residual microemulsion and aqueous phases containing the catalyst, ligand and ionic liquid were reused by adding formic acid (2 equiv) to regenerate sodium formate. Fresh acetophenone was added into the aqueous solution, and the next cycle of the reaction was started under the same conditions.

(R)-2-Phenylethanol:⁵⁰ $^1\text{H NMR}$ (400 MHz; CDCl_3) δ : 1.38 (3H, d, $J = 6.5$ Hz, CH_3), 2.89 (1H, s, OH), 4.73 (1H, q, $J = 6.4$ Hz, CH_2CH), 7.19–7.28 (5H, m, H -arom). Determination of enantiomeric excess: DAICEL Chiracel IB column, *n*-hexane/*i*-PrOH, 98.5/1.5 V/V, 1.0 mL min^{-1} , 25 °C, UV 254 nm: t_R (*R*) = 14.8 min, t_R (*S*) = 16.7 min (95% ee).

(R)-1-(4-Chlorophenyl)ethanol:⁵⁰ $^1\text{H NMR}$ (400 MHz; CDCl_3) δ : 1.41 (3H, d, CH_3 , $J = 6.3$ Hz), 3.16 (1H, s, OH), 4.77 (1H, q, $J = 6.4$ Hz, CH_2CH), 7.25 (4H, quin., H -arom). Determination of enantiomeric excess: DAICEL Chiracel IB column, *n*-hexane/*i*-PrOH, 98.5/1.5 V/V, 1.0 mL min^{-1} , 25 °C, UV 254 nm: t_R (*R*) = 15.5 min, t_R (*S*) = 14.8 min (87% ee).

(R)-1-(*p*-Tolyl)ethanol:⁵⁰ $^1\text{H NMR}$ (400 MHz; CDCl_3) δ : 1.50 (3H, d, $J = 6.4$ Hz, CH_3), 2.39 (3H, s, CCH_3), 2.66 (1H, s, OH), 4.83 (1H, q, $J = 6.4$ Hz, CH_2CH), 7.17–7.30 (4H, m, H -arom). Determination of enantiomeric excess: DAICEL Chiracel IB column, *n*-hexane/*i*-PrOH, 98.5/1.5 V/V, 1.0 mL min^{-1} , 25 °C, UV 254 nm: t_R (*R*) = 18.4 min, t_R (*S*) = 16.3 min (97% ee).

(R)-1-(1'-Naphthyl)ethanol:⁵¹ $^1\text{H NMR}$ (400 MHz; CDCl_3) δ : 1.50 (3H, d, $J = 6.7$ Hz, CH_3), 2.23 (1H, s, OH), 5.45 (1H, q, $J = 6.4$ Hz, CH_2CH), 7.18–7.96 (7H, m, H -arom). Determination of enantiomeric excess: DAICEL Chiracel IB column, *n*-heptane/*i*-PrOH, 93/7 V/V, 1.0 mL min^{-1} , 25 °C, UV 254 nm: t_R (*R*) = 12.1 min, t_R (*S*) = 9.3 min (86% ee).

(R)-1-(4-Methoxyphenyl)ethanol:⁵⁰ $^1\text{H NMR}$ (400 MHz; CDCl_3) δ : 1.33 (3H, d, $J = 6.3$ Hz, CH_3), 2.53 (1H, s, OH), 3.67 (3H, s, CH_3), 4.67 (1H, q, $J = 6.5$ Hz, CH_2CH), 6.74 (2H, d, $J = 8.7$ Hz, H -arom), 7.15 (2H, d, H -arom, $J = 8.6$ Hz). Determination of enantiomeric excess: DAICEL Chiracel IB column, *n*-hexane/*i*-PrOH, 98.5/1.5 V/V, 1.0 mL min^{-1} , 25 °C, UV 254 nm: t_R (*R*) = 21.6 min, t_R (*S*) = 23.3 min (88% ee).

(R)-1-Phenylpropan-1-ol:⁵⁰ $^1\text{H NMR}$ (400 MHz; CDCl_3) δ : 0.85 (3H, d, $J = 7.3$ Hz, CH_3), 1.67–1.77 (3H, m, OH, CH_2CH_2), 4.52 (1H, t, $J = 6.2$ Hz, CH_2CHC), 7.18–7.29 (5H, m, H -arom). Determination of enantiomeric excess: DAICEL Chiracel IB column, *n*-hexane/*i*-PrOH, 98.5/1.5 V/V, 1.0 mL min^{-1} , 25 °C, UV 254 nm: t_R (*R*) = 11.6 min, t_R (*S*) = 12.8 min (84% ee).

(R)-Methyl 3-hydroxy-3-phenylpropanoate:⁵² $^1\text{H NMR}$ (400 MHz; CDCl_3) δ : 1.25 (3H, t, $J = 7.1$ Hz, CH_3), 2.71 (2H, q, $J = 8.0$ Hz, CH_2CH_2), 3.41 (1H, s, OH), 4.15 (2H, q, $J = 14.0$ Hz, CHCH_2), 5.11 (1H, q, $J = 5.2$ Hz, CH), 7.30–7.37 (5H, m, H -arom). Determination of enantiomeric excess: AS-H column, *n*-heptane/*i*-PrOH 98/2 V/V, of 0.7 mL min^{-1} , 25 °C, UV 254 nm: t_R (*R*) = 17.8 min, t_R (*S*) = 19.1 min (94% ee).

(*S*)-Ethyl 2-hydroxy-2-phenylacetate:⁵³ ¹H NMR (400 MHz; CDCl₃) δ: 1.14 (3H, t, *J* = 7.1 Hz, CH₃), 3.40 (1H, s, OH), 4.09–4.17 (2H, m, CH₂CH₂), 5.07 (1H, s, CH), 7.24–7.33 (5H, m, *H*-arom). Determination of enantiomeric excess: AS-H column, *n*-heptane/*i*-PrOH 98/2 V/V, of 0.7 mL min⁻¹, 25 °C, UV 254 nm: *t*_R (*R*) = 11.0 min, *t*_R (*S*) = 9.2 min (64% ee).

(*R*)-1,3-Diphenylpropan-1-ol:⁵⁴ ¹H NMR (400 MHz; CDCl₃) δ: 1.94–2.07 (3H, m, OH, CHCH₂), 2.59–2.71 (2H, m, CH₂CH₂C), 4.59 (1H, q, *J* = 4.0 Hz, CH₂CHC), 7.14–7.27 (10H, m, *H*-arom). Determination of enantiomeric excess: DAICEL Chiracel IB column, *n*-heptane/*i*-PrOH, 93/7 V/V, 1.0 mL min⁻¹, 25 °C, UV 254 nm: *t*_R (*R*) = 14.3 min, *t*_R (*S*) = 11.8 min (58% ee).

(*S*)-Octan-2-ol:⁵⁵ ¹H NMR (400 MHz; CDCl₃) δ: 0.86 (3H, t, *J* = 7.04 Hz, CH₃), 1.15 (3H, d, *J* = 6.2 Hz, CHCH₃), 1.26–1.44 (10H, m, CH₂), 2.15 (1H, s, OH), 3.73–3.77 (1H, m, CH). Determination of Enantiomeric Excess. 2-Octanol (0.1 mmol) was dissolved in anhydrous dichloromethane (1 mL). Triethylamine (21 μL, 0.15 mmol) and (*S*)-Mosher's acid chloride (22 μL, 0.12 mmol) were added, and the reaction mixture was stirred at 25 °C. After completion, 5 mL of dichloromethane was added, and the organic phase was successively washed with 0.5 M Na₂CO₃ and water, dried over Na₂SO₄, and concentrated *in vacuo*. The enantiomeric composition was analyzed by ¹⁹F{¹H} NMR measurement. ¹⁹F{¹H} NMR (100 MHz; CDCl₃) δ: -70.02, (minor diastereomer), -71.69 (major diastereomer) (38% ee).

1-Phenyl-1,2,3,4-tetrahydroisoquinoline:⁵⁶ ¹H NMR (400 MHz; CDCl₃) δ: 2.00 (1H, brs, NH), 2.73–2.78 (1H, m, CH_{2a}-NH), 2.94–3.06 (2H, m, CH₂-CH₂-NH), 3.19–3.23 (1H, m, CH_{2b}-NH), 5.04 (1H, s, CH-NH), 6.68 (1H, d, *J* = 7.6 Hz, *H*-arom), 6.94–6.98 (1H, m, *H*-arom), 7.07–7.08 (2H, m, *H*-arom), 7.19–7.26 (5H, m, *H*-arom). Determination of enantiomeric excess: DAICEL Chiracel IB column, *n*-hexane/EtOH, 85/15 V/V, 1.0 mL min⁻¹, 25 °C, UV 254 nm: *t*_R (*R*) = 4.9 min, *t*_R (*S*) = 5.5 min (26% ee).

(*R*)-*P,P*-Diphenyl-*N*-(1-phenylethylidene)phosphinic amide:⁵⁷ ¹H NMR (400 MHz; CDCl₃) δ: 1.48 (3H, d, *J* = 6.74, CH₃), 3.32 (1H, brs, NH), 4.31 (1H, q, *J* = 6.74, CH₃CH), 7.19–7.38 (11H, m, *H*-arom), 7.70–7.87 (4H, m, *H*-arom). Determination of enantiomeric excess: DAICEL Chiracel IB column, *n*-hexane/EtOH, 90/10 V/V, 1.0 mL min⁻¹, 25 °C, UV 254 nm: *t*_R (*R*) = 7.0 min, *t*_R (*S*) = 10.3 min (15% ee).

(*R*)-*N*-(1-(Naphthalen-1-yl)ethyl)-*P,P*-diphenylphosphinic amide:⁵⁷ ¹H NMR (400 MHz; CDCl₃) δ: 1.62 (3H, d, *J* = 6.67, CH₃), 3.26 (1H, brs, NH), 5.15 (1H, quin., *J* = 6.70, CH₃CH), 7.27–7.83 (17H, m, *H*-arom). Determination of enantiomeric excess: DAICEL Chiracel IB column, *n*-hexane/EtOH, 90/10 V/V, 1.0 mL min⁻¹, 25 °C, UV 254 nm: *t*_R (*R*) = 21.5 min, *t*_R (*S*) = 19 min (42% ee).

■ ASSOCIATED CONTENT

Supporting Information

The Supporting Information is available free of charge on the ACS Publications website at DOI: 10.1021/acs.oprd.9b00150.

Phase diagrams, kinetic study for the ATH of acetophenone, and copies of NMR spectra of all compounds (PDF)

■ AUTHOR INFORMATION

Corresponding Author

*E-mail: katharina.schroeder@tuwien.ac.at. Tel: +43 1 58801 163601.

ORCID

Katharina Bica-Schröder: 0000-0002-2515-9873

Notes

The authors declare no competing financial interest.

■ ACKNOWLEDGMENTS

Financial support by the Austrian Science Fund (FWF project P25504-N28 and P29146-N34) is gratefully acknowledged. The authors are grateful to Prof. Andreas Limbeck (Institute of Chemical Technologies and Analytics) for help and assistance with ICP measurements.

■ REFERENCES

- (1) Kang, G.; Lin, S.; Shiwakoti, A. B.; Ni, B. Imidazolium ion tethered TsDPENs as efficient water-soluble ligands for rhodium catalyzed asymmetric transfer hydrogenation of aromatic ketones. *Ni. Catal. Commun.* **2014**, *57*, 111–114.
- (2) Wang, D.; Astruc, D. The golden age of transfer hydrogenation. *Chem. Rev.* **2015**, *115*, 6621–6686.
- (3) Karakaş, D. E.; Durap, F.; Baysal, A.; Ocak, Y. S.; Rafikova, K.; Kaya, E. Ç.; Zazybin, A.; Temel, H.; Kayan, C.; Meriç, N.; Aydemir, M. Transfer hydrogenation reaction using novel ionic liquid based Rh(I) and Ir(III)-phosphinite complexes as catalyst. *J. Organomet. Chem.* **2016**, *824*, 25–32.
- (4) Fujii, A.; Hashiguchi, S.; Uematsu, N.; Ikariya, T.; Noyori, R. Ruthenium(II)-Catalyzed Asymmetric Transfer Hydrogenation of Ketones Using a Formic Acid–Triethylamine Mixture. *J. Am. Chem. Soc.* **1996**, *118*, 2521–2522.
- (5) Nishibayashi, Y.; Singh, J. D.; Arikawa, Y.; Uemura, S.; Hidai, M. Rhodium(I)-, iridium(I)-, and ruthenium(II)-catalyzed asymmetric transfer hydrogenation of ketones using diferrocenyl dichalcogenides as chiral ligands. *J. Organomet. Chem.* **1997**, *531*, 13–18.
- (6) Noyori, R.; Takaya, H. BINAP: an efficient chiral element for asymmetric catalysis. *Acc. Chem. Res.* **1990**, *23*, 345–350.
- (7) Hashiguchi, S.; Fujii, A.; Takehara, J.; Ikariya, T.; Noyori, R. Asymmetric Transfer Hydrogenation of Aromatic Ketones Catalyzed by Chiral Ruthenium(II) Complexes. *J. Am. Chem. Soc.* **1995**, *117*, 7562–7563.
- (8) Bubert, C.; Blacker, J.; Brown, S. M.; Crosby, J.; Fitzjohn, S.; Muxworthy, J. P.; Thorpe, T.; Williams, J. M. Synthesis of water-soluble aminosulfonamide ligands and their application in enantioselective transfer hydrogenation. *Tetrahedron Lett.* **2001**, *42*, 4037–4039.
- (9) Li, J.; Li, X.; Ma, Y.; Wu, J.; Wang, F.; Xiang, J.; Zhu, J.; Wang, Q.; Deng, J. Surfactant-accelerated asymmetric transfer hydrogenation with recyclable water-soluble catalyst in aqueous media. *RSC Adv.* **2013**, *3*, 1825–1834.
- (10) Liu, X.; Chen, C.; Xiu, Y.; Chen, A.; Guo, L.; Zhang, R.; Chen, J.; Hou, Z. Asymmetric transfer hydrogenation of ketones catalyzed by thermoregulated ionic liquid-regulating ruthenium complexes. *Catal. Commun.* **2015**, *67*, 90–94.
- (11) Rhyoo, H. Y.; Park, H.-E.; Chung, Y. K. The first Ru(II)-catalyzed asymmetric hydrogen transfer reduction of aromatic ketones in aqueous media. *Chem. Commun.* **2001**, 2064–2065.
- (12) Rhyoo, H. Y.; Park, H.-J.; Suh, W. H.; Chung, Y. K. Use of surfactants in water-soluble ruthenium(II) complex-catalyzed asymmetric hydrogen-transfer reduction of aromatic ketones. *Tetrahedron Lett.* **2002**, *43*, 269–272.
- (13) Cortez, N. A.; Aguirre, G.; Parra-Hake, M.; Somanathan, R. Water-soluble chiral monosulfonamide-cyclohexane-1,2-diamine-RhCp* complex and its application in the asymmetric transfer

hydrogenation (ATH) of ketones. *Tetrahedron Lett.* **2007**, *48*, 4335–4338.

(14) Zhou, Z.; Ma, Q.; Sun, Y.; Zhang, A.; Li, L. Ruthenium(II)-catalyzed asymmetric transfer hydrogenation of aromatic ketones in water using novel water-soluble chiral monosulfonamide ligands. *Heteroat. Chem.* **2010**, *21*, 505–514.

(15) Vasiliou, M.; Gaertner, P.; Zirbs, R.; Bica, K. Coordinating Chiral Ionic Liquids: Design, Synthesis, and Application in Asymmetric Transfer Hydrogenation under Aqueous Conditions. *Eur. J. Org. Chem.* **2015**, *2015*, 2374–2381.

(16) Kalsin, A. M.; Peganova, T. y. A.; Novikov, V. V.; Zhamoytina, A. I.; Gonsalvi, L.; Peruzzini, M. Transfer Hydrogenation of Ketones Catalyzed by Surface-Active Ruthenium and Rhodium Complexes in Water. *Chem. - Eur. J.* **2014**, *20*, 846–854.

(17) Li, X.; Chen, W.; Hems, W.; King, F.; Xiao, J. Asymmetric transfer hydrogenation of ketones with a polymer-supported chiral diamine. *Tetrahedron Lett.* **2004**, *45*, 951–953.

(18) Vasiliou, M.; Rainer, D.; Gaertner, P.; Reichel, C.; Schroeder, C.; Bica, K. Basic chiral ionic liquids: A novel strategy for acid-free organocatalysis. *Catal. Today* **2013**, *200*, 80–86.

(19) Vasiliou, M.; Leder, S.; Gaertner, P.; Mereiter, K.; Bica, K. Coordinating chiral ionic liquids. *Org. Biomol. Chem.* **2013**, *11*, 8092–8102.

(20) Pálvolgyi, Á. M.; Bitai, J.; Zeindlhofer, V.; Schröder, C.; Bica, K. Ion-Tagged Chiral Ligands for Asymmetric Transfer Hydrogenations in Aqueous Medium. *ACS Sustainable Chem. Eng.* **2019**, *7* (3), 3414–3423.

(21) Muldoon, M. J. Modern multiphase catalysis: new developments in the separation of homogeneous catalysts. *Dalton Trans.* **2010**, *39*, 337–348.

(22) Schwarze, M.; Pogrzeba, T.; Seifert, K.; Hamerla, T.; Schomäcker, R. Recent developments in hydrogenation and hydroformylation in surfactant systems. *Catal. Today* **2015**, *247*, 55–63.

(23) Dwars, T.; Paetzold, E.; Oehme, G. Reactions in Micellar Systems. *Angew. Chem., Int. Ed.* **2005**, *44*, 7174–7199.

(24) Hejazifar, M.; Earle, M.; Seddon, K. R.; Weber, S.; Zirbs, R.; Bica, K. Ionic Liquid-Based Microemulsions in Catalysis. *J. Org. Chem.* **2016**, *81*, 12332–12339.

(25) Nowothnick, H.; Blum, J.; Schomäcker, R. Suzuki Coupling Reactions in Three-Phase Microemulsions. *Angew. Chem., Int. Ed.* **2011**, *50*, 1918–1921.

(26) Rost, A.; Brunsch, Y.; Behr, A.; Schomaecker, R. Comparison of the Activity of a Rhodium-Biphosphos Catalyst in Thermomorphic Solvent Mixtures and Microemulsions. *Chem. Eng. Technol.* **2014**, *37*, 1055–1064.

(27) Behr, A.; Kämper, A.; Kuhlmann, R.; Vorholt, A. J.; Franke, R. First efficient catalyst recycling for the iridium-catalyzed hydroformylation of 1-octene. *Catal. Sci. Technol.* **2016**, *6*, 208–214.

(28) Batarseh, C.; Nairoukh, Z.; Volovych, I.; Schwarze, M.; Schomäcker, R.; Fanun, M.; Blum, J. Catalytic transfer hydrogenation of hydrophobic substrates by water-insoluble hydrogen donors in aqueous microemulsions. *J. Mol. Catal. A: Chem.* **2013**, *366*, 210–214.

(29) Winsor, P. Hydrotropy, solubilisation and related emulsification processes. *Trans. Faraday Soc.* **1948**, *44*, 376–398.

(30) Li, X.; Wu, X.; Chen, W.; Hancock, F. E.; King, F.; Xiao, J. Asymmetric Transfer Hydrogenation in Water with a Supported Noyori–Ikariya Catalyst. *Org. Lett.* **2004**, *6*, 3321–3324.

(31) Wang, J.; Qin, R.; Fu, H.; Chen, J.; Feng, J.; Chen, H.; Li, X. Asymmetric hydrogenation of α,β -unsaturated ketones catalyzed by Ru–TPPTS–(S,S)-DPENDS complex in ionic liquids. *Tetrahedron: Asymmetry* **2007**, *18*, 847–851.

(32) Jiang, J.-Z.; Cai, C. Copper- and ligand-free Sonogashira reaction catalyzed by palladium in microemulsion. *J. Colloid Interface Sci.* **2007**, *307*, 300–303.

(33) Ma, Y.; Liu, H.; Chen, L.; Cui, X.; Zhu, J.; Deng, J. Asymmetric Transfer Hydrogenation of Prochiral Ketones in Aqueous Media with New Water-Soluble Chiral Vicinal Diamine as Ligand. *Org. Lett.* **2003**, *5*, 2103–2106.

(34) Ahlford, K.; Lind, J.; Mäler, L.; Adolfsson, H. Rhodium-catalyzed asymmetric transfer hydrogenation of alkyl and aryl ketones in aqueous media. *Green Chem.* **2008**, *10*, 832–835.

(35) Jiang, Q.; Jiang, Y.; Xiao, D.; Cao, P.; Zhang, X. Highly Enantioselective Hydrogenation of Simple Ketones Catalyzed by a Rh–PennPhos Complex. *Angew. Chem., Int. Ed.* **1998**, *37*, 1100–1103.

(36) Gladiali, S.; Alberico, E. Asymmetric transfer hydrogenation: chiral ligands and applications. *Chem. Soc. Rev.* **2006**, *35*, 226–236.

(37) Li, W.; Hou, G.; Wang, C.; Jiang, Y.; Zhang, X. Asymmetric hydrogenation of ketones catalyzed by a ruthenium(II)-indan–ambox complex. *Chem. Commun.* **2010**, *46*, 3979–3981.

(38) Martins, J. E.; Clarkson, G. J.; Wills, M. Ru(II) Complexes of N-Alkylated TsDPEN Ligands in Asymmetric Transfer Hydrogenation of Ketones and Imines. *Org. Lett.* **2009**, *11*, 847–850.

(39) Foubelo, F.; Yus, M. Catalytic Asymmetric Transfer Hydrogenation of Imines: Recent Advances. *Chem. Rec.* **2015**, *15*, 907–924.

(40) Aberg, J. B.; Samec, J. S. M.; Bäckvall, J.-E. Mechanistic investigation on the hydrogenation of imines by $[p\text{-}(\text{Me}_2\text{CH})\text{-C}_6\text{H}_4\text{Me}]\text{RuH}(\text{NH}_2\text{CHPhCHPhNSO}_2\text{C}_6\text{H}_4\text{-}p\text{-CH}_3)$. Experimental support for an ionic pathway. *Chem. Commun.* **2006**, *26*, 2771–2773.

(41) Václavík, J.; Kuzma, M.; Přeč, J.; Kačer, P. Asymmetric Transfer Hydrogenation of Imines and Ketones Using Chiral $\text{Ru}^{\text{II}}\text{Cl}(\eta^6\text{-}p\text{-cymene})[(\text{S,S})\text{-N-TsDPEN}]$ as a Catalyst: A Computational Study. *Organometallics* **2011**, *30*, 4822–4829.

(42) Uematsu, N.; Fujii, A.; Hashiguchi, S.; Ikariya, T.; Noyori, R. Asymmetric Transfer Hydrogenation of Imines. *J. Am. Chem. Soc.* **1996**, *118*, 4916–4917.

(43) Hall, A. M. R.; Dong, P.; Codina, A.; Lowe, J. P.; Hintermair, U. Kinetics of Asymmetric Transfer Hydrogenation, Catalyst Deactivation, and Inhibition with Noyori Complexes As Revealed by Real-Time High-Resolution FlowNMR Spectroscopy. *ACS Catal.* **2019**, *9*, 2079–2090.

(44) Geldbach, T. J.; Dyson, P. J. A Versatile Ruthenium Precursor for Biphasic Catalysis and Its Application in Ionic Liquid Biphasic Transfer Hydrogenation: Conventional vs Task-Specific Catalysts. *J. Am. Chem. Soc.* **2004**, *126*, 8114–8115.

(45) Dimroth, J.; Keilitz, J.; Schedler, U.; Schomäcker, R.; Haag, R. Immobilization of a Modified Tethered Rhodium(III)-*p*-Toluene-sulfonyl-1,2-diphenylethylenediamine Catalyst on Soluble and Solid Polymeric Supports and Successful Application to Asymmetric Transfer Hydrogenation of Ketones. *Adv. Synth. Catal.* **2010**, *352*, 2497–2506.

(46) Cognigni, A.; Gaertner, P.; Zirbs, R.; Peterlik, H.; Prochazka, K.; Schroeder, C.; Bica, K. Surface-active ionic liquids in micellar catalysis: impact of anion selection on reaction rates in nucleophilic substitutions. *Phys. Chem. Chem. Phys.* **2016**, *18*, 13375–13384.

(47) Pecháček, J.; Václavík, J.; Přeč, J.; Šot, P.; Januščák, J.; Vilhanová, B.; Vavřík, J.; Kuzma, M.; Kačer, P. Asymmetric transfer hydrogenation of imines catalyzed by a Noyori-type Ru(II) complex – a parametric study. *Tetrahedron: Asymmetry* **2013**, *24*, 233–239.

(48) Yonggui, Z.; Lei, S.; Guangshou, F.; Yue, J. Method for solvent accelerated selective dehydrogenation of tetrahydroisoquinoline type compound. Chinese Patent No. CN106699657A, 2017.

(49) Huang, J.; Liu, X.; Wen, Y.; Qin, B.; Feng, X. Enantioselective Strecker Reaction of Phosphinoyl Ketoimines Catalyzed by in Situ Prepared Chiral N,N'-Dioxides. *J. Org. Chem.* **2007**, *72*, 204–208.

(50) Chen, X.; Lu, Z. Iminophenyl Oxazolonylphenylamine for Enantioselective Cobalt-Catalyzed Hydrosilylation of Aryl Ketones. *Org. Lett.* **2016**, *18*, 4658–4661.

(51) Xu, Y.; Alcock, N. W.; Clarkson, G. J.; Docherty, G.; Woodward, G.; Wills, M. Asymmetric Hydrogenation of Ketones Using a Ruthenium(II) Catalyst Containing BINOL-Derived Monodonor Phosphorus-Donor Ligands. *Org. Lett.* **2004**, *6*, 4105–4107.

(52) Xu, C.; Yuan, C. *Candida Rugosa* lipase-catalyzed kinetic resolution of β -hydroxy- β -arylpropionates and δ -hydroxy- δ -aryl- β -oxo-pentanoates. *Tetrahedron* **2005**, *61*, 2169–2186.

(53) Brown, H. C.; Cho, B. T.; Park, W. S. Asymmetric reduction of α -keto esters with potassium-9-O-(1,2:5,6-di-O-isopropylidene- α -D-glucopyranose)-9-boratabicyclo-[3.3.1]nonane. Chiral synthesis of α -hydroxy esters with optical purity approaching 100% ee. *J. Org. Chem.* **1986**, *51*, 3396–3398.

(54) Schmidt, F.; Rudolph, J.; Bolm, C. Catalyzed Enantioselective Synthesis of Allyl Alcohols from Aldehydes and Alkenylboronic Acids. *Synthesis* **2006**, *2006*, 3625–3630.

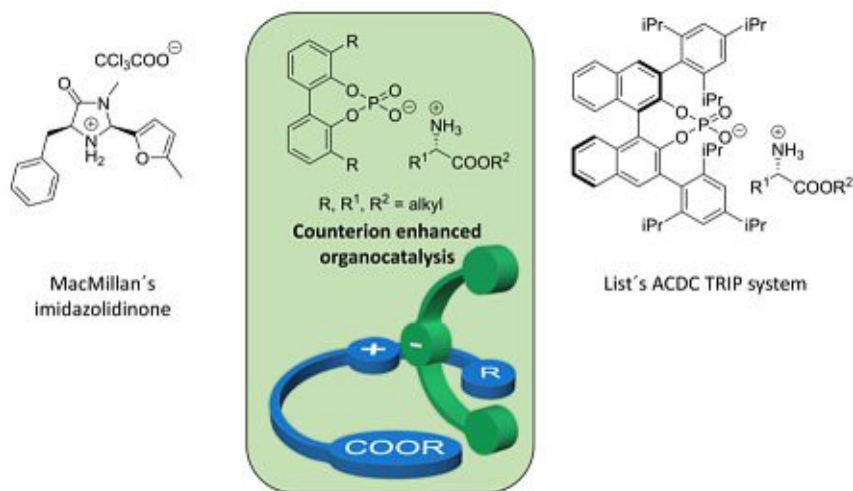
(55) Cheung, F. K.; Hayes, A. M.; Morris, D. J.; Wills, M. The use of a [4 + 2] cycloaddition reaction for the preparation of a series of 'tethered' Ru(II)-diamine and aminoalcohol complexes. *Org. Biomol. Chem.* **2007**, *5*, 1093–1103.

(56) Ji, Y.; Shi, L.; Chen, M.-W.; Feng, G.-S.; Zhou, Y.-G. Concise Redox Deracemization of Secondary and Tertiary Amines with a Tetrahydroisoquinoline Core via a Nonenzymatic Process. *J. Am. Chem. Soc.* **2015**, *137*, 10496–10499.

(57) Krzyżanowska, B.; Stec, W. A Study of the Synthesis of Optically Active Amines from Prochiral *N*-Phosphinylimines. *Synthesis* **1982**, *1982*, 270–273.

3. Counterion-enhanced organocatalysis: A novel approach for the asymmetric transfer hydrogenation of enones

The regio- and stereoselective reduction of 3-substituted carbonyl compounds is particularly challenging *via* transition metal catalysis because of the possible reduction of the carbonyl center. The introduction of biomimetic hydrogen sources like Hantzsch esters and benzothiazolines provides a metal-free, purely organocatalytic alternative for the ATH of enals and enones. As neither gaseous hydrogen, nor transition metals are required, such reactions can provide a safer and simpler alternative to traditional hydrogenations; moreover, they feature high air and moisture tolerance. To date, two main methodologies emerged as particularly applicable for the ATH of α,β -unsaturated ketones. Chiral imidazolidinones are in general very powerful catalysts for the ATH of enals; however, they show inferior performance for enone substrates and also high catalyst loadings are required (Scheme 41, left).³⁹ Expanding their previously described concept of “Asymmetric Counteranion-Directed Catalysis (ACDC)”, the List group developed a very efficient method for the ATH of enones, relying on the non-natural BINOL-based phosphoric acid TRIP (Scheme 41, right).⁵² Even though this is certainly an elegant and powerful alternative for ATH reactions, its major drawback arises from the use of TRIP: its synthesis requires a multi-step strategy including tedious purifications, which results in a particularly expensive catalyst. In order to overcome these issues; a significantly simpler, cheaper and natural-derived catalyst framework of L-amino acid esters and natural-derived achiral/racemic phosphoric acids should be developed (Scheme 41, middle). After fine-tuning the catalyst properties and reaction parameters, the optimized catalyst system should then be used for the ATH of various 3-substituted cyclic enones.



Scheme 41. Different catalytic concepts for the ATH of cyclic enones: MacMillan's imidazolidinone (left), List's TRIP phosphate *via* ACDC catalysis (right) and our novel concept of counterion enhanced catalysis (middle).

In parallel with the experimental work, the influence of chiral and achiral cations on the enantiomerization of different biphenyl anions, as well as a possible chirality transfer between the ions was investigated *via* polarizable MD simulations.

The following manuscripts will be presented in this chapter:

- 1.) Scharinger, F.; Pálvölgyi, Á. M.; Zeindlhofer, V.; Schnürch, M.; Schröder, C.; Bica-Schröder, K. Counterion Enhanced Organocatalysis: A Novel Approach for the Asymmetric Transfer Hydrogenation of Enones. *ChemCatChem* **2020**, *12* (14), 3776–3782.

As a main author with equal contribution, I planned the experiments and performed them together with Fabian Scharinger. Furthermore, I also had a major contribution to the manuscript preparation.

- 2.) Zeindlhofer, V.; Hudson, P.; Pálvölgyi, Á. M.; Welsch, M.; Almarashi, M.; Woodcock, H. L.; Brooks, B.; Bica-Schröder, K.; Schröder, C. Enantiomerization of Axially Chiral Biphenyls: Polarizable MD Simulations in Water and Butylmethylether. *Int. J. Mol. Sci.* **2020**, *21*, 6222–6240.

As a co-author, I participated in the conceptualization and contributed in the manuscript preparation.

Counterion Enhanced Organocatalysis: A Novel Approach for the Asymmetric Transfer Hydrogenation of Enones

Fabian Scharinger^{+, [a]} Ádám Márk Pálvölgyi^{+, [a]} Veronika Zeindlhofer,^[b] Michael Schnürch,^[a] Christian Schröder,^[b] and Katharina Bica-Schröder^{*[a]}

Dedicated to Prof. Johannes Fröhlich on the occasion of his 60th birthday

We present a novel strategy for organocatalytic transfer hydrogenations relying on an ion-paired catalyst of natural L-amino acids as main source of chirality in combination with racemic, atropisomeric phosphoric acids as counteranion. The combination of a chiral cation with a structurally flexible anion resulted in a novel chiral framework for asymmetric transfer hydrogenations with enhanced selectivity through synergistic effects. The optimized catalytic system, in combination with a Hantzsch

ester as hydrogen source for biomimetic transfer hydrogenation, enabled high enantioselectivity and excellent yields for a series of α,β -unsaturated cyclohexenones under mild conditions. Moreover, owing to the use of readily available and chiral pool-derived building blocks, it could be prepared in a straightforward and significantly cheaper way compared to the current state of the art.

Introduction

Asymmetric transfer hydrogenation has emerged as a powerful and convenient tool for the reduction of prochiral carbonyl compounds.^[1] The selective reduction of enones is a particularly challenging task due to the inherent question of regio- and stereoselectivity.^[2] Among many catalytic protocols that have been described for this particular reaction, the flourishing area of organocatalysis offers attractive solutions, and iminium-based asymmetric transfer hydrogenations provide an efficient and metal-free alternative for the selective reduction of enones via 1,4-addition.^[3–5]

Over the past years, two types of catalysts have emerged as particularly well suited for organocatalytic transfer hydrogenations of enals and enones. In 2004, the group of MacMillan reported a series of imidazolidinone derivatives as powerful benchmark catalysts for highly asymmetric conjugate hydrogenations of α,β -unsaturated aldehydes and ketones (Figure 1, left).^[5,6] In parallel, List and co-workers described a novel

method for the non-asymmetric transfer hydrogenation of cinnamaldehyde derivatives using secondary ammonium salts as catalysts.^[7] Two years later, a new methodology in asymmetric transfer hydrogenation was reported by Mayer and List as they observed high catalytic activity and enantioselectivity in the reaction of enals and enones catalyzed by ammonium salts composed of an achiral or chiral cation and an enantiopure sterically demanding phosphate anion, TRIP (Figure 1, right).^[8,9] Based on the early success of List's catalytic system, a new general concept emerged in the field of organocatalysis, known as Asymmetric Counteranion-Directed Catalysis (ACDC), which refers to any catalytic reaction, in which the enantiodiscrimination is induced through the tight ion-pairing of a cationic intermediate with an enantiomerically pure anion.^[10] The ion-bound nature of this attractive approach for chiral induction offers considerable flexibility for fine-tuning of the electronic and steric properties compared to conventional covalent ligand systems.^[11] Since the discovery of ACDC, or in general, of asymmetric ion-pairing catalysis, several other highly enantioselective reactions proceeding through cationic intermediates have been reported.^[12–15] While different asymmetric induction modes can be realized in asymmetric ion-pairing catalysis, the formation of ion pairs between ammonium cations and bulky chiral phosphate anions is particularly prominent.^[16–21]

While these elegant strategies are certainly among the most important discoveries in the field of organocatalysis for the last decades, they still do have some limitations. MacMillan's imidazolidinones are excellent catalysts for the asymmetric transfer hydrogenation of enals; however, the reactivity for enones is inferior thus requiring higher catalyst loadings.^[6] In contrast, List et al. could successfully reach high reactivity and selectivity for the asymmetric transfer hydrogenation of enals and enones even with low catalyst loading based on the chiral TRIP counteranion. However, this approach requires a rather expensive catalyst, prepared in a five-step synthesis with rather

[a] F. Scharinger,⁺ Á. Márk Pálvölgyi,⁺ Prof. M. Schnürch, Prof. K. Bica-Schröder
Institute of Applied Synthetic Chemistry
TU Wien

Getreidemarkt 9/163
1060 Wien (Austria)

E-mail: katharina.schroeder@tuwien.ac.at

[b] V. Zeindlhofer, Prof. C. Schröder
Department of Computational Biological Chemistry
University of Vienna

Währinger Str. 17
1090 Wien (Austria)

[⁺] These authors contributed equally to this manuscript.

Supporting information for this article is available on the WWW under <https://doi.org/10.1002/cctc.202000414>

© 2020 The Authors. Published by Wiley-VCH Verlag GmbH & Co. KGaA. This is an open access article under the terms of the Creative Commons Attribution License, which permits use, distribution and reproduction in any medium, provided the original work is properly cited.

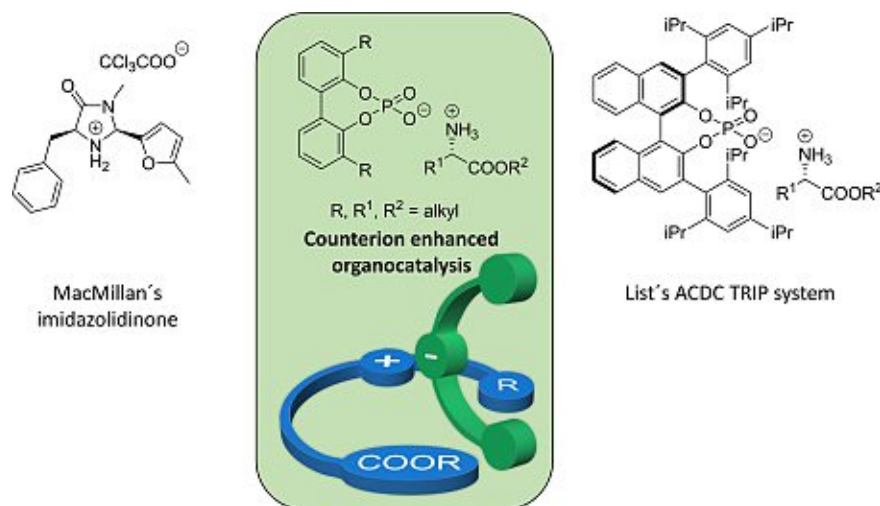


Figure 1. Iminium-based organocatalytic reduction of enones and different catalytic systems, including MacMillan's imidazolidinone catalyst (left), List's TRIP phosphate (right) as well as the novel counterion enhanced approach reported in here (middle).

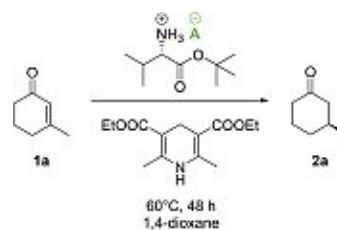
low overall yields. Moreover, a careful structural optimization is required for the bulky phosphate anion of the catalyst: while the TRIP counteranion provides indeed high selectivity in the ATH of ketones and aldehydes, a significant decrease in the enantiodiscrimination could be observed just with a slight modification of the phosphate unit, resulting in moderate selectivity or even close-to-racemic products. Given these limitations; a straightforward, cheaper and chiral-pool derived catalytic system that combines high catalytic activity with excellent enantioselectivity would be highly desirable.

In here, we propose a novel concept of asymmetric ion-paired organocatalysis with a fixed element of chirality based on ion aggregation between a chiral amino acid cation and C_2 -symmetric atropisomeric phosphate anion. This concept of an ion-paired catalyst framework offers novel opportunities for ligand design with unprecedented flexibility compared to conventional ligand design relying on covalently constructed ligands. Eventually, this unique approach results in an easily accessible, cheap and chiral pool-derived a catalytic system that is yet able to reduce a set of α,β -unsaturated ketones with high yields and selectivity.

Results and Discussion

To prove the concept of counterion enhanced asymmetric transfer hydrogenations, we initially focused on the reduction of 3-methyl-2-cyclohexenone. The reaction was performed with the common Hantzsch ethyl ester as mild reductant using standard conditions that have been previously established by List et al (Scheme 1).^[5]

For a first evaluation of the concept, different salts of (L)-valine *t*-butyl ester, including the non-chiral trifluoroacetate salt, but also salts with tropoisomeric biphenyl phosphate as well as enantiopure or racemic binaphthyl phosphate anions were used as catalysts (Table 1). While no reaction was



Scheme 1. Proof of concept: asymmetric transfer hydrogenation of 3-methyl-2-cyclohexenone (1a) by using different salts of L-valine *t*-butyl ester.

observed with the biphenolate anion **3** due to the lower acidity of 2,2'-biphenol (Table 1, entry 1), the reaction proceeded with moderate yield in the presence of biphenyl phosphate **4** (Table 1, entries 4 and 5). Most importantly, an increase of enantioselectivity to 64%ee – an increase by 10%ee compared to the trifluoroacetate salt – could be observed, indicating that the tropoisomeric and C_2 -symmetric biphenyl phosphate anion plays a role in enantiodiscrimination (Table 1, entries 2 vs. 4). It is worthwhile noticing that this is not the case with different binaphthyl phosphate anions, as the observed enantioselectivity with racemic or enantiopure binaphthyl phosphate was identical to the values obtained for trifluoroacetate (Table 1, entries 2 vs. 6–8). This clearly shows that matched/mismatched effects between the chiral amino acid and the counteranion do not influence the enantioselectivity of the product.

Further studies showed that this effect is even more pronounced in MTBE as a solvent, where an enantioselectivity of 74%ee compared to 51%ee obtained with the trifluoroacetate anion was found (Table 1, entries 3 vs. 5). In fact, when studying the impact of different solvents in this reaction, we found that the best selectivity is observed in solvents with low dielectric constants such as MTBE ($\epsilon=4.5$) or toluene ($\epsilon=2.4$), whereas lower enantioselectivity was found in more polar solvents such as water ($\epsilon=80.1$), see ESI Table S2, page S24 for details.

Table 1. Proof of concept in the counterion enhanced asymmetric transfer hydrogenation of 3-methyl-2-cyclohexenone (1a) using (L)-valine *t*-butyl ester as cation source.

| Entry ^[a] | Anion | Conv. ^[c] [%] | Yield ^[c] [%] | ee ^[c] [%] | Δee ^[d] |
|----------------------|-------|--------------------------|--------------------------|-----------------------|--------------------|
| 1 | | < 1 | < 1 | n.d. | n.d. |
| 2 | | 78 | 49 | 54 | - |
| 3 ^[b] | | 92 | 88 | 51 | - |
| 4 | | 40 | 27 | 64 | 10 |
| 5 ^[b] | | 75 | 72 | 74 | 23 |
| 6 | | 13 | 13 | 54 | 0 |
| 7 | | 22 | 13 | 54 | 0 |
| 8 | | 20 | 15 | 54 | 0 |

[a] Performed with 0.18 mmol 3-methyl-2-cyclohexenone (1a), 20 mol% catalyst and 0.22 mmol Hantzsch ethyl ester in 0.55 mL 1,4-dioxane for 48 hours at 60 °C, [b] MTBE used as solvent, [c] Determined by GC analysis on BGB5 column using *n*-dodecane as internal standard and chiral GC analysis using a BGB175 chiral capillary column, [d] Δee defined as the difference between the reaction with phosphate anion 4 and trifluoroacetate anion in 1,4-dioxane and MTBE, respectively.

This increase in the enantioselectivity can be attributed to the solvent's polarity, resulting in the formation of contact ion pairs in apolar solvents and hence a stronger interaction between cation and anion in the catalyst. In contrast to conventional salts that are defined by a strictly charge-ordered structure of atomic ions without dipole moment, organic salts, e.g. ionic liquids, possess a complex network with remarkable structural heterogeneity of the composing molecular ions.^[22] On a supramolecular length scale, ion pairs, or more precisely ion aggregates exist for a lifetime of a few picoseconds; however, ion pair destabilization occurs as pairs readily dissociate into individual ions in pure salt melts. This situation changes drastically when organic salts are dissolved in molecular solvents: A number of experimental techniques, including NMR measurements or cyclic voltammetry proved the existence of long-lived ion pairs, suggesting that the ion pair formation is insignificant in neat salts but dominant in electrolyte solutions. Although a key feature of organic salts in solution, ion aggregation has been scarcely exploited for interionic chirality transfer. An outstanding example in this regard was published by Leitner and co-workers in their work on asymmetric hydrogenations featuring a proline-based chiral ionic liquid as solvent

or additive in combination with atropisomeric phosphine ligands.^[23] Impressive enantioselectivity was obtained through a complex of $[[\text{(R)-binap}]\text{Rh}\{\text{(S)-MeProl}\}]^+$, accompanied by *N*-bis-(trifluoromethane)sulfonimide anion.

We reasoned that the catalytic system could be improved by tuning the steric demand and rotation barrier of the atropisomeric phosphate anion. For this purpose, a set of biphenyl phosphoric acids were prepared via microwave-assisted oxidative coupling of phenols with *t*-butyl peroxide. This straightforward coupling step, followed by reaction with POCl₃ and successive hydrolysis gave access to the phosphoric acids (4–7) with variable substituent pattern in acceptable overall yield, starting from cheap and readily available phenols (see ESI S10–S13 for details). With this set of phosphoric acids in hand, the selectivity in asymmetric transfer hydrogenation could be considerably improved and varied between 74 and 80%ee. Best results were obtained with the isopropyl substituted phosphoric acid 6 as anion source, providing up to 80%ee with nearly quantitative yield (Figure 2, also see ESI Table S3, page S25 for details). Furthermore, other acids traditionally used in organocatalysis have been investigated. The ee values were below 60% for all cases under the same reaction conditions, further highlighting the benefits of the atropisomeric phosphoric acids 4–7 (see ESI Table S4, page S26 for details).

Successively, we performed an extensive screening of the amino acid as cation source for further optimization of the catalytic system. Little difference in enantioselectivity (between 72–80%ee) were found between (L)-valine, (L)-leucine, (L)-isoleucine and (L)-*t*-leucine *t*-butyl esters, whereas aromatic species such as (L)-phenylalanine *t*-butyl ester where less efficient. (L)-Proline *t*-butyl ester with a secondary ammonium cation gave also significantly lower selectivity (see ESI Table S5, page S27 for details). Finally, modifications on the ester moiety

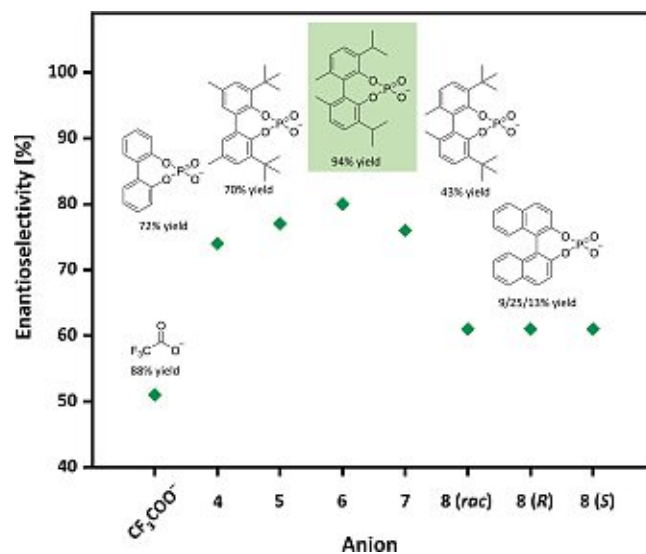
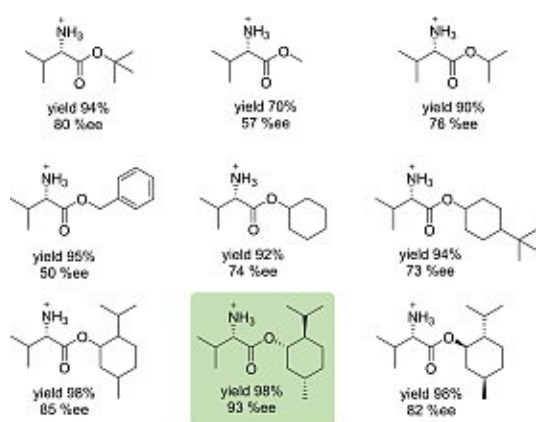


Figure 2. Impact of different phosphate anions vs. TFA anion on the enantioselectivity. All reactions were carried out in MTBE at 60 °C using L-valine *t*-butyl ester as cation source.

of (L)-valine revealed that sterically demanding aliphatic groups such as *t*-butyl, 4-*t*-butyl cyclohexyl or menthyl are indeed required for reaching high selectivity, as can be easily seen when comparing the results with those obtained for methyl or benzyl esters. Eventually, the best results were obtained when matching (L)-valine with the (+)-(1*S*,2*R*,5*S*) menthol, as the resulting ester in combination with phosphoric acid **6** resulted in an excellent yield of 98% and an enantioselectivity of 93% ee. This is in contrast to the mismatched ester-system obtained with (–)-(1*R*,2*S*,5*R*) menthol, which gave only 82% ee (Scheme 2).

With the ideal cationic and anionic moiety identified, it was also possible to reduce the catalyst loading to lower amounts: When studying different catalyst loadings at 25 °C, the high selectivity was maintained even at 5 mol% catalyst, although



Scheme 2. Optimization of the (L)-valine ester moiety as cations source for. All reactions were carried out in MTBE at 60 °C using phosphate anion **6**.

Table 2. Optimization of conditions and parameters for the asymmetric transfer hydrogenation of 3-methyl-2-cyclohexenone (**1a**) using (L)-valine (+)-(1*R*,3*R*,4*S*) menthyl ester and the isopropyl substituted phosphoric acid **6** as anion source.

| Entry ^[a] | T [°C] | Catalyst [mol%] | Hantzsch ester | Yield ^[b] /% | ee ^[c] [%] |
|----------------------|--------|-----------------|------------------|-------------------------|-----------------------|
| 1 | 60 | 20 | ethyl | 98 | 93 |
| 2 | 50 | 20 | ethyl | 98 | 95 |
| 3 | 40 | 20 | ethyl | 96 | 95 |
| 4 | 25 | 20 | ethyl | 59 | 96 |
| 5 | 25 | 10 | ethyl | 43 | 96 |
| 6 | 25 | 5 | ethyl | 29 | 96 |
| 7 | 25 | 1 | ethyl | 11 | 96 |
| 8 | 50 | 10 | ethyl | 99 | 94 |
| 9 | 50 | 5 | ethyl | 98 | 95 |
| 10 | 50 | 1 | ethyl | 68 | 93 |
| 11 ^[d] | 25 | 20 | methyl | 14 | 83 |
| 12 ^[d] | 25 | 20 | ethyl | 17 | 88 |
| 13 ^[d] | 25 | 20 | <i>i</i> -propyl | 58 | 69 |
| 14 ^[d] | 25 | 20 | <i>t</i> -butyl | 58 | 67 |

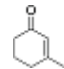
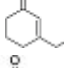
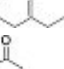
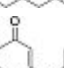
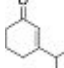
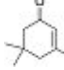
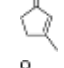
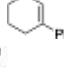
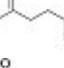
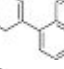
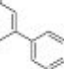
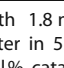
[a] Performed with 0.18 mmol 3-methyl-2-cyclohexenone, 0.009–0.036 mmol catalyst and 0.22 mmol Hantzsch ester in 0.55 mL MTBE at the given temperature for 48 hours, [b] Determined by GC analysis on a BGB5 column using *n*-dodecane as internal standard, [c] Determined by chiral GC analysis using a BGB175 chiral capillary column, [d] Performed with (L)-valine *t*-butyl ester instead of (L)-valine (+)-(1*R*,3*R*,4*S*) menthyl ester.

losses in yield had to be taken into account. Eventually, a reaction temperature of 50 °C provided an ideal compromise between yield and selectivity, providing the desired product **2a** in 98% yield and 95% ee (Table 2, entry 9).

For further studies on scope and limitation of the newly established catalytic system, the substrate pool was widened to investigate the asymmetric transfer hydrogenation of different 3-substituted cyclohexenones under the previously optimized reaction conditions (Table 3). Enantioselectivity exceeded 90% frequently, thereby demonstrating the versatility and broad application range of the newly established system.

In general, atropisomerism is a type of axial chirality that may arise in systems where free rotation about a single covalent

Table 3. Substrate scope for the counterion enhanced transfer hydrogenation of enones.

| Entry ^[a] | Substrate | Yield ^[d] [%] | ee ^[e] [%] |
|----------------------|--|----------------------------------|-----------------------|
| 1 |  | 1a 98 (72) ^[f] | 95 (S) |
| 2 |  | 1b 85 (76) ^[f] | 92 (S) |
| 3 |  | 1c 70 (55) ^[f] | 91 (S) |
| 4 |  | 1d 91 (87) | 93 (S) |
| 5 |  | 1e 85 (60) ^[f] | 86 (S) |
| 6 |  | 1f 75 (68) ^[f] | 88 (S) |
| 7 ^[b] |  | 1g 66 (60) | 92 (S) |
| 8 ^[c] |  | 1h 94 (80) ^[f] | 89 (S) |
| 9 |  | 1i 86 (84) | 82 (S) |
| 10 |  | 1j 94 (91) | 90 (S) |
| 11 |  | 1k 65 (62) | 94 (S) |
| 12 |  | 1l 89 (86) | 70 (S) |

[a] Performed with 1.8 mmol ketone, 5 mol% catalyst and 2.2 mmol Hantzsch ethyl ester in 5.5 mL MTBE at 50 °C for 48 hours, [b] 20 mol% catalyst, [c] 10 mol% catalyst, [d] Determined by GC or GC–MS analysis. Isolated yields after flash column chromatography are given in parenthesis, [e] Determined by chiral GC analysis using a BGB175 or BGB173 chiral capillary column, or by chiral HPLC analysis using a Diacel Chiralcel AS–H column. Absolute configurations have been determined by measuring the optical rotation and comparing with literature data, [f] Lower isolated yield because of high volatility of the product.

bond is hindered.^[24] The isomerization pathways of biphenyls with bulky ortho-substituents were studied in detail by Masson, showing that conformers with isomerization barriers > 23 kcal/mol can be separated at room temperature.^[25] Less information is available for biphenols or biphenyl phosphoric acids. For more insight on the behavior of the atropisomeric phosphoric

acids, we calculated isomerization barriers for compounds 4–8 (Table 4). The pure electrostatic barriers were corrected by frequency contributions to result in the Gibbs free energy barrier (ΔG) at a temperature of 333.15 K. Optimizations, energy evaluations and frequency calculations were performed on the B3LYP-D3/def2TZVP^[26–28] level of theory with the program package ORCA.^[29] Correlation in the uniform electron gas was modeled according to the Vosko-Wilk-Nusair VWN5 formalism.^[30] A detailed description of the computational methodology can be found in the ESI (S32–S33).

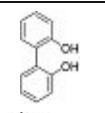
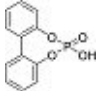
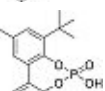
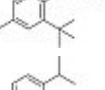
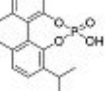
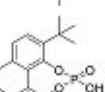
In general, comparison of the isomerization barriers between biphenols and biphenyl phosphoric acids is not straightforward. In case of biphenol, at least five ground state isomers can be identified, resulting in multiple isomerization pathways.^[31] Sahnoun et al. estimate a value of 11.5 kcal/mol for the lowest possible pathway.^[31]

Due to the additional O–P–O bridge, the phosphoric acids are restricted in the rotation of the aryl-aryl bond, hence allowing only one pathway. The phosphoric acids 4 and 5 have similar rotational barriers of 10 and 12 kcal/mol, indicating that substituents in 3,3'-position have only a minor impact on the rotation barrier. As visible from Figure 3 (top), their transition states for the isomerization are both planar. However, barriers for the acids 6 and 7 increase to 41.2 and 48.2 kcal/mol, respectively, which can be attributed to the methyl groups in 6,6'-position. Apart from the steric hindrance of the rotation, this substitution pattern also forces an out-of-plane transition state (Figure 3, bottom).

Moreover, the optimal dihedral angle of 2,2'-biphenol and biphenyl phosphoric acid differs significantly due to the constraints of the phosphate bridge on the rotation of the two phenyl rings (Table 4). In case of 2,2'-biphenol two hydroxyl hydrogens are able to form hydrogen bonds to the opposite oxygen.

The rotational barrier itself cannot explain the different enantioselectivity observed in the ATH reaction. For example,

Table 4. Barrier energies for the phosphoric acids on the B3LYP-D3/def2TZVP level of theory.

| Entry | Biphenol/ Phosphoric acid | Isomerization barrier ΔG [kcal/mol] | Dihedral angle around the aryl-aryl bond | |
|-------|---|---|--|------------------|
| | | | Ground state | Transition state |
| 1 |  | 11.5 ^[31] | 110° | 0° |
| 2 |  | 10.0 | 43° | 0° |
| 3 |  | 12.0 | 49° | 0° |
| 4 |  | 41.2 | 56° | 21° |
| 5 |  | 48.2 | 61° | 29° |
| 6 |  | 42.7 ^[25] | 75° | 26° |

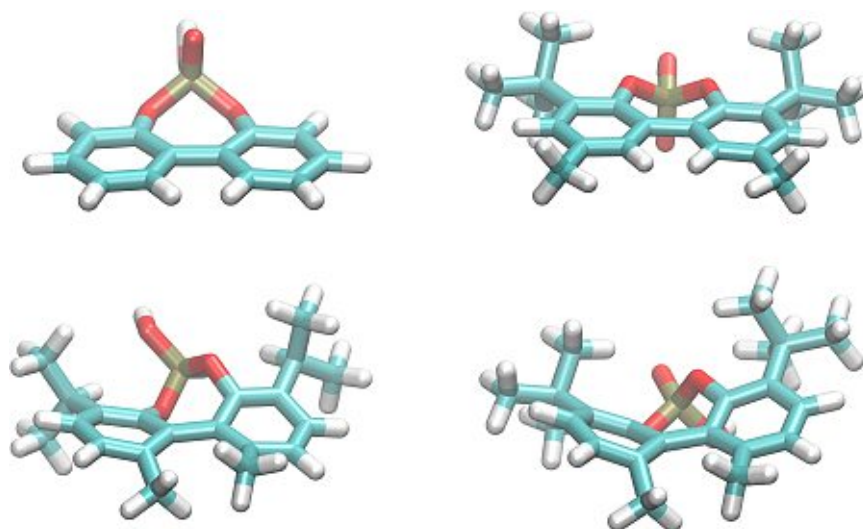


Figure 3. Optimized geometry of the transition states of compounds 4–7.

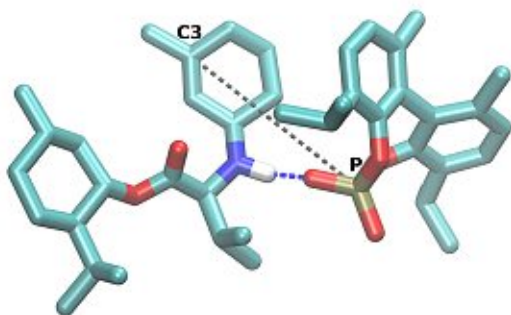
anions arising from phosphoric acid **5** and **7** gave similar enantioselectivity, despite a considerable difference in their rotational barriers (Figure 2). Additionally, the rotational barrier of the binaphthyl phosphate **8** is considerably higher compared to biphenyl phosphate **4**. However, the latter resulted in considerably higher yield and enantioselectivity (see Table 1, entries 4 vs. 6–8), indicating that a complex interplay of the steric demand, anion geometry and rotation barrier is responsible for the different performance in the ATH reaction.

The most promising catalyst system was investigated further via non-polarizable molecular dynamics simulations. To model the ion pair prior to the enantioselective reaction step, we further investigated the iminium cation formed (+)-(1*S*,2*R*,5*S*) menthyl-L-valinate and 3-methyl-2-cyclohexenone, in combination with phosphate anion **6**. Simulations were performed for one intermediate ion pair at 60 °C in methyl

butyl ether, a solvent with a comparable dielectric constant to MTBE (see ESI S34–S37 for details). To explore any structural difference in the ion pairs, the (*E*) and (*Z*) form of the cation and both enantiomers of the anion were considered in four different simulations. The ion pairs incorporating the (*R*)-enantiomer of the anion are shown in Figure 4.

From the average interionic distance calculated respective to center of mass, it can be seen that the ions form stable pairs throughout the simulation. In all systems, the hydrogen bond between cation and anion (see Figure 4 and Table 5) is present for more than 85 % of the simulation time. This hydrogen bond promotes a certain orientation of the ion pair, with the phosphate group of the anion oriented towards the nitrogen of the cation. This also affects the average distance between the prochiral C3-atom of the cation and the P-atom of the anion. In the unfavored (*Z*)-form, the methyl group bound to the prochiral C3 points on the opposite side of the nitrogen-bound hydrogen, resulting in an interionic distance of approx. 6.5 Å away. In contrast, the C3–P distance is shorter by about 1 Å in the favored (*E*)-form, providing a closer ion pair and thus might be ideal for chiral induction.

(*Z*)-cation/(*R*)-anion



(*E*)-cation/(*R*)-anion

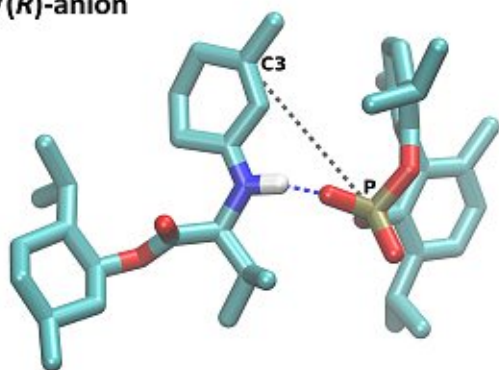


Figure 4. Snapshots of the (*Z*)-cation/(*R*)-anion (top) and (*E*)-cation/(*R*)-anion (bottom) pairs from the simulations. All solvent molecules as well as all hydrogens except the nitrogen-bound hydrogen were omitted for clarity.

Table 5. Average number of hydrogen bonds and interionic distances obtained from molecular dynamics simulations.

| Ion pair | Average number of hydrogen bonds | Average interionic distance (center of mass) [Å] | Average distance C3–P [Å] |
|------------|----------------------------------|--|---------------------------|
| Z-cat/R-an | 0.90 ± 0.04 | 7.2 ± 0.8 | 6.7 ± 0.5 |
| Z-cat/S-an | 0.85 ± 0.07 | 6.9 ± 0.9 | 6.6 ± 0.6 |
| E-cat/R-an | 0.90 ± 0.05 | 7.1 ± 0.9 | 5.5 ± 0.4 |
| E-cat/S-an | 0.87 ± 0.03 | 6.8 ± 0.9 | 5.2 ± 0.4 |

Conclusion

In here, we reported a novel concept of counterion catalysis for organocatalytic asymmetric transfer hydrogenations. The ion-paired catalysts, based on cheap amino acid-derived cations and flexible phosphate anions could be readily synthesized from natural compounds, providing a significantly cheaper alternative to the current state-of-the-art ACDC methodology. After careful parameter optimization, a series of different enones could be reduced with high yields and enantioselectivity under mild conditions even with low catalyst loadings.

From the simulation data, we can conclude that interionic interactions are strong enough to form a stable ion pair in apolar solvents such as MTBE, and that the hydrogen bond both favors a certain arrangement of the ion pair, with the C3 atom relatively close to the anion. The exact interplay between the ions, and the mechanism of a possible chirality transfer remains unclear, and it will be further evaluated in future studies addressing the influence of aggregate formation rather than a single ion pair.

Current investigations focus on the exploration of the reaction scope for counterion enhanced organocatalysis with chiral amino acid derived cations and atropisomeric phosphate anions. Overall, we expect that the concept of counterion enhanced catalysis relying on chiral cations and atropisomeric anions will find broad utility in organocatalysis, but also in transition metal catalyzed process.

Experimental Section

Representative procedure for the asymmetric transfer hydrogenation

A glass vial equipped with a magnetic stir bar was charged with ketone (1.8 mmol, 1.0 equiv.) in MTBE (5.5 mL, 0.33 M), followed by the addition of the catalyst (55.4 mg, 0.09 mmol, 5 mol%) and Hantzsch ester (552 mg, 2.2 mmol, 1.2 equiv.). The reaction mixture was stirred at 50 °C for 48 h. After cooling to room temperature, diethyl ether (5 mL) and 4 M HCl (10 mL) was added and the mixture was stirred until the phases were transparent (30 min). The phases were separated and the organic phase was washed with 4 M HCl (3 × 20 mL). The organic phase was dried over Na₂SO₄ and concentrated under reduced pressure. Purification by column chromatography (15% Et₂O: PE, vanillin staining agent or UV visualization) gave the 3-substituted cyclohexanones.

Acknowledgements

Financial support by the Austrian Science Fund (project P29146-N34) is gratefully acknowledged.

Conflict of Interest

The authors declare no conflict of interest.

Keywords: organocatalysis · asymmetric synthesis · transfer hydrogenation · ion aggregation · phosphoric acid · counterion catalysis

- [1] D. Wang, D. Astruc, *Chem. Rev.* **2015**, *115*, 6621–6686.
- [2] W. S. Mahoney, J. M. Stryker, *J. Am. Chem. Soc.* **1989**, *111*, 8818–8823.
- [3] A. Erkkilä, I. Majander, P. M. Pihko, *Chem. Rev.* **2007**, *107*, 5416–5470.
- [4] R. P. Herrera, *Top. Curr. Chem.* **2016**, *374*, 29.
- [5] S. G. Ouellet, J. B. Tuttle, D. W. C. MacMillan, *J. Am. Chem. Soc.* **2005**, *127*, 32–33.
- [6] J. B. Tuttle, S. G. Ouellet, D. W. C. MacMillan, *J. Am. Chem. Soc.* **2006**, *128*, 12662–12663.

- [7] J. W. Yang, M. T. Hechavarria Fonseca, B. List, *Angew. Chem. Int. Ed.* **2004**, *43*, 6660–6662; *Angew. Chem.* **2004**, *116*, 6829–6832.
- [8] S. Mayer, B. List, *Angew. Chem. Int. Ed.* **2006**, *45*, 4193–4195; *Angew. Chem.* **2006**, *118*, 4299–4301.
- [9] N. J. A. Martin, B. List, *J. Am. Chem. Soc.* **2006**, *128*, 13368–13369.
- [10] M. Mahlau, B. List, *Angew. Chem. Int. Ed.* **2013**, *52*, 518–533; *Angew. Chem.* **2013**, *125*, 540–556.
- [11] K. Brak, E. N. Jacobsen, *Angew. Chem. Int. Ed.* **2013**, *52*, 534–561; *Angew. Chem.* **2013**, *125*, 558–588.
- [12] G. L. Hamilton, E. J. Kang, M. Mba, F. D. Toste, *Science* **2007**, *317*, 496–499.
- [13] S. Liao, B. List, *Angew. Chem. Int. Ed.* **2010**, *49*, 628–631; *Angew. Chem.* **2010**, *122*, 638–641.
- [14] P. García-García, F. Lay, C. Rabalakos, B. List, *Angew. Chem. Int. Ed.* **2009**, *48*, 4363–4366; *Angew. Chem.* **2009**, *121*, 4427–4430.
- [15] V. Rauniyar, Z. J. Wang, H. E. Burks, F. D. Toste, *J. Am. Chem. Soc.* **2011**, *133*, 8486–8489.
- [16] D. Qian, J. Sun, *Chem. Eur. J.* **2019**, *25*, 3740–3751.
- [17] G. B. Rowland, E. B. Rowland, Y. Liang, J. A. Perman, J. C. Antilla, *Org. Lett.* **2007**, *9*, 2609–2611.
- [18] L. Ren, T. Lei, L.-Z. Gong, *Chem. Commun.* **2011**, *47*, 11683.
- [19] X. Cheng, S. Vellalath, R. Goddard, B. List, *J. Am. Chem. Soc.* **2008**, *130*, 15786–15787.
- [20] M. Rueping, E. Sugiono, C. Azap, T. Theissmann, M. Bolte, *Org. Lett.* **2005**, *7*, 3781–3783.
- [21] R. I. Storer, D. E. Carrera, Y. Ni, D. W. C. MacMillan, *J. Am. Chem. Soc.* **2006**, *128*, 84–86.
- [22] R. Hayes, G. G. Warr, R. Atkin, *Chem. Rev.* **2015**, *115*, 6357–6426.
- [23] D. Chen, M. Schmitkamp, G. Franciò, J. Klankermayer, W. Leitner, *Angew. Chem. Int. Ed.* **2008**, *47*, 7339–7341; *Angew. Chem.* **2008**, *120*, 7449–7451.
- [24] J. Chandrasekhar, R. Dick, J. Van Veldhuizen, D. Koditek, E.-I. Lepist, M. E. McGrath, L. Patel, G. Phillips, K. Sedillo, J. R. Somoza, et al., *J. Med. Chem.* **2018**, *61*, 6858–6868.
- [25] E. Masson, *Org. Biomol. Chem.* **2013**, *11*, 2859.
- [26] A. D. Becke, *J. Chem. Phys.* **1993**, *98*, 5648–5652.
- [27] S. Grimme, J. Antony, S. Ehrlich, H. Krieg, *J. Chem. Phys.* **2010**, *132*, 154104.
- [28] F. Weigend, R. Ahlrichs, *Phys. Chem. Chem. Phys.* **2005**, *7*, 3297.
- [29] F. Neese, *Wiley Interdiscip. Rev.: Comput. Mol. Sci.* **2012**, *2*, 73–78.
- [30] S. H. Vosko, L. Wilk, M. Nusair, *Can. J. Phys.* **1980**, *58*, 1200–1211.
- [31] R. Sahnoun, S. Koseki, Y. Fujimura, *J. Phys. Chem. A* **2006**, *110*, 2440–2447.

Manuscript received: March 9, 2020
 Revised manuscript received: April 22, 2020
 Accepted manuscript online: April 28, 2020
 Version of record online: June 15, 2020



Article

Enantiomerization of Axially Chiral Biphenyls: Polarizable MD Simulations in Water and Butylmethylether

Veronika Zeindlhofer ¹, Phillip Hudson ^{2,3} , Ádám Márk Pálvölgyi ⁴ , Matthias Welsch ¹, Mazin Almarashi ¹, H. Lee Woodcock ³ , Bernard Brooks ² and Katharina Bica-Schröder ⁴ and Christian Schröder ^{1,*}

¹ Department of Computational Biological Chemistry, University of Vienna, Währingerstraße 17, 1090 Vienna, Austria; veronika.zeindlhofer@univie.ac.at (V.Z.); m.welsch@chello.at (M.W.); a01619644@unet.univie.ac.at (M.A.)

² Laboratory of Computational Biology, National Heart, Lung, and Blood Institute (NHLBI), National Institutes of Health (NIH), Bethesda, MD 20892, USA; phillip.hudson@nih.gov (P.H.); brb@mail.nih.gov (B.B.)

³ Department of Chemistry, University of South Florida, Tampa, FL 33620, USA; hlw@mail.usf.edu

⁴ Institute of Applied Synthetic Chemistry, TU Wien, Getreidemarkt 9/163, 1060 Vienna, Austria; adam.palvoelgyi@tuwien.ac.at (Á.M.P.); katharina.schroeder@tuwien.ac.at (K.B.-S.)

* Correspondence: christian.schroeder@univie.ac.at

Received: 10 July 2020; Accepted: 25 August 2020; Published: 28 August 2020



Abstract: In this study, we investigate the influence of chiral and achiral cations on the enantiomerization of biphenylic anions in *n*-butylmethylether and water. In addition to the impact of the cations and solvent molecules on the free energy profile of rotation, we also explore if chirality transfer between a chiral cation and the biphenylic anion is possible, i.e., if pairing with a chiral cation can energetically favour one conformer of the anion via diastereomeric complex formation. The quantum-mechanical calculations are accompanied by polarizable MD simulations using umbrella sampling to study the impact of solvents of different polarity in more detail. We also discuss how accurate polarizable force fields for biphenylic anions can be constructed from quantum-mechanical reference data.

Keywords: chiral ionic liquids; biphenyl; chirality transfer; molecular dynamics simulations

1. Introduction

Over the last 20 years, chiral ionic liquids (CILs) have been in the focus of a rapidly growing field of research [1–4]. Although the first synthesis of a CIL was reported in 1997 [5], it took seven more years until the first successful chirality transfer by a CIL in an asymmetric Baylis–Hillman reaction was realized by Pégot et al. in 2004 [6]. However, since then the reports on successful applications of CILs in analytics [7–10] and asymmetric synthesis have been increasing steadily. In asymmetric synthesis, CILs can be used either as reaction solvent [11–13] or incorporated into the catalytic system, for example, as chiral ligand [3,14–16] or chiral organocatalyst [17,18].

Although chirality transfer via ion pairing in asymmetric synthesis (counterion directed catalysis) has been successfully realized in many high-impact studies [19–23], few examples that utilize ion aggregation in CILs for asymmetric synthesis exist. High selectivities of an aza-Baylis–Hillman reaction with a CIL as reaction medium were reported by Leitner and coworkers, while Wasserscheid and coworkers demonstrated chirality transfer in a CIL with prochiral cations and chiral anions in asymmetric hydrogenation reactions [2,11,13]. A better understanding of ion aggregation and chirality

transfer in CILs is necessary to enable the rational design of new catalytically active ionic liquids (ILs). Computer simulations can be a valuable tool in this respect since they offer a molecular view on ion aggregation in solution.

Many examples of successful chirality transfer experiments employ axially chiral compounds [20,21], which renders them promising for the design of new CILs. The rotational barrier of axially chiral *tropos* compounds is below 22.3 kcal/mol, meaning they can racemize at room temperature. The term racemization describes the irreversible conversion of an optically active compound (due to surplus of one enantiomer) into an optically inactive compound, where equal amounts of enantiomers are present [24]. If the rotational barrier of axially chiral compounds is greater than 22.3 kcal/mol, enantiomers are stable for more than 15 min at room temperature [25,26] and are called atropisomers [27], stemming from the ancient Greek word for “atropos” = “immutable, inflexible” [28]. Ligand and receptor chirality have a significant impact on biomolecular interactions, which is particularly essential for drug design, since two different enantiomers of a drug can differ significantly in their biological activity [29]. LaPlante et al. [25] discriminated between three classes of axial chirality based on the height of the rotational barrier: Class I molecules possess a barrier of less than 20 kcal/mol, which corresponds to a racemic mixture at room temperature in experiment. Class II molecules have a torsional barrier between 20 kcal/mol and 30 kcal/mol, which makes them problematic for drug design as the racemization can take place from within several minutes up to a month. This also hampers experimental analysis since the conversion between enantiomers can occur during measurements. However, class I and II molecules could be potentially interesting for chirality transfer as the switch from R_a to S_a or vice versa induced by the counter-ion may happen on a time scale of reactions. Class III molecules with rotational barriers higher than 30 kcal/mol are optimal for drug design as the racemization would take several years. In other words, the R_a and the S_a enantiomer can be synthesized separately. Class I molecules are *tropos*, while Class II and Class III molecules are atropisomers. Apart from being important for drug development, the use of atropisomeric, simple 1,1'-Bi-2-naphthol (BINOL)-derived chiral compounds already found a tremendously broad range of application in the field of asymmetric synthesis. In 1979 Noyori and co-workers published the use of a BINOL-based chiral reagent (BINAL-H) for asymmetric hydrogenations [30]. Since then, the classical BINOL-derived Class III compounds were proven to be extremely efficient for a large number of reactions as asymmetric catalysis as well [31]. Recently, another hot topic emerged in the field of asymmetric catalysis using atropisomeric and enantiomerically pure phosphoric acids. Starting from the first years of the 21st century, this field is constantly growing, providing a good alternative for a wide range of asymmetric transformations [32–34].

In this study, we are interested in the interconversion between enantiomers (enantiomerization [24]) of anionic biphenyls **1** and **2** (see Figure 1) in gasphase, *n*-butylmethylether (BuOMe) and water.

Anionic biphenyl **1** was chosen because experimental studies suggest chirality induction between its neutral form and a chiral diamine [35,36]. The phosphate bridged anion **2** was successfully used for selectivity enhancement in asymmetric transfer hydrogenation of enones [37]. In addition to the influence of the solvent, we want to investigate the effect of achiral and chiral cations on the enantiomerization barrier of the biphenyl anions **1** and **2**. We want to test if diastereomeric complex formation with a chiral cation can induce preference of one anion conformer, which would result in two diastereomerization barriers instead of a single enantiomerization barrier [38]. Figure 2 schematically illustrates the free energy profile of the enantiomerization process, and how chiral induction would be reflected as an asymmetry in the profile.

Despite their differing rotational barriers (see Results Section), both chiral anions **1** and **2** belong to Class I and are thus ideal candidates for the analysis of chirality transfer as the barrier may be overcome at room temperature. The amino-functionalized cations **3** and **4** are achiral and differ in their capability of hydrogen bonding to the anion. As already mentioned before, the neutral analog of cation **5** has been successfully applied in chirality transfer experiments [36].

Although the analysis of the rotational barriers of the biphenyls can be performed on a quantum-mechanical level, the enantiomerization process in various solvents is out of reach with this level of theory. Since we want to investigate the effect of hydrogen bonding between the distinct hydrogen bonding sites of the anion to both cation and solvent, explicit treatment of the solvent is preferable over dielectric continuum models. Hence, we augment our quantum-mechanical analysis of the rotational barrier with polarizable molecular dynamics simulations using umbrella sampling [39] to study the influence of the cations and the solvent on the interconversion.

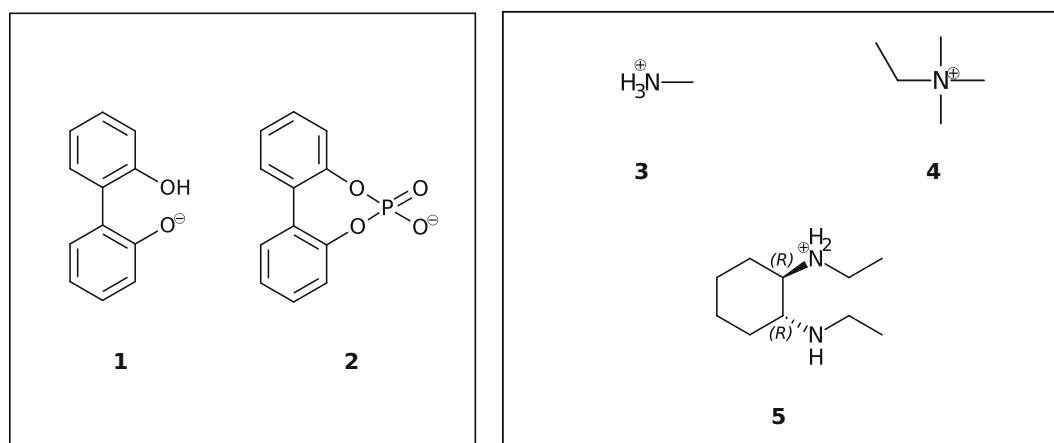


Figure 1. Axially chiral biphenyl-based anions (1, 2) and achiral (3, 4) and chiral cations (5) investigated in this study.

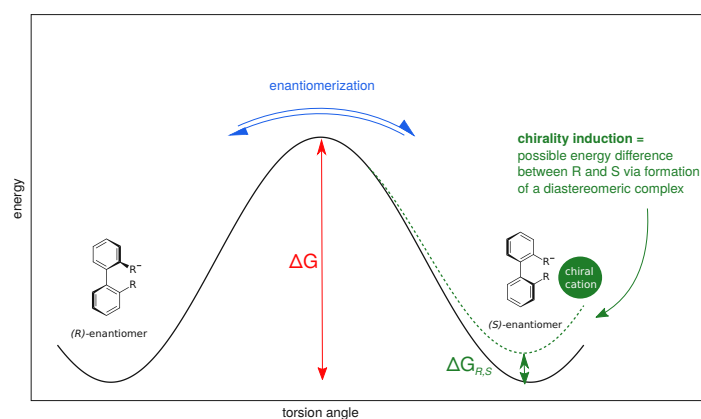


Figure 2. Schematic free energy profile of the enantiomerization in axially chiral biphenyl anions. The interconversion barrier ΔG determines the enantiomerization rate. If one conformer becomes energetically more favourable, e.g., due to formation of a diastereomeric complex with a chiral counterpart, the profile is rendered asymmetric (dashed line), resulting in two different diastereomerization barriers.

2. Results

This study is organized in two parts: First, we present the generation of quantum-mechanical (QM) target data and construction of force fields from the target data for ortho-substituted biphenyl anions. Second, we apply these force fields in molecular dynamics (MD) simulation to study ion pairing and chirality induction of single ion pairs in solution.

2.1. Enantiomerization Barriers of Ortho-Substituted Biphenyls

Since for axially chiral biphenyl derivatives the transition between enantiomers proceeds via rotation around the aryl-aryl bond, it is crucial that the corresponding torsional energy profile is

represented correctly in the force field, which is not the case for many standard force fields of unsubstituted biphenyl [40,41]. Our force fields are based on the CHARMM Drude force field [42], in which the general approach for fitting flexible degrees of freedom is to target QM scans on the MP2/6-31G(d) (6-31+G(d,p) for ions) level of theory. In the case of biphenyl-based anions **1** and **2**, care must be taken when generating QM target data in that way for several reasons: First and foremost, the QM treatment of biphenyl-based structures is not straightforward. Computing rotation barriers for simple unsubstituted biphenyl has been a particular challenge addressed in several studies [43–47], and has only been resolved in 2008 by Johansson and Olsen [41,48] by using a high-level coupled-cluster approach combined with several extrapolation schemes. The situation seems less challenging for substituted biphenyls, since good results have been obtained with standard DFT and ab initio approaches [49–51] in some cases. However, most of these studies investigate only small sets of specific biphenyls, and do not allow to make conclusions about the general applicability of specific QM methods for substituted biphenyls. To the best of our knowledge, the most systematic computational study on rotational barriers in substituted biphenyls so far was published by Masson in 2013 [52]. In this study, barrier energies of 13 substituted biphenyls computed with different density functional theory (DFT) methods are compared against the experiment. The author found that the B3LYP and B97 functionals augmented by an empirical dispersion correction [53,54] and a large triple-zeta basis set (def2-TZVPP [55]) gave the best agreement with experiment.

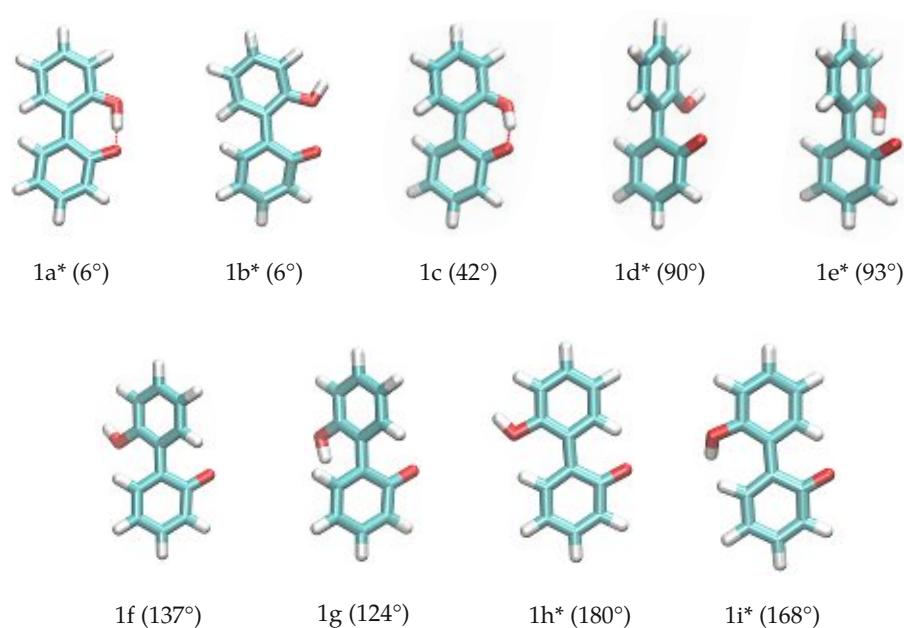
Another crucial prerequisite for precise barrier energies is the accuracy of transition state geometries. In ortho-substituted biphenyls, steric repulsion between the substituents can influence the transition state. When ortho-substituents have rotational degrees of freedom, different transition states depending on the rotational conformation of the ortho-substituent are possible (see Figure 3), which is the case for anion **1**. The rotational position of the hydroxy-hydrogen influences the energy of the transition states and, consequently, a simple one-dimensional dihedral scan does not suffice to describe the enantiomerization pathway and a two-dimensional scan exploring both the aryl-aryl dihedral as well as the rotation of the hydrogen, respectively, is necessary. However, in case of **1**, this 2D potential energy surface exhibits significant energy jumps because additional degrees of freedom change abruptly for particular conformations. For example, the strong intramolecular hydrogen bond causes significant changes in the O-H bond length and distortions in the geometry when the bond is broken during rotation. For **2**, the rotation cannot be described with one degree of freedom either, since the O-P-O-C and C-C-O-P dihedrals all change during the rotation. Consequently, we constructed the potential energy surface from QM ground and transition state optimizations without constraints (transition state 1b was omitted from the fit for **1** due to the high barrier). This gives fewer but more reliable points on the potential energy surface associated with the enantiomeric transition. The geometries of all ground and transition states optimized on the RI-MP2/6-31+G(d) level of theory are depicted in Figure 3. Although interconversion will likely proceed via the lowest-lying path and will not include all structures depicted in Figure 3, optimizing all possible ground and transition states is necessary in order to identify the most favorable pathway.

To probe the performance of different functionals and basis sets, we have optimized the structures in gas phase using two different levels of theory (RI-MP2/6-31+G(d) and B3LYP-D3/def2-TZVPP) and subsequently performed single point calculations on both structure sets using four different methods (listed in Figure 3). RI-MP2/6-31+G(d) and RI-MP2/cc-pVQZ were chosen as these methods are parts of the CHARMM Drude force field parametrization philosophy, and B3LYP-D3/def2-TZVPP was successfully applied by Masson in his work [52]. The DLPNO-CCSD(T)/def2-TZVP [56] level of theory is employed as a reference since we have used this level of theory successfully in a previous study [37]. The results are listed in Figure 3. It is of particular importance that the energy difference between ground state 1c and transition state 1a* is correctly reproduced since it is the lowest barrier through which interconversion can occur. Based on the data in Figure 3, it is clear that the RI-MP2/6-31+G(d) level is not sufficient to represent the barrier properly since it is about 40% higher compared to the DLPNO-CCSD(T)/def2-TZVP reference energy in the case of the RI-MP2 optimized geometries,

and even 60% higher in case of the B3LYP-optimized geometries. The B3LYP-D3/def2-TZVPP barrier is lower by 1 kcal/mol, while barriers on the RI-MP2/cc-pVQZ and DLPNO-CCSD(T)/def2-TZVP level of theory coincide, justifying the use of RI-MP2/cc-pVQZ energies as target values for the force field fitting. Furthermore, the obtained geometries show a dependence on the optimization method with energies differing by approximately 0.5 kcal/mol. Since we aim at consistency with the existing CHARMM Drude force field, we will use the geometries optimized on the RI-MP2/6-31+G(d) level of theory. It is visible from the data that the lowest-energy pathway for the full rotation proceeds with the hydroxy-hydrogen pointed towards the second ring.

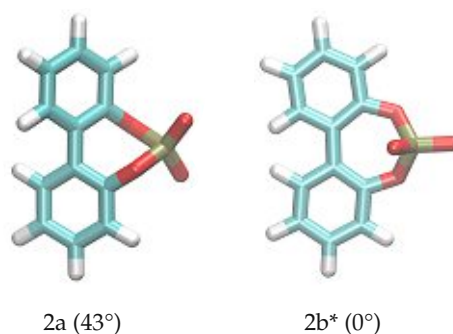
The enantiomerization pathway for anion **2** is comparably simple, with the bridged phosphate group allowing only one possible transition state (Figure 4). The same QM analysis as for anion **1** has been performed for anion **2**, with the resulting energies being shown in Figure 4. In contrast to compound **1**, the level of theory used for the optimization is not as significant as for **1**, with the most substantial difference being 0.3 kcal/mol between barriers. However, it is also clear that RI-MP2/6-31+G(d) gives insufficient energies that are about 40% higher than the DLPNO-CCSD(T)/def2-TZVP results. The B3LYP-D3/def2-TZVPP energies are closer to the DLPNO-CCSD(T)/def2-TZVP barriers than for **1**, and again the RI-MP2/cc-pVQZ level of theory gives satisfying results that can be used in the force field fit.

Both anions definitely belong to class I of axially chiral molecules concerning the rotational barrier at 0°. The lowest barriers are less than 10 kcal/mol and thus more or less frequently crossed during polarizable MD simulations.



| Level of Theory | | E_{el} [kcal/mol] | | | | | | | | | |
|---------------------|-------------------------|---------------------|------|-----|------|------|------|------|------|------|--|
| Optimization | Energy Evaluation | 1a* | 1b* | 1c | 1d* | 1e* | 1f | 1g | 1h* | 1i* | |
| RI-MP2/6-31+G(d) | RI-MP2/6-31+G(d) | 8.5 | 41.8 | 0.0 | 23.4 | 12.6 | 21.5 | 11.8 | 26.2 | 26.2 | |
| | RI-MP2/cc-pVQZ | 6.2 | 41.0 | 0.0 | 25.5 | 15.0 | 22.3 | 13.4 | 25.4 | 25.2 | |
| | B3LYP-D3/def2-TZVPP | 5.2 | 39.3 | 0.0 | 24.9 | 14.4 | 21.4 | 13.0 | 23.8 | 23.7 | |
| | DLPNO-CCSD(T)/def2-TZVP | 6.2 | 40.8 | 0.0 | 24.6 | 14.1 | 21.9 | 12.9 | 25.2 | 24.9 | |
| B3LYP-D3/def2-TZVPP | RI-MP2/6-31+G(d) | 9.0 | 42.5 | 0.0 | 23.2 | 12.4 | 21.4 | 11.7 | 26.4 | 26.8 | |
| | RI-MP2/cc-pVQZ | 5.7 | 40.7 | 0.0 | 25.9 | 15.3 | 22.6 | 13.6 | 25.1 | 24.7 | |
| | B3LYP-D3/def2-TZVPP | 4.8 | 38.7 | 0.0 | 25.1 | 14.6 | 21.5 | 13.1 | 23.5 | 23.0 | |
| | DLPNO-CCSD(T)/def2-TZVP | 5.7 | 40.2 | 0.0 | 24.7 | 14.1 | 22.0 | 13.1 | 25.0 | 25.0 | |

Figure 3. Ground and transition state geometries and their relative energies of anion **1** for the rotation around the aryl-aryl bond. The value in brackets is the corresponding dihedral angle. Transition states are marked with an asterisk (*). Only one enantiomer is shown for every state.



| Level of theory | | E_{el} [kcal/mol] | |
|---------------------|-------------------------|---------------------|------|
| Optimization | Energy evaluation | 2a | 2b* |
| RI-MP2/6-31+G(d) | RI-MP2/6-31+G(d) | 0.0 | 11.5 |
| | RI-MP2/cc-pVQZ | 0.0 | 8.5 |
| | B3LYP-D3/def2-TZVPP | 0.0 | 7.9 |
| | DLPNO-CCSD(T)/def2-TZVP | 0.0 | 8.3 |
| B3LYP-D3/def2-TZVPP | RI-MP2/6-31+G(d) | 0.0 | 11.6 |
| | RI-MP2/cc-pVQZ | 0.0 | 8.2 |
| | B3LYP-D3/def2-TZVPP | 0.0 | 7.6 |
| | DLPNO-CCSD(T)/def2-TZVP | 0.0 | 8.1 |

Figure 4. Ground and transition state geometries and their relative energies of anion **2** for the rotation around the aryl-aryl bond. The value in brackets is the corresponding dihedral angle. The transition state is marked with an asterisk (*). Only one enantiomer is shown for every state.

2.2. Construction of the Polarizable Force Field

Using the generated QM data on the RI-MP2/cc-pVQZ//RI-MP2/6-31+G(d) level of theory as target data, dihedral potentials associated with the rotation around the aryl-aryl-bond were fitted. To generate molecular mechanics (MM) energies, the aryl-aryl dihedral in both anions, as well as the dihedral associated with rotation of the ortho-substituent in **1** were held fixed at values obtained from the QM geometry optimizations and all other remaining degrees of freedom were minimized. Improper dihedrals were added to prevent unwanted out-of-plane-bending, which allowed exploring the enantiomerization pathway along this one degree of freedom. For **1**, the aryl-aryl dihedral parameters as well as the H-O-C-C dihedral parameters were fitted. For **2**, the aryl-aryl dihedral parameters and the C-O-P-O and C-C-O-P dihedral parameters were fitted to reproduce the torsional profile. The parameter values can be found in Supplementary Material 8.

Before discussing the fit results, it is necessary to analyze the effect of the intramolecular hydrogen bond in anion **1**. Via this hydrogen bond, charge can be transferred from the negatively charged oxygen, resulting in different charge distributions in the most favorable *syn* and *anti* ground states (**1c** and **1g** in Figure 3) as depicted in Figure 5. Since the *syn* ground state (containing the hydrogen bond) is preferred by about 13 kcal/mol, it is unlikely that the *anti* conformation is visited in simple equilibrium simulations. However, since we want to explore the full rotation around the aryl-aryl bond and cannot exclude competitive hydrogen bonding of other ions, we need to consider that the charge distribution will change once the hydrogen bond is broken. To investigate the effect of the two different charge distributions, we have constructed two different force fields for compound **1** -one uses partial charges computed on the geometry of **1c**, the other one charges computed on the geometry of **1g**. The two different partial charge distributions will be labelled as *anti* (distribution corresponding to geometry **1g**) and *syn* (distribution of geometry **1c**) throughout the text. As the hydroxy-proton is partially shared by both oxygens in the *syn* configuration, the negative partial charges of the oxygens are more similar compared to the *anti* configuration. Here, the oxygen without the attached hydrogen is far more negatively charged. Consequently, a stronger intramolecular hydrogen bond is expected for the *anti* partial charge distribution (see left Figure 5).

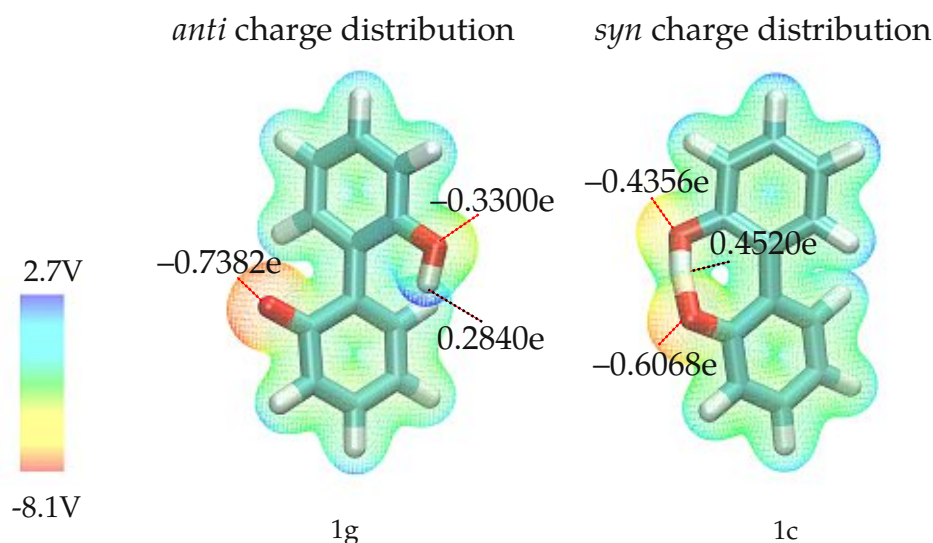


Figure 5. Molecular electrostatic potential for geometries 1g (left) and 1c (right), computed on the RI-MP2/Sadlej-TZ level of theory and mapped to the electron density surface at $0.002 \text{ e}/\text{\AA}^3$. Please note that the shown partial charges are the charges used in the force field, which differ from the QM partial charges since polarizable force fields with Drude particles require refitting of the QM charges.

The results of the torsional fit for both charge distributions are depicted in Figure 6. While the lower energy differences are well captured by the fitted parameters, higher-energy parameters are not reproduced as well but play a minor role in enantiomerization due to their much higher energy compared to the 0° barrier. As rotation is most likely to proceed via the lowest-energy pathway, the resulting fit is satisfying. Consequently, in the simulations the torsional potential will only be computed from -160° to 160° for anion **1**. In case of the bridged anion, the scan is restricted from -60° to 60° .

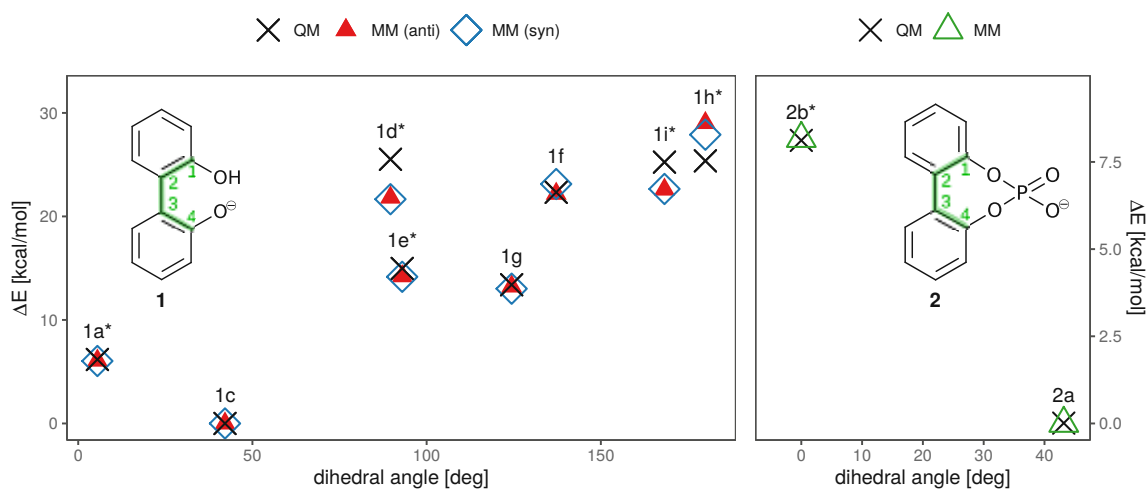


Figure 6. QM and MM torsional profile of compounds **1** and **2**, constructed from the structures shown in Figures 3 and 4. For **1**, results for both the *syn* and *anti* charge set are depicted. The dihedral plotted on the x axis is marked in green in the insets. Points represent the conformations shown in Figures 3 and 4 and are labelled accordingly. Again, transition states are marked with an asterisk (*). Since the profiles are symmetric, only one half is shown.

2.3. Effect of the Solvent

To investigate the influence of the solvent and counterion on the enantiomeric stability of the anion, we have conducted umbrella sampling simulations to compute the free energy profile of rotation around the aryl-aryl bond (10° increments, additional windows at -15° , -5° , 5° and 15° for anion **2**, see Figures S1 and S2 for a more detailed discussion). To investigate the effect of the solvent, we will investigate systems of a single ion pair of cation **3** and one anion (either **1** or **2**) in water and *n*-butylmethylether (BuOMe). In Figure 7, the free energy torsional profile of the rotation around the aryl-aryl-bond of the anion is shown for a single ion pair of cation **3** together with anion **1** and **2**, respectively (gasphase profile is single anion only). The shaded areas depict the standard deviation of the respective energy profile.

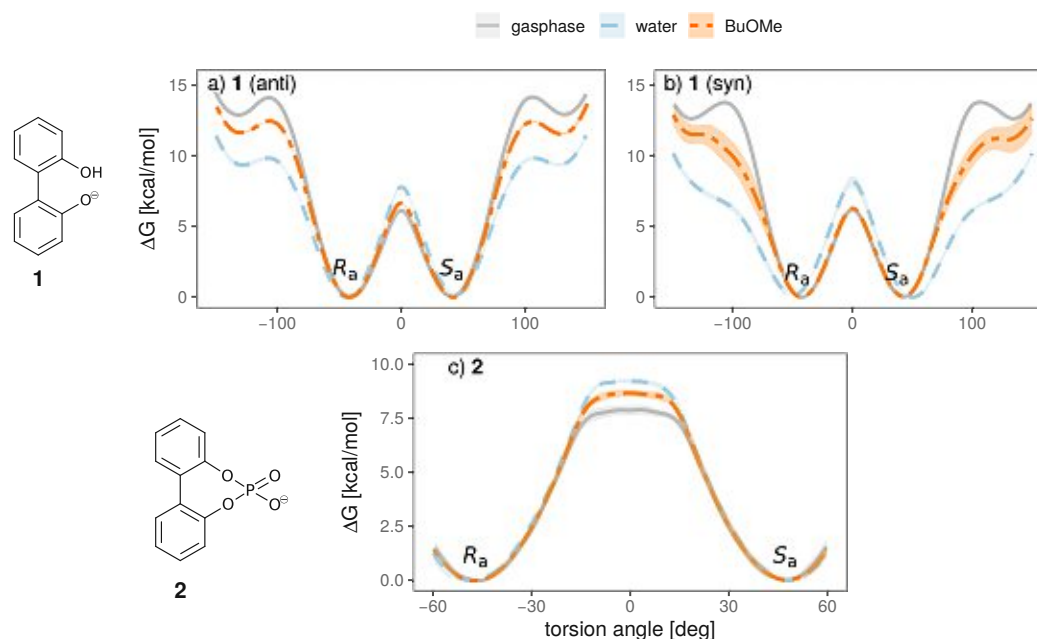


Figure 7. Free energy torsional profile of the aryl-aryl bond rotation in **1** (a,b, top panel) and **2** (c, bottom panel), for a single molecule in gasphase (grey) and a single ion pair with cation **3** in water (blue) and BuOMe (orange). For **1**, profiles obtained with both charge distributions (*anti* in a, *syn* in b) are shown.

It is clearly visible that the solvent strongly influences the profile. The 0° barrier, which is the lowest and hence the most important one, is increased in water compared to the less polar BuOMe and gasphase. Contrary, the barriers at 90° are lowered by approximately 2.5 kcal/mol compared to BuOMe, which is likely caused by hydrogen bonding with water molecules. The influence of solvent on rotational barrier energies has been reported in literature [57,58]. Demir-Ordu et al. observed an increase in barrier energies of an axially chiral compound by hydrogen bonding to the solvent [59]. QM studies on ortho-substituted biphenyls by Masson [52] suggest that solvent effects are even more pronounced when the biphenyl compound bears charged substituents in the ortho-positions, such as the biphenyls used in this study. The effect of water on the torsional barrier is stronger for the *syn* partial charge distribution (see Figure 7a,b). Furthermore, the minima of the torsional potential are slightly shifted in water for the *syn* configuration by 15° to higher absolute angles (see Figure 7b). Thus, the interaction of the *syn* partial charge distribution with water seems stronger.

Interestingly, the torsional barrier at 0° of the phosphoric acid bridged anion **2** in water is only 1 kcal/mol higher than the corresponding barrier of the biphenolat **1**. Apparently, the ring tension is not significantly higher compared to the intramolecular hydrogen bond of compound **1**. Additionally, the rotational barrier of **2** exhibits a small plateau which is broader compared to **1**.

Hydrogen bonds are most probably the strongest interaction between the anions **1** and **2** and the solvent. In Figure 8 the average number of hydrogen bonds is depicted for the oxygens and the hydroxy-proton of **1**. Hydrogen bonds to the solvent (blue for water, orange for BuOMe) are displayed as solid lines, whereas the intramolecular hydrogen bond is shown as a dashed line. As expected from the energy profiles in Figure 7a,b, the number of hydrogen bonds between the *syn* compound and water shows a stronger dependence on the dihedral angle and consequently, the rotational barrier changes. However, the average number of hydrogen bonds to the oxygens is roughly the same for *anti* and *syn*. The intramolecular hydrogen bond between -60° and 60° seems to be neither a function of the dihedral angle nor of the solvent as visualized by the dashed lines in the middle of Figure 8. Butylmethylether can only accept hydrogen bonds. The only hydrogen which may act as hydrogen donor of **1** is the hydroxy proton. The hydrogen is a much stronger donor in the *syn* charge distribution, as it carries a higher partial charge (0.4520e compared to 0.2840e). This difference in hydrogen bonding likely causes the discrepancy between the *syn* and *anti* profiles for water in Figure 7, also because the position of the hydrogen influences the rotational barrier as shown in Figure 3.

In anion **2**, hydrogen bonds to the solvent are only possible with water, and there is no dependence on the dihedral angle. The oxygens adjacent to the rings form on average 0.6 hydrogen bonds with water, while the terminal oxygens form 2.4 on average (data shown in Figure S6).

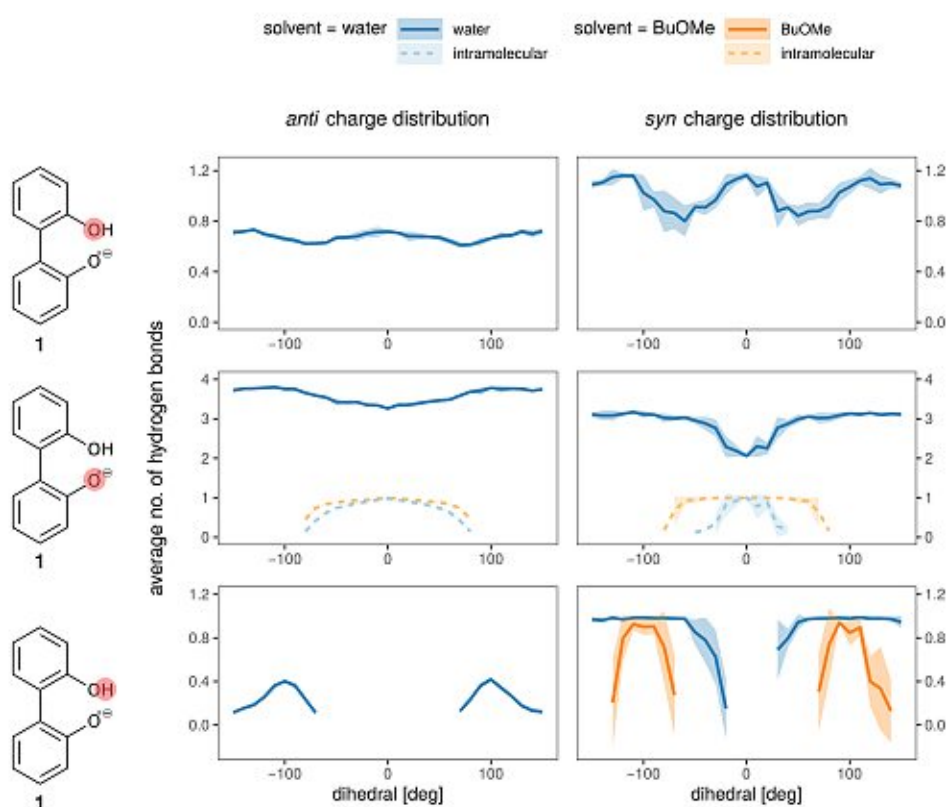


Figure 8. Hydrogen bonding to all hydrogen bonding sites of the anion (single ion pair of **1** and **3** in solvent).

2.4. Effect of the Counterion

The initial idea behind using cation **5** was to explore a possible chirality transfer between cation and anion, since experimental studies on successful chirality transfer between the neutral analogs of chiral cation **5** and anion **1** exist [36]. In these studies, the authors suggest formation of a complex where the neutral form of **5** acts as a “bidentate” ligand that accepts hydrogen bonds from the

hydroxy groups of the neutral form of **1**. Although anion **1** can donate only one hydrogen bond and intramolecular bonding is stronger in the ionic form, we nevertheless want to explore the possibility of chiral induction, since charged compounds drastically increase the chance of complex formation. Furthermore, the cation acts as a stronger hydrogen bond donor due to its free protic hydrogens. If a diastereomeric complex between the chiral cation **5** and anion in which either R_a or S_a is preferred is formed, this should be visible in the free energy profile.

As water is a polar solvent with a dielectric constant of roughly 80, the probability of ion pairing is low as each ion is surrounded by its own hydration shell. Consequently, we expect only weak chirality transfer. As shown in Figure 9a,c the dihedral potential of the anion **1** is symmetric in water and does not depend on the cation, since simulations containing the achiral cations **3** and **4** result in the same free energy profile as the simulation using the chiral cation **5**. The picture does not change in the apolar BuOMe, which has a dielectric constant of 4.5 and consequently a much higher probability for ion pairing. For the *anti* charge distribution, the free energy profile is still not a function of the cation as shown in Figure 9b,d. For the *syn* charge distribution, there is a slight cation dependence of the profile in the regions around -100° and 100° , but the profile in between is similar for all three cations. The profiles are still symmetric, indicating no preference of either enantiomer. These results suggest that hydrogen bonding of the anion to the cation plays a negligible role, as the achiral cation **4** cannot form hydrogen bonds in contrast to **3**. For anion **2**, no notable influence of the cation on the profiles can be detected in Figure 9e,f either, and as for compound **1**, the profiles indicate no preference for one enantiomer

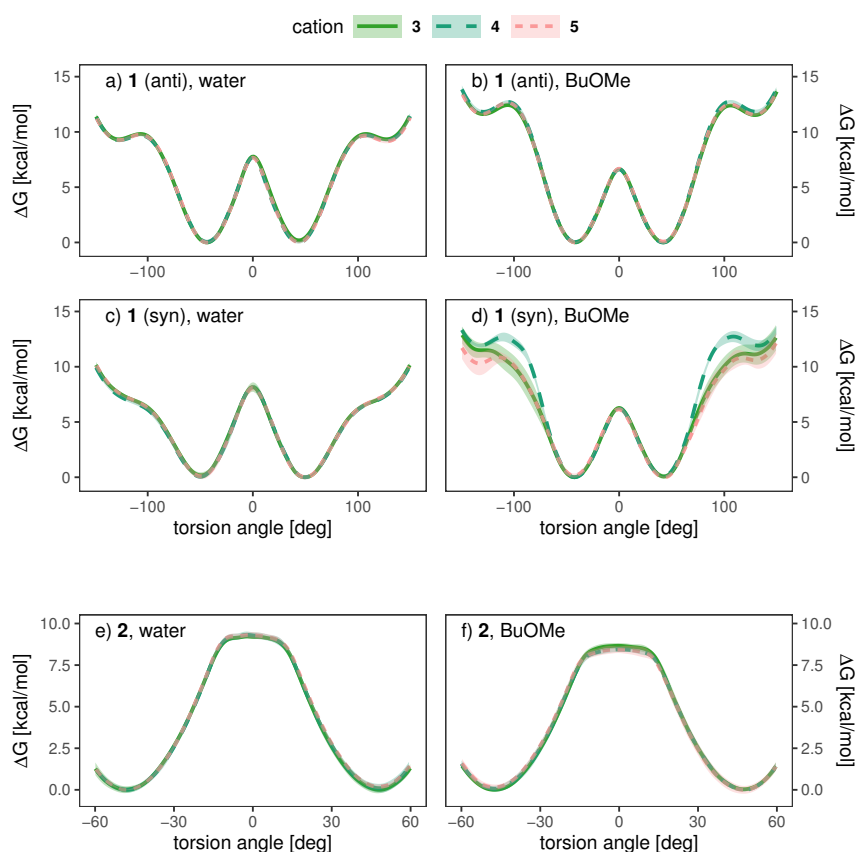


Figure 9. Dependence of the free energy torsional profile of anions **1** (*anti* (a,b, top) and *syn* (c,d, middle) charge distribution) and **2** (e,f, bottom) on the counterion, for a single ion pair in water (a,c,e, left) and BuOMe (b,d,f, right).

The hydrogen bonding of both charge distributions of anion **1** to the cations is shown in Figure 10 for the BuOMe solution. As already discussed, **4** cannot form hydrogen bonds and consequently only

the intramolecular hydrogen bond of biphenyl **1** is depicted. The intramolecular hydrogen bond (violet dashed and solid lines) is similar for both charge distributions, and is hardly affected by cation choice. The intermolecular hydrogen bond between the anion and cations **3** and **5** is still not a function of the cation, but there are some differences between the *syn* (dashed lines) and *anti* charge distribution (solid lines).

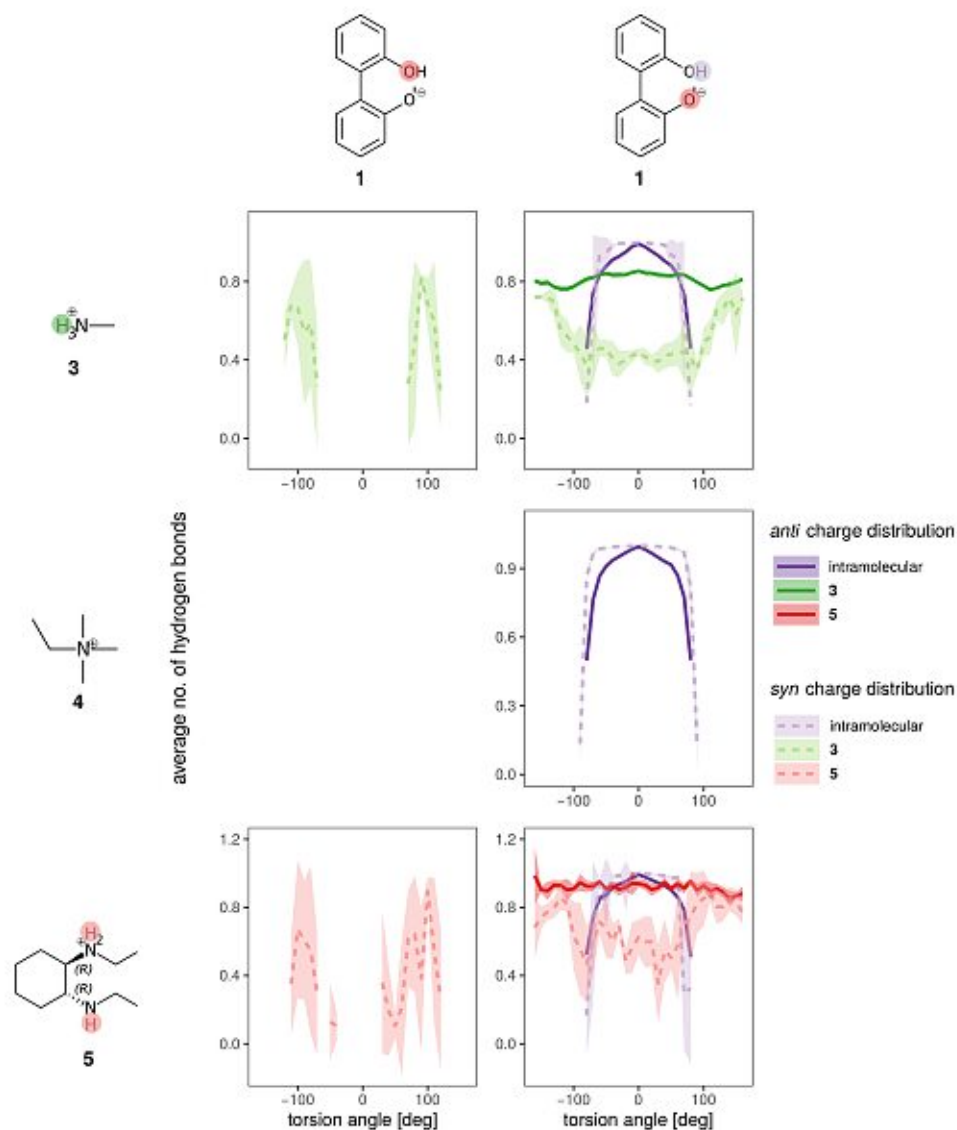


Figure 10. Hydrogen bonding of anion **1** for the *syn* (lighter dashed lines) and *anti* charge distribution (darker solid lines) for the different counterions in BuOMe.

As the partial charges of the oxygens for the *syn* charge distribution differ less compared to the *anti* (see Figure 5), the overall U-shaped hydrogen bonding profile of the *syn* oxygens as a function of the dihedral angle resembles each other. Only the minimum for the hydroxy-oxygen is lower as no hydrogen bonding occurs around 0° . In case of the anionic oxygen, the minimal number of hydrogen bonds is still 0.4 at 0° . The situation drastically changes for the *anti* charge distribution. Here, the hydroxy-oxygen has zero hydrogen bonds to the cations irrespective of the dihedral angle. The anionic oxygen with the much more negative partial charge ($-0.7382e$) forms 0.8 hydrogen bonds on average to the cations which is also not a function of the dihedral angle. The strongest change in

the hydrogen bonding as a function of the dihedral angle can be found at -100 and $+100^\circ$ for the *syn* charge distribution. At the same angles, the deviations in the free energy profiles in Figure 9d occur indicating that the hydroxy oxygen plays a major role.

Only the terminal oxygens of the anion **2** form hydrogen bonds to the cations **3** and **5**. The number of hydrogen bonds is not a function of the dihedral angle and on average, 0.45 and 0.5 hydrogen bonds exist, respectively (data shown in Figure S7).

3. Concluding Discussion

For the analysis of the enantiomerization of axially chiral biphenyls in solution, a dual method approach is preferable. If multiple degrees of freedom are necessary to describe the aryl-aryl torsion in a QM scan, ground and transition state optimizations without restraints can be used to construct the potential energy surface. To obtain accurate barrier energies for substituted biphenyls, high-level methods such as the RI-MP2/cc-pVQZ level used in this study are necessary. Since the influence of the solvent and cation are out of reach for high-level quantum-mechanical methods, we used the QM data to parametrize a polarizable force field. In molecular dynamics simulations the free energy ΔG of the aryl-aryl torsion as a function of the cations and solvent is accessible. In this work, we have shown that the solvents *n*-butylmethylether and water affect the free energy profile of the torsion. In water, the lowest energy barrier at a dihedral of 0° is increased compared to *n*-butylmethylether. However, the nature of the cations has only a marginal impact on $\Delta G(\phi)$, and symmetric profiles are obtained in all cases. We therefore conclude that for the systems investigated in this work, no chirality transfer has taken place although the cations form hydrogen bonds to the anion. We have observed no preference for R_a or S_a in the simulations.

Another important factor in the force field development for biphenyl-based compounds is the influence of the configuration on the partial charge distribution, which is especially important for anion **1** due to the intramolecular hydrogen bond. In this study we have shown that the *syn* and *anti* configuration of **1** result in different partial charge distributions which influence the hydrogen bonding behavior. Although dihedral parameters were adapted independently to reproduce the target QM energies as closely as possible, different hydrogen bonding with the solvent results in different profiles, which is especially problematic when the simulation aims at exploring conformations that differ from the one used for generation of partial charges. As classical molecular dynamics simulations operate with fixed partial charges, a switch between *syn* and *anti* partial charge distribution would be desirable. However, since this is not viable in long-term molecular dynamics simulations, at least polarizable simulations are preferable as the induced dipoles may model the change of the electrostatic potential as a function of the aryl-aryl dihedral angle to some extent. Although the anions investigated in this work belong to class I of axially chiral molecules with rotational barriers of less than 20 kcal/mol, the computation of the free energy ΔG requires exceptionally long molecular dynamics simulations, as even simulations of more than 100 ns did not yield adequate statistics. Consequently, enhanced sampling techniques such as the umbrella sampling used in this study are strongly recommended.

4. Materials and Methods

4.1. Quantum-Mechanical Calculations

All QM calculations were performed with the quantum-chemistry package ORCA [60]. Ground and transition state geometry optimizations were performed on the the RI-MP2/6-31+G(d) (auxiliary basis for RI-MP2: def2-TZVP) and B3LYP-D3/def2-TZVP level of theory. In all calculations employing the B3LYP functional, correlation of the uniform electron gas was modeled according to the Vosko-Wilk-Nusair VWN5 formalism [61]. Transition state geometries were optimized in a two-step procedure: In the first step, a constraint minimization with a restraint on the aryl-aryl-dihedral (0° , 90° or 180° for the respective transition states) was performed, and the resulting structure used

as input for unrestrained transition state optimization. Transition states were verified by subsequent frequency calculations. On the obtained geometries, single point calculations with a set of different methods and basis sets were performed with ORCA (see Figure 3 for an overview of the employed methods). For the RI-MP2/cc-pVQZ calculations, a cc-pVQZ auxiliary basis was used. The molecular electrostatic potentials shown in Figure 5 were computed with ORCA on the RI-MP2/Sadlej-TZ level of theory and mapped to the electron density surface at $0.002 \text{ e}/\text{\AA}^3$.

4.2. Force Field Parametrization

In all simulations, electronic polarizability was included via Drude oscillators. Parameters were based on the existing CHARMM Drude force field (see reference [42] and references therein) which is available from http://mackerell.umaryland.edu/charmm_drude_ff.shtml. Ions 3 and 4 as well as the solvents (*n*-butylmethylether BuOMe and the SWM4 water model) were readily available from this force field, ions 1, 2 and 5 required additional parametrization.

The optimization targeted quantum-mechanically calculated reference data. All QM calculations were performed with ORCA [60] and PSI4 [62]. Parametrization proceeded in two main steps: In the first, electrostatic parameters (partial charges, atomic polarizabilities, Thole screening factors) were optimized, followed by optimization of bonded parameters. Lennard-Jones parameters were not optimized, but taken from the CHARMM Drude force field. Atomic polarizabilities and charges in gas phase were computed according to protocols described in detail in references [63–65] using geometries optimized at the RI-MP2/6-31+G(d) level of theory: Atomic polarizabilities were obtained on the RI-MP2/Sadlej-TZ level of theory using the methodology described in references [63–65]. According to suggestions in reference [42], polarizabilities were subsequently scaled by empirical factors, 0.85 for the cation, 0.724 for anion 1 and 0.6 for anion 2. Initial Thole screening factors were taken from similar structures already included in the CHARMM Drude force field and subsequently modified to reproduce the components of the molecular polarizability.

Initial atomic charges were obtained via restrained electrostatic potential (RESP) fitting [66,67] on the RI-MP2/Sadlej-TZ [68] level of theory. Charges were then modified to reproduce the components of the molecular dipole moment as well as interaction energies of hydrogen bonding sites with water, all computed with single point RI-MP2/cc-pVQZ energy evaluations on structures optimized at RI-MP2/6-31+G(d) [69]. Compound 1 can form a relatively stable intramolecular hydrogen bond, which influences the charge distribution—to investigate this, two charge distributions were computed for 1—one with and one without the hydrogen bond (*syn* and *anti*, see Figure 5 and Figure S5). A more thorough discussion of this issue can be found in the Results section.

In a second step, bonded parameters were optimized. To ensure compatibility with the existing CHARMM Drude force field, only parameters not already included in the force field were optimized. To alleviate the cost of parametrization, we assigned parameters by similarity as often as possible and explicitly fitted only those that have no resembling parameters and/or are crucial to the overall conformation of the molecule. Fitted parameters are marked explicitly in the force field (see Supplementary Material 8). For the parameters that were explicitly fitted, QM relaxed scans of the relevant degree of freedom on the RI-MP2/6-31+G(d) level of theory were conducted. Parameters were then fitted to target these scans using the lsfitpar program [70] as well as manual fitting in some cases. The aryl-aryl bond torsion of compounds 1 and 2 was fitted as described in the results section - the potential energy surface was constructed from ground and transition state optimizations without geometry restraints. The specific dihedrals fitted to reproduce the aryl-aryl torsion are marked in the force fields (see Supplementary Material 8). Optimizations were performed on the RI-MP2/6-31+G(d) level of theory, followed by energy evaluations on the RI-MP2/cc-pVQZ level of theory. Furthermore, improper dihedrals were added to prevent unwanted out-of-plane bending for the biphenyl-based compounds.

5. Umbrella Sampling

All simulations were performed with a GPU-capable version of the program package CHARMM [71,72]. In all simulations, the Velocity-Verlet integrator [73] with a timestep of 0.5 fs was employed. All simulations made use of a dual thermostat, using the Andersen-Hoover equations at constant pressure and the Nosé-Hoover equations at constant volume. The SHAKE algorithm was applied to fix lengths of bonds to hydrogen atoms [74]. Drude masses were set to 0.4 amu.

5.1. Gasphase Simulations

For simulations of a single ion in gas phase at $T=300\text{K}$, an infinite cut-off was applied and electrostatic interactions were calculated explicitly. For the Umbrella sampling [39], a harmonic restraint with a force constant of $100\text{ kcal mol}^{-1}\text{ rad}^{-2}$ (CONS DIHE command in CHARMM) was placed on the torsion angles depicted in Figure 11.

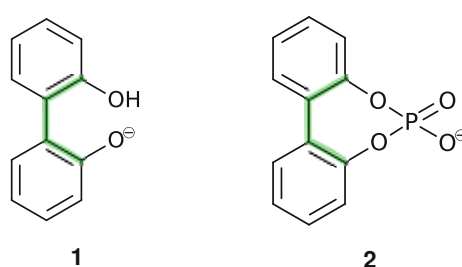


Figure 11. During production runs, the dihedral angles marked in green were held fixed at a certain value by a harmonic restraint.

Separate simulations at 10° intervals were used to generate umbrella sampling data, with a range of -160° to 160° for anion **1** and a range of -60 to 60° for anion **2**. For anion **2**, additional windows at -15 , -5 , 5 , and 15° were added (see Figure S1 for further discussion). After applying the restraint, each simulation was equilibrated for 250 ps, followed by a production phase of 5 ns (see Figure S3 for further discussion). Data was written to disk every 500 ps. The free energy profile was obtained in a post-processing step with the vFEP (variational free energy profile) program [75]. By splitting the data into five blocks and computing individual profiles for each block, the standard deviation was estimated.

5.2. Simulations in Solution

Simulations were performed at $T=300\text{ K}$ and atmospheric pressure. In all simulations, periodic boundary conditions were applied. A non-bonded cut-off of 12 \AA and a smooth switching function between 10 and 12 \AA were used. Electrostatic interactions were calculated with the Particle Mesh Ewald Method, employing a grid of approximately 1 \AA , cubic splines of order 6 and $\kappa = 0.41\text{ \AA}^{-1}$. For each system, five replica simulations were performed. Data for each replica was generated as follows: Initial configurations of a single ion pair in solution were generated with PACKMOL [76] and equilibrated in the NpT ensemble for 0.5 ns. Subsequently, the dihedral restraint was applied according to the protocol used in the gas phase. After applying the restraint, the system was allowed to equilibrate for 0.25 ns in the NVT ensemble, followed by a production phase of 1 ns in the NVT ensemble. Data was written to disk every 0.5 ps, resulting in 2000 data points per replica. 5 replica per window were generated this way, resulting in an overall simulation times of 5 ns (10,000 data points) per window, see Figure S4. An overview of the simulations can be found in Supplementary Material 6. Dihedral values were extracted with CHARMM in a post-processing step. The free energy profiles were again computed with the vFEP program. Hydrogen bonds for every replica simulation were analyzed with CHARMM, using distance and angle cut-offs of 2.4 \AA and 135° , respectively. Standard deviations for free energy profiles and hydrogen bonding were computed from the five

replica simulations. Figures were created using VMD [77] and the ggplot2 package within the R program suite [78,79].

Supplementary Materials: The following are available at <http://www.mdpi.com/1422-0067/21/17/6222/s1>.

Author Contributions: Conceptualization, P.H., Á.M.P., K.B.-S. and C.S.; Formal analysis, V.Z., M.W. and M.A.; Funding acquisition, K.B.-S. and C.S.; Investigation, V.Z.; Methodology, P.H., Á.M.P., K.B.-S. and C.S.; Project administration, K.B.-S. and C.S.; Resources, H.L.W., B.B. and K.B.-S.; Supervision, H.L.W., B.B., K.B.-S. and C.S.; Visualization, V.Z.; Writing—original draft, V.Z., Á.M.P. and C.S.; Writing—review & editing, Á.M.P., M.W. and M.A. All authors analyzed the results and substantively revised the work. All authors read and approved the final manuscript.

Funding: V.Z., C.S., A.P., and K.B.-S. were funded by Austrian Science fund (project P29146). P.S.H acknowledges funding support from the Intramural Research Program of the NIH, NHLBI. H.L.W. would like to highlight that this material is based upon work supported by the National Science Foundation under CHE-1464946. Additionally, research reported in this publication was supported by NIGMS of the National Institutes of Health under award number R01GM129519. Open Access Funding by the Austrian Science Fund (FWF).

Conflicts of Interest: The authors declare no conflict of interest.

Abbreviations

The following abbreviations are used in this manuscript:

| | |
|-------|----------------------------|
| CIL | Chiral ionic liquid |
| QM | Quantum-mechanical |
| MM | Molecular mechanics |
| MD | Molecular dynamics |
| BuOMe | <i>n</i> -butylmethylether |

References

- Vasiloiu, M.; Leder, S.; Gaertner, P.; Mereiter, K.; Bica, K. Coordinating Chiral Ionic Liquids. *Org. Biomol. Chem.* **2013**, *11*, 8092–8102. [CrossRef] [PubMed]
- Schneiders, K.; Bösmann, A.; Schulz, P.S.; Wasserscheid, P. Chirality Transfer in Imidazolium Camphorsulfonate Ionic Liquids through Ion Pairing Effects. *Adv. Synth. Catal.* **2009**, *351*, 432–440. [CrossRef]
- Bica, K.; Gaertner, P. Applications of Chiral Ionic Liquids. *Eur. J. Org. Chem.* **2008**, *2008*, 3235–3250. [CrossRef]
- Payagala, T.; Armstrong, D.W. Chiral Ionic Liquids: A Compendium of Syntheses and Applications (2005–2012). *Chirality* **2012**, *24*, 17–53. [CrossRef]
- Howarth, J.; Hanlon, K.; Fayne, D.; McCormac, P. Moisture Stable Dialkylimidazolium Salts as Heterogeneous and Homogeneous Lewis Acids in the Diels-Alder Reaction. *Tetrahedron Lett.* **1997**, *38*, 3097–3100. [CrossRef]
- Pégot, B.; Vo-Thanh, G.; Gori, D.; Loupy, A. First Application of Chiral Ionic Liquids in Asymmetric Baylis–Hillman Reaction. *Tetrahedron Lett.* **2004**, *45*, 6425–6428. [CrossRef]
- Tran, C.D.; Oliveira, D.; Yu, S. Chiral Ionic Liquid That Functions as Both Solvent and Chiral Selector for the Determination of Enantiomeric Compositions of Pharmaceutical Products. *Anal. Chem.* **2006**, *78*, 1349–1356. [CrossRef]
- Zhao, L.; Ai, P.; Duan, A.H.; Yuan, L.M. Single-Walled Carbon Nanotubes for Improved Enantioseparations on a Chiral Ionic Liquid Stationary Phase in GC. *Anal. Bioanal. Chem.* **2011**, *399*, 143–147. [CrossRef]
- Zhang, J.; Du, Y.; Zhang, Q.; Chen, J.; Xu, G.; Yu, T.; Hua, X. Investigation of the Synergistic Effect with Amino Acid-Derived Chiral Ionic Liquids as Additives for Enantiomeric Separation in Capillary Electrophoresis. *J. Chromatogr. A* **2013**, *1316*, 119–126. [CrossRef]
- Kapnissi-Christodoulou, C.P.; Stavrou, I.J.; Mavroudi, M.C. Chiral Ionic Liquids in Chromatographic and Electrophoretic Separations. *J. Chromatogr. A* **2014**, *1363*, 2–10. [CrossRef]
- Wagner, V.; Schulz, P.S.; Wasserscheid, P. Asymmetric Hydrogenation Catalysis via Ion-Pairing in Chiral Ionic Liquids. *J. Mol. Liq.* **2014**, *192*, 177–184. [CrossRef]

12. Gausepohl, R.; Buskens, P.; Kleinen, J.; Bruckmann, A.; Lehmann, C.W.; Klankermayer, J.; Leitner, W. Highly Enantioselective Aza-Baylis–Hillman Reaction in a Chiral Reaction Medium. *Angew. Chem. Int. Ed.* **2006**, *45*, 3689–3692. [[CrossRef](#)] [[PubMed](#)]
13. Schulz, P.S.; Müller, N.; Bösmann, A.; Wasserscheid, P. Effective Chirality Transfer in Ionic Liquids through Ion-Pairing Effects. *Angew. Chem. Int. Ed.* **2007**, *46*, 1293–1295. [[CrossRef](#)] [[PubMed](#)]
14. Doherty, S.; Goodrich, P.; Hardacre, C.; Knight, J.G.; Nguyen, M.T.; Pârvulescu, V.I.; Paun, C. Recyclable Copper Catalysts Based on Imidazolium-Tagged Bis(Oxazolines): A Marked Enhancement in Rate and Enantioselectivity for Diels–Alder Reactions in Ionic Liquid. *Adv. Synth. Catal.* **2007**, *349*, 951–963. [[CrossRef](#)]
15. Vasiloiu, M.; Rainer, D.; Gaertner, P.; Reichel, C.; Schröder, C.; Bica, K. Basic Chiral Ionic Liquids: A Novel Strategy for Acid-Free Organocatalysis. *Catal. Today* **2013**, *200*, 80–86. [[CrossRef](#)]
16. Vasiloiu, M.; Gaertner, P.; Zirbs, R.; Bica, K. Coordinating Chiral Ionic Liquids: Design, Synthesis, and Application in Asymmetric Transfer Hydrogenation under Aqueous Conditions: Coordinating Chiral Ionic Liquids. *Eur. J. Org. Chem.* **2015**, *2015*, 2374–2381. [[CrossRef](#)]
17. Luo, S.; Mi, X.; Zhang, L.; Liu, S.; Xu, H.; Cheng, J.P. Functionalized Chiral Ionic Liquids as Highly Efficient Asymmetric Organocatalysts for Michael Addition to Nitroolefins. *Angew. Chem. Int. Ed.* **2006**, *45*, 3093–3097. [[CrossRef](#)]
18. Lombardo, M.; Pasi, F.; Easwar, S.; Trombini, C. An Improved Protocol for the Direct Asymmetric Aldol Reaction in Ionic Liquids, Catalysed by Onium Ion-Tagged Prolines. *Adv. Synth. Catal.* **2007**, *349*, 2061–2065. [[CrossRef](#)]
19. Lacour, J.; Hebbe-Viton, V. Recent Developments in Chiral Anion Mediated Asymmetric Chemistry. *Chem. Soc. Rev.* **2003**, *32*, 373–382. [[CrossRef](#)]
20. Lacour, J.; Moraleda, D. Chiral Anion-Mediated Asymmetric Ion Pairing Chemistry. *Chem. Commun.* **2009**, *46*, 7073. [[CrossRef](#)]
21. Brak, K.; Jacobsen, E.N. Asymmetric Ion-Pairing Catalysis. *Angew. Chem. Int. Ed.* **2013**, *52*, 534–561. [[CrossRef](#)] [[PubMed](#)]
22. Chi, Y.; Gellman, S.H. Enantioselective Organocatalytic Aminomethylation of Aldehydes: A Role for Ionic Interactions and Efficient Access to *B2*-Amino Acids. *J. Am. Chem. Soc.* **2006**, *128*, 6804–6805. [[CrossRef](#)] [[PubMed](#)]
23. Ohmatsu, K.; Ito, M.; Kunieda, T.; Ooi, T. Ion-Paired Chiral Ligands for Asymmetric Palladium Catalysis. *Nature Chem.* **2012**, *4*, 473–477. [[CrossRef](#)] [[PubMed](#)]
24. Schurig, V.; Jung, M.; Schleimer, M.; Klärner, F.G. Investigation of the Enantiomerization Barrier of Homofuran by Computer Simulation of Interconversion Profiles Obtained by Complexation Gas Chromatography. *Chemische Berichte* **1992**, *125*, 1301–1303. [[CrossRef](#)]
25. LaPlante, S.R.; Edwards, P.J.; Fader, L.D.; Jakalian, A.; Hucke, O. Revealing Atropisomer Axial Chirality in Drug Discovery. *ChemMedChem* **2011**, *6*, 505–513. [[CrossRef](#)]
26. Brandt, J.R.; Salerno, F.; Fuchter, M.J. The Added Value of Small-Molecule Chirality in Technological Applications. *Nat. Rev. Chem.* **2017**, *1*, 0045. [[CrossRef](#)]
27. Mikami, K.; Aikawa, K.; Yusa, Y.; Jodry, J.J.; Yamanaka, M. Tropos or Atropos? That Is the Question! *Synlett* **2002**, *2002*, 1561–1578. [[CrossRef](#)]
28. Montanari, F.; Goh, M.; Schroeder, C.; Nagy, G.; Muellner, L. *The Brill Dictionary of Ancient Greek*; Brill: Leiden/Boston, MA, USA, 2015.
29. Brooks, W.; Guida, W.; Daniel, K. The Significance of Chirality in Drug Design and Development. *Curr. Top. Med. Chem.* **2011**, *11*, 760–770. [[CrossRef](#)]
30. Noyori, R.; Tomino, I.; Tanimoto, Y. Virtually Complete Enantioface Differentiation in Carbonyl Group Reduction by a Complex Aluminum Hydride Reagent. *J. Am. Chem. Soc.* **1979**, *101*, 3129–3131. [[CrossRef](#)]
31. Chen, Y.; Yekta, S.; Yudin, A.K. Modified BINOL Ligands in Asymmetric Catalysis. *Chem. Rev.* **2003**, *103*, 3155–3212. [[CrossRef](#)]
32. Parmar, D.; Sugiono, E.; Raja, S.; Rueping, M. Complete Field Guide to Asymmetric BINOL-Phosphate Derived Brønsted Acid and Metal Catalysis: History and Classification by Mode of Activation; Brønsted Acidity, Hydrogen Bonding, Ion Pairing, and Metal Phosphates. *Chem. Rev.* **2014**, *114*, 9047–9153. [[CrossRef](#)] [[PubMed](#)]

33. You, S.L. Recent Developments in Asymmetric Transfer Hydrogenation with Hantzsch Esters: A Biomimetic Approach. *Chem. Asian J.* **2007**, *2*, 820–827. [[CrossRef](#)] [[PubMed](#)]
34. Bartoli, G.; Bencivenni, G.; Dalpozzo, R. Organocatalytic Strategies for the Asymmetric Functionalization of Indoles. *Chem. Soc. Rev.* **2010**, *39*, 4449–4465. [[CrossRef](#)] [[PubMed](#)]
35. Mizutani, T.; Takagi, H.; Hara, O.; Horiguchi, T.; Ogoshi, H. Axial Chirality Induction in Flexible Biphenols by Hydrogen Bonding and Steric Interactions. *Tetrahedron Lett.* **1997**, *38*, 1991–1994. [[CrossRef](#)]
36. Etxebarria, J.; Degenbeck, H.; Felten, A.S.; Serres, S.; Nieto, N.; Vidal-Ferran, A. Supramolecular-Directed Chiral Induction in Biaryl Derivatives. *J. Org. Chem.* **2009**, *74*, 8794–8797. [[CrossRef](#)]
37. Scharinger, F.; Pálvölgyi, Á.M.; Zeindlhofer, V.; Schnürch, M.; Schröder, C.; Bica-Schröder, K. Counterion Enhanced Organocatalysis: A Novel Approach for the Asymmetric Transfer Hydrogenation of Enones. *ChemCatChem* **2020**, *12*, 3776–3782. [[CrossRef](#)]
38. Wolf, C. *Dynamic Stereochemistry of Chiral Compounds: Principles and Applications*; Royal Society of Chemistry: London, UK, 2007.
39. Torrie, G.M.; Valleau, J.P. Nonphysical Sampling Distributions in Monte Carlo Free-Energy Estimation: Umbrella Sampling. *J. Comput. Phys.* **1977**, *23*, 187–199. [[CrossRef](#)]
40. Simón, L.; Goodman, J.M. Theoretical Study of the Mechanism of Hantzsch Ester Hydrogenation of Imines Catalyzed by Chiral BINOL-Phosphoric Acids. *J. Am. Chem. Soc.* **2008**, *130*, 8741–8747. [[CrossRef](#)]
41. Sancho-García, J.C.; Cornil, J. Anchoring the Torsional Potential of Biphenyl at the Ab Initio Level: The Role of Basis Set versus Correlation Effects. *J. Chem. Theory Comput.* **2005**, *1*, 581–589. [[CrossRef](#)]
42. Lemkul, J.A.; Huang, J.; Roux, B.; MacKerell, A.D. An Empirical Polarizable Force Field Based on the Classical Drude Oscillator Model: Development History and Recent Applications. *Chem. Rev.* **2016**, *116*, 4983–5013. [[CrossRef](#)]
43. Tsuzuki, S.; Tanabe, K. Ab Initio Molecular Orbital Calculations of the Internal Rotational Potential of Biphenyl Using Polarized Basis Sets with Electron Correlation Correction. *J. Phys. Chem.* **1991**, *95*, 139–144. [[CrossRef](#)]
44. Rubio, M.; Merchán, M.; Ortí, E. The Internal Rotational Barrier of Biphenyl Studied with Multiconfigurational Second-Order Perturbation Theory (CASPT2). *Theoret. Chim. Acta* **1995**, *91*, 17–29. [[CrossRef](#)]
45. Karpfen, A.; Choi, C.H.; Kertesz, M. Single-Bond Torsional Potentials in Conjugated Systems: A Comparison of Ab Initio and Density Functional Results. *J. Phys. Chem. A* **1997**, *101*, 7426–7433. [[CrossRef](#)]
46. Grein, F. Twist Angles and Rotational Energy Barriers of Biphenyl and Substituted Biphenyls. *J. Phys. Chem. A* **2002**, *106*, 3823–3827. [[CrossRef](#)]
47. Grein, F. New Theoretical Studies on the Dihedral Angle and Energy Barriers of Biphenyl. *J. Mol. Struct.* **2003**, *624*, 23–28. [[CrossRef](#)]
48. Johansson, M.P.; Olsen, J. Torsional Barriers and Equilibrium Angle of Biphenyl: Reconciling Theory with Experiment. *J. Chem. Theory Comput.* **2008**, *4*, 1460–1471. [[CrossRef](#)] [[PubMed](#)]
49. Ceccacci, F.; Mancini, G.; Mencarelli, P.; Villani, C. Determination of the Rotational Barrier of a Chiral Biphenyl: Comparison of Theoretical and Experimental Data. *Tetrahedron Asymmetry* **2003**, *14*, 3117–3122. [[CrossRef](#)]
50. Mazzanti, A.; Lunazzi, L.; Minzoni, M.; Anderson, J.E. Rotation in Biphenyls with a Single Ortho-Substituent. *J. Org. Chem.* **2006**, *71*, 5474–5481. [[CrossRef](#)]
51. Lunazzi, L.; Mancinelli, M.; Mazzanti, A.; Lepri, S.; Ruzziconi, R.; Schlosser, M. Rotational Barriers of Biphenyls Having Heavy Heteroatoms as Ortho-Substituents: Experimental and Theoretical Determination of Steric Effects. *Org. Biomol. Chem.* **2012**, *10*, 1847–1855. [[CrossRef](#)]
52. Masson, E. Torsional Barriers of Substituted Biphenyls Calculated Using Density Functional Theory: A Benchmarking Study. *Org. Biomol. Chem.* **2013**, *11*, 2859. [[CrossRef](#)]
53. Grimme, S.; Antony, J.; Ehrlich, S.; Krieg, H. A Consistent and Accurate Ab Initio Parametrization of Density Functional Dispersion Correction (DFT-D) for the 94 Elements H-Pu. *J. Chem. Phys.* **2010**, *132*, 154104. [[CrossRef](#)]

54. Grimme, S.; Ehrlich, S.; Goerigk, L. Effect of the Damping Function in Dispersion Corrected Density Functional Theory. *J. Comput. Chem.* **2011**, *32*, 1456–1465. [[CrossRef](#)] [[PubMed](#)]
55. Weigend, F.; Ahlrichs, R. Balanced Basis Sets of Split Valence, Triple Zeta Valence and Quadruple Zeta Valence Quality for H to Rn: Design and Assessment of Accuracy. *Phys. Chem. Chem. Phys.* **2005**, *7*, 3297–3305. [[CrossRef](#)] [[PubMed](#)]
56. Riplinger, C.; Neese, F. An Efficient and near Linear Scaling Pair Natural Orbital Based Local Coupled Cluster Method. *J. Chem. Phys.* **2013**, *138*, 034106. [[CrossRef](#)] [[PubMed](#)]
57. Colebrook, L.D.; Giles, H.G.; Granata, A.; Icli, S.; Fehlner, J.R. Restricted Internal Rotation in 1-Arylhydantoins, 3-Arylhydantoins, and 3-Aryl-2-Thiohydantoins: Reversal of the Effective Sizes of Methyl and Chlorine. *Can. J. Chem.* **1973**, *51*, 3635–3639. [[CrossRef](#)]
58. Kishikawa, K.; Yoshizaki, K.; Kohmoto, S.; Yamamoto, M.; Yamaguchi, K.; Yamada, K. Control of the Rotational Barrier and Spatial Disposition of the N-(2'-Methylphenyl) Group in Succinimides Bysubstituent and Solvent Effects. *J. Chem. Soc. Perkin Trans. 1* **1997**, *1*, 1233–1240. [[CrossRef](#)]
59. Demir-Ordu, Ö.; Yilmaz, E.M.; Doğan, İ. Determination of the Absolute Stereochemistry and the Activation Barriers of Thermally Interconvertible Heterocyclic Compounds Bearing a Naphthyl Substituent. *Tetrahedron Asymmetry* **2005**, *16*, 3752–3761. [[CrossRef](#)]
60. Neese, F. The ORCA Program System. *Wiley Interdiscip. Rev. Comput. Mol. Sci.* **2012**, *2*, 73–78. [[CrossRef](#)]
61. Vosko, S.H.; Wilk, L.; Nusair, M. Accurate Spin-Dependent Electron Liquid Correlation Energies for Local Spin Density Calculations: A Critical Analysis. *Can. J. Phys.* **1980**, *58*, 1200–1211. [[CrossRef](#)]
62. Parrish, R.M.; Burns, L.A.; Smith, D.G.A.; Simmonett, A.C.; DePrince, A.E., III; Hohenstein, E.G.; Bozkaya, U.; Sokolov, A.Y.; Di Remigio, R.; Richard, R.M.; et al. Psi4 1.1: An Open-Source Electronic Structure Program Emphasizing Automation, Advanced Libraries, and Interoperability. *J. Chem. Theory Comput.* **2017**, *13*, 3185–3197. [[CrossRef](#)]
63. Heid, E.; Schmode, S.; Chatterjee, P.; MacKerell, A.D.; Schröder, C. Solvation Dynamics: Improved Reproduction of the Time-Dependent Stokes Shift with Polarizable Empirical Force Field Chromophore Models. *Org. Biomol. Chem.* **2019**, *21*, 17703–17710. [[CrossRef](#)] [[PubMed](#)]
64. Heid, E.; Hunt, P.A.; Schröder, C. Evaluating Excited State Atomic Polarizabilities of Chromophores. *Org. Biomol. Chem.* **2018**, *20*, 8554–8563. [[CrossRef](#)]
65. Heid, E.; Szabadi, A.; Schröder, C. Quantum Mechanical Determination of Atomic Polarizabilities of Ionic Liquids. *Phys. Chem. Chem. Phys.* **2018**, *20*, 10992–10996. [[CrossRef](#)] [[PubMed](#)]
66. Bayly, C.I.; Cieplak, P.; Cornell, W.; Kollman, P.A. A Well-Behaved Electrostatic Potential Based Method Using Charge Restraints for Deriving Atomic Charges: The RESP Model. *J. Phys. Chem.* **1993**, *97*, 10269–10280. [[CrossRef](#)]
67. Alenaizan, A.; Burns, L.A.; Sherrill, C.D. Python Implementation of the Restrained Electrostatic Potential Charge Model. *Int. J. Quantum Chem.* **2020**, *120*, e26035. [[CrossRef](#)]
68. Sadlej, A.J. Medium-Size Polarized Basis Sets for High-Level-Correlated Calculations of Molecular Electric Properties. *Theoret. Chim. Acta* **1992**, *81*, 339–354. [[CrossRef](#)]
69. Bernholdt, D.E.; Harrison, R.J. Large-Scale Correlated Electronic Structure Calculations: The RI-MP2 Method on Parallel Computers. *Chem. Phys. Lett.* **1996**, *250*, 477–484. [[CrossRef](#)]
70. Vanommeslaeghe, K.; Yang, M.; MacKerell, A.D. Robustness in the Fitting of Molecular Mechanics Parameters. *J. Comput. Chem.* **2015**, *36*, 1083–1101. [[CrossRef](#)]
71. Heid, E.; Boresch, S.; Schröder, C. Polarizable Molecular Dynamics Simulations of Ionic Liquids: Influence of Temperature Control. *J. Chem. Phys.* **2020**, *152*, 094105. [[CrossRef](#)]
72. Brooks, B.R.; Brooks, C.L., III; Mackerell, A.D., Jr.; Nilsson, L.; Petrella, R.J.; Roux, B.; Won, Y.; Archontis, G.; Bartels, C.; Boresch, S.; et al. CHARMM: The Biomolecular Simulation Program. *J. Comput. Chem.* **2009**, *30*, 1545. [[CrossRef](#)]
73. Lamoureux, G.; Roux, B. Modeling Induced Polarization with Classical Drude Oscillators: Theory and Molecular Dynamics Simulation Algorithm. *J. Chem. Phys.* **2003**, *119*, 3025–3039. [[CrossRef](#)]
74. Ryckaert, J.P.; Ciccotti, G.; Berendsen, H.J. Numerical Integration of the Cartesian Equations of Motion of a System with Constraints: Molecular Dynamics of n-Alkanes. *J. Comput. Phys.* **1977**, *23*, 327–341. [[CrossRef](#)]
75. Lee, T.S.; Radak, B.K.; Pabis, A.; York, D.M. A New Maximum Likelihood Approach for Free Energy Profile Construction from Molecular Simulations. *J. Chem. Theory Comput.* **2013**, *9*, 153–164. [[CrossRef](#)] [[PubMed](#)]

76. Martínez, L.; Andrade, R.; Birgin, G.; Martínez, J.M. PACKMOL: A Package for Building Initial Configurations for Molecular Dynamics Simulations. *J. Comput. Chem.* **2009**, *30*, 2157. [[CrossRef](#)] [[PubMed](#)]
77. Humphrey, W.; Dalke, A.; Schulten, K. VMD: Visual Molecular Dynamics. *J. Mol. Graph.* **1996**, *14*, 33–38. [[CrossRef](#)]
78. Wickham, H. *Ggplot2: Elegant Graphics for Data Analysis*; Springer: New York, NY, USA, 2016.
79. R Core Team. *A Language and Environment for Statistical Computing*; version 3.5.2; R core team: Vienna, Austria, 2018.



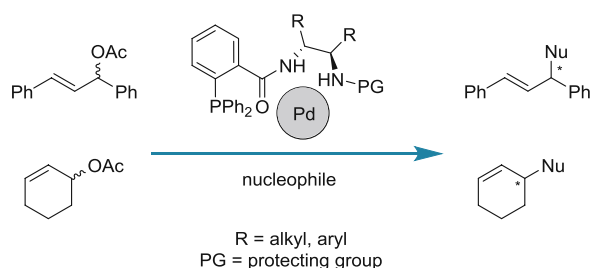
© 2020 by the authors. Licensee MDPI, Basel, Switzerland. This article is an open access article distributed under the terms and conditions of the Creative Commons Attribution (CC BY) license (<http://creativecommons.org/licenses/by/4.0/>).

4. Asymmetric allylic alkylations

Since the pioneering work of J. Tsuji and B. M. Trost, asymmetric allylic alkylation (AAA) plays a crucial role for the synthesis of optically active compounds. Such reactions require mild reaction conditions and provide operational simplicity; moreover, AAA shows a remarkable functional group tolerance which makes it compatible with a broad range of nucleophiles and allylic electrophiles.

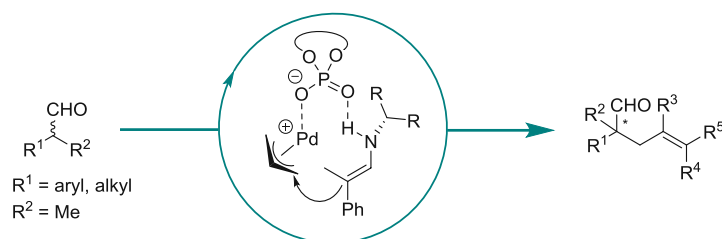
In this particular chapter, palladium-catalyzed asymmetric allylic alkylations using activated and non-activated allylic electrophiles will be discussed.

- 1.) As a possible *P,O*-chelating alternative to the classical Trost Modular Ligands (TMLs), a small set of chiral diamine-based carbamate-monophosphine ligands was synthesized and their catalytic efficiency was evaluated in the asymmetric allylic alkylation of activated allylic electrophiles (Scheme 42).



Scheme 42. Classical Tsuji-Trost reaction with activated allylic electrophiles.

- 2.) By merging the fields of transition metal-catalysis and organocatalysis, poorly nucleophilic substrates like aldehydes or ketones can be readily allylated *via* Pd/enamine dual activation.⁹¹ When using an additional acidic activator, such reactions can be performed with simple allylic alcohol reagents, which is both environmentally and economically highly desired.^{84,85,86} Relying on a Pd-precursor, a simple chiral amine and an achiral or racemic phosphoric acid, a three-component catalyst system was developed for the direct α -allylation of α -branched aldehydes. Apart from the optimization of such “counterion-enhanced” catalytic system, the effect of different aldehydes and allylic alcohols was investigated as well (Scheme 43).



Scheme 43. Counterion-enhanced direct α -allylation of α -branched aldehydes with allylic alcohols.

The following manuscripts will be presented in this chapter:

- 1.) Pálvölgyi, Á. M.; Schnürch, M.; Bica-Schröder K. Carbamate-base *P,O*-ligands for asymmetric allylic alkylations. *Tetrahedron* **2020**, *76*, 131246.

As a first author I planned and performed the experimental work. Furthermore, I also wrote the manuscript.

- 2.) Pálvölgyi, Á. M.; Smith, J.; Schnürch, M.; Bica-Schröder Counterion Enhanced Pd/Enamine-Catalysis: A Simple Methodology for the Direct Asymmetric α -Allylation of Aldehydes with Allylic Alcohols. *J. Org. Chem.* **2020**, *86*, 850-860.

As a first author I planned and performed the major part of the experimental work and I wrote the manuscript.



Carbamate-based *P,O*-ligands for asymmetric allylic alkylations

Ádám Márk Pálvölgyi, Michael Schnürch, Katharina Bica-Schröder*

Institute of Applied Synthetic Chemistry, TU Wien, Getreidemarkt 9/163, A-1060, Vienna, Austria

ARTICLE INFO

Article history:

Received 29 March 2020
Received in revised form
22 April 2020
Accepted 25 April 2020
Available online 4 May 2020

Keywords:

Chiral *P,O*-ligands
Tsuji-Trost reaction
Asymmetric synthesis
Palladium-catalyzed allylation

ABSTRACT

Herein we report the design and successful catalytic application of modified *Trost*-ligands in asymmetric allylic alkylation (AAA) reactions. A small set of carbamate-monophosphine *P,O*-ligands has been prepared in a straightforward two-step synthetic procedure. After optimization of the reaction conditions, high catalytic activities and excellent enantioselectivity up to >99% have been attained.

© 2020 Elsevier Ltd. All rights reserved.

1. Introduction

Highly functionalized and optically active allylic intermediates are invaluable building blocks for the total synthesis of numerous biologically active compounds [1–4]. In this field, palladium-catalyzed asymmetric allylic alkylation (AAA) provides a useful synthetic tool and thanks to its indisputable advantages, such as mild reaction conditions and operational simplicity, it is still one of the most relevant strategies for the synthesis of substituted allylic compounds [5]. The class of C_2 -symmetric diamine-based chiral diphosphines, such as **1** and **2** have been already proven to be really efficient ligands for asymmetric allylic alkylation, resulting in high catalytic activities and excellent stereocontrol (Fig. 1) [6].

Despite the wide variety of other available chiral ligands including (bis)oxazolines [7,8], amino acid-derived ligands [9,10], or diphosphines featuring axial and planar chirality [11–14], the *Trost*-type chiral diamine-based *P,P*-ligands still remain one of the most important tools in the field of asymmetric allylic alkylation. While such ligands have been already quite well studied, the chiral diamine-based monophosphine-analogues did not gain too much of attention. In 1994, *Trost* reported the first application of chiral diamine-based analogues bearing only one phosphine unit for asymmetric allylations, however low reactivities (20–50% yield) and poor enantioselectivity (<20% ee) were observed [15]. Since then, only a few examples in the area of chiral diamine-based monophosphine ligands have been reported, but the

enantioselectivity could not be improved significantly in any case. In 2000, *Kim* et al. reported the synthesis of novel *P,N*-monophosphine ligands based on an (*R,R*)-1,2-diaminocyclohexane (*R,R*-DACH) core and in the absence of the second phosphine unit, they observed strong *P,N*- and *P,O*-chelation [16]. In contrast with the previous results, they could reach significantly higher enantioselectivity (up to 75% ee), indicating that there is still potential in such diamine-based *P,N* and *P,O*-ligands for asymmetric allylic allylations.

Inspired by these results and based on our previous success with carbamate-based ligands in asymmetric transfer hydrogenations [17], herein we report the synthesis and application of chiral diamine-based, carbamate-derived monophosphine ligands for asymmetric allylic allylations.

2. Results and discussion

Starting from the cheap and easily accessible chiral pool of diamines **3–4**, a small library of carbamate-monophosphine ligands (**11–16**) has been prepared according to a straightforward two-step procedure (Scheme 1). At first, the chiral diamines have been

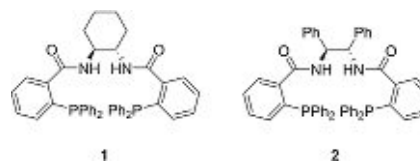
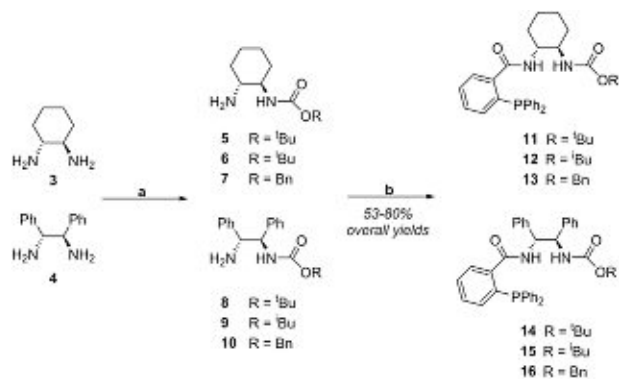


Fig. 1. Typical *Trost*-type bidentate *P,P*-ligands for AAA reactions.

* Corresponding author.

E-mail address: katharina.schroeder@tuwien.ac.at (K. Bica-Schröder).

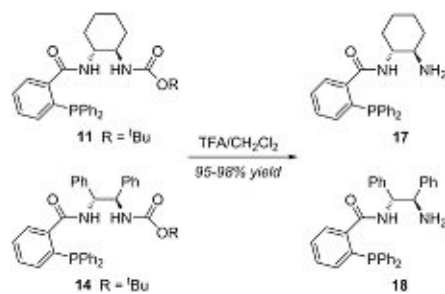


Scheme 1. Design of carbamate-based *P,O*-ligands. Reagents and conditions: (a) HCl, anhydride or chloroformate, anhydrous MeOH or EtOH, 0–25 °C (b) 2-PPh₂-PhCOOH, DCC/DMAP, anhydrous CH₂Cl₂, 0–25 °C.

reacted with the corresponding anhydride or chloroformate by using a temporary masking on one of the amino groups by means of HCl salt, resulting in the corresponding mono carbamate-protected intermediates as major products. These intermediates (**5–10**) have then been coupled with 2-(diphenylphosphino)-benzoic acid *via* simple DCC/DMAP coupling procedure, affording the chiral ligand **11–16** in good overall yields (Scheme 1).

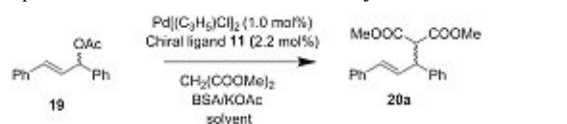
In order to investigate whether the carbamate carbonyl group plays an important role in the complexation, the unprotected analogues of ligand **11** and **14** have also been synthesized (Scheme 2).

After the successful synthesis and characterization of the ligands, we investigated the asymmetric allylic alkylation of racemic (*E*)-1,3-diphenylallyl acetate (**19**) with dimethyl malonate as a benchmark reaction (Table 1). The initial screening aiming to find



Scheme 2. Deprotection of carbamate ligands **11** and **14**.

Table 1
Parameter optimization for the AAA reaction of the allylic acetate **19**.



| Entry ^a | Solvent | Conversion (%) ^b | Yield (%) ^b | ee (%) ^c |
|--------------------|---------------------------------|-----------------------------|------------------------|---------------------|
| 1 | CH ₂ Cl ₂ | 98 | 95 | 49 (R) |
| 2 ^d | CH ₂ Cl ₂ | 75 | 70 | 48 (R) |
| 3 | EtOAc | 85 | 55 | 70 (R) |
| 4 | THF | 91 | 89 | 73 (R) |
| 5 | MTBE | 96 | 93 | 75 (R) |
| 6 | Et ₂ O | 95 | 94 (93) | >99 (R) |
| 7 ^e | Et ₂ O | 95 | 94 (93) | >99 (R) |
| 8 | Toluene | 60 | 57 | >99 (R) |

^a Performed with 0.50 mmol rac-(*E*)-1,3-diphenylallyl acetate (**19**) using 0.011 mmol (2.2 mol%) chiral ligand **11**, 0.005 mmol (1.0 mol%) [Pd(C₃H₅)Cl]₂, 0.60 mmol (1.2 equiv.) dimethyl malonate, 1.0 mmol (2.0 equiv.) BSA and 2 mg (2 mol%) KOAc in 1 mL solvent at 25 °C for 24 h.

^b Determined by GC analysis. Isolated yield in parenthesis.

^c Determined by chiral HPLC analysis using Diacel Chiralcel IB column.

^d Cs₂CO₃ instead of BSA/KOAc.

^e Reaction time was 6 h.

the most suitable solvent and base has been carried out by using 1.0 mol% of Pd-precursor and 2.2 mol% chiral ligand (**11**) at room temperature for 24 h. As it can be seen from Table 1, ether-type solvents like THF and MTBE afforded the desired product **20a** with higher enantioselectivity than dichloromethane, without significantly affecting the catalytic activity (Table 1, entries 1 vs. 4–5.). To our delight, the product **20a** could be obtained in 93% isolated yield and excellent enantioselectivity (>99% ee) by using diethyl ether as solvent in the presence of the chiral ligand **11** at room temperature (Table 1, entry 6.). Moreover, the reaction time could be also reduced to 6 h without any loss in catalytic activity (Table 1, entries 6 vs. 7.). Similarly, high enantioselectivity was observed in toluene albeit the catalytic activity was significantly decreased compared to those reactions in other solvents (Table 1, entries 6–7 vs. 8).

After determining the optimal reaction conditions, the catalytic efficiency of the chiral ligands was also evaluated (Fig. 2).

The catalyst screening revealed that the (*R,R*)-1,2-diaminocyclohexane based ligands are in general superior over the (*R,R*)-1,2-diphenylethylenediamine analogues yielding the desired product **20a** with slightly higher yields and significantly higher enantiomeric excess (ligand **11–13** vs. **14–16**). Moreover, the presence of the bulky Boc-group was also found to be beneficial. Importantly, the compound **17** and **18** – the corresponding amino-monophosphine analogues of ligand **11** and **14** – gave basically no product under identical conditions, indicating that the presence of the carbamate unit is indeed crucial for the complex formation.

Encouraged by these results, a series of different nucleophiles have been successfully applied for the asymmetric allylic alkylation of racemic (*E*)-1,3-diphenylallyl acetate (**19**) under the previously optimized reaction conditions. As it can be seen from Scheme 3, the corresponding products could be obtained with high isolated yields (87–98%) and excellent stereocontrol (84–>99%). While the C-allylated products have been formed mainly in (*R*)-configuration, interestingly the reaction with diethyl-acetamidomalonnate resulted in the formation of the (*S*)-**20d** as a major product, indicating that the -NHAc group might alter the chelation mode during the reaction. The high catalytic activity and selectivity were eventually retained by using *N*-nucleophiles as well, affording the amines **20g–i** in high yields and 84–92% ee. For all amine products, the (*S*)-

Effect of ligand structure on the yield and enantioselectivity

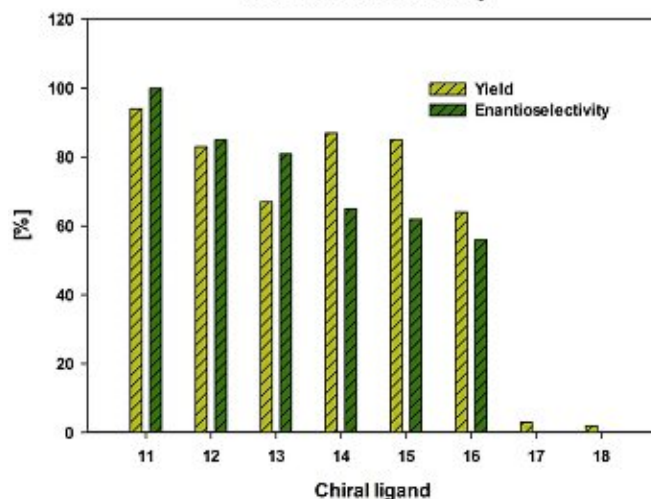
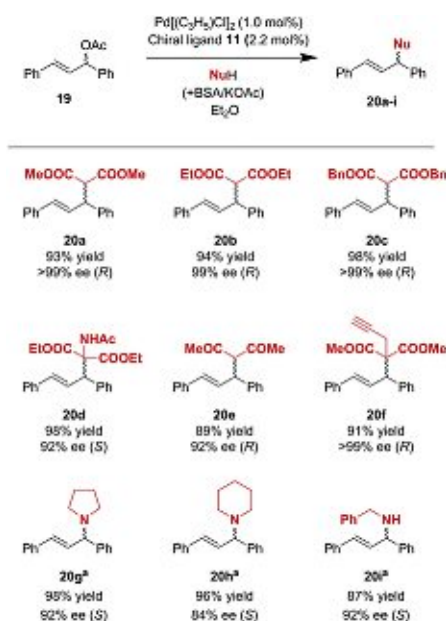


Fig. 2. Catalyst screening for the AAA reaction of allylic acetate **19**. The reaction conditions and monitoring were identical to those used in Table 1, entry 7.

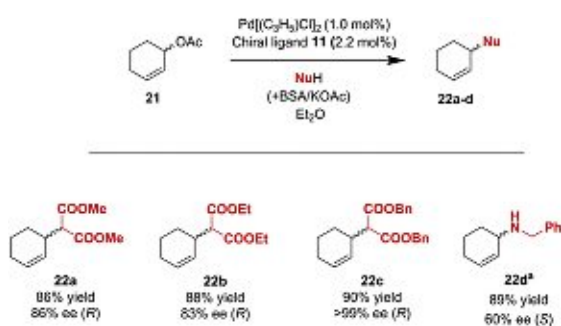


Scheme 3. Screening of different nucleophiles for the AAA reaction of allylic acetate **19** by using 0.50 mmol substrate, 0.011 mmol (2.2 mol%) chiral ligand **11**, 0.005 mmol (1.0 mol%) $[\text{Pd}(\text{C}_3\text{H}_5)\text{Cl}]_2$, 0.60 mmol (1.2 equiv.) nucleophile, 1.0 mmol (2.0 equiv.) BSA and 2 mg (2 mol%) KOAc in 1 mL Et_2O at 25 °C for 6 h. Yields refer to the pure products after preparative TLC/column chromatography. Enantiomeric excess values have been determined by chiral HPLC analysis. Absolute configuration was determined by comparison of the optical rotation with literature data. ^a Without BSA/KOAc.

enantiomer has been predominantly formed.

Eventually, we further expanded our reaction scope with the asymmetric allylic alkylation of racemic 3-acetoxy-1-cyclohexene (**21**). By using diphenyl malonate as nucleophile, the product **22c** could be isolated in high yield and excellent enantiopurity (>99% ee), while the other products could be also obtained in good yields and moderate to good enantioselectivity (Scheme 4).

In order to get more insight into the chelation mode, $^{31}\text{P}\{^1\text{H}\}$ NMR analysis of the *in-situ* formed $(\pi\text{-allyl})\text{Pd}$ complex **11*** was carried out by using 1.0 equivalent of $[\text{Pd}(\text{C}_3\text{H}_5)\text{Cl}]_2$ and 2.0 equivalents of chiral ligand **11** ($\text{Pd}/\text{L}^* = 1$). As shown in Fig. 3, only one doublet of the complex at $\delta = 25.6$ ppm with a coupling constant of $^2J(\text{P},\text{O}) = 37.1$ Hz was formed. This indicates, that basically only one type of chelation takes place and there is no competition between the different complexation modes which can be sometimes



Scheme 4. Screening of different nucleophiles for the AAA reaction of allylic acetate **21** by using 0.50 mmol substrate, 0.011 mmol (2.2 mol%) chiral ligand **11**, 0.005 mmol (1.0 mol%) $[\text{Pd}(\text{C}_3\text{H}_5)\text{Cl}]_2$, 0.60 mmol (1.2 equiv.) nucleophile, 1.0 mmol (2 equiv.) BSA and 2 mg (2 mol%) KOAc in 1 mL Et_2O at 25 °C for 24 h. Yields refer to the pure products after column chromatography. Enantiomeric excess values have been determined by chiral HPLC analysis. Absolute configuration was determined by comparison of the optical rotation with literature data. ^a Without BSA/KOAc.

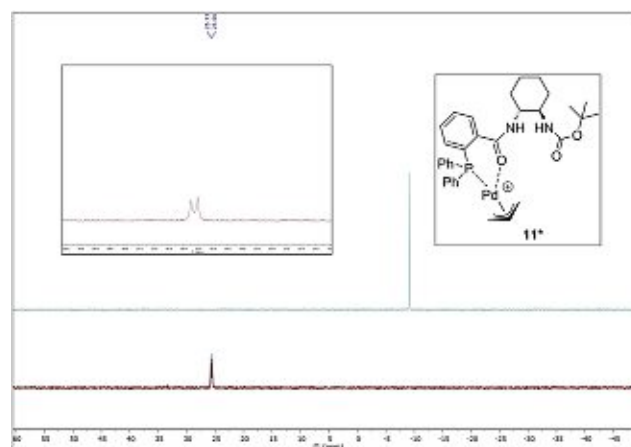


Fig. 3. $^{31}\text{P}\{^1\text{H}\}$ NMR spectra of the pure chiral ligand **11** (top, green), and the *in-situ* formed $(\pi\text{-allyl})\text{Pd}$ complex **11*** (bottom, red) showing only one major chelation mode.

observed with the *P,P*-bidentate Trost ligands [18]. Based on the literature, the major complex should have a *P,O*-chelation motif in which the carboxamide oxygen acts as an *O*-ligand. While there is no direct proof for the carbamate unit participating in the chelation mode; based on the results, its presence is certainly crucial in order to reach high enantioselectivity.

3. Conclusion

Herein, we have reported the synthesis and application of carbamate-based *P,O*-ligands for palladium-catalyzed asymmetric allylic alkylation. After optimization of the catalyst structure and reaction conditions, the chiral ligand **11** bearing a bulky Boc-protecting group could be successfully applied for the AAA reaction of an aromatic and an aliphatic model substrate by using a series of different *C*- and *N*-nucleophiles. High isolated yields and excellent stereocontrol could be attained for all products of racemic (*E*)-1,3-diphenylallyl acetate (**19**), while moderate to excellent enantioselectivity was obtained in the AAA reaction of racemic 3-acetoxy-1-cyclohexene (**21**).

4. Experimental section

4.1. General remarks

All reagents were purchased from commercial suppliers and used without further purification unless noted otherwise. Solvents intended for anhydrous reactions were pre-distilled and desiccated on Al_2O_3 columns (PURESOLV, Innovative Technology). Chromatography solvents were distilled prior to use. Column chromatography was performed on standard manual glass columns using silica gel from Merck (40–63 μm). TLC-analysis was carried out using precoated and aluminum-backed plates purchased from Merck (silica gel 60 F₂₅₄). UV active compounds were detected at 254 nm, while non-UV active compounds were detected by using potassium permanganate solution as staining agent. ^1H , ^{13}C and ^{31}P NMR spectra were recorded from CDCl_3 and MeOD solutions on a Bruker AC 200 (200 MHz) or Bruker Advance UltraShield 400 (400 MHz) spectrometer and chemical shifts (δ) are reported in ppm, using tetramethylsilane as internal standard. Coupling constants (*J*) are reported in Hertz (Hz). The following abbreviations were used to explain the multiplicities: s = singlet, d = doublet, t = triplet, q = quartet, qvin. = quintett, sex = sextet, m = multiplet, brs = broad singlet. Melting points above room temperature were

measured on an automated melting point system OPTI MELT of Stanford Research Systems and are uncorrected. Infrared spectra were recorded on a PerkinElmer Spectrum 65 FT IR spectrometer equipped with a specac MK II Golden Gate Single Reflection ATR unit. HR-MS analysis was carried out from methanol solutions ($c = 10$ ppm) by using an HTPAL system auto sampler (CTC Analytics AG), an Agilent 1100/1200 HPLC with binary pumps, a degasser and a column thermostat (Agilent Technologies) and an Agilent 6230 AJS ESI-TOF mass spectrometer. Chiral HPLC analysis were carried out on a DIONEX UPLC, equipped with a PDA plus detector (190–360 nm) using Chiralcel Diacel IB, AS-H, OJ and OD columns (250 × 4.60 mm) as stationary phases. GC measurements have been performed on a Thermo Scientific Focus instrument, equipped with an FID detector using a BGB5 column. Optical rotation was measured on an Anton Paar MCP500 polarimeter at the specific conditions and the results have been compared to literature values. Concentrations are given in g/100 mL.

4.2. Synthesis of mono-protected carbamates (5–10)

4.2.1. *tert*-Butyl ((1*R*,2*R*)-2-aminocyclohexyl)carbamate (5)

Prepared according to the modified literature procedure [19]. (1*R*,2*R*)-DACH (780 mg, 6.83 mmol, 1.0 equiv.) was dissolved in anhydrous MeOH (15 mL) and cooled *via* ice bath. 37% HCl (600 μL, 7.18 mmol, 1.05 equiv.) was diluted with 5 mL anhydrous MeOH, and it was added to the reaction mixture dropwise at 0 °C. The mixture was allowed to warm up, and it was stirred for 30 min. Then, di-*tert*-butyl dicarbonate (2.22 g, 10.25 mmol, 1.50 equiv.) in anhydrous MeOH (10 mL) was added dropwise at 0 °C. The mixture was stirred at room temperature for 4 h. After evaporation of the MeOH, water was added, and the insoluble byproduct was filtered off. The aqueous layer was basified with 2 M NaOH, extracted with CH_2Cl_2 (4×), dried over Na_2SO_4 and concentrated *in vacuo*, affording compound **5** as a white solid, which was found to be pure without further purification (1.29 g, 88% yield). $^1\text{H NMR}$ (400 MHz, CDCl_3) δ : 4.43 (brs, 1H, NHCOO), 3.13 (brs, 1H, CH–NHCOO), 2.32 (td, $J = 10.2$ Hz, 1H, CH–NH₂), 1.98 (t, $J = 6.0$ Hz, 2H, CH₂–CH), 1.70 (d, $J = 6.02$ Hz, 2H, CH₂–CH), 1.45–1.40 (m, 11H, C–(CH₃)₃, CH–NH₂), 1.28–1.07 (m, 4H, CH₂–CH₂); $^{13}\text{C NMR}$ (100 MHz, CDCl_3) δ : 156.3 (NHCOO), 79.4 (C–(CH₃)₃), 57.9 (CH–NHCOO), 55.8 (CH–NH₂), 35.4 (CH₂–CH), 33.0 (CH₂–CH), 28.5 (C–(CH₃)₃), 25.3 (CH₂–CH₂), 25.2 (CH₂–CH₂).

4.2.2. *Isobutyl* ((1*R*,2*R*)-2-aminocyclohexyl)carbamate (6)

Prepared according to the procedure for the synthesis of compound **5** by using (1*R*,2*R*)-DACH (456 mg, 4.0 mmol, 1.0 equiv.), 37% HCl (351 μL, 4.2 mmol, 1.05 equiv.), isobutyl chloroformate (778 μL, 6.0 mmol, 1.50 equiv.) and anhydrous MeOH (10 + 5 + 10 mL) to afford product **6** as a light brown solid, which was found to be pure without further purification (705 mg, 82% yield). **M.p.**: 100–101 °C; **HRMS (ESI-TOF) m/z** : [M+H]⁺ calculated for C₁₁H₂₃N₂O₂ 215.1760, found 215.1762; α_D^{20} : +10.5 (c 1.0, CHCl₃); **IR** (ν_{max} /cm⁻¹): 3358 (N–H ν), 2904 (C–H ν), 16,852 (C=O ν), 1607 (C–C ν), 1511 (N–H δ), 1437 (CH₂ δ); 1242 (C–O ν); $^1\text{H NMR}$ (400 MHz, CDCl_3) δ : 4.65 (brs, 1H, NHCOO), 3.82 (d, $J = 8.0$ Hz, 2H, CH₂–CH(CH₃)₂), 3.15 (brs, 1H, CH–NHCOO), 2.33 (td, $J = 10.2$ Hz, 1H, CH–NH₂), 2.00–1.92 (m, 3H, CH₂–CH, CH₂–CH(CH₃)₂), 1.71–1.68 (m, 2H, CH₂–CH), 1.24–1.02 (m, 6H, CH₂–CH₂, CH–NH₂), 0.85 (d, $J = 4.0$ Hz, 6H, CH₂–CH(CH₃)₂); $^{13}\text{C NMR}$ (100 MHz, CDCl_3) δ : 157.0 (NHCOO), 71.0 (CH₂–CH(CH₃)₂), 57.9 (CH–NHCOO), 55.4 (CH–NH₂), 35.2 (CH₂–CH), 32.9 (CH₂–CH), 28.0 (CH₂–CH(CH₃)₂), 25.2 (CH₂–CH₂), 19.1 (CH₂–CH(CH₃)₂).

4.2.3. *Benzyl* ((1*R*,2*R*)-2-aminocyclohexyl)carbamate (7)

Prepared according to the literature procedure [20]. (1*R*,2*R*)-

DACH (456 mg, 4.0 mmol, 1.0 equiv.) was dissolved in 10 mL anhydrous EtOH, and the solution of benzyl-phenyl-carbonate (790 μL, 4.0 mmol, 1.0 equiv.) in anhydrous EtOH (10 mL) was added dropwise at room temperature. The reaction mixture was stirred for 24 h and the EtOH was removed *in vacuo*. 10 M HCl (960 μL) was added, the formed precipitate was filtered off and it was successively washed with diethyl ether (2×) and H₂O (2×). Then, it was treated with a solution of NaOH (355 mg) in H₂O (2.40 mL). In a few minutes, the precipitate was filtered off, and it was washed with H₂O (3 × 10 mL), affording compound **7** as an off-white solid, which was found to be pure without further purifications (655 mg, 66% yield). $^1\text{H NMR}$ (200 MHz, CDCl_3) δ : 7.26–7.18 (m, 5H, *H*-arom), 4.99 (brs, 3H, arom-CH₂, CH–NHCOO), 3.11–3.01 (m, 1H, NHCOO), 2.28 (td, $J = 10.2$ Hz, 1H, CH–NH₂), 1.91–1.78 (m, 2H, CH₂–CH), 1.60–1.57 (m, 2H, CH₂–CH), 1.26–0.95 (m, 6H, CH₂–CH₂, CH–NH₂); $^{13}\text{C NMR}$ (100 MHz, CDCl_3) δ : 156.7 (NHCOO), 136.6 (C-arom), 128.5 (C-arom), 128.1 (C-arom), 66.7 (arom-CH₂), 58.2 (CH–NHCOO), 55.4 (CH–NH₂), 35.3 (CH₂–CH), 32.8 (CH₂–CH), 25.1 (CH₂–CH₂), 25.0 (CH₂–CH₂).

4.2.4. *tert*-Butyl ((1*R*,2*R*)-2-amino-1,2-diphenylethyl)carbamate (8)

Prepared according to the procedure for the synthesis of compound **5** by using (1*R*,2*R*)-DPEN (1.93 g, 9.1 mmol, 1.0 equiv.), 37% HCl (900 μL, 10.8 mmol, 1.05 equiv.), di-*tert*-butyl dicarbonate (2.93 g, 13.5 mmol, 1.50 equiv.) and anhydrous MeOH (30 + 15 + 15 mL). After the work-up, the obtained crude product was dissolved in ethyl acetate and the solid residue was removed over a patch of silica. The solvent was removed under reduced pressure to yield **8** as a white solid (2.18 g, 77% yield). $^1\text{H NMR}$ (400 MHz, CDCl_3) δ : 7.28–7.14 (m, 10H, *H*-arom), 5.80 (d, $J = 8.51$ Hz, 1H, CH–NHCOO), 4.77 (brs, 1H, NHCOO), 4.24 (s, 1H, CH–NH₂), 1.37 (s, 2H, CH–NH₂), 1.22 (s, 9H, C–(CH₃)₃); $^{13}\text{C NMR}$ (100 MHz, CDCl_3) δ : 155.9 (NHCOO), 142.4 (C-arom), 141.2 (C-arom), 128.7 (C-arom), 128.5 (C-arom), 127.6 (C-arom), 127.4 (C-arom), 127.0 (C-arom), 126.6 (C-arom), 79.4 (C–(CH₃)₃), 60.0 (CH–NHCOO, CH–NH₂), 28.5 (C–(CH₃)₃).

4.2.5. *Isobutyl* ((1*R*,2*R*)-2-amino-1,2-diphenylethyl)carbamate (9)

Prepared according to the procedure for the synthesis of compound **5** by using (1*R*,2*R*)-DPEN (2.36 mmol, 500 mg), 37% HCl (207 μL, 2.48 mmol, 1.05 equiv.) and isobutyl chloroformate (460 μL, 3.54 mmol, 1.50 equiv.) and anhydrous MeOH (10 + 5 + 5 mL). After the work-up, the obtained crude product was purified by column chromatography (15 g silica, light petrol: ethyl acetate 1:1 + 1 V/V % Et₃N), affording **9** as a white powder (479 mg, 65% yield). $^1\text{H NMR}$ (400 MHz, CDCl_3) δ : 7.31–7.18 (m, 10H, *H*-arom), 5.91 (d, $J = 7.84$ Hz, 1H, CH–NHCOO), 4.80 (brs, 1H, NHCOO), 4.29 (s, 1H, CH–NH₂), 3.64 (s, 2H, CH₂–CH(CH₃)₂), 1.74 (s, 1H, CH₂–CH(CH₃)₂), 1.46 (brs, 2H, CH–NH₂), 0.78 (s, 5H, CH₂–CH(CH₃)₂), 0.52 (s, 1H, CH₂–CH(CH₃)₂); $^{13}\text{C NMR}$ (100 MHz, CDCl_3) δ : 156.7 (NHCOO), 142.3 (C-arom), 141.1 (C-arom), 128.8 (C-arom), 128.7 (C-arom), 127.8 (C-arom), 127.6 (C-arom), 127.0 (C-arom), 126.6 (C-arom), 71.2 (CH₂–CH(CH₃)₂), 60.4 (CH–NHCOO), 60.0 (CH–NH₂), 28.2 (CH₂–CH(CH₃)₂), 19.2 (CH₂–CH(CH₃)₂).

4.2.6. *Benzyl* ((1*R*,2*R*)-2-amino-1,2-diphenylethyl)carbamate (10)

Prepared according to the synthesis of compound **7** by using (1*R*,2*R*)-DPEN (2.36 mmol, 500 mg), 10 mL anhydrous EtOH, and benzyl-phenyl-carbonate (2.36 mmol, 540 mg, 1.0 equiv.), affording the product **10** as an off-white solid (570 mg, 70% yield). $^1\text{H NMR}$ (400 MHz, CDCl_3) δ : 7.29–7.20 (m, 15H, *H*-arom), 6.05 (d, $J = 7.24$ Hz, 1H, CH–NHCOO), 4.91 (s, 2H, CH₂-arom), 4.83 (brs, 1H, NHCOO), 4.29 (s, 1H, CH–NH₂), 1.32 (brs, 2H, CH–NH₂); $^{13}\text{C NMR}$ (100 MHz, CDCl_3) δ : 156.3 (NHCOO), 142.3 (C-arom), 141.0 (C-arom),

136.9 (C-arom), 128.8 (C-arom), 128.7 (C-arom), 128.2 (C-arom), 127.8 (C-arom), 127.6 (C-arom), 126.9 (C-arom), 126.6 (C-arom), 66.8 (CH₂-arom), 60.6 (CH–NHCOO), 60.0 (CH–NH₂).

4.3. General procedure for the ligand synthesis (11–16)

Compound 11–16 have been prepared according to the literature procedure [16]. To the solution of 2-(diphenylphosphino) benzoic acid (1.05 equiv.) in anhydrous CH₂Cl₂ at 0 °C, DCC (2.0 mmol, 1.05 equiv.) was added and the mixture was stirred at 0 °C for 15 min. To this, the solution of monoprotected carbamate 5–10 (1.0 equiv.) and DMAP (0.1 equiv.) in anhydrous CH₂Cl₂ was slowly added at 0 °C. The mixture was allowed to warm up to room temperature and it was stirred overnight. The reaction mixture was cooled at 5 °C for 1 h, filtered and washed with cold CH₂Cl₂ to remove the majority of the dicyclohexyl urea. The filtrate was successively washed with 0.5 M HCl (3×), sat. NaHCO₃ (3×) and water (2×). After evaporation of the solvent, the crude products were purified by column chromatography.

4.3.1. tert-Butyl ((1R,2R)-2-(2-(diphenylphosphanyl)benzamido)-cyclohexyl)carbamate (11)

Prepared from compound 5 following the general procedure on a 1.9 mmol scale. Flash column chromatography (silica gel, light petrol:ethyl-acetate 4:1) afforded 11 as a white solid (870 mg, 91% yield). ¹H NMR (400 MHz, CDCl₃)δ: 7.51 (brs, 1H, NHCO), 7.25–7.20 (m, 12H, H-arom), 6.86 (brs, 1H, H-arom), 6.38 (brs, 1H, H-arom), 4.74 (d, J = 8.0 Hz, 1H, NHCOO), 3.61–3.58 (m, 1H, CH–NHCO), 3.29–3.26 (m, 1H, CH–NHCOO), 1.93 (d, J = 8.0 Hz, 1H, CH_{2a}-CH), 1.82 (d, J = 8.0 Hz, 1H, CH_{2b}-CH), 1.63 (brs, 1H, CH_{2a}-CH), 1.55 (brs, 1H, CH_{2b}-CH), 1.31 (s, 9H, C-(CH₃)₃), 1.20–1.12 (m, 3H, CH₂-CH_{2a}), 0.92–0.88 (m, 1H, CH₂-CH_{2b}); ³¹P NMR (167 MHz, CDCl₃)δ: –9.15; ¹³C NMR (100 MHz, CDCl₃)δ: 169.2 (NHCO), 156.9 (NHCOO), 141.1 (C-arom), 140.9 (C-arom), 137.8 (C-arom), 134.5 (C-arom), 134.2 (C-arom), 130.3 (C-arom), 128.7 (C-arom), 127.6 (C-arom), 79.7 (C-(CH₃)₃), 55.1 (CH–NHCO), 54.3 (CH–NHCOO), 33.0 (CH₂-CH), 32.4 (CH₂-CH), 28.6 (C-(CH₃)₃), 25.2 (CH₂-CH₂), 24.7 (CH₂-CH₂).

4.3.2. Isobutyl ((1R,2R)-2-(2-(diphenylphosphanyl)benzamido)-cyclohexyl)carbamate (12)

Prepared from compound 6 following the general procedure on a 1.4 mmol scale. Flash column chromatography (silica gel, light petrol:ethyl-acetate 4:1) afforded 12 as a white solid (610 mg, 87% yield). **M.p.:** 90–92 °C; **HRMS (ESI-TOF) m/z:** [M+H]⁺ Calculated for C₃₀H₃₆N₂O₃P 503.2464, found 503.2463; α_D²⁰: +35.5 (c 1.0, CHCl₃); **IR (ν_{max}/cm⁻¹):** 3332 (N–H ν), 2930 (C–H ν), 1680 (C=O ν), 1635 (C=O ν), 1526 (N–H δ), 1452 (C=C ν), 1432 (CH₂ δ); 1240 (C–O ν), 1150 (C–N ν), 743 (C–H arom δ), 695 (C–H arom δ); ¹H NMR (400 MHz, CDCl₃)δ: 7.48 (brs, 1H, NHCO), 7.25–7.20 (m, 12H, H-arom), 6.88 (brs, 1H, H-arom), 6.16 (brs, 1H, H-arom), 5.01 (d, J = 8.0 Hz, 1H, NHCOO), 3.73–3.63 (m, 3H, CH–NHCO, CH₂-CH(CH₃)₂), 3.34–3.32 (m, 1H, CH–NHCOO), 1.87–1.85 (m, 1H, CH₂-CH(CH₃)₂), 1.82–1.80 (m, 2H, CH₂-CH), 1.65–1.50 (m, 2H, CH₂-CH), 1.26–1.11 (m, 4H, CH₂-CH₂), 0.81 (d, J = 8.0 Hz, 6H, CH₂-CH(CH₃)₂); ³¹P NMR (167 MHz, CDCl₃)δ: –9.78; ¹³C NMR (100 MHz, CDCl₃)δ: 169.2 (NHCO), 157.3 (NHCOO), 141.2 (C-arom), 140.9 (C-arom), 137.6 (C-arom), 137.3 (C-arom), 136.4 (C-arom), 136.2 (C-arom), 133.7 (C-arom), 130.2 (C-arom), 128.4 (C-arom), 127.3 (C-arom), 71.0 (CH₂-CH(CH₃)₂), 55.0 (CH–NHCO), 54.0 (CH–NHCOO), 32.7 (CH₂-CH), 32.0 (CH₂-CH), 27.9 (CH₂-CH(CH₃)₂), 24.7 (CH₂-CH₂), 24.5 (CH₂-CH₂), 19.0 (CH₂-CH(CH₃)₂).

4.3.3. Benzyl ((1R,2R)-2-(2-(diphenylphosphanyl)benzamido)-cyclohexyl)carbamate (13)

Prepared from compound 7 following the general procedure on a 1.27 mmol scale. Flash column chromatography (silica gel, light petrol:ethyl-acetate 4:1) afforded 13 as a white solid (540 mg, 83% yield). **M.p.:** 101–103 °C; **HRMS (ESI-TOF) m/z:** [M+H]⁺ calculated for C₃₃H₃₄N₂O₃P 537.2307, found 537.2310; α_D²⁰: +30.1 (c 1.0, CHCl₃); **IR (ν_{max}/cm⁻¹):** 3301 (N–H ν), 2923 (C–H ν), 1691 (C=O ν), 1637 (C=O ν), 1529 (N–H δ), 1450 (C=C ν), 1436 (CH₂ δ); 1250 (C–O ν), 1158 (C–N ν), 743 (C–H arom δ), 694 (C–H arom δ); ¹H NMR (400 MHz, CDCl₃)δ: 7.45 (brs, 1H, NHCO), 7.31–7.21 (m, 17H, H-arom), 6.94–6.92 (m, 1H, H-arom), 6.27 (d, J = 8.0 Hz, 1H, H-arom), 5.33 (d, J = 8.0 Hz, 1H, NHCOO), 5.05 (s, 2H, arom-CH₂) 3.79–3.68 (m, 1H, CH–NHCO), 3.38–3.36 (m, 1H, CH–NHCOO), 2.05 (m, 1H, CH_{2a}-CH), 1.88–1.86 (m, 1H, CH_{2b}-CH), 1.71–1.69 (m, 2H, CH₂-CH), 1.25–1.22 (m, 3H, CH₂-CH_{2a}), 0.96–0.89 (m, 1H, CH₂-CH_{2b}); ³¹P NMR (167 MHz, CDCl₃)δ: –9.34; ¹³C NMR (100 MHz, CDCl₃)δ: 169.5 (NHCO), 157.1 (NHCOO), 141.5 (C-arom), 141.0 (C-arom), 137.9 (C-arom), 136.7 (C-arom), 134.4 (C-arom), 134.2 (C-arom), 133.9 (C-arom), 133.8 (C-arom), 130.3 (C-arom), 128.8 (C-arom), 128.1 (C-arom), 127.5 (C-arom), 66.7 (arom-CH₂), 55.6 (CH–NHCO), 54.0 (CH–NHCOO), 32.9 (CH₂-CH), 32.2 (CH₂-CH), 24.9 (CH₂-CH₂), 24.8 (CH₂-CH₂).

4.3.4. tert-Butyl((1R,2R)-2-(2-(diphenylphosphanyl)benzamido)-1,2-diphenylethyl)carbamate (14)

Prepared from compound 8 following the general procedure on a 1.0 mmol scale. Flash column chromatography (silica gel, light petrol:ethyl-acetate 4:1) afforded 14 as a white solid (540 mg, 83% yield). **M.p.:** 110–112 °C; **HRMS (ESI-TOF) m/z:** [M+H]⁺ calculated for C₃₈H₃₈N₂O₃P 601.2620, found 601.2615; α_D²⁰: +44.7 (c 1.0, CHCl₃); **IR (ν_{max}/cm⁻¹):** 3318 (N–H ν), 2933 (C–H ν), 1682 (C=O ν), 1639 (C=O ν), 1526 (N–H δ), 1450 (C=C ν), 1241 (C–O ν), 1170 (C–N ν), 742 (C–H arom δ), 695 (C–H arom δ); ¹H NMR (400 MHz, CDCl₃)δ: 7.67 (brs, 1H, NHCO), 7.34–6.90 (m, 25H, H-arom), 5.75 (d, J = 8.0 Hz, 1H, CH–NHCO), 5.26 (t, J = 8.0 Hz, 1H, CH–NHCOO), 4.92 (t, J = 12.0 Hz, 1H, NHCOO), 1.36 (s, 9H, C-(CH₃)₃); ³¹P NMR (167 MHz, CDCl₃)δ: –11.15; ¹³C NMR (100 MHz, CDCl₃)δ: 169.2 (NHCO), 156.4 (NHCOO), 141.1 (C-arom), 139.4 (C-arom), 138.4 (C-arom), 134.3 (C-arom), 134.2 (C-arom), 133.8 (C-arom), 133.5 (C-arom), 130.3 (C-arom), 128.7 (C-arom), 128.5 (C-arom), 128.4 (C-arom), 128.1 (C-arom), 127.6 (C-arom), 127.5 (C-arom), 79.8 (C-(CH₃)₃), 60.8 (CH–NHCO), 59.6 (CH–NHCOO), 28.4 (C-(CH₃)₃).

4.3.5. Isobutyl ((1R,2R)-2-(2-(diphenylphosphanyl)benzamido)-1,2-diphenylethyl)carbamate (15)

Prepared from compound 9 following the general procedure on a 1.0 mmol scale. Flash column chromatography (silica gel, light petrol:ethyl-acetate 4:1) afforded 15 as a white solid (505 mg, 78% yield). **M.p.:** 106–108 °C **HRMS (ESI-TOF) m/z:** [M+H]⁺ calculated for C₃₈H₃₈N₂O₃P 601.2620, found 601.2619; α_D²⁰: +43.4 (c 1.0, CHCl₃); **IR (ν_{max}/cm⁻¹):** 3321 (N–H ν), 2930 (C–H ν), 1680 (C=O ν), 1641 (C=O ν), 1530 (N–H δ), 1451 (C=C ν), 1243 (C–O ν), 1173 (C–N ν), 740 (C–H arom δ), 696 (C–H arom δ); ¹H NMR (400 MHz, CDCl₃)δ: 7.74 (brs, 1H, NHCO), 7.49–7.33 (m, 20H, H-arom), 7.12–7.08 (m, 1H, H-arom), 7.08–6.89 (m, 3H, H-arom), 6.25 (d, J = 8.0 Hz, 1H, CH–NHCO), 5.45 (t, J = 8.0 Hz, 1H, CH–NHCOO), 5.09 (t, J = 12.0 Hz, 1H, NHCOO), 3.91 (d, J = 6.0 Hz, 2H, CH₂-CH(CH₃)₂), 1.93 (brs, 1H, CH₂-CH(CH₃)₂), 1.38–1.34 (m, 1H, CH₂-CH(CH₃)₂), 0.99–0.96 (m, 5H, CH₂-CH(CH₃)₂); ³¹P NMR (167 MHz, CDCl₃)δ: –11.22; ¹³C NMR (100 MHz, CDCl₃)δ: 169.9 (NHCO), 157.3 (NHCOO), 141.4 (C-arom), 139.7 (C-arom), 138.2 (C-arom), 134.5 (C-arom), 134.1 (C-arom), 134.0 (C-arom), 133.8 (C-arom), 130.6 (C-arom), 128.9 (C-arom), 128.5 (C-arom), 127.8 (C-arom), 127.6 (C-arom), 71.5

(CH₂–CH(CH₃)₂), 61.7 (CH–NHCO), 59.4 (CH–NHCOO), 28.2 (CH₂–CH(CH₃)₂), 19.3 (CH₂–CH(CH₃)₂).

4.3.6. Benzyl ((1*R*,2*R*)-2-(2-(diphenylphosphanyl)benzamido)-1,2-diphenylethyl)carbamate (**16**)

Prepared from compound **10** following the general procedure on a 1.0 mmol scale. Flash column chromatography (silica gel, light petrol: ethyl-acetate 4:1) afforded **16** as a white solid (505 mg, 75% yield). **M.p.**: 100–104 °C; **HRMS (ESI-TOF) m/z**: [M+H]⁺ calculated for C₄₁H₃₆N₂O₃P 635.2464, found 635.2466; α_D²⁰: +47.8 (c 1.0, CHCl₃); **IR (ν_{max}/cm⁻¹)**: 3311 (N–H ν), 3010 (C–H ν), 1695 (C=O ν), 1630 (C–C ν), 1525 (N–H δ), 1450 (C=C ν), 1170 (C–N ν), 742 (C–H arom δ), 696 (C–H arom δ); **¹H NMR (400 MHz, CDCl₃)δ**: 7.44 (brs, 1H, NHCO), 7.21–7.03 (m, 26H, *H*-arom), 6.86 (brs, 1H, *H*-arom), 6.71 (d, *J* = 8.0 Hz, 2H, *H*-arom), 6.28 (d, *J* = 8.0 Hz, 1H, CH–NHCO), 5.24 (t, *J* = 8.0 Hz, 1H, CH–NHCOO), 4.99–4.85 (m, 3H, NHCOO, CH₂-arom); **³¹P NMR (167 MHz, CDCl₃)δ**: –11.16; **¹³C NMR (100 MHz, CDCl₃) δ**: 169.8 (NHCO), 156.7 (NHCOO), 141.4 (C-arom) 139.4 (C-arom), 137.3 (C-arom), 136.8 (C-arom), 136.5 (C-arom), 134.3 (C-arom), 134.0 (C-arom), 133.8 (C-arom), 133.5 (C-arom), 130.4 (C-arom), 128.8 (C-arom), 128.6 (C-arom), 128.5 (C-arom), 128.3 (C-arom), 127.9 (C-arom), 127.8 (C-arom), 127.6 (C-arom), 127.5 (C-arom), 66.7 (CH₂-arom), 61.8 (CH–NHCO), 59.2 (CH–NHCOO).

4.4. General procedure for ligand deprotection (**17**–**18**)

Prepared according to the literature procedure [16]. To a solution of **17** or **18** (0.5 mmol, 1.0 equiv.) in anhydrous CH₂Cl₂ (1.5 mL), trifluoroacetic acid (765 μL, 10.0 mmol, 20.0 equiv.) was added, and the reaction mixture was stirred at room temperature for 4 h. Then, the mixture was poured onto saturated NaHCO₃ solution, and it was extracted with CH₂Cl₂ (4×). The crude product was purified by flash column chromatography. All data were in accordance with the literature [16,21].

4.4.1. *N*-((1*R*,2*R*)-2-aminocyclohexyl)-2-(diphenylphosphanyl)benzamide (**17**)

The crude product was purified by column chromatography (silica gel, CH₂Cl₂: MeOH 30:1) affording **17** as a white solid (197 mg, 98% yield). **¹H NMR (400 MHz, CDCl₃)δ**: 7.32 (brs, 1H, NHCO), 7.28–7.21 (m, 13H, *H*-arom), 6.92 (m, 1H, *H*-arom) 5.76 (d, *J* = 8.0 Hz, 1H, CH–NHCO), 3.59 (m, 1H, CH–NH₂), 2.19–2.14 (m, 1H, CH_{2a}-CH), 1.90–1.86 (m, 2H, CH₂-CH), 1.69–1.63 (m, 3H, CH_{2b}-CH, CH–NH₂), 1.26–1.21 (m, 3H, CH_{2a}-CH₂), 0.89–0.86 (m, 1H, CH_{2b}-CH₂).

4.4.2. *N*-((1*R*,2*R*)-2-amino-1,2-diphenylethyl)-2-(diphenylphosphanyl)benzamide (**18**)

The crude product was purified by column chromatography (silica gel, CH₂Cl₂: MeOH 30:1) affording **18** as a white solid (240 mg, 96% yield). **¹H NMR (400 MHz, CDCl₃)δ**: 7.45 (brs, 1H, NHCO), 7.31–7.18 (m, 21H, *H*-arom), 7.05 (d, *J* = 8.0 Hz, 2H, *H*-arom), 6.96 (brs, 1H, *H*-arom), 5.25 (dd, *J* = 8.0 Hz, 4.0 Hz, 1H, CH–NHCO), 4.28 (d, *J* = 4.0 Hz, 1H, CH–NH₂), 1.69 (brs, 2H, CH–NH₂).

4.5. Synthesis of the allylic acetates

4.5.1. (±)-(E)-1,3-diphenylallyl acetate (**19**)

Prepared according to the literature procedure [22]. (±)-(E)-1,3-Diphenylallyl alcohol (28.6 mmol, 6.0 g, 1.0 equiv.) was dissolved in anhydrous CH₂Cl₂ (70 mL) and Et₃N (34.8 mmol, 4.83 mL, 1.22 equiv.) was added. The mixture was cooled to 0 °C *via* ice bath, and a solution of acetyl chloride (34.3 mmol, 2.46 mL, 1.20 equiv.) in anhydrous CH₂Cl₂ was slowly added. Then, the solution was

allowed to warm up to room temperature and it was stirred for 4 h. The reaction mixture was washed with 2 M NaOH (3×), water (2×) and brine (2×) successively, dried over Na₂SO₄, filtered and evaporated. The crude product was purified by *Kugelrohr* distillation (0.35 mBar, 150–170 °C) to obtain the product **19** as a light-yellow oil (6.84 g, 95% yield). **¹H NMR (400 MHz, CDCl₃)δ**: 7.37–7.21 (m, 10H, *H*-arom), 6.56 (d, *J* = 16.0 Hz, 1H, arom-CH=CH), 6.37 (d, *J* = 8.0 Hz, 1H, arom-CH=CH), 6.27 (dd, *J* = 16.0 Hz, 4.0 Hz, 1H, arom-CH), 2.09 (s, 3H, CH₃-CO); **¹³C NMR (100 MHz, CDCl₃)δ**: 170.3 (CH₃-CO), 139.5 (C-arom), 136.4 (arom-CH), 132.8 (arom-CH=CH), 128.9 (C-arom), 128.8 (C-arom), 128.4 (C-arom), 128.3 (C-arom), 127.7 (C-arom), 127.3 (arom-CH=CH), 126.9 (C-arom), 76.4 (arom-CH), 21.6 (CH₃-CO).

4.5.2. (±)-3-acetoxy-1-cyclohexene (**21**)

Prepared according to literature procedure [23]. Freshly distilled 3-bromo-1-cyclohexene (30.3 mmol, 3.5 mL, 1.0 equiv.) was dissolved in acetone (60 mL). Glacial acetic acid (0.3 mol, 17.5 mL, 10.0 equiv.) was added, followed by the dropwise addition of Et₃N (0.31 mol, 43 mL, 10.2 equiv.) at 0 °C. The mixture was allowed to warm up and it was subsequently stirred at room temperature overnight. The solvent was removed *in vacuo* and the residue was dissolved in diethyl ether. The organic layer was washed with 0.5 M HCl (3×), saturated NaHCO₃-solution (3×), brine (1×) and water (1×) successively, dried over Na₂SO₄ and concentrated *in vacuo*. Vacuum distillation (20 mBar, 85 °C) afforded product **21** as a colourless liquid (3.56 g, 84% yield). **¹H NMR (400 MHz, CDCl₃)δ**: 5.96–5.93 (m, 1H, CH–CH=CH), 5.71–5.67 (m, 1H, CH–CH=CH), 5.26–5.23 (m, 1H, CH–CH=CH), 2.12–2.09 (m, 1H, CH₂–CH_{2a}-CH), 2.04 (s, 3H, CH₃-CO), 2.01–1.98 (m, 1H, CH₂–CH_{2b}-CH), 1.89–1.83 (m, 1H, CH_{2a}-CH₂-CH), 1.77–1.68 (m, 1H, CH₂-CH=CH), 1.66–1.60 (m, 1H, CH_{2b}-CH₂-CH); **¹³C NMR (100 MHz, CDCl₃)δ**: 170.9 (CH₃-CO), 132.8 (CH–CH=CH), 125.8 (CH–CH=CH), 68.2 (CH–CH=CH), 28.4 (CH–CH₂-CH₂), 25.0 (CH₂-CH=CH), 21.5 (CH₃-CO), 19.0 (CH–CH₂-CH₂).

4.6. General procedure for the asymmetric allylic alkylation

A mixture of [Pd(C₃H₅)Cl]₂ (1.83 mg, 0.005 mmol, 1.0 mol%) and the chiral ligand (0.011 mmol, 2.2 mol%) in 0.5 mL solvent was stirred for 30 min under argon atmosphere to form the active catalyst species. The allylic acetate (0.5 mmol, 1.0 equiv.) was dissolved in 0.5 mL solvent, and it was added to the reaction mixture. After an additional 10 min of stirring, the corresponding malonate or amine (0.60 mmol, 1.2 equiv.), and optionally BSA (250 μL, 1.0 mmol, 2.0 equiv.) and KOAc (2 mg, 2.0 mol%) were added. The mixture was stirred at room temperature. After completion, 5 mL diethyl ether was added. In case of C-allylation reactions the organic layer was washed with saturated NH₄Cl solution and water, dried over Na₂SO₄ and concentrated under reduced pressure. For the *N*-allylations, the reaction mixtures were simply concentrated *in vacuo*. The crude products were purified by column chromatography or preparative TLC.

4.6.1. Dimethyl-(*R,E*)-2-(1,3-diphenylallyl)malonate (**20a**) [24]

Purification by preparative TLC (light petrol: ethyl acetate 10:1, UV visualization) afforded the pure product as a colorless liquid (151 mg, 93% yield; >99% ee). α_D²⁰: +12.4 (c 1.0, CHCl₃); **¹H NMR (400 MHz, CDCl₃)δ**: 7.29–7.17 (m, 10H, *H*-arom), 6.45 (d, *J* = 16.0 Hz, 1H, arom-CH=CH), 6.30 (dd, *J* = 16.0 Hz, 8.0 Hz, 1H, arom-CH=CH), 4.24 (dd, *J* = 12.0 Hz, 8.0 Hz, 1H, arom-CH), 3.91 (d, *J* = 12.0 Hz, 1H, CH(COOCH₃)), 3.66 (s, 3H, COOCH₃), 3.47 (s, 3H, COOCH₃); **Chiral HPLC analysis**: (chiralcel IB column, ⁿhexane: EtOH 99:1 V/V, 1.0 mL/min, 25 °C, UV 254 nm) t_R = 7.71 min (R).

4.6.2. Diethyl-(*R,E*)-2-(1,3-diphenylallyl)malonate (**20b**) [24]

Purification by preparative TLC (light petrol: ethyl acetate 10:1, UV visualization) afforded the pure product as a colorless oil (166 mg, 94% yield; 99% ee). α_D^{20} : +17.0 (c 1.0, CHCl₃); **¹H NMR (400 MHz, CDCl₃)**δ: 7.23–7.16 (m, 10H, *H*-arom), 6.44 (d, *J* = 16.0 Hz, 1H, arom-CH=CH), 6.28 (dd, *J* = 16.0 Hz, 8.0 Hz, 1H, arom-CH=CH), 4.28–4.08 (m, 3H, arom-CH, COOCH₂CH₃), 3.91–3.85 (m, 3H, COOCH₂CH₃, CH(COOCH₂CH₃)), 1.20 (t, *J* = 8.0 Hz, 3H, COOCH₂CH₃), 0.97 (t, *J* = 8.0 Hz, 3H, COOCH₂CH₃); **Chiral HPLC analysis**: (chiralcel IA column, ⁿhexane: 2-propanol 90:10 V/V, 0.5 mL/min, 25 °C, UV 254 nm) *t*_R = 11.3 min (*R*), *t*_R = 13.5 min (*S*).

4.6.3. Dibenzyl-(*R,E*)-2-(1,3-diphenylallyl)malonate (**20c**) [24]

Purification by preparative TLC (light petrol: ethyl acetate 10:1, UV visualization) afforded the pure product as a colorless oil (233 mg, 98% yield; >99% ee). α_D^{20} : +7.0 (c 1.0, CHCl₃); **¹H NMR (400 MHz, CDCl₃)**δ: 7.27–7.22 (m, 18H, *H*-arom), 7.05 (d, *J* = 8.0 Hz, 2H, *H*-arom), 6.42 (d, *J* = 16.0 Hz, 1H, arom-CH=CH), 6.31 (dd, *J* = 16.0 Hz, 8.0 Hz, 1H, arom-CH=CH), 5.11 (dd, *J* = 16.0 Hz, 12.0 Hz, CH₂-arom), 4.94 (dd, *J* = 16.0 Hz, 12.0 Hz, CH₂-arom), 4.30 (dd, *J* = 12.0 Hz, 8.0 Hz, 1H, arom-CH), 4.05 (d, *J* = 12.0 Hz, 1H, CH(COOCH₂Ph)); **Chiral HPLC analysis**: (chiralcel IA column, ⁿhexane: 2-propanol 90:10 V/V, 0.5 mL/min, 25 °C, UV 254 nm) *t*_R = 21.0 min (*R*).

4.6.4. Diethyl-(*S,E*)-2-acetamido-2-(1,3-diphenylallyl)malonate (**20d**) [25]

Purification by preparative TLC (light petrol: ethyl acetate 10:1, UV visualization) afforded the pure product as a white solid (200 mg, 98% yield; 92% ee). α_D^{20} : +44.0 (c 1.0, EtOH); **¹H NMR (400 MHz, CDCl₃)**δ: 7.29–7.21 (m, 9H, *H*-arom), 7.16–7.12 (m, 1H, *H*-arom), 6.74 (dd, *J* = 16.0 Hz, 8.0 Hz, 1H, arom-CH=CH), 6.56 (brs, 1H, NH), 6.27 (d, *J* = 16.0 Hz, 1H, arom-CH=CH), 4.75 (d, *J* = 12.0 Hz, 1H, arom-CH), 4.29–4.20 (m, 2H, COOCH₂CH₃), 4.13–3.99 (m, 2H, COOCH₂CH₃), 1.94 (s, 3H, CH₃-CO), 1.23 (t, *J* = 8.0 Hz, 1H, COOCH₂CH₃), 1.14 (t, *J* = 8.0 Hz, 3H, COOCH₂CH₃); **Chiral HPLC analysis**: (chiralcel IA column, ⁿhexane: 2-propanol 90:10 V/V, 0.5 mL/min, 25 °C, UV 254 nm) *t*_R = 12.9 min (*S*), *t*_R = 15.1 min (*R*).

4.6.5. (*R,E*)-3-(1,3-Diphenylallyl)pentane-2,4-dione (**20e**) [26]

Purification by preparative TLC (light petrol: ethyl acetate 10:1, UV visualization) afforded the pure product as a white solid (130 mg, 95% yield; 92% ee). α_D^{20} : –11.0 (c 1.0, CHCl₃); **¹H NMR (400 MHz, CDCl₃)**δ: 7.32–7.18 (m, 10H, *H*-arom), 6.41 (d, *J* = 16.0 Hz, 1H, arom-CH=CH), 6.19–6.15 (m, 1H, arom-CH=CH), 4.33–4.31 (m, 2H, arom-CH, CH(COCH₃)), 2.23 (s, 3H, COCH₃), 1.91 (s, 3H, COCH₃); **Chiral HPLC analysis**: (chiralcel OJ column, ⁿhexane: 2-propanol 98:2 V/V, 0.5 mL/min, 25 °C, UV 254 nm) *t*_R (major) = 37.3 min (*R*), *t*_R (minor) = 47.5 min (*S*).

4.6.6. Dimethyl (*R,E*)-2-(1,3-diphenylallyl)-2-(prop-2-yn-1-yl)malonate (**20f**)

Purification by preparative TLC (light petrol: ethyl acetate 10:1, UV visualization) afforded the pure product as a light-yellow oil (165 mg, 94% yield; 99% ee). α_D^{20} : +15.2 (c 1.0, CHCl₃); **¹H NMR (400 MHz, CDCl₃)**δ: 7.34–7.19 (m, 10H, *H*-arom), 6.76 (dd, *J* = 16.0 Hz, 8.0 Hz, 1H, arom-CH=CH), 6.43 (d, *J* = 16.0 Hz, 1H, arom-CH=CH), 4.42 (d, *J* = 12.0 Hz, 1H, arom-CH), 3.76 (s, 3H, COOCH₃), 3.69 (s, 3H, COOCH₃), 2.80 (d, *J* = 20.0 Hz, 1H, CHCCH_{2a}), 2.62 (d, *J* = 20.0 Hz, 1H, CHCCH_{2b}), 2.11–2.09 (m, 1H, CHCCH₂); **Chiral HPLC analysis**: (chiralcel IA column, ⁿhexane: 2-propanol 99:1 V/V, 0.5 mL/min, 25 °C, UV 254 nm) *t*_R = 20.1 min (*R*).

4.6.7. (*S,E*)-1-(1,3-diphenylallyl)pyrrolidine (**20g**) [27]

Purification by preparative TLC (light petrol: ethyl acetate 7:1, UV visualization) afforded the pure product as a yellow oil (129 mg, 98% yield; 92% ee). α_D^{20} : +4.1 (c 1.0, CHCl₃); **¹H NMR (400 MHz, CDCl₃)**δ: 7.35–7.12 (m, 10H, *H*-arom), 6.49 (d, *J* = 16.0 Hz, 1H, arom-CH=CH), 6.34 (dd, *J* = 16.0 Hz, 8.0 Hz, arom-CH=CH), 3.69 (d, *J* = 8.0 Hz, 1H, arom-CH), 2.50–2.49 (m, 2H, N-CH₂), 2.37–2.35 (m, 2H, N-CH₂), 1.73–1.69 (m, 2H, N-CH₂-CH₂), 1.51 (brs, 2H, N-CH₂-CH₂); **Chiral HPLC analysis**: (chiralcel OD column, ⁿhexane: 2-propanol 99.5:0.5 V/V, 0.5 mL/min, 25 °C, UV 254 nm) *t*_R = 10.1 min (*R*), *t*_R = 10.9 min (*S*).

4.6.8. (*S,E*)-1-(1,3-diphenylallyl)piperidine (**20h**) [27]

Purification by preparative TLC (light petrol: ethyl acetate 7:1, UV visualization) afforded the pure product as a yellow oil (133 mg, 98% yield; 84% ee). α_D^{20} : +5.2 (c 1.0, CHCl₃); **¹H NMR (400 MHz, CDCl₃)**δ: 7.33–7.12 (m, 10H, *H*-arom), 6.45 (d, *J* = 16.0 Hz, 1H, arom-CH=CH), 6.26 (dd, *J* = 16.0 Hz, 8.0 Hz, arom-CH=CH), 3.74 (d, *J* = 8.0 Hz, 1H, arom-CH), 2.43–2.38 (m, 2H, N-CH₂), 2.30–2.25 (m, 2H, N-CH₂), 1.51–1.47 (m, 4H, N-CH₂-CH₂), 1.39–1.35 (m, 2H, N-(CH₂)₂-CH₂); **Chiral HPLC analysis**: (chiralcel OD column, ⁿhexane: 2-propanol 99.5:0.5 V/V, 0.5 mL/min, 25 °C, UV 254 nm) *t*_R = 9.6 min (*R*), *t*_R = 10.5 min (*S*).

4.6.9. (*S,E*)-*N*-benzyl-1,3-diphenylprop-2-en-1-amine (**20i**) [27]

Purification by preparative TLC (light petrol: ethyl acetate 7:1, UV visualization) afforded the pure product as a light-yellow oil (131 mg, 87% yield; 92% ee). α_D^{20} : +29.5 (c 1.5, CHCl₃); **¹H NMR (400 MHz, CDCl₃)**δ: 7.36 (d, *J* = 8.0 Hz, 2H, *H*-arom), 7.29–7.10 (m, 13H, *H*-arom), 6.50 (d, *J* = 16.0 Hz, 1H, arom-CH=CH), 6.24 (dd, *J* = 16.0 Hz, 8.0 Hz, 1H, arom-CH=CH), 4.32 (d, *J* = 8.0 Hz, 1H, arom-CH), 3.71 (dd, *J* = 16.0 Hz, 12.0 Hz, 2H, arom-CH₂), 1.63 (brs, 1H, NH); **Chiral HPLC analysis**: (chiralcel OD column, ⁿhexane: 2-propanol 99.5:0.5 V/V, 0.5 mL/min, 25 °C, UV 254 nm) *t*_R = 24.66 min (*R*), *t*_R = 27.4 min (*S*).

4.6.10. Dimethyl 2-(cyclohex-2-en-1-yl)malonate (**22a**) [28]

Purification by column chromatography (light petrol: diethyl ether 10:1, visualization by potassium permanganate stain) afforded the pure product as a colorless oil (91 mg, 86% yield; 86% ee). α_D^{20} : +35.2 (c 1.0, CHCl₃); **¹H NMR (400 MHz, CDCl₃)**δ: 5.80–5.76 (m, 1H, CH-CH=CH), 5.51 (d, *J* = 12.0 Hz, 1H, CH-CH=CH), 3.73 (s, 6H, 2 x COOCH₃), 3.29 (d, *J* = 8.0 Hz, 1H, CH-CH=CH), 2.93–2.87 (m, 1H, CH(COOCH₃)₂), 2.00–1.97 (m, 2H, CH₂-CH), 1.79–1.73 (m, 2H, CH₂-CH₂-CH), 1.60–1.54 (m, 1H, CH_{2a}-(CH₂)₂-CH), 1.40–1.33 (m, 1H, CH_{2b}-(CH₂)₂-CH); **Chiral HPLC analysis**: (chiralcel AS-H column, ⁿhexane: 2-propanol 95:5 V/V, 1.0 mL/min, 25 °C, UV 220 nm) *t*_R = 6.6 min (*R*), *t*_R = 7.7 min (*S*).

4.6.11. Diethyl 2-(cyclohex-2-en-1-yl)malonate (**22b**) [28]

Purification by column chromatography (light petrol: diethyl ether 10:1, visualization by potassium permanganate stain) afforded the pure product as a colorless oil (106 mg, 88% yield; 83% ee). α_D^{20} : +23.2 (c 1.0, CHCl₃); **¹H NMR (400 MHz, CDCl₃)**δ: 5.73–5.65 (m, 1H, CH-CH=CH), 5.48 (d, *J* = 12.0 Hz, 1H, CH-CH=CH), 4.13 (q, 4H, 2 x COOCH₂H₃), 3.17 (d, *J* = 8.0 Hz, 1H, CH-CH=CH), 2.87–2.77 (m, 1H, CH(COOCH₂CH₃)₂), 1.95–1.91 (m, 2H, CH₂-CH), 1.75–1.35 (m, 4H, CH₂-CH₂-CH, CH_{2a}-(CH₂)₂-CH, CH_{2b}-(CH₂)₂-CH), 1.20 (t, *J* = 12.0 Hz, 2 x COOCH₂CH₃); **Chiral HPLC analysis**: (chiralcel OJ column, ⁿhexane: 2-propanol 98:2 V/V, 0.5 mL/min, 25 °C, UV 220 nm) *t*_R = 10.5 min (*R*), *t*_R = 10.9 min (*S*).

4.6.12. Dibenzyl 2-(cyclohex-2-en-1-yl)malonate (**22c**)

Purification by column chromatography (light petrol: diethyl

ether 10:1, visualization by potassium permanganate stain) afforded the pure product (90% yield; 99% ee). α_D^{20} : +17.8 (c 1.0, CHCl₃); ¹H NMR (400 MHz, CDCl₃) δ : 7.34–7.29 (m, 10H, *H*-arom), 5.77–5.72 (m, 1H, CH–CH=CH), 5.53 (d, *J* = 12.0 Hz, 1H, CH–CH=CH), 5.15 (dd, *J* = 16.0 Hz, 8.0 Hz, 4H, 2 x CH₂-arom), 3.39 (d, *J* = 8.0 Hz, 1H, CH–CH=CH), 2.99–2.91 (m, 1H, CH(COOCH₂Ph)₂), 1.98–1.94 (m, 2H, CH₂-CH), 1.77–1.66 (m, 2H, CH₂-CH₂-CH), 1.51–1.47 (m, 1H, CH_{2a}-(CH₂)₂-CH), 1.39–1.34 (m, 1H, CH_{2b}-(CH₂)₂-CH); **Chiral HPLC analysis**: (chiralcel IA column, ⁿhexane: 2-propanol 90:10 V/V, 0.5 mL/min, 25 °C, UV 254 nm) *t*_R = 10.8 min (R).

4.6.13. (*S*)-*N*-Benzylcyclohex-2-en-1-amine (**22d**)

Purification by column chromatography (light petrol: diethyl ether 5:1, visualization by potassium permanganate stain) afforded the pure product as a light-yellow oil (84 mg, 89% yield; 60% ee). α_D^{20} : +1.8 (c 0.5, CHCl₃); ¹H NMR (400 MHz, CDCl₃) δ : 7.25–7.17 (m, 5H, *H*-arom) 5.73–5.65 (m, 2H, CH–CH=CH, CH–CH=CH), 3.78 (dd, *J* = 16.0 Hz, *J* = 8.0 Hz, 2H, CH₂-arom), 3.17–3.14 (m, 1H, CH–NH), 1.94–1.92 (m, 2H, CH₂-CH), 1.84–1.72 (m, 2H, CH₂-CH₂-CH), 1.70–1.65 (m, 1H, CH_{2a}-(CH₂)₂-CH), 1.52–1.40 (m, 1H, CH_{2b}-(CH₂)₂-CH); **Chiral HPLC analysis**: (chiralcel OD column, ⁿhexane: 2-propanol 99.5:0.5 V/V, 1.0 mL/min, 25 °C, UV 220 nm) *t*_R = 19.1 min (*S*), *t*_R = 21.1 min (R).

Declaration of interests

The authors declare that they have no known competing financial interests or personal relationships that could have appeared to influence the work reported in this paper.

Acknowledge

Financial support by the Austrian Science Fund (FWF, project P29146–N34) is gratefully acknowledged.

Appendix A. Supplementary data

Supplementary data to this article can be found online at <https://doi.org/10.1016/j.tet.2020.131246>.

References

- [1] H. Yoshizaki, H. Satoh, Y. Sato, S. Nukui, M. Shibasaki, M. Mori, *J. Org. Chem.* 60

- (1995) 2016–2021.
- [2] J. Kobayashi, M. Ishibashi, H. Nakamura, Y. Ohizumi, *Tetrahedron Lett.* 27 (1986) 5755–5758.
- [3] B.M. Trost, J.D. Chisholm, S.J. Wroblewski, M. Jung, *J. Am. Chem. Soc.* 124 (2002) 12420–12421.
- [4] B.M. Trost, M.L. Crawley, *Chem. Rev.* 103 (2003) 2921–2944.
- [5] For selected reviews, see: a) B.M. Trost, D.L. Van Vranken, *Chem. Rev.* 96 (1996) 395–422; b) B.M. Trost, *Tetrahedron* 71 (2015) 5708–5733; c) J.T. Mohr, B.M. Stoltz, *Chem. Asian J.* 2 (2007) 1486–1491; d) G. Poli, G. Prestat, F. Liron, C. Kammerer-Pentier, *Top. Organomet. Chem.* 38 (2011) 1–64.
- [6] For selected advances with P,P-bidentate ligands, see: a) B.M. Trost, G.M. Schroeder, *J. Am. Chem. Soc.* 121 (1999) 6759–6760; b) B.M. Trost, D.E. Patterson, E.J. Hembre, *J. Am. Chem. Soc.* 121 (1999) 10834–10835; c) B.M. Trost, R. Radinov, E.M. Grenzer, *J. Am. Chem. Soc.* 119 (1997) 7879–7880; d) B.M. Trost, *Chem. Pharm. Bull.* 50 (2002) 1–14; e) Z. Lu, S. Ma, *Angew. Chem. Int. Ed.* 47 (2008) 258–297.
- [7] C.M. Reeves, D.C. Behenna, B.M. Stoltz, *Org. Lett.* 16 (2014) 2314–2317.
- [8] J.T. Mohr, D.C. Behenna, A.M. Harned, B.M. Stoltz, *Angew. Chem. Int. Ed.* 44 (2005) 6924–6927.
- [9] Y. Tanaka, T. Mino, K. Akita, M. Sakamoto, T. Fujita, *J. Org. Chem.* 69 (2004) 6679–6687.
- [10] G.S. Mahadiq, S.R. Hitchcock, *Tetrahedron: Asymmetry* 1 (2010) 33–38.
- [11] R. Kuwano, K.-I. Uchida, Y. Ito, *Org. Lett.* 5 (2003) 2177–2179.
- [12] M. Ogasawara, H.L. Ngo, T. Sakamoto, T. Takahashi, *Org. Lett.* 7 (2005) 2881–2884.
- [13] W. Zhang, T. Kida, Y. Nakatsuji, I. Ikeda, *Tetrahedron Lett.* 44 (1996) 7995–7998.
- [14] D. Liu, F. Xie, W. Zhang, *J. Org. Chem.* 72 (2007) 6992–6997.
- [15] B.M. Trost, B. Breit, M.G. Organ, *Tetrahedron Lett.* 35 (1994) 5817–5820.
- [16] Y.K. Kim, S.J. Lee, K.H. Ahn, *J. Org. Chem.* 65 (2000) 7807–7813.
- [17] Á.M. Pálvölgyi, J. Bitai, V. Zeindlhofer, C. Schröder, K. Bica, *ACS Sustain. Chem. Eng.* 7 (2019) 3414–3423.
- [18] G.C. Lloyd-Jones, S.C. Stephen, I.J.S. Fairlamb, A. Martorell, B. Dominguez, P.M. Tomlin, M. Murray, J.M. Fernandez, J.C. Jeffery, T. Riis-Johannes, T. Guereziz, *Pure Appl. Chem.* 76 (2004) 589–601.
- [19] D.W. Lee, H. Ha, W.K. Lee, *Synth. Commun.* 37 (2007) 252–255.
- [20] A.S. Kucherenko, D.E. Siyutkin, S.G. Nigmatov, A.O. Chizhov, S.G. Zlotin, *Adv. Synth. Catal.* 16 (2012) 3078–3086.
- [21] Y. Xiong, Z. Du, H. Chen, Z. Yang, Q. Tan, C. Zhang, L. Zhu, M. Zhang, *J. Am. Chem. Soc.* 141 (2019) 961–971.
- [22] I.D.G. Watson, S.A. Styler, A.K. Yudin, *J. Am. Chem. Soc.* 126 (2004) 5086–5087.
- [23] S. Fuchs, V. Berl, J.-P. Lepoittevin, *Eur. J. Org. Chem.* (2007) 1145–1152.
- [24] X. Du, H. Liu, D.-M. Du, *Eur. J. Org. Chem.* (2010) 786–793.
- [25] P. Von Matt, A. Pfaltz, *Angew. Chem.* 105 (1993) 614–615.
- [26] G. Blay, L. Cardona, J.R. Pedro, *Chem. Eur. J.* 18 (2012) 12966–12969.
- [27] D. Smyth, H. Tye, C. Eldred, N.W. Alcock, M. Wills, *J. Chem. Soc. Perkin Trans.* (2001) 2840–2849.
- [28] J. Ma, C. Li, D. Zhang, Y. Lei, M. Li, R. Jiang, W. Chen, *RSC Adv.* 5 (2015) 35888–35892.

Counterion-Enhanced Pd/Enamine Catalysis: Direct Asymmetric α -Allylation of Aldehydes with Allylic Alcohols by Chiral Amines and Achiral or Racemic Phosphoric Acids

Ádám Márk Pálvölgyi, Jakob Smith, Michael Schnürch, and Katharina Bica-Schröder*



Cite This: *J. Org. Chem.* 2021, 86, 850–860



Read Online

ACCESS |



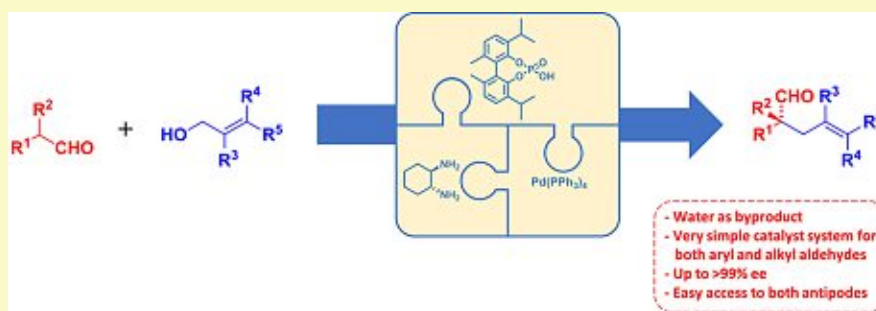
Metrics & More



Article Recommendations



Supporting Information



ABSTRACT: We report a straightforward and efficient Pd/enamine catalytic procedure for the direct asymmetric α -allylation of branched aldehydes. The use of simple chiral amines and easily prepared achiral or racemic phosphoric acids, together with a suitable Pd-source resulted in a highly active and enantioselective catalyst system for the allylation of various α -branched aldehydes with different allylic alcohols. The reported procedure could provide an easy access to both product antipodes. Furthermore, two possible orthogonal derivatizations of the enantioenriched aldehydes were performed without any decrease in enantioselectivity.

INTRODUCTION

Carbon–carbon bond-forming reactions were always in the focus of organic chemistry. The synthesis of asymmetric all-carbon quaternary centers is particularly challenging, and despite the growing numbers of advances in this field, it is still a difficult task because of the substantial steric repulsion between the reactants.^{1,2}

Optically active molecules bearing an allylic motif are invaluable intermediates for the total synthesis of biologically active compounds.^{3,4} Based on the pioneering work of Jirō Tsuji and Barry M. Trost, the palladium-catalyzed asymmetric allylation involving an in situ-generated allylpalladium– π complex is of special interest in this field. Thanks to the indisputable advantages such as mild reaction conditions and operational simplicity, it is still a crucial tool for the synthesis of allylic compounds.⁵

While the traditional Tsuji–Trost allylation requires both a good nucleophile and an allylic compound with a suitable leaving group, several advances have been published to overcome this problem by merging organo- and transition-metal catalyses. In 2003, Krische and coworkers achieved enone cycloallylations via dual activation of latent nucleophilic and electrophilic partners.⁶ Three years later, Córdova reported the first Pd/enamine dual catalyst system relying on Pd(PPh₃)₄ and pyrrolidine in the direct α -allylation of nonbranched aldehydes and ketones with activated allylic

electrophiles.⁷ Since then, enamine catalysis has played an important role in the field of asymmetric allylation.^{8–11} A few elegant procedures have also been found for the asymmetric α -allylation of branched aldehydes including the synergistic use of a Pd-source with modified primary amino acids (Yoshida, Scheme 1a) or iridium catalysis with double stereocontrol (Carreira).^{12–16} By expanding the use of their previously established concept of asymmetric counteranion-directed catalysis to asymmetric allylations, the List group developed a three-component-catalyst system composed of a Pd-complex, an amine, and a chiral Brønsted acid known as TRIP (Scheme 1b).^{17–20} Even though the synthesis of TRIP requires a multistep procedure and results in a rather pricy catalyst, they achieved impressive catalytic activities together with a high degree of enantioselectivity (Scheme 1b).²⁰

Herein, we propose a concept of counterion-enhanced catalysis for the enantioselective α -allylation of α -branched aldehydes with allylic alcohols (Scheme 1c). The combination of simple chiral amines together with readily prepared achiral

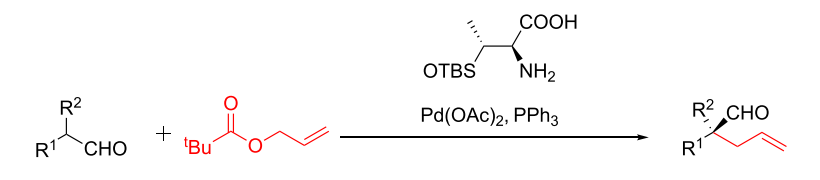
Received: October 8, 2020

Published: December 15, 2020

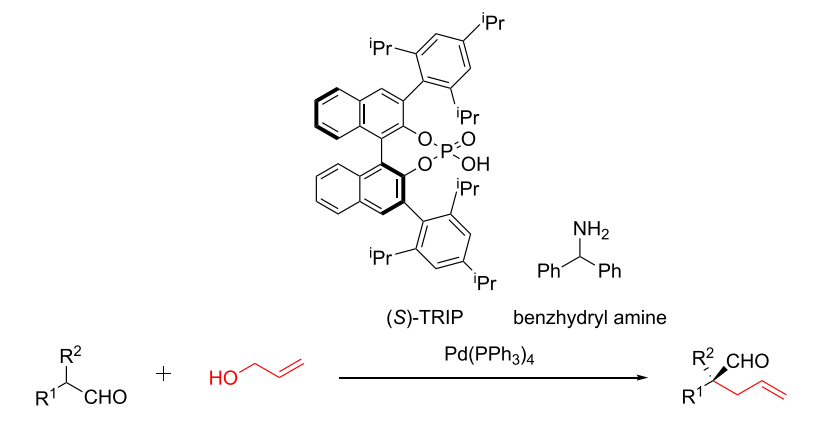


Scheme 1. Concepts for the α -Allylation of Branched Aldehydes

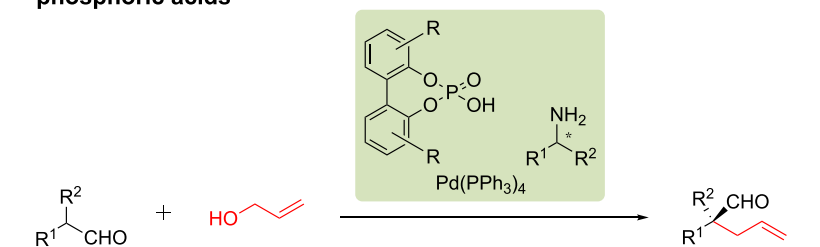
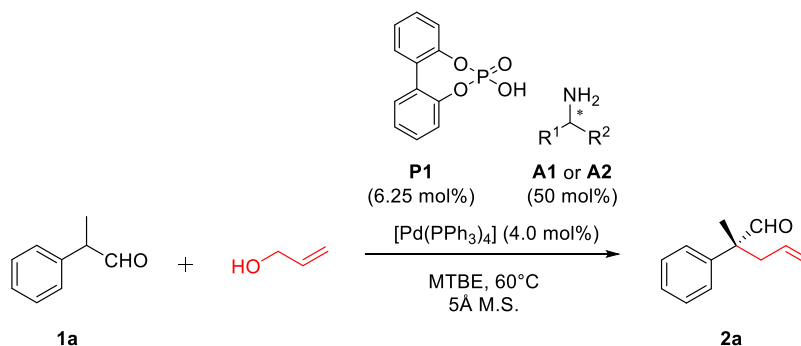
a) Yoshida's method using D-amino acids



b) List's three-catalyst system featuring (S)-TRIP and an achiral amine



c) Our concept: the use of simple chiral amines and achiral or racemic phosphoric acids

Scheme 2. Asymmetric α -Allylation of 2-Phenylpropanal

or racemic phosphoric acids and $\text{Pd}(\text{PPh}_3)_4$ resulted in high catalytic activities and excellent stereocontrol. As no extensive catalyst preparation is required, this methodology could provide a good alternative to current state-of-the-art methods.

RESULTS AND DISCUSSION

To establish the new concept, we were initially interested in the asymmetric α -allylation of 2-phenylpropanal (**1a**). Based on our previous observations for asymmetric counterion-enhanced catalysis, *L*-valine *tert*-butyl ester (**A1**) was chosen as

the amine source, together with the phosphoric acid **P1** (Scheme 2).²¹ MTBE as an apolar aprotic solvent was used as its low dielectric constant might facilitate the formation of stronger contact ion pairs. In accordance with the relevant literature, high amine loadings were used.²⁰ After the initial screening for proper concentrations and desiccant, the product **2a** could be obtained in good yield, albeit with moderate enantioselectivity (Table 1, entry 1). Gratifyingly, the ee could be dramatically increased to 78% by simply changing the amine source to the C_2 -symmetric diamine (*R,R*)-**A2**, also increasing

Table 1. Initial Screening and Proof of Concept

| entry ^a | amine | comment | yield (%) ^b | ee (%) ^c |
|--------------------|----------|---|------------------------|---------------------|
| 1 | (S)-A1 | | 82 | 31 (S) |
| 2 | | | 87 | 78 (R) |
| 3 | (R,R)-A2 | 0 mol % [Pd(PPh ₃) ₄] | 0 | n.d. |
| 4 | | 0 mol % P1 | 37 | 35 (R) |
| 5 | | 0 mol % (R,R)-A2 | 81 | 0 |

^aPerformed on a 0.375 mmol scale by using 4.0 mol % Pd(PPh₃)₄, 50 mol % amine, 6.25 mol % P1, 190 mg 5 Å molecular sieves, and 0.75 mmol allyl alcohol in 0.75 mL MTBE at 60 °C for 16 h. ^bDetermined by gas chromatography (GC) analysis. ^cDetermined by chiral high-performance liquid chromatography (HPLC) analysis using a Diacel Chiralcel AS-H column. Absolute configurations were determined by measuring the optical rotations and comparing with the literature data.

the yield (Table 1, entry 2). As can be seen, all three catalytic components are essential for achieving high catalytic activity and selectivity. In the absence of Pd(PPh₃)₄, the formation of 2a could not be observed (Table 1, entry 3). Without the amine source, the reaction presumably follows a pure enol pathway catalyzed by the phosphoric acid P1, consequently resulting in a racemic product (Table 1, entry 5). Nevertheless,

the use of the phosphoric acid was also found to be crucial, as both the reactivity and the selectivity drastically decrease in the absence of compound P1 (Table 1, entry 4).

To further tune our catalytic system, a series of different achiral or racemic phosphoric acids have been synthesized following a straightforward one- or two-step reaction procedure using cheap and easily accessible phenols and bisphenols as starting materials. The use of P1–P7 yielded the allylation product 2a in high to excellent yields and enantioselectivity (Figure 1). The best result was obtained with the thymol-derived analogue P5, resulting in 98% yield and 94% ee. To investigate whether the stereochemistry of the racemic phosphoric acids plays a role in the reaction, the BINOL-derived acid P8 was tested in the enantiopure form (both isomers) and also as a racemic mixture. In all three cases, product 2a was obtained with basically the same enantioselectivity (73%), suggesting that match/mismatch scenarios between the chiral amine and the racemic phosphoric acid do not affect the degree of asymmetric induction. This is in good agreement with our previous observations for organocatalytic asymmetric transfer hydrogenations.²¹ Furthermore, diphenyl phosphate as well as other Brønsted and Lewis acids traditionally used for organocatalysis were also tested. Only

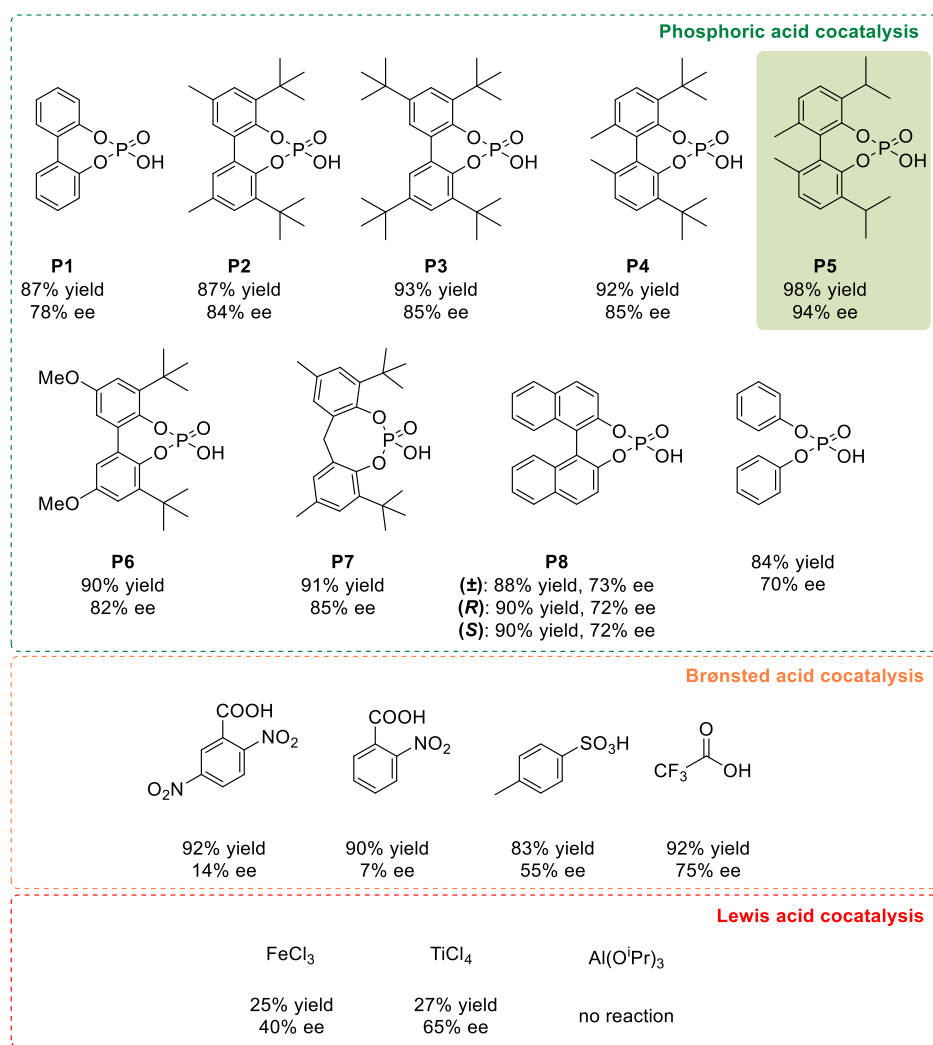
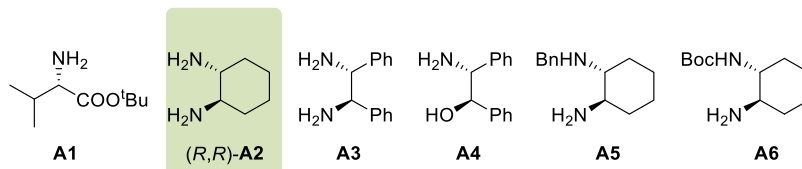


Figure 1. Effect of different acidic cocatalysts in the asymmetric α -allylation of 1a. The reaction conditions were identical to those used in Table 1, entry 2.

Table 2. Different Amines for the Asymmetric α -Allylation of **1a**

| entry ^a | amine | yield (%) ^b | ee (%) ^c |
|--------------------|-------------------|------------------------|---------------------|
| 1 | A1 | 89 | 31 (S) |
| 2 | (<i>R,R</i>)-A2 | 98 | 94 (<i>R</i>) |
| 3 | (<i>S,S</i>)-A2 | 97 | 94 (<i>S</i>) |
| 4 | A3 | 89 | 37 (<i>R</i>) |
| 5 | A4 | 89 | 21 (<i>R</i>) |
| 6 | A5 | 90 | 60 (<i>R</i>) |
| 7 | A6 | 97 | 44 (<i>R</i>) |

^aPerformed on a 0.375 mmol scale by using 4.0 mol % Pd(PPh₃)₄, 50 mol % amine, 6.25 mol % **P5**, 190 mg 5 Å molecular sieves, and 0.75 mmol allyl alcohol in 0.75 mL MTBE at 60 °C for 16 h. ^bDetermined by GC analysis. ^cDetermined by chiral HPLC analysis using a Diacel Chiralcel AS-H column. Absolute configurations were determined by measuring the optical rotations and comparing with the literature data.

trifluoroacetic acid led to a comparable result of 75% ee; all others resulted in significantly inferior results, highlighting the particular advantages associated with the use of achiral or racemic phosphoric acids **P1–P7** (Figure 1, also see Supporting Information Tables S2 and S3, pages S4–S6).

Next, a small set of chiral amines (**A1–A6**) was screened. While the product **2a** was formed in high yields in all cases, the enantioselectivity was moderate when using an amine other than (*R,R*)-A2 (Table 2). Presumably, the high rigidity of amine (*R,R*)-A2 results in a significantly increased energy difference between the diastereomorphous transition states, therefore results in higher enantioselectivity.

Furthermore, by simply changing the amine source from (*R,R*)-A2 to (*S,S*)-A2, the product (*S*)-**2a** could be obtained with the same excellent enantioselectivity of 94% ee (Table 2, entries 2–3). However, given the economic considerations, the (*R,R*)-A2 analogue was used for further optimizations, as well as for investigating the scope and limitations.

With the suitable amine [(*R,R*)-A2] and phosphoric acid (**P5**) in hand, we sought to optimize the ratio of these two components. Eventually, we found that the selectivity of the product **2a** highly depends on the amine-to-acid ratio. As the allylic aldehyde **2a** was obtained in rather high yield even in the absence of the amine source (Table 1, entry 5), it is likely that the level of asymmetric induction is determined by competing enamine- and enol-mediated pathways (see the plausible key intermediates in Figure 2). Decreasing the amine-to-acid ratio leads to an increase in the enol-mediated product, consequently resulting in lower ee values (Figure 2, left side, see also Supporting Information Table S5, page S8). By increasing the amine-to-acid ratio, the level of asymmetric induction increases rapidly. Because of the higher nucleophilicity of the enamine, it can suppress the formation of the enol intermediate and, therefore, lead to an optically active product; however—in accordance with the observations of List—a rather high amine loading was necessary to achieve this. Based on the results, it seems that the initially used amine-to-acid ratio of 8:1 gives the best results (Figure 2, middle), while a further increase in the amine loading could possibly increase the free amine-to-enamine ratio to an undesired level: this would lead to the phosphoric acid reacting with the free amine rather than the enamine, thus hampering the selectivity (Figure 2, right side).

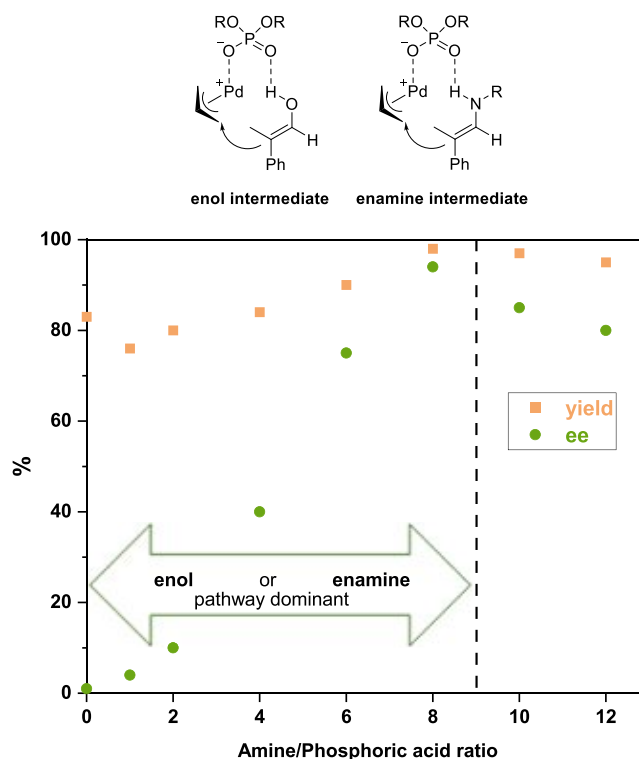


Figure 2. Effect of different amine-to-phosphoric acid ratios in the asymmetric α -allylation of **1a** using amine (*R,R*)-A2 and phosphoric acid **P5** (bottom), and the plausibly competing key intermediates for the enol and enamine pathways (top).

Finally, the effect of the solvent was also investigated. Only slight differences in the catalytic activity and selectivity were observed (see Supporting Information Table S6, page S9) as the allylic aldehyde **2a** could be obtained in rather high yield and enantioselectivity even in green, bio-derived solvents like 2-MeTHF. Most importantly, the solvent screening showed that the use of toluene allowed both the reaction temperature and the catalyst loadings to be decreased successfully. However—similar to previous reports—a relatively high absolute amine loading was necessary to retain a high level of asymmetric induction.

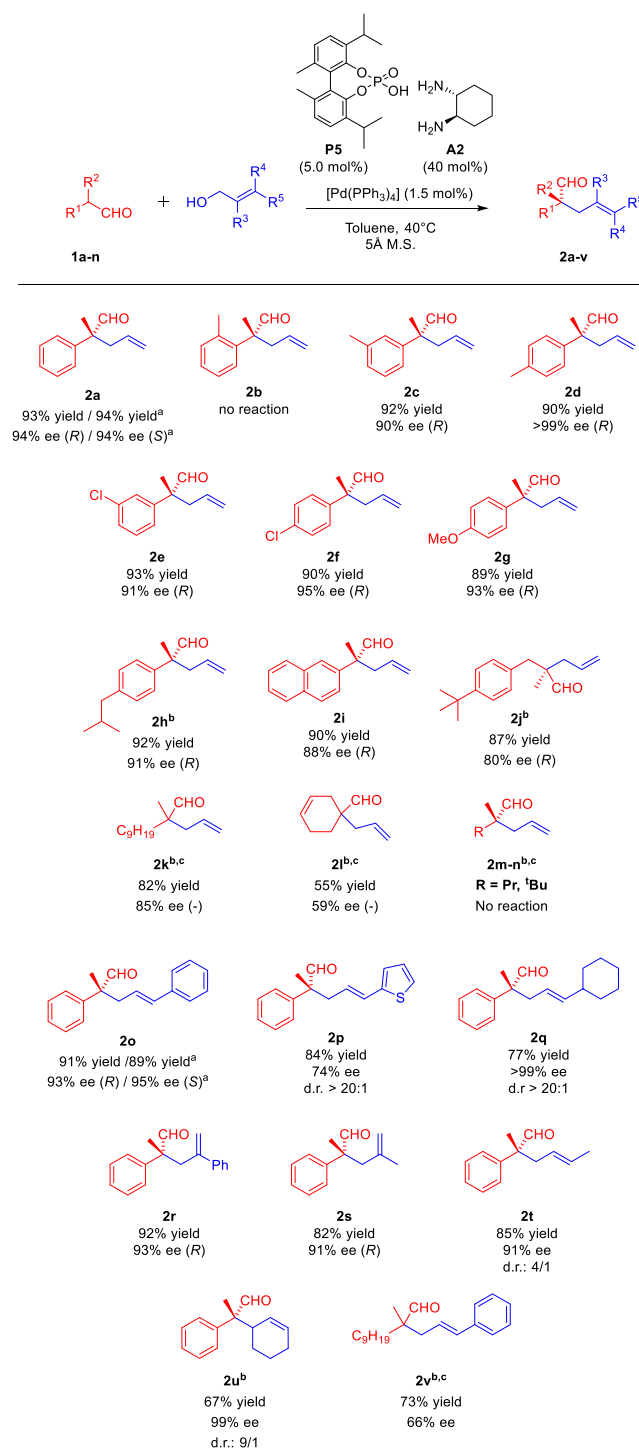
Having optimized and established the catalytic system, we explored the scope and limitations of the reaction by testing different α -branched aldehydes (Scheme 3). Electron-withdrawing and -donating groups in the meta and para positions of the aryl group were well tolerated, resulting in high yields and enantioselectivity up to >99% ee for the allylic aldehydes **2c–j** under the previously optimized reaction conditions; however, no reaction was observed when using the ortho-substituted aldehyde **1b**. Eventually, we also tried to expand the scope to aliphatic aldehydes. Gratifyingly, both a linear and a cyclic aliphatic substrate could be allylated by simply increasing the temperature to 90 °C, yielding the corresponding products (**2k–l**) with moderate to high yield and enantioselectivity; even though still no reaction was observed for short-chained aliphatic aldehydes (**2m–n**).

Furthermore, our catalyst system was found to well tolerate different substituted allylic alcohols as well (Scheme 3). Aliphatic and aromatic primary allylic alcohols readily furnished the corresponding products (**2o, 2r–2t**) in good to excellent yield and in excellent enantiopurity. Moreover, acyclic and cyclic secondary allylic alcohols were also found to be suitable reagents for the synthesis of **2p–q** and **2u**, with the first two resulting in the rearranged, linear allylic aldehydes **2p** and **2q** as major products (Scheme 3). Our procedure could also give an easy access to both product enantiomers: when using (*S,S*)-**A2** for the allylation of **1a** with allyl alcohol and cinnamyl alcohol, the (*S*)-product antipodes [(*S*)-**2a** and (*S*)-**2o**] could be obtained with the same excellent 94 and 95% ee, respectively (Scheme 3).

The proposed reaction mechanism comprises three catalytic cycles (Figure 3). In the enamine cycle (marked with red), the substrate **1a** reacts with the free amine (*R,R*)-**A2** to form the enamine **I**. The allylpalladium- π complex **II** is generated in the second catalytic cycle (green) via acidic activation of the allylic alcohol and subsequent oxidative addition to the Pd⁰ species. The enamine intermediate **I** is then allylated with complex **II** through the key intermediate **III** involving all three catalyst components. This is then dissociated, resulting in the formation of the imine **IV**, meanwhile the phosphoric acid and the Pd⁰ are regenerated (green and orange cycles). Finally, hydrolysis of imine **IV** yields the product **2a**. Alternatively, the free amine (*R,R*)-**A2** could also be allylated directly to give **VI**; however—given the high catalytic efficiency—this must dissociate as the reaction proceeds. Based on our observations and in accordance with the literature, a rather high amine loading is necessary.²⁰ We suspect that the hydrolysis of the imine **IV** is rather slow, therefore a relatively high amine loading is necessary to speed it up and thus ensure that the enamine pathway outperforms the competing enol-mediated reaction (see Figure 3). Our plausible mechanism is supported by analytical studies, as the mass of the enamine **I**, the imine **IV**, the allylpalladium- π complex **II**, and the activated allylic alcohol **V** intermediates could all be detected via electron spin ionization-mass spectrometry (ESI-MS) analysis (see Supporting Information page S67 for details). A similar study was carried out by using the amine **A1** via GC-MS analysis, resulting in the same type of proposed catalytic cycle (see Supporting Information pages S67–S70 for details).

Furthermore, the enantioenriched allylic aldehyde **2a** could be smoothly and orthogonally converted into the corresponding formate **3** and into the dicarbonyl compound **4** via Baeyer–Villiger oxidation and Wacker-oxidation, respectively, retaining the excellent enantioselectivity of **2a** (Scheme 4).

Scheme 3. Scope and Limitations in the Asymmetric α -Allylation of α -Branched Aldehydes^a



^aReactions were performed on a 0.75 mmol scale by using 1.5 mol % Pd(PPh₃)₄, 40 mol % amine(*R,R*)-**A2**, 5.0 mol % **P5**, 190 mg 5 Å molecular sieves, and 1.50 mmol (substituted) allylic alcohol in 1.50 mL toluene at 40 °C for 16 h. Yields refer to pure products after isolation by flash column chromatography. The enantioselectivity was determined by chiral HPLC and chiral GC analysis. Absolute configurations were determined by measuring the optical rotations and comparing with the literature data. ^a(*S,S*)-**A2**, as the amine source, resulting in the formation of (*S*)-**2a**. ^bA higher catalyst loading of 4.0 mol % Pd(PPh₃)₄, 50 mol % (*R,R*)-**A2**, and 6.25 mol % **P5** were used. ^cReaction performed at 90 °C.

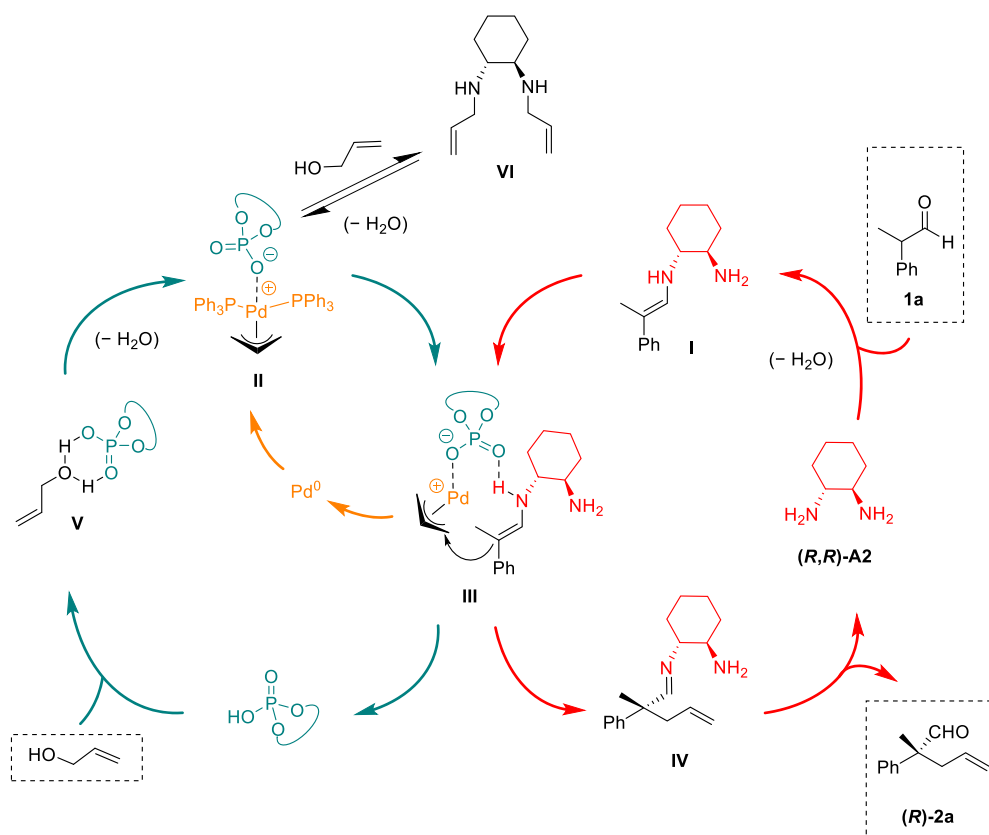
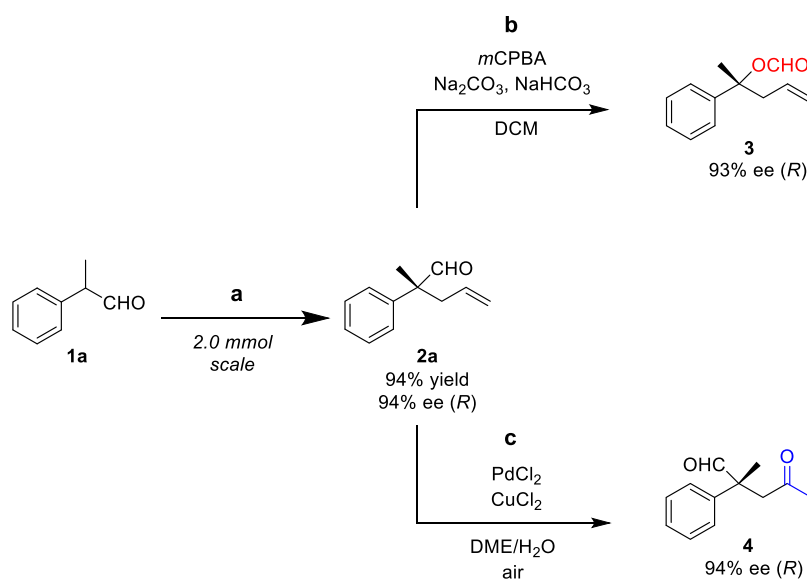


Figure 3. Plausible reaction mechanism for the direct α -allylation of α -branched aldehyde **1a** by using (R,R) -A2, phosphoric acid **P5** and $\text{Pd}(\text{PPh}_3)_4$. The product enantiomer generated in excess [(R) -2a] is illustrated in the cycle for clarity.

Scheme 4. Utilization of **2a** for the Synthesis of the α -Branched Quaternary Allylic Formate **3** and Dicarbonyl Compound **4**^a



^a(a) Performed on a 2.0 mmol scale by using 40 mol % amine (R,R) -A2, 5.0 mol % **P5**, 1.5 mol % $\text{Pd}(\text{PPh}_3)_4$, 190 mg 5 Å molecular sieves, and 4.0 mmol allyl alcohol in 4.0 mL toluene at 40 °C for 16 h. Yield refers to pure **2a** after flash column chromatography. (b) Performed on a 1.0 mmol scale by using 2.1 mmol *m*CPBA, 1.5 mmol NaHCO_3 , and 1.2 mmol Na_2CO_3 in anhydrous CH_2Cl_2 at 25 °C for 24 h. Purified by flash column chromatography. (c) Performed on a 0.9 mmol scale by using 0.09 mmol PdCl_2 and 0.09 mmol CuCl_2 in a mixture of DME and water (v/v 9/1). Purified by flash column chromatography.

CONCLUSIONS

Herein, we reported a concept of counterion enhanced Pd/enamine catalysis for the asymmetric α -allylation of α -branched aldehydes. Our multicomponent catalyst system

relying on a commercially available chiral amine, a readily synthesized phosphoric acid, and $\text{Pd}(\text{PPh}_3)_4$ resulted in a simple and rather cheap chiral framework. The catalyst system was found to be quite versatile, tolerating different aromatic

and aliphatic aldehydes, as well as substituted primary and secondary allylic alcohols. Furthermore, the possible orthogonal derivatization of the enantioenriched aldehydes was demonstrated through the synthesis of the α -branched quaternary allylic formate **3** and the dicarbonyl compounds **4**.

EXPERIMENTAL SECTION

General Experimental Information. All purchased chemicals from commercial suppliers were used without further purification. Dry solvents were predistilled and desiccated on aluminum oxide columns (PureSolv, Innovative Technology). Column chromatography was performed on standard manual glass columns using Merck (40–60 μm) silica gel with predistilled solvents (EtOAc: ethyl acetate, Et₂O: diethyl ether). For TLC analysis, precoated aluminum-backed plates were purchased from Merck (silica gel 60 F₂₅₄). UV-active compounds were detected at 254 nm. Non UV-active compounds were detected using Hanesian's stain solution (cerium molybdate stain). ¹H, ¹³C, and ³¹P nuclear magnetic resonance (NMR) spectra were recorded on a Bruker Advance UltraShield 200 or 400 MHz spectrometer, and chemical shifts are reported in ppm using TMS (tetramethylsilane) as the internal standard. Coupling constants (*J*) are given in Hz. The following abbreviations are used to explain multiplicities: s (singlet), d (doublet), t (triplet), q (quartet), m (multiplet), brs (broad singlet), dd (doublet of doublets), ddd (doublets of doublets of doublets), and td (triplet of doublets). GC measurements were performed on a Thermo Scientific Focus instrument, by using the BGB5 column and a flame ionization detector. Chiral HPLC measurements were carried out on a DIONEX ultraperformance liquid chromatograph equipped with a PDA plus detector (190–360 nm), using Diacel Chiralcel AS-H, OJ, or IB columns (250 \times 4.60 mm, 5 μm). Chiral GC measurements were carried out on a Thermo Scientific Focus instrument, by using a BGB173 column and a flame ionization detector. To determine the absolute configuration, optical rotation was measured on an Anton Paar MCP500 polarimeter under the specific conditions and the results were compared to literature values. Concentrations are given in g/100 mL. High-resolution MS analysis was performed using a HTC PAL system autosampler, an Agilent 1100/1200 high-performance liquid chromatograph, and an Agilent 6230 AJS ESI-time-of-flight mass spectrometer. Microwave reactions were performed in a Biotage Initiator Classic microwave reactor in sealed, 20 ml pressure tight glass vials. Infrared (IR) spectra were recorded on a PerkinElmer Spectrum 65 Fourier transform IR spectrometer equipped with a specac MK II Golden Gate Single Reflection ATR unit.

Amine(S)-**A1**, (R,R)-**A5**, and (R,R)-**A6** were prepared according to literature procedures.^{22–24}

General Procedures for the Phosphoric Acid Synthesis. Phosphoric acids **P1**, **P7**, and **P8** were prepared by direct phosphorylation of the corresponding diols.²⁵ Phosphoric acids **P2–P6** were prepared in a two-step fashion via oxidative coupling of the corresponding phenols (method A or B) followed by subsequent phosphorylation.^{26–28}

4,8-Di-tert-butyl-6-hydroxy-2,10-dimethyldibenzo[d,f]-[1,3,2]-dioxaphosphepine 6-oxide (P2) (Method A). In a pressure-tight MW-vial, 2-(tert-butyl)-4-methylphenol (1.5 g, 12.0 mmol, 1.0 equiv) was dissolved in chlorobenzene (7.2 mL, 1.66 M solution) and di-tert-butyl peroxide (2.3 mL, 12.6 mmol, 1.05 equiv) was added. The vial was sealed, and it was stirred for 15 min at room temperature. The vial was then placed in a microwave reactor and the reaction mixture was stirred for 15 min (160 °C, high absorption setting and 10 bar pressure limit to avoid safety issues). The reaction mixture was allowed to cool down, and volatiles were removed in vacuo. Column chromatography (silica gel, 1.5% EtOAc in light petrol) afforded 3,3'-di-tert-butyl-5,5'-dimethyl-[1,1'-biphenyl]-2,2'-diol as a pale yellow solid (845 mg, 56% yield). To the solution of this diol (800 mg, 2.45 mmol, 1.0 equiv) in pyridine (7 mL), POCl₃ (0.51 mL, 5.4 mmol, 2.2 equiv) was slowly added via a syringe at 0 °C. The reaction mixture was stirred for 24 h at 95 °C (heating mantle, IKA). After being cooled down to room temperature, distilled H₂O (4 mL) was added,

and the resulting clear solution was stirred for another 18 h at 95 °C (heating mantle, IKA). After cooling down to room temperature, 4 N HCl (25 mL) was slowly added. The precipitate was filtered off, and it was washed with 4 N HCl. The product was further washed and hydrolyzed by redissolving it in CH₂Cl₂ and washing several times with 4 N HCl. After being dried over Na₂SO₄, removal of the solvent yielded the phosphoric acid **P2** as a lightly grayish solid (630 mg, 66% yield). ¹H NMR (400 MHz, CDCl₃): δ (ppm) 7.48 (br s, 1H, POOH), 7.26 (s, 2H, H-arom), 7.02 (s, 2H, H-arom), 2.36 (s, 6H, 2 \times CH₃), 1.50 (s, 18H, 6 \times CH₃-C); ³¹P NMR (162 MHz, CDCl₃): δ (ppm) 0.48. Analytical data were in accordance with the literature.

2,4,8,10-Tetra-tert-butyl-6-hydroxydibenzo[d,f]-[1,3,2]-dioxaphosphepine 6-oxide (P3) (Method B). A solution of 3-tert-butyl-4-hydroxyanisole (2.47 g, 12.0 mmol, 1.0 equiv) in methanol (75 mL) was prepared and a solution of KOH (2.77 g, 49.0 mmol, 4.1 equiv) and K₃Fe(CN)₆ (4.58 g, 14.0 mmol, 1.17 equiv) in water (75 mL) was added dropwise over 1 h at room temperature. The mixture was stirred for 2 h before the addition of 50 mL of water. The suspension was extracted with ethyl acetate (3 \times 50 mL) and the combined organic phases were washed with brine. After being dried over Na₂SO₄, removal of the solvents under reduced pressure afforded a light brown solid. After washing with *n*-hexane, 3,3',5,5'-tetra-tert-butyl-[1,1'-biphenyl]-2,2'-diol was obtained as an off-white powder (1.80 g, 73% yield). The subsequent phosphorylation was carried out according to the synthesis of **P2** on a 4.4 mmol scale, yielding phosphoric acid **P3** as an off-white solid (1.97 g, 95% yield). HRMS [(ESI-time-of-flight (TOF)) *m/z*: [M + Na]⁺ calcd for C₂₈H₄₁O₄PNa, 495.2640; found, 495.2640; IR ATR (ν_{max} /cm⁻¹): 2955 (O–H), 2867 (C–H), 1615 (C=C), 1302 (C–O), 1025 (C–H), 899 (C–H arom), 701 (C–H arom); ¹H NMR (400 MHz, CDCl₃): δ (ppm) 10.57 (br s, 1H), 7.42 (br s, 2H), 7.12 (d, *J* = 2.0 Hz, 2H), 1.45 (s, 18H), 1.27 (s, 18H); ³¹P NMR (162 MHz, CDCl₃): δ (ppm) 0.40; ¹³C{¹H} NMR (100 MHz, CDCl₃): δ 147.9, 144.3, 144.1, 140.2, 140.1, 130.1, 126.5, 125.3, 35.5, 34.7, 31.5, 31.3.

4,8-Di-tert-butyl-6-hydroxy-1,11-dimethyldibenzo[d,f]-[1,3,2]-dioxaphosphepine 6-oxide (P4). 3,3'-Di-tert-butyl-6,6'-dimethyl-[1,1'-biphenyl]-2,2'-diol was prepared via method A on a 12.0 mmol scale. Column chromatography (silica gel, 1.5% EtOAc in light petrol) afforded the diol as a white solid (910 mg, 45% yield). The subsequent phosphorylation was carried out according to the synthesis of **P2** on a 3.4 mmol scale, yielding phosphoric acid **P4** as a white solid (900 mg, 69% yield). HRMS (ESI-TOF) *m/z*: [M + Na]⁺ calcd for C₂₂H₂₉O₄PNa, 411.1701; found, 411.1732; IR ATR (ν_{max} /cm⁻¹): 2961 (O–H), 2872 (C–H), 1610 (C=C), 1308 (C–O), 1023 (C–H), 901 (C–H arom), 700 (C–H arom); ¹H NMR (400 MHz, CDCl₃): δ (ppm) 7.38 (dd, *J* = 8.0, 1.5 Hz, 2H), 7.11 (dd, *J* = 11.8, 8.2 Hz, 2H), 2.01 (d, *J* = 27.3 Hz, 6H), 1.48 (d, *J* = 12.4 Hz, 18H); ³¹P NMR (162 MHz, CDCl₃): δ (ppm) 3.99; ¹³C{¹H} NMR (100 MHz, CDCl₃): δ (ppm) 144.5, 144.3, 140.8, 140.7, 134.8, 130.1, 129.9, 128.9, 35.2, 31.3, 21.1.

6-Hydroxy-4,8-diisopropyl-1,11-dimethyldibenzo[d,f]-[1,3,2]-dioxaphosphepine-6-oxide (P5). 3,3'-Diisopropyl-6,6'-dimethyl-[1,1'-biphenyl]-2,2'-diol was prepared via method A on a 20.0 mmol scale. Column chromatography (silica gel, 2.0% EtOAc in light petrol) afforded the diol as a pale yellow liquid (2.03 g, 68% yield). The subsequent phosphorylation was carried out according to the synthesis of **P2** on a 6.7 mmol scale, yielding phosphoric acid **P5** as an amorphous brown solid (2.0 g, 83% yield). HRMS (ESI-TOF) *m/z*: [M + Na]⁺ calcd for C₂₀H₂₅O₄PNa, 383.1388; found, 383.1389; IR ATR (ν_{max} /cm⁻¹): 2963 (O–H), 2872 (C–H), 1610 (C=C), 1204 (C–O), 967 (C–H), 818 (C–H arom), 696 (C–H arom); ¹H NMR (400 MHz, CDCl₃): δ (ppm) 8.24 (br s, 1H), 7.27 (d, *J* = 8.0 Hz, 2H), 7.15 (d, *J* = 8.0 Hz, 2H), 3.49–3.45 (m, 2H), 2.14 (s, 6H), 1.27 (dd, *J* = 25.5, 6.9 Hz, 12H); ³¹P NMR (162 MHz, CDCl₃): δ (ppm) 2.40; ¹³C{¹H} NMR (100 MHz, CDCl₃): δ (ppm) 145.4, 137.7, 136.1, 128.0, 127.1, 126.3, 26.6, 24.1, 22.8, 19.7.

4,8-Di-tert-butyl-6-hydroxy-2,10-dimethoxydibenzo[d,f]-[1,3,2]-dioxaphosphepine-6-oxide (P6). 3,3'-Di-tert-butyl-5,5'-dimethoxy-[1,1'-biphenyl]-2,2'-diol was prepared according to literature procedure (method B) on a 4.0 mmol scale. The subsequent

124.9, 119.1, 84.2, 46.8, 25.1; chiral HPLC analysis: (Chiralcel IB column, *n*-hexane/2-propanol 99.8/0.2 v/v %, 1 mL/min, λ = 210 nm) t_R (R) = 8.8 min, t_R (S) = 9.3 min.

(*R*)-2-Methyl-4-oxo-2-phenylpentanal (**4**). Prepared according to the literature procedure.³² To a solution of the enantioenriched allylic aldehyde **2a** (157.0 mg, 0.9 mmol, 1.0 equiv) in a mixture of H₂O and dimethoxyethane (4.5 mL, 1/9 v/v) was added PdCl₂ (15.9 mg, 0.09 mmol, 0.1 equiv) and CuCl₂ (12.1 mg, 0.09 mmol, 0.1 equiv) and the resulting suspension was stirred overnight. The solvent was evaporated in vacuo and the crude product was purified by flash column chromatography (light petrol/EtOAc 5:1) affording the product **4** as a light yellow oil (124 mg, 72% yield, 94% ee). [α]_D²⁰ –66.0 (*c* 1.0, CHCl₃); ¹H NMR (200 MHz, CDCl₃): δ (ppm) 9.49 (s, 1H), 7.31–7.16 (m, 5H), 3.04 (dd, *J* = 26.0 Hz, 18.0 Hz, 2H), 2.00 (s, 3H), 1.54 (s, 3H); ¹³C{¹H} NMR (100 MHz, CDCl₃): δ (ppm) 206.0, 201.0, 139.2, 129.0, 127.5, 126.8, 51.8, 50.4, 30.9, 19.9; chiral HPLC analysis: (Chiralcel IB column, *n*-hexane/2-propanol 95/5 v/v %, 1 mL/min, λ = 220 nm) t_R (S) = 10.3 min, t_R (R) = 11.8 min.

■ ASSOCIATED CONTENT

SI Supporting Information

The Supporting Information is available free of charge at <https://pubs.acs.org/doi/10.1021/acs.joc.0c02385>.

Detailed parameter optimization, NMR spectra, and chiral HPLC traces (PDF)

■ AUTHOR INFORMATION

Corresponding Author

Katharina Bica-Schröder – Institute of Applied Synthetic Chemistry, TU Wien, A-1060 Vienna, Austria; orcid.org/0000-0002-2515-9873; Email: katharina.schroeder@tuwien.ac.at

Authors

Ádám Márk Pálvölgyi – Institute of Applied Synthetic Chemistry, TU Wien, A-1060 Vienna, Austria

Jakob Smith – Institute of Applied Synthetic Chemistry, TU Wien, A-1060 Vienna, Austria

Michael Schnürch – Institute of Applied Synthetic Chemistry, TU Wien, A-1060 Vienna, Austria; orcid.org/0000-0003-2946-9294

Complete contact information is available at:

<https://pubs.acs.org/doi/10.1021/acs.joc.0c02385>

Notes

The authors declare no competing financial interest.

■ ACKNOWLEDGMENTS

Financial support by the Austrian Science Fund (project P29146-N34) is gratefully acknowledged. The authors thank F. Scharinger for kindly providing phosphoric acids P6–P7.

■ REFERENCES

(1) For selected reviews, see: (a) Martin, S. F. Methodology for the Construction of Quaternary Carbon Centers. *Tetrahedron* **1980**, *36*, 419–460. (b) Fuji, K. Asymmetric Creation of Quaternary Carbon Centers. *Chem. Rev.* **1993**, *93*, 2037–2066. (c) Douglas, C. J.; Overman, L. E. Catalytic Asymmetric Synthesis of All-Carbon Quaternary Stereocenters. *Proc. Natl. Acad. Sci. U.S.A.* **2004**, *101*, 5363–5367. (d) Quasdorf, K. W.; Overman, L. E. Catalytic Enantioselective Synthesis of Quaternary Carbon Stereocenters. *Nature* **2014**, *516*, 181–191. (e) Corey, E. J.; Guzman-Perez, A. The Catalytic Enantioselective Construction of Molecules with Quaternary Carbon Stereocenters. *Angew. Chem., Int. Ed.* **1998**, *37*,

388–401. (f) Trost, B. M.; Jiang, C. Catalytic Enantioselective Construction of All-Carbon Quaternary Stereocenters. *Synthesis* **2006**, 369–396. (g) Feng, J.; Holmes, M.; Krische, M. J. Acyclic Quaternary Carbon Stereocenters via Enantioselective Transition Metal Catalysis. *Chem. Rev.* **2017**, *117*, 12564–12580.

(2) For selected advances, see: (a) Mikami, K.; Motoyama, Y.; Terada, M. Asymmetric Catalysis of Diels-Alder Cycloadditions by an MS-free Binaphthol-Titanium Complex: Dramatic Effect of MS, Linear vs Positive Nonlinear Relationship, and Synthetic Application. *J. Am. Chem. Soc.* **1994**, *116*, 2812–2820. (b) Sasai, H.; Emori, E.; Arai, T.; Shibasaki, M. Catalytic Asymmetric Michael Reactions Promoted by the La-Na-BINOL Complex (LSB). Enantioface Selection on Michael Donors. *Tetrahedron Lett.* **1996**, *37*, 5561–5564. (c) Ooi, T.; Miki, T.; Taniguchi, M.; Shiraiishi, M.; Takeuchi, M.; Maruoka, K. Highly enantioselective construction of quaternary stereocenters on beta-keto esters by phase-transfer catalytic asymmetric alkylation and Michael reaction. *Angew. Chem., Int. Ed.* **2003**, *42*, 3796–3798. (d) Wu, J.; Mampreian, D. M.; Hoveyda, A. H. Enantioselective Synthesis of Nitroalkanes Bearing All-Carbon Quaternary Stereogenic Centers through Cu-Catalyzed Asymmetric Conjugate Additions. *J. Am. Chem. Soc.* **2005**, *127*, 4584–4585. (e) Zhao, W.; Wang, Z.; Chu, B.; Sun, J. Enantioselective Formation of All-Carbon Quaternary Stereocenters from Indoles and Tertiary Alcohols Bearing A Directing Group. *Angew. Chem., Int. Ed.* **2014**, *54*, 1910–1913. (f) Murphy, J. J.; Bastida, D.; Paria, S.; Fagnoni, M.; Melchiorre, P. Asymmetric catalytic formation of quaternary carbons by iminium ion trapping of radicals. *Nature* **2016**, *532*, 218–222.

(3) Trost, B. M.; Chisholm, J. D.; Wroblewski, S. T.; Jung, M. Ruthenium-Catalyzed Alkene-Alkyne Coupling: Synthesis of the Proposed Structure of Amphidinolide A. *J. Am. Chem. Soc.* **2002**, *124*, 12420–12421.

(4) Trost, B. M.; Crawley, M. L. Asymmetric Transition-Metal-Catalyzed Allylic Alkylations: Applications in Total Synthesis. *Chem. Rev.* **2003**, *103*, 2921–2944.

(5) For selected reviews, see: (a) Trost, B. M. Metal Catalyzed Allylic Alkylation: Its Development in the Trost Laboratories. *Tetrahedron* **2015**, *71*, 5708–5733. (b) Trost, B. M.; Van Vranken, D. L. Asymmetric Transition Metal-Catalyzed Allylic Alkylations. *Chem. Rev.* **1996**, *96*, 395–422. (c) Diéguez, M.; Oscar, P. Biaryl Phosphites: New Efficient Adaptive Ligands for Pd-Catalyzed Asymmetric Allylic Substitution Reactions. *Acc. Chem. Res.* **2010**, *43*, 312–322. (d) Hong, A. Y.; Stoltz, B. M. The Construction of All-Carbon Quaternary Stereocenters by Use of Pd-Catalyzed Asymmetric Allylic Alkylation Reactions in Total Synthesis. *Eur. J. Org. Chem.* **2013**, 2745–2759.

(6) Jellerichs, B. G.; Kong, J.-R.; Krische, M. J. Catalytic Enone Cycloallylation via Concomitant Activation of Latent Nucleophilic and Electrophilic Partners: Merging Organic and Transition Metal Catalysis. *J. Am. Chem. Soc.* **2003**, *125*, 7758–7759.

(7) Ibrahim, I.; Córdova, A. Direct Catalytic Intermolecular α -Allylic Alkylation of Aldehydes by Combination of Transition-Metal and Organocatalysis. *Angew. Chem., Int. Ed.* **2006**, *45*, 1952–1956.

(8) Weix, D. J.; Hartwig, J. F. Regioselective and Enantioselective Iridium-Catalyzed Allylation of Enamines. *J. Am. Chem. Soc.* **2007**, *129*, 7720–7721.

(9) Liu, D.; Xie, F.; Zhang, W. Palladium-catalyzed asymmetric allylic alkylation with an enamine as the nucleophilic reagent. *Tetrahedron Lett.* **2007**, *48*, 7591–7594.

(10) Shibasaki, M.; Yasuda, S.; Kumagai, N. Direct Asymmetric α -Allylation of Ketones with Allylic Alcohols via Pd/Enamine Cooperative Function. *Heterocycles* **2012**, *86*, 745–757.

(11) Silvi, M.; Arceo, E.; Jurberg, I. D.; Cassani, C.; Melchiorre, P. Enantioselective Organocatalytic Alkylation of Aldehydes and Enals Driven by the Direct Photoexcitation of Enamines. *J. Am. Chem. Soc.* **2015**, *137*, 6120–6123.

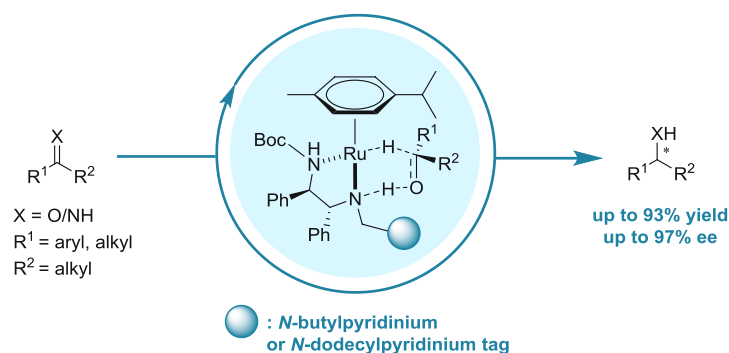
(12) Yoshida, M.; Terumine, T.; Masaki, E.; Hara, S. Direct Asymmetric α -Allylation of α -Branched Aldehydes by Two Catalytic Systems with an Achiral Pd Complex and a Chiral Primary α -Amino Acid. *J. Org. Chem.* **2013**, *78*, 10853–10859.

- (13) Yoshida, M.; Masaki, E.; Terumine, T.; Hara, S. Asymmetric α -Allylation of α -Branched Aldehydes with Allyl Alcohols by Synergistic Catalysis Using an Achiral Palladium Complex and a Chiral Primary Amino Acid. *Synthesis* **2014**, *46*, 1367–1373.
- (14) Krautwald, S.; Schafroth, M. A.; Sarlah, D.; Carreira, E. M. Stereodivergent α -Allylation of Linear Aldehydes with Dual Iridium and Amine Catalysis. *J. Am. Chem. Soc.* **2014**, *136*, 3020–3023.
- (15) Krautwald, S.; Sarlah, D.; Schafroth, M. A.; Carreira, E. M. Enantio- and Stereodivergent Dual Catalysis: α -Allylation of Branched Aldehydes. *Science* **2013**, *340*, 1065–1068.
- (16) Wang, P.-S.; Lin, H.-C.; Han, Z.-Y.; Gong, L.-Z. Chiral Counteranion Strategy for Asymmetric Oxidative C(sp³)-H/C(sp³)-H Coupling: Enantioselective α -Allylation of Aldehydes with Terminal Alkenes. *Angew. Chem., Int. Ed.* **2014**, *126*, 12414.
- (17) For a general review on asymmetric counteranion-directed catalysis, see: Mahlau, M.; List, B. Asymmetric Counteranion-Directed Catalysis: Concept, Definition, and Applications. *Angew. Chem., Int. Ed.* **2013**, *52*, 518–533.
- (18) Hoffmann, S.; Nicoletti, M.; List, B. Catalytic Asymmetric Reductive Amination of Aldehydes via Dynamic Kinetic Resolution. *J. Am. Chem. Soc.* **2006**, *128*, 13074–13075.
- (19) Mukherjee, S.; List, B. Chiral Counteranions in Asymmetric Transition-Metal Catalysis: Highly Enantioselective Pd/Brønsted Acid-Catalyzed Direct α -Allylation of Aldehydes. *J. Am. Chem. Soc.* **2007**, *129*, 11336–11337.
- (20) Jiang, G.; List, B. Direct Asymmetric α -Allylation of Aldehydes with Simple Allylic Alcohols Enabled by the Concerted Action of Three Different Catalysts. *Angew. Chem., Int. Ed.* **2011**, *50*, 9471–9474.
- (21) Scharinger, F.; Márk Pálvölgyi, Á.; Zeindlhofer, V.; Schnürch, M.; Schröder, C.; Bica-Schröder, K. Counterion Enhanced Organocatalysis: A Novel Approach for the Asymmetric Transfer Hydrogenation of Enones. *ChemCatChem* **2020**, *12*, 3776–3782.
- (22) Chen, H.; Feng, Y.; Xu, Z.; Ye, T. The total synthesis and reassignment of stereochemistry of dragonamide. *Tetrahedron* **2005**, *61*, 11132–11140.
- (23) Mohamadi, A.; Miller, L. W. Efficient route to pre-organized and linear polyaminopolycarboxylates: Cy-TTHA, Cy-DTPA and mono/di- reactive, tert-butyl protected TTHA/Cy-TTHA. *Tetrahedron Lett.* **2017**, *58*, 1441–1444.
- (24) Lee, D. W.; Ha, H.; Lee, W. K. Selective Mono-BOC Protection of Diamines. *Synth. Commun.* **2007**, *37*, 737.
- (25) Kuchen, W.; Mahler, H. F. Dibenzo(d, f)-1,3,2-Dioxaphosphoropine und Metallkomplexe von 2,2'-Biphenylphosphorsäuren. *Phosphorus Sulfur Relat. Elem.* **1980**, *8*, 139–145.
- (26) Grant-Overton, S.; Buss, J. A.; Smith, E. H.; Gutierrez, E. G.; Moorhead, E. J.; Lin, V. S.; Wenzel, A. G. Efficient Microwave Method for the Oxidative Coupling of Phenols. *Synth. Commun.* **2015**, *45*, 331–337.
- (27) Gutierrez, E. G.; Moorhead, E. J.; Smith, E. H.; Lin, V.; Ackerman, L. K. G.; Knezevic, C. E.; Sun, V.; Grant, S.; Wenzel, A. G. Electron-Withdrawing, Biphenyl-2,2'-diol-Based Compounds for Asymmetric Catalysis. *Eur. J. Org. Chem.* **2010**, 3027–3031.
- (28) van der Vlugt, J. I.; Hewat, A. C.; Neto, S.; Sablong, R.; Mills, A. M.; Lutz, M.; Spek, A. L.; Müller, C.; Vogt, D. Sterically Demanding Diphosphonite Ligands – Synthesis and Application in Nickel-Catalyzed Isomerization of 2-Methyl-3-Butenenitrile. *Adv. Synth. Catal.* **2004**, *346*, 993–1003.
- (29) Kimura, M.; Horino, Y.; Mukai, R.; Tanaka, S.; Tamaru, Y. Strikingly Simple Direct α -Allylation of Aldehydes with Allyl Alcohols: Remarkable Advance in the Tsuji–Trost Reaction. *J. Am. Chem. Soc.* **2001**, *123*, 10401–10402.
- (30) Murahashi, S.; Makabe, Y.; Kunita, K. Palladium(0)-Catalyzed Rearrangement of N-Allylenamines. Synthesis of γ,δ -Unsaturated Imines and γ,δ -Unsaturated Carbonyl Compounds. *J. Org. Chem.* **1988**, *53*, 4489–4495.
- (31) Horn, A.; Kazmaier, U. Purified mCPBA, a Useful Reagent for the Oxidation of Aldehydes. *Eur. J. Org. Chem.* **2018**, 2531–2536.
- (32) Kulkarni, M.; Davawala, S.; Doke, A.; Pendharkar, D. An Expedient Protocol for Cyclopentenone Annulation. *Synthesis* **2004**, 2919–2926.

5. Conclusions

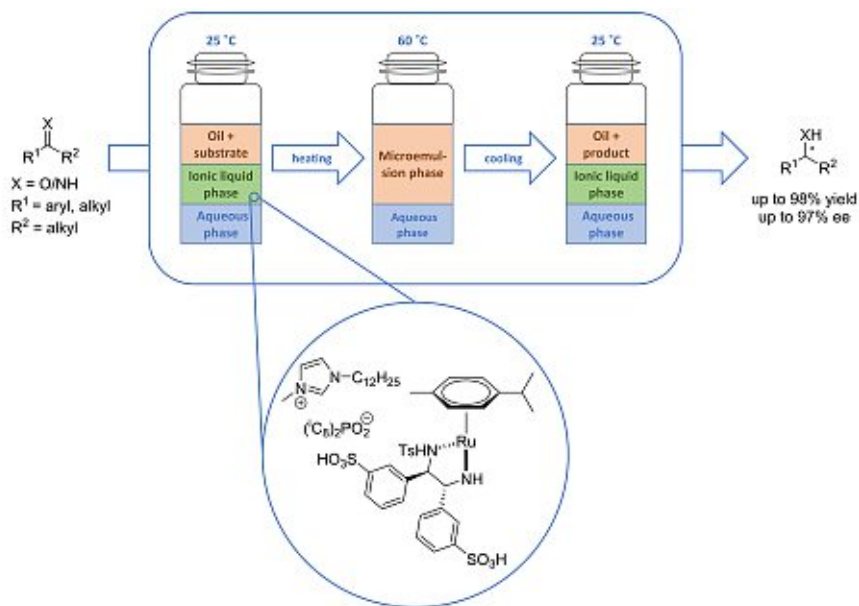
In the first part of the thesis, novel methods for the transition-metal-catalyzed ATH of ketones and imines were investigated in alternative reaction media.

In the first sub-project, a set of chiral-pool derived, ion-tagged chiral ligands was developed in a simple three-step synthetic pathway starting from commercially available (1*R*,2*R*)-diphenylethylenediamine. After the successful synthesis and characterization, these ligands were used for ruthenium-catalyzed ATH reactions in aqueous media. The ligand screening revealed that the ion-tags bearing bulky Boc protecting groups were particularly suitable for ATH reactions. Adjusting the alkyl chain-length of such ligands, both aromatic and aliphatic ketones could be reduced to the corresponding optically active secondary alcohols with excellent enantioselectivity. Moreover, a simple change in the hydrogen source allowed also the highly enantioselective ATH of imine substrates. This concept provides a simple and surfactant-free alternative for asymmetric transfer hydrogenation in environmentally friendly reaction media (Scheme 44).



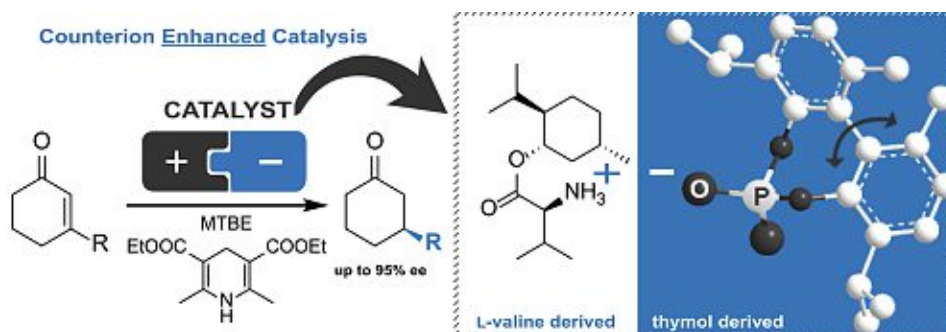
Scheme 44. Ion-tagged chiral ligands for aqueous ATH reactions.

In the second sub-project, ruthenium-catalyzed ATH reactions in ionic liquid-based microemulsions were investigated (Scheme 45). It has been shown, that microemulsions based on surface active ionic liquids can be applied for the ATH of ketones. As a result of the temperature-dependent multiphase behavior of the microemulsion, a rather simple product separation could be achieved. Using a sulfonated TsDPEN ligand possessing enhanced hydrophilicity; it was also possible to immobilize the catalyst in the intermediate layer and prevent its leaching into the organic phase. A series of aromatic ketones could be reduced with excellent yield and ee, while the ATH of aliphatic ketones and imines gave inferior results.



Scheme 45. Ionic liquid-based microemulsions for ATH reactions.

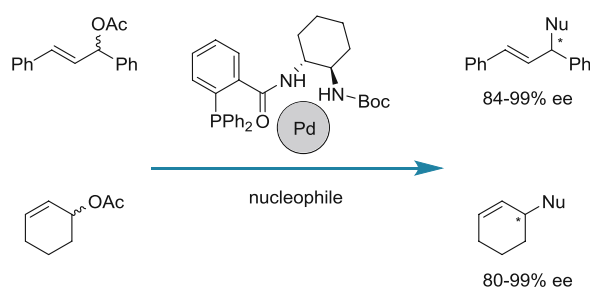
In the second part of the thesis, a novel concept of counterion enhanced catalysis was applied for the organocatalytic ATH reaction of cyclic enones (Scheme 46). The ion-paired catalyst of simple, natural-derived L-amino acid esters with achiral or racemic phosphoric acids could be prepared in a two-step, parallel reaction pathway. After optimizing the reaction conditions including solvent, amino acid, amino acid ester and phosphoric acid screenings, it was found that the ion-paired catalyst of L-valine-D-menthyl ester in combination with a thymol-derived phosphoric acid provided excellent reactivity and high enantioselectivity for the ATH of 3-methylcyclohexenone even when using a moderate catalyst loading of 5 mol%. This catalyst system could be then applied for the ATH of various 3-substituted cyclic enones resulting in good yields and excellent stereocontrol. The ion-paired catalyst system could be synthesized in a straightforward fashion starting from cheap and natural compounds; therefore, it could provide a promising alternative to current state-of-art methodologies.



Scheme 46. Counterion enhanced ATH of cyclohexenones.

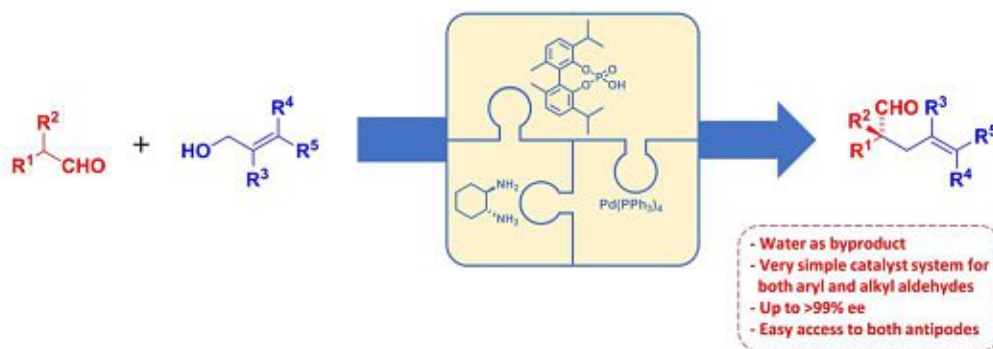
In the third part of this thesis, methods for asymmetric allylic alkylations with activated and non-activated allylic electrophiles have been developed, respectively.

In the first sub-project, a small set of C_2 -symmetric diamine-derived carbamate-monophosphine ligands was prepared. After finding the most suitable reaction parameters and ligand, a series of C - and N -nucleophiles could be successfully reacted with allylic acetates in good to excellent yields and enantioselectivity (Scheme 47).



Scheme 47. Classical Tsuji-Trost allylation with activated allylic electrophiles.

In the second sub-project, the direct asymmetric α -allylation of α -branched aldehydes was investigated. A three-component catalyst system was developed, allowing the direct reaction of aldehydes with allylic alcohols without pre-functionalization *via* Pd/enamine catalysis (Scheme 48). The rather simple catalyst composing of (*R,R*)-diaminocyclohexane, a thymol-derived racemic phosphoric acid and $[Pd(PPh_3)_4]$ could provide high catalytic activities and excellent stereoselection for a range of aromatic and also a few aliphatic substrates. The catalyst system could well tolerate different allylic alcohols as well resulting in a rather broad reaction scope; furthermore, two possible orthogonal derivatizations of the allylic aldehyde products were also demonstrated. As a quite simple still rather versatile catalyst, our system could offer a valuable alternative to the current state-of-art.



Scheme 48. Direct α -allylation of aldehydes with allylic alcohols.

In this thesis, novel and highly efficient asymmetric catalytic methodologies were developed both for the field of transition-metal- and organocatalysis.

Appendix A

Supporting information:

Ion-tagged chiral ligands for the asymmetric transfer hydrogenation in aqueous medium

Ion-tagged chiral ligands for the asymmetric transfer hydrogenation in aqueous medium

Ádám Márk Pálvölgyi^a, Jacqueline Bitai^a, Veronika Zeindlhofer^b, Christian Schröder^b and

Katharina Bica^{a,}*

^a *Institut für Angewandte Synthesechemie, Technische Universität Wien, Getreidemarkt
9/163-OC, 1060 Vienna, Austria*

^b *Department of Computational Biological Chemistry, University of Vienna, Währinger
Str. 17, 1090 Vienna, Austria*

E-mail: katharina.schroeder@tuwien.ac.at

| | |
|---|-----|
| I. General Remarks | 118 |
| II. Ligand Synthesis | 119 |
| III. Synthesis of imine substrates for ATH reactions | 130 |
| IV. General procedure for the asymmetric transfer hydrogenation | 132 |
| V. Analytical data of ATH products | 134 |
| VI. Reference..... | 138 |

I. General Remarks

All reagents were purchased from commercial suppliers and used without further purification unless noted otherwise. Dichloromethane, methanol and toluene intended for anhydrous reactions were pre-distilled and desiccated on Al₂O₃ columns (PURESOLV, Innovative Technology).

Chromatography solvents were distilled prior to use. Column chromatography was performed on standard manual glass columns using silica gel from Merck (40-63 μm) with the eluates stated.

Preparative HPLC was performed on a Reveleris® Prep Purification System using a Maisch ReproSil 100 C18 column (250 mm x 4.6 mm ID, 5 μm) and H₂O/acetonitrile as eluent at a flowrate of 15 mL/min.

TLC-analysis was carried out using precoated aluminum-backed plates purchased from Merck (silica gel 60 F₂₅₄). UV active compounds were detected at 254 nm. Non UV active compounds were detected using *p*-Anisaldehyde (1) or Ceric Sulfate (2) as staining solution.

| Staining Solution 1 | | Staining Solution 2 | |
|---------------------|--------------------------------------|---------------------|---------------------------------------|
| 3.7 mL | <i>p</i> -anisaldehyde | 0.1 g | Ce(IV)(SO ₄) ₂ |
| 1.5 mL | AcOH (99%) | 4.5 g | Phosphormolybdic acid |
| 5 mL | H ₂ SO ₄ (98%) | 100 mL | H ₂ SO ₄ (10%) |
| 135 mL | EtOH anhydr. | | |

¹H, ¹³C and ¹⁹F NMR spectra were recorded from CDCl₃, MeOD or D₂O solutions on a Bruker AC 200 (200 MHz) or Bruker Advance UltraShield 400 (400 MHz) spectrometer and chemical shifts (δ) are reported in ppm, using tetramethylsilane as internal standard. Coupling constants (J) are reported in Hertz (Hz). The following abbreviations were used to explain the multiplicities: s = singlet, d = doublet, t = triplet, q = quartet, sex = sextet, m = multiplet, brs = broad singlet.

Melting points above room temperature were measured on an automated melting point system OPTI MELT of Stanford ResearchSystems and are uncorrected.

Infrared spectra were recorded on a Perkin-Elmer Spectrum 65 FT IR spectrometer equipped with a specac MK II Golden Gate Single Reflection ATR unit.

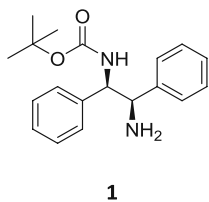
HR-MS analysis was carried out from methanol solutions (c10 ppm) by using an HTPAL system auto sampler (CTC Analytics AG), an Agilent 1100/1200 HPLC with binary pumps, degasser and column thermostat (Agilent Technologies) and Agilent 6230 AJS ESI-TOF mass spectrometer.

ChiralHPLC analysis were carried out on a DAIONEX UPLC, equipped with a PDA plus detector (190-360 nm) using CHIRACEL DAICEL IB or AS-H columns (250x 4.60 mm) as stationary phases.

Chiral GC analysis were done on a, equipped with a FID detector, using chiral BGB 173 column (30 m x 0.25 mm x 0.25 μm).

II. Ligand Synthesis

II.1. *tert*-Butyl((1*R*,2*R*)-2-amino-1,2-diphenylethyl)carbamate (**1**)

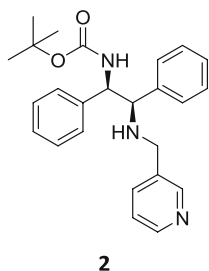


Compound **1** was prepared following the literature procedure.ⁱ

(1*R*,2*R*)-1,2-Diphenyl-1,2-ethanediamine (9.1 mmol, 1.93 g) was dissolved in 15 mL anhydrous MeOH and cooled via ice bath. A 1M solution of HCl in MeOH (10.8 mmol, 10.5 mL) was slowly added and the mixture was subsequently stirred at r.t. for 15 min. The formed precipitate was again dissolved by the addition of 1 mL H₂O.

Di-*tert*-butyl dicarbonate (13.5 mmol, 2.93 g) was dissolved in 5 mL anhydrous MeOH and slowly added to the reaction mixture, which was subsequently stirred at room temperature for 4 h. After completion, 10 mL H₂O was added to the mixture and MeOH was removed under reduced pressure. The obtained suspension was washed with Et₂O, basified with 2 M NaOH solution and extracted with CH₂Cl₂. The combined organic phases were dried over Na₂SO₄ and concentrated *in vacuo*. The obtained crude product was dissolved in EtOAc and the solid residue was removed over a patch of silica. The solvent was removed under reduced pressure to yield **1** as an off-white solid (2.18 g, 77%). **M.p.**: 103-105 °C; **HRMS (ESI-TOF) m/z**: [M + H]⁺Calculated for C₁₉H₂₅N₂O₂ 313.1911, Found 313.1912; α_D^{20} : +34.4 (c 1.0, MeOH); **IR (v_{max}/cm⁻¹)**: 3378 (N-H v), 2978 (C-H v), 1684 (C=O v), 1605 (C-C v), 1514 (N-H δ), 1454 (C=C v), 1160 (C-N v), 696 (C-H arom δ); **¹H NMR (400 MHz, CDCl₃) δ** : 7.32 – 7.09 (m, 10H, *H*-arom), 5.81 (d, *J* = 8.51 Hz, 1H, *CH*-NHCO), 4.77 (brs, 1H, *NH*-CO), 4.25 (d, *J* = 3.79 Hz, 1H, *CH*-NH), 1.38 (s, 2H, NH₂), 1.22 (s, 9H, C-(CH₃)₃); **¹³C NMR (100 MHz, CDCl₃) δ** : 155.6 (s, 1C, NH-CO), 142.2 (s, 1C, *C*-arom), 141.0 (s, 1C, *C*-arom), 128.5 (d, 2C, *C*-arom), 128.3 (d, 2C, *C*-arom), 127.4 (d, 2C, *C*-arom), 127.2 (d, 2C, *C*-arom), 126.8 (d, 2C, *C*-arom), 79.3 (s, 1C, C-(CH₃)₃), 60.0 (d, 1C, *CH*-NHCO), 59.9 (d, 1C, *CH*-NH₂), 28.3 (q, 3C, C-(CH₃)₃).

II.2. *tert*-Butyl((1*R*,2*R*)-1,2-diphenyl-2-((pyridin-3-ylmethyl)amino)ethyl)carbamate (**2**)

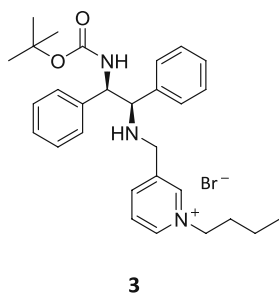


Procedure adapted from literature.ⁱⁱ

Amine **1** (1.0 g, 3.2 mmol) was dissolved in 30 mL anhydrous MeOH. Freshly activated molecular sieve 4 Å (2.0 g), and freshly distilled pyridine-3-carboxaldehyde (300 μ L, 343 mg, 3.2 mmol) were added, and the reaction mixture was refluxed until total conversion. The reaction mixture was cooled to room temperature, NaBH₄ (182 mg, 4.8 mmol) was added, and the reaction was stirred again until total conversion. The mixture was filtered over a batch of silica and subsequently hydrolyzed with H₂O. Methanol was removed under reduced pressure, and the remaining aqueous phase was extracted with CH₂Cl₂. The combined organic phases were dried over Na₂SO₄ and the solvent removed under reduced pressure. The crude product was purified by column chromatography (light petrol: ethyl acetate 1:1 + Et₃N) to obtain pure product **2** as a colorless solid (843 mg, 65%). **M.p.**: 90-91 °C; **HRMS (ESI-TOF) m/z**: [M + H]⁺Calculated for C₂₅H₃₀N₃O₂ 404.2333,

Found 404.2333; α_D^{20} : +2.2 (c 1.25, MeOH); IR ($\nu_{\max}/\text{cm}^{-1}$):3379 (N-H ν), 2977 (C-H ν), 1684 (C=O ν), 1595 (C-C ν), 1510 (N-H δ), 1454 (C=C ν), 1164 (C-N ν), 754 (C-H pyridine δ),696 (C-H arom δ); $^1\text{H NMR}$ (400 MHz, CDCl_3) δ : 8.39 (d, J = 4.05 Hz, 1H, H -pyridine), 8.28 (s, 1H, H -pyridine), 7.36 (d, J = 6.88 Hz, 1H, H -pyridine), 7.27 – 7.04 (m, 11H, H -pyridine, H -arom), 5.51 (d, J = 7.69 Hz, 1H, CH-NHCO), 4.78 (brs, 1H, NH-CO), 3.86 (s, 1H, CH-NH), 3.57 (d, J = 13.48 Hz, 1H, NH-CH_2), 3.34 (d, J = 13.48 Hz, 1H, NH-CH_2), 1.75 (brs, 1H, NH-CH_2), 1.27 (s, 9H, $\text{C-(CH}_3)_3$); $^{13}\text{C NMR}$ (100 MHz, CDCl_3) δ : 155.5 (s, 1C, NH-CO), 149.5 (d, 1C, C -pyridine), 148.5 (d, 1C, C -pyridine), 140.2 (s, 1C, C -pyridine), 139.6 (s, 1C, C -arom), 135.6 (d, 1C, C -pyridine), 135.2 (s, 1C, C -arom), 128.4 (d, 2C, C -arom), 127.8 (d, 2C, C -arom), 127.6 (d, 2C, C -arom), 127.3 (d, 2C, C -arom), 126.5 (d, 2C, C -arom), 123.3 (d, 1C, C -pyridine), 79.5 (s, 1C, $\text{C-(CH}_3)_3$), 66.6 (d, 1C, CH-NH), 59.8 (d, 1C, CH-NHCO), 48.4 (t, 1C, NH-CH_2), 28.3 (q, 3C, $\text{C-(CH}_3)_3$).

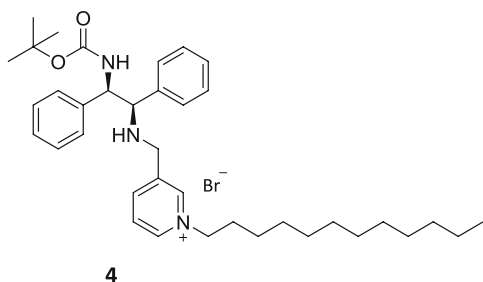
II.3. 1-Butyl-3-((((1R,2R)-2-((*tert*-butoxycarbonyl)amino)-1,2-diphenylethyl)amino) methyl)pyridin-1-ium bromide (3)



3

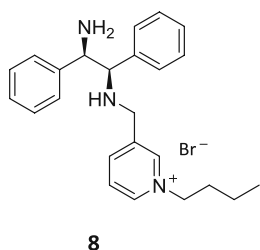
Finely powdered **2** (1.8 mmol, 753 mg) was mixed with *n*-butyl bromide (2.2 mmol, 307 mg), sealed and heated to 80 °C for 20 h. Excess of *n*-butyl bromide was removed under reduced pressure to yield **3** as a yellow foam (1.0 g, >99%), which was used without further purification. For analytical purpose the product was purified via preparative HPLC. **HRMS (ESI-TOF) m/z**: $[\text{M}]^+$ Calculated for $\text{C}_{29}\text{H}_{38}\text{N}_3\text{O}_2$ 460.2959, Found 460.2974; α_D^{20} : +20.1 (c 1.0, MeOH); IR ($\nu_{\max}/\text{cm}^{-1}$):3242 (N-H ν), 2963 (C-H ν), 1692 (C=O ν), 1632 (C-C ν), 1496 (N-H δ), 1459 (C=C ν), 1161 (C-N ν), 757 (C-H pyridine δ),699 (C-H arom δ); $^1\text{H NMR}$ (400 MHz, MeOD) δ : 8.83 (d, J = 5.87 Hz, 1H, H -pyridine), 8.78 (s, 1H, H -pyridine), 8.31 (d, J = 7.94 Hz, 1H, H -pyridine), 7.90 (t, J = 6.91 Hz, 1H, H -pyridine), 7.27 – 7.10 (m, 10H, H -arom), 4.81 (brs, 1H, CH-NHCO), 4.55 (t, J = 7.25 Hz, 2H, N-CH_2), 4.03 (d, J = 7.94 Hz, 1H, CH-NH), 3.94 – 3.80 (m, 2H, NH-CH_2), 2.01 – 1.89 (m, 2H, $\text{N-CH}_2\text{-CH}_2$), 1.53 – 1.21 (m, 11H, $\text{N-(CH}_2)_2\text{-CH}_2$, $\text{C-(CH}_3)_3$), 1.02 (t, J = 7.25 Hz, 3H, $\text{N-(CH}_2)_3\text{-CH}_3$); $^{13}\text{C NMR}$ (100 MHz, MeOD) δ : 156.5 (s, 1C, NH-CO), 144.6 (d, 1C, C -pyridine), 143.5 (d, 1C, C -pyridine), 142.9 (s, 1C, C -pyridine), 142.4 (d, 1C, C -pyridine), 140.8 (s, 1C, C -arom), 139.9 (s, 1C, C -arom), 128.1 (d, 2C, C -arom), 128.0 (d, 2C, C -arom), 127.7 (d, 2C, C -arom), 127.2 (d, 2C, C -arom), 127.1 (d, 2C, C -arom), 126.7 (d, 1C, C -pyridine), 79.0 (s, 1C, $\text{C-(CH}_3)_3$), 67.2 (d, 1C, CH-NH), 61.3 (t, 1C, N-CH_2), 60.6 (d, 1C, CH-NHCO), 47.4 (t, 1C, NH-CH_2), 33.0 (t, 1C, $\text{N-CH}_2\text{-CH}_2$), 27.5 (q, 3C, $\text{C-(CH}_3)_3$), 19.1 (t, 1C, $\text{N-(CH}_2)_2\text{-CH}_2$), 12.6 (q, 1C, $\text{N-(CH}_2)_3\text{-CH}_3$).

II.4. 1-Dodecyl-3-((((1*R*,2*R*)-2-((*tert*-butoxycarbonyl)amino)-1,2-diphenylethyl)amino) methyl)pyridin-1-ium bromide (**4**)



Finely powdered **2** (1.2 mmol, 500 mg) was mixed with *n*-dodecyl bromide (1.4 mmol, 370 mg), sealed and heated to 80 °C for 20 h. Excess *n*-dodecyl bromide was removed by refluxing the crude product with *n*-hexane. Remaining volatile compounds were removed under reduced pressure to yield **4** as an orange foam (800 mg, 99%). The product was used without further purification. For analytical purpose the product was purified via preparative HPLC. **HRMS (ESI-TOF) m/z:** [M]⁺Calculated for C₃₇H₅₄N₃O₂ 572.4211, Found 572.4215; α_D^{20} : +13.4 (*c* 1.05, MeOH); **IR (v_{max}/cm⁻¹):** 3245 (N-H v), 2924 (C-H v), 1697 (C=O v), 1633 (C-C v), 1497 (N-H δ), 1454 (C=C v), 1166 (C-N v), 758 (C-H pyridine δ), 700 (C-H arom δ); **¹H NMR (400 MHz, MeOD) δ:** 8.86 – 8.80 (m 2H, *H*-pyridine), 8.36 (d, *J* = 7.56 Hz, 1H, *H*-pyridine), 7.92 (t, *J* = 7.07 Hz, 1H, *H*-pyridine), 7.27 – 7.12 (m, 10H, *H*-arom), 4.88 (brs, 1H, *CH*-NHCO), 4.56 (t, *J* = 7.47 Hz, 2H, N-CH₂), 4.14 (brs, 1H, *CH*-NH), 4.01 – 3.87 (m, 2H, NH-CH₂), 2.03 – 1.93 (m, 2H, N-CH₂-CH₂), 1.47 – 1.25 (m, 27H, C-(CH₃)₃, N-(CH₂)₂-(CH₂)₉), 0.91 (t, *J* = 6.80 Hz, 3H, N-(CH₂)₁₁-CH₃); **¹³C NMR (100 MHz, MeOD) δ:** 157.8 (s, 1C, NH-CO), 146.2 (d, 1C, C-pyridine), 145.2 (d, 1C, C-pyridine), 144.0 (d, 1C, C-pyridine), 141.7 (s, 1C, C-pyridine), 137.9 (s, 1C, C-arom), 129.6 (d, 1C, C-arom), 129.4 (d, 2C, C-arom), 129.0 (d, 2C, C-arom), 128.9 (d, 2C, C-arom), 128.6 (d, 2C, C-arom), 128.4 (d, 2C, C-arom), 128.1 (d, 1C, C-pyridine), 80.5 (s, 1C, C-(CH₃)₃), 68.4 (d, 1C, CH-NH), 62.9 (t, 1C, N-CH₂), 61.6 (d, 1C, CH-NHCO), 47.4 (t, 1C, NH-CH₂), 33.0 (t, 1C, N-CH₂-CH₂), 32.4 (t, 1C, N-(CH₂)₂-CH₂), 30.6 (t, 1C, N-(CH₂)₃-CH₂), 30.6 (t, 1C, N-(CH₂)₄-CH₂), 30.4 (t, 1C, N-(CH₂)₅-CH₂), 30.4 (t, 1C, N-(CH₂)₆-CH₂), 30.1 (t, 1C, N-(CH₂)₇-CH₂), 28.7 (q, 3C, C-(CH₃)₃), 27.1 (t, 1C, N-(CH₂)₈-CH₂), 23.6 (t, 1C, N-(CH₂)₉-CH₂), 14.4 (q, 1C, N-(CH₂)₁₁-CH₃).

II.5. 1-Butyl-3-((((1*R*,2*R*)-2-Amino-1,2-diphenylethyl)amino)methyl)pyridin-1-ium bromide (**8**)

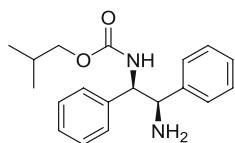


Reaction protocol adapted from literature.ⁱⁱⁱ

Compound **3** (1.0 mmol, 540 mg) was dissolved in 20 mL CH₂Cl₂ and cooled via ice bath. Hydrogen bromide (33% in AcOH, 10 mmol, 1.75 mL) was slowly added under argon atmosphere. The reaction mixture was allowed to warm to room temperature and stirred for 4 h. After neutralization with saturated Na₂CO₃ solution, the phases were separated and the aqueous phase was extracted with CH₂Cl₂. The combined organic phases were dried over Na₂SO₄ and the solvent removed under reduced pressure. The crude product was purified via column chromatography (60 g silica, MeOH/H₂O/AcOH 5:4:1), to yield **8** as orange foam (148 mg, 34%). **HRMS (ESI-TOF) m/z:** [M]⁺Calculated for C₂₄H₃₀N₃ 360.2434, Found 360.2435; α_D^{20} : +76.8 (*c* 0.95, MeOH); **IR (v_{max}/cm⁻¹):** 3386 (N-H v), 2945 (C-H v), 1637 (C-C v), 1569 (N-H δ), 1499 (C=C v), 1155 (C-N v), 758 (C-H pyridine δ), 699 (C-H arom δ); **¹H NMR (400 MHz, MeOD) δ:** 8.93 (s, 1H, *H*-pyridine), 8.83 (d, *J* = 6.20 Hz, 1H, *H*-pyridine), 8.46 (d, *J* = 7.97 Hz, 1H, *H*-

pyridine), 8.00 – 7.94 (m, 1H, *H*-pyridine), 7.18 – 7.09 (m, 10H, *H*-arom), 4.60 (t, *J* = 7.63 Hz, 2H, N-CH₂), 4.11 (d, *J* = 8.84 Hz, 1H, CH-NH₂), 3.91 (d, *J* = 15.46 Hz, 1H, NH-CH₂), 3.84 (d, *J* = 15.46 Hz, 1H, NH-CH₂), 3.80 (d, *J* = 8.84 Hz, 1H, CH-NH), 2.03 – 1.95 (m, 2H, N-CH₂-CH₂), 1.48 – 1.39 (m, 2H, N-(CH₂)₂-CH₂), 1.04 (t, *J* = 7.43 Hz, 3H, N-(CH₂)₃-CH₃); ¹³C NMR (100 MHz, MeOD) δ: 146.1 (d, 1C, C-pyridine), 145.4 (d, 1C, C-pyridine), 143.9 (d, 1C, C-pyridine), 143.7 (s, 1C, C-pyridine), 139.6 (s, 1C, C-arom), 136.0 (s, 1C, C-arom), 130.0 (d, 2C, C-arom), 129.8 (d, 2C, C-arom), 129.6 (d, 2C, C-arom), 129.3 (d, 2C, C-arom), 129.0 (d, 2C, C-arom), 128.6 (d, 1C, C-pyridine), 67.5 (d, 1C, CH-NH), 62.8 (t, 1C, N-CH₂), 61.4 (d, 1C, CH-NH₂), 48.8 (t, 1C, NH-CH₂), 34.5 (t, 1C, N-CH₂-CH₂), 20.5 (t, 1C, N-(CH₂)₂-CH₂), 13.8 (q, 1C, N-(CH₂)₃-CH₃).

II.6. Isobutyl ((1*R*,2*R*)-2-amino-1,2-diphenylethyl)carbamate (**14**)

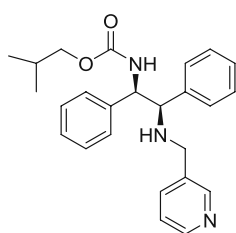


14

(1*R*,2*R*)-1,2-Diphenylethylenediamine (2.36 mmol, 500 mg) was dissolved in 10 mL anhydrous acetonitrile, and it was cooled to 0°C *via* ice bath. 1M solution of HCl in acetonitrile (2.83 mmol, 2.77 mL) was dropwisely added, and the mixture was subsequently stirred at room temperature for 15 minutes. The formed precipitate was re-dissolved by the addition of 0.5 mL H₂O. Isobutyl

chloroformate (3.54 mmol, 460 μL) was diluted with 5 mL anhydrous acetonitrile, then it was dropwise added to the reaction mixture, which was subsequently stirred at room temperature for 10 hours. The reaction monitoring and the subsequent work-up were in accordance with those used for the synthesis of compound **1**. The crude product was then purified by column chromatography (15 g silica, light petrol: ethyl acetate 1:1 + Et₃N), afforded **14** as a white powder (460 mg, 63 %). **M.p.**: 112-113 °C; **HRMS (ESI-TOF) m/z** : [M + H]⁺ calculated for C₁₉H₂₅N₂O₂ 313.1911, Found 313.1919; [α]_D²⁰ : + 8.4 (c 1.0, CHCl₃); **IR (ATR, cm⁻¹)** : 3364 (N-H v), 2960 (C-H v), 1683 (C=O v), 1518 (N-H δ), 1454 (C-H δ), 699 (C-H arom δ); **¹H NMR (400 MHz, MeOD) δ** : 7.31 - 7.17 (m, 10H, *H*-arom), 5.92 (d, *J* = 7.84 Hz, 1H, CH-NHCO), 4.81 (brs, 1H, NH), 4.30 (s, 1H, CH-NH₂), 3.64 (s, 2H, CH₂-CH(CH₃)₂), 1.74 (s, 1H, CH₂-CH(CH₃)₂), 1.46 (brs, 2H, NH₂), 0.79 (s, 5H, CH₂-CH(CH₃)₂), 0.52 (s, 1H, CH₂-CH(CH₃)₂); **¹³C NMR (100 MHz, MeOD) δ** : 157.51 (s, 1C, NH-CO), 141.31 (s, 1C, C-arom), 140.57 (s, 1C, C-arom), 127.84 (d, 2C, C-arom), 127.80 (d, 2C, C-arom), 127.08 (d, 2C, C-arom), 126.99 (d, 1C, C-arom), 126.85 (d, 1C, C-arom), 126.78 (d, 2C, C-arom), 70.74 (t, 1C, CH₂-CH(CH₃)₂), 62.02 (d, 1C, CH-NHCO), 60.19 (d, 1C, CH-NH₂), 27.89 (d, 1C, CH₂-CH(CH₃)₂), 17.93 (q, 2C, CH₂-CH(CH₃)₂).

II.7. Isobutyl((1*R*,2*R*)-1,2-diphenyl-2-((pyridin-3-ylmethyl)amino)ethyl)carbamate (15)

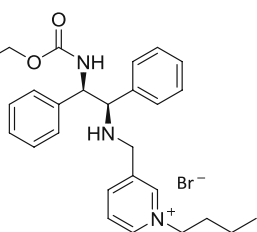


15

Procedure adapted from literature: ²

According to the synthesis of compound **2**: substrate (**14**, 0.96 mmol, 300 mg), pyridine-3-carboxaldehyde (0.96 mmol, 90 μ L), molecular sieve 4 \AA (1.0 g) in 10 mL anhydrous MeOH, and then reduction with NaBH₄ (1.92 mmol, 55 mg). The work-up was done according with those for compound **2**. Column chromatographic purification (30 g silica, light petrol: ethyl acetate 1:1 + Et₃N) afforded product **15** as white crystals (275 mg, 71 %). **M.p.**: 95-96 °C; **HRMS (ESI-TOF) m/z** : [M + H]⁺Calculated for C₂₅H₃₀N₃O₂ 404.2333, Found 404.2336; [α]_D²⁰ : + 9.7 (c 1.0, CHCl₃); **IR (ATR, cm⁻¹)** : 3354 (N-H v), 2962 (C-H v), 1691 (C=O v), 1494 (N-H δ), 1453 (C-H δ), 755 (C-H arom δ), 699 (C-H arom δ); **¹H NMR (400 MHz, CDCl₃) δ** : 8.41 (d, *J* = 3.60 Hz, 1H, *H*-pyridine), 8.28 (s, 1H, *H*-pyridine), 7.39 (d, *J* = 7.62 Hz, 1H, *H*-pyridine), 7.24 – 7.09 (m, 11H, *H*-pyridine, *H*-arom), 5.72 (d, s, 1H, *CH*-NHCO), 4.82 (brs, 1H, *NH*-CO), 3.91 (s, 1H, *CH*-NH), 3.66 – 3.58 (m, 3H, *CH*₂-CH(CH₃)₂, *NH*-CH₂), 3.37 (d, *J* = 13.78 Hz, 1H, *NH*-CH₂), 1.77 (brs, 2H, *CH*₂-CH(CH₃)₂, *NH*-CH₂), 0.81 (s, 6H, *CH*₂-CH(CH₃)₂); **¹³C NMR (100 MHz, MeOD) δ** : 157.50 (s, 1C, *NH*-CO), 148.54 (d, 1C, *C*-pyridine), 147.11 (d, 1C, *C*-pyridine), 140.55 (s, 1C, *C*-pyridine), 139.86 (s, 1C, *C*-arom), 136.82 (d, 1C, *C*-pyridine), 136.47 (s, 1C, *C*-arom), 128.31 (d, 2C, *C*-arom), 128.02 (d, 1C, *C*-arom), 127.89 (d, 1C, *C*-arom), 127.69 (d, 1C, *C*-arom), 127.45 (d, 1C, *C*-arom), 127.23 (d, 1C, *C*-arom), 127.13 (d, 1C, *C*-arom), 126.92 (d, 1C, *C*-arom), 126.72 (d, 1C, *C*-arom), 123.66 (d, 1C, *C*-pyridine), 70.75 (t, 1C, *CH*₂-CH(CH₃)₂), 66.83 (d, 1C, *CH*-NH), 61.04 (d, 1C, *CH*-NHCO), 47.95 (t, 1C, *NH*-CH₂), 27.88 (d, 1C, *CH*₂-CH(CH₃)₂), 17.92 (q, 2C, *CH*₂-CH(CH₃)₂).

II.8. 3-((((1*R*,2*R*)-2-((isobutoxycarbonyl)amino)-1,2-diphenylethyl)amino)methyl)-1-butylpyridin-1-ium bromide (5)



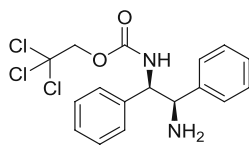
5

In accordance with the synthesis of compound **3**: substrate **15** (0.37 mmol, 150 mg), ⁿBuBr (0.44 mmol, 47.5 μ L). The mixture was stirred at 80°C for 20 hours. After concentration *in vacuo*, product **5** was obtained as an orange foam (198 mg, 99 %).

The analytical sample was purified by preparative HPLC. **HRMS (ESI-TOF) m/z** : [M]⁺ Calculated for C₂₉H₃₈N₃O₂ 460.2959, Found 460.2979; [α]_D²⁰ : + 11.0 (c 1.0, CHCl₃); **IR (ATR, cm⁻¹)** : 3252 (N-H v), 2968 (C-H v), 1693 (C=O v), 1496 (N-H v), 1453 (C-H δ), 755 (C-H arom δ), 700 (C-H arom δ); **¹H NMR (400 MHz, MeOD) δ** : 8.66 (t, *J* = 8.40 Hz, 2H, *H*-pyridine), 8.22 (d, *J* = 7.96 Hz, 1H, *H*-pyridine), 7.80 (t, *J* = 8.10 Hz, 1H, *H*-pyridine), 7.10 – 7.00 (m, 10H, *H*-arom), 4.43 (t, *J* = 7.58 Hz, 2H, *N*-CH₂), 3.89 (s, 1H, *CH*-NH), 3.77 – 3.75 (m, 2H, *NH*-CH₂), 3.68 (brs, 2H, *CH*₂-CH(CH₃)₂), 1.90 – 1.77 (m, 3H, *CH*₂-CH(CH₃)₂, *N*-CH₂-CH₂), 1.30 (sex., *J* = 8.44 Hz, 2H, *N*-CH₂-CH₂), 0.92 (t, *J* = 7.72 Hz, 3H, *N*-(CH₂)₂-CH₃), 0.82 (s, 6H, *CH*₂-CH(CH₃)₂); **¹³C NMR (100 MHz, MeOD) δ** : 158.86 (s, 1C, *NH*-CO), 146.06 (d, 1C, *C*-pyridine), 145.00 (d, 1C, *C*-pyridine), 144.30 (s, 1C, *C*-pyridine), 143.86 (d, 1C, *C*-pyridine), 142.07 (s, 1C, *C*-arom), 141.18 (s, 1C, *C*-arom), 129.57 (d, 2C, *C*-arom), 129.41 (d, 2C, *C*-arom), 129.17 (d, 2C, *C*-arom), 128.66 (d, 2C, *C*-arom), 128.57 (d, 2C, *C*-arom), 128.21 (d, 1C, *C*-pyridine), 72.22 (t, 1C, *CH*₂-CH(CH₃)₂), 68.61 (d, 1C, *CH*-NH), 62.75 (t, 1C, *N*-CH₂), 62.74 (d, 1C, *CH*-

NHCO), 48.86 (t, 1C, NH-CH₂), 34.45 (t, 1C, N-CH₂-CH₂), 29.29 (d, 1C, CH₂-CH(CH₃)₂), 20.48 (t, 1C, N-(CH₂)₂-CH₂), 19.46 (q, 2C, CH₂-CH(CH₃)₂), 13.93 (q, 1C, N-(CH₂)₃-CH₃).

II.9. 2,2,2-Trichloroethyl ((1*R*,2*R*)-2-amino-1,2-diphenylethyl)carbamate (**16**)

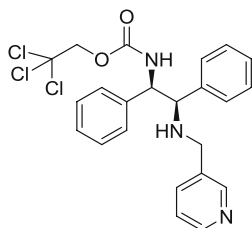


16

Similarly to the synthesis of amine **14**: (*R,R*)-DPEN (2.36 mmol, 500 mg), 1M solution of HCl in acetonitrile (2.83 mmol, 2.77 mL), 0.5 mL H₂O, 2,2,2-trichloroethyl chloroformate (3.54 mmol, 486 μ L), 10mL anhydrous acetonitrile. The reaction mixture was stirred for 4 hours at room temperature.

The work-up and the isolation were the same, that those for compound **14**, affording product **16** as a pale white solid (520 mg, 57 %). **M.p.**: 83-84°C; **HRMS (ESI-TOF) m/z**: [M + H]⁺ calculated for C₁₇H₁₈Cl₃N₂O₂ 387.0434, Found 387.0439; [α]_D²⁰: + 7.2 (c 1.0, CHCl₃); **IR (ATR, cm⁻¹)**: 3360 (N-H), 2955 (C-H v), 1690 (C=O v), 1517 (N-H δ), 1452 (C-H δ), 760 (C-Cl v), 696 (C-H arom δ); **¹H NMR (200 MHz, CDCl₃) δ** : 7.35 - 7.19 (m, 10H, *H*-arom), 6.34 (d, *J* = 7.80 Hz, 1H, *CH*-NHCO), 4.84 (s, 1H, *NH*), 4.53 (s, 2H, Cl₃CCH₂), 4.36 (s, 1H, *CH*-NH₂), 1.35 (brs, 2H, *NH*₂); **¹³C NMR (100 MHz, MeOD) δ** : 155.20 (s, 1C, NH-CO), 141.32 (s, 1C, *C*-arom), 140.17 (s, 1C, *C*-arom), 127.87 (d, 2C, *C*-arom), 127.83 (d, 2C, *C*-arom), 127.09 (d, 2C, *C*-arom), 126.99 (d, 2C, *C*-arom), 126.90 (d, 2C, *C*-arom), 95.76 (s, 1C, Cl₃CCH₂), 74.10 (t, 1C, Cl₃CCH₂), 62.58 (d, 1C, *CH*-NHCO), 60.12 (d, 1C, *CH*-NH₂).

II.10. 2,2,2-Trichloroethyl((1*R*,2*R*)-1,2-diphenyl-2-((pyridin-3-ylmethyl)amino)ethyl)carbamate (**17**)

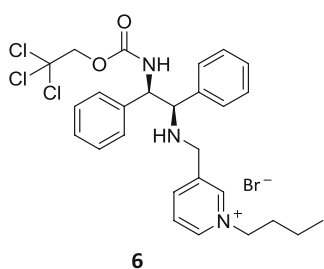


17

Procedure adapted from literature: ²

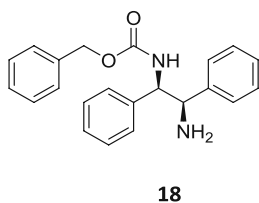
Similarly to the synthesis of compound **2**: Compound **16** (0.77 mmol, 300 mg), pyridine-3-carboxaldehyde (0.77 mmol, 72 μ L), molecular sieve 4 Å (1.0 g) in 10 mL anhydrous MeOH. The subsequent reduction was performed with NABH₄ (1.54 mmol, 44 mg). The work-up and purification were in accordance with those for compound **2**. After column chromatography (30 g silica, light petrol: ethyl acetate 1:1 + Et₃N), product **17** was obtained as a white solid (196 mg, 53 %). **M.p.**: 72-74 °C; **HRMS (ESI-TOF) m/z**: [M + H]⁺Calculated for C₂₃H₂₃Cl₃N₃O₂ 478.0856, Found 478.0859; [α]_D²⁰: + 9.4 (c 1.0, CHCl₃); **IR (ATR, cm⁻¹)** : 3202 (N-H v), 3030 (C-H v), 1725 (C=O v), 1542 (N-H δ), 1494 (C-H δ), 762 (C-Cl v), 752 (C-H arom δ), 697 (C-H arom δ); **¹H NMR (400 MHz, CDCl₃) δ** : 8.40 (d, *J* = 4.56 Hz, 1H, *H*-pyridine), 8.27 (s, 1H, *H*-pyridine), 7.36 (d, *J* = 7.08 Hz, 1H, *H*-pyridine), 7.24 – 7.12 (m, 11H, *H*-pyridine, *H*-arom), 6.06 (d, *J* = 6.88 Hz, 1H, *CH*-NHCO), 4.84 (brs, 1H, *NH*), 4.57 (dd, *J* = 15.36 Hz, 12.00 Hz, 2H, Cl₃CCH₂), 3.95 (s, 1H, *CH*-NH₂), 3.59 (d, *J* = 13.76 Hz, 1H, *NH*-CH₂), 3.36 (d, *J* = 13.72 Hz, 1H, *NH*-CH₂), 1.75 (brs, 1H, *NH*-CH₂); **¹³C NMR (100 MHz, MeOD) δ** : 155.20 (s, 1C, NH-CO), 148.54 (d, 1C, *C*-pyridine), 147.12 (d, 1C, *C*-pyridine), 140.03 (s, 1C, *C*-pyridine), 139.74 (s, 1C, *C*-arom), 136.83 (d, 1C, *C*-pyridine), 136.49 (s, 1C, *C*-arom), 128.04 (d, 2C, *C*-arom), 127.93 (d, 2C, *C*-arom), 127.71 (d, 2C, *C*-arom), 127.16 (d, 1C, *C*-arom), 127.01 (d, 2C, *C*-arom), 126.84 (d, 1C, *C*-arom), 123.66 (d, 1C, *C*-pyridine), 95.79 (s, 1C, Cl₃CCH₂), 74.08 (t, 1C, Cl₃CCH₂), 66.58 (d, 1C, *CH*-NH₂), 61.49 (d, 1C, *CH*-NHCO), 47.99 (t, 1C, *NH*-CH₂).

II.11. 1-Butyl-3-((((1*R*,2*R*)-1,2-diphenyl-2-(((2,2,2-trichloroethoxy)carbonyl)amino)ethyl)amino) methyl)pyridin-1-ium bromide (**6**)



In accordance with the synthesis of chiral ligand **3**: compound **17** (0.37 mmol, 150 mg) and ⁿBuBr (0.44 mmol, 47.5 μL). The mixture was stirred at 80°C for 20 hours. After concentration *in vacuo*, product **6** was obtained as an orange foam (181 mg, 95 %). The analytical sample was purified by preparative HPLC. **HRMS (ESI-TOF) m/z**: [M]⁺ Calculated for C₂₇H₃₁Cl₃N₃O₂ 535.1560, Found 534.1551; [α]_D²⁰ : + 11.0 (c 1.0, CHCl₃); **IR (ATR, cm⁻¹)** : 3252 (N-H v), 2968 (C-H v), 1693 (C=O v), 1496 (N-H v), 1453 (C-H δ), 764 (C-Cl v), 750 (C-H arom δ), 700 (C-H arom δ); **¹H NMR (400 MHz, MeOD) δ** : 8.67-8.62 (m, 2H, *H*-pyridine), 8.24 (d, *J* = 7.84 Hz, 1H, *H*-pyridine), 7.80 (t, *J* = 6.92 Hz, 1H, *H*-pyridine), 7.09 - 7.03 (m, 10H, *H*-arom), 4.64 (dd, *J* = 21.0 Hz, 12.52 Hz, 2H, Cl₃CCH₂), 4.42 (t, *J* = 7.60 Hz, 2H, N-CH₂), 3.90 (d, *J* = 8.64 Hz, 1H, CH-NH), 3.80 - 3.71 (m, 2H, NH-CH₂), 1.83 (sex., *J* = 7.52 Hz, 2H, N-CH₂-CH₂), 1.30 (q, *J* = 7.52 Hz, 2H, N-(CH₂)₂-CH₂), 0.92 (t, *J* = 7.36 Hz, 3H, N-(CH₂)₃-CH₃); **¹³C NMR (100 MHz, MeOD) δ** : 155.22 (s, 1C, NH-CO), 144.61 (d, 1C, C-pyridine), 143.49 (d, 1C, C-pyridine), 143.23 (s, 1C, C-pyridine), 142.40 (d, 1C, C-pyridine), 140.11 (s, 1C, C-arom), 139.77 (s, 1C, C-arom), 128.08 (d, 2C, C-arom), 128.00 (d, 2C, C-arom), 127.78 (d, 2C, C-arom), 127.25 (d, 2C, C-arom), 127.17 (d, 2C, C-arom), 126.91 (d, 1C, C-pyridine), 95.79 (s, 1C, Cl₃CCH₂), 74.13 (t, 1C, Cl₃CCH₂), 67.12 (d, 1C, CH-NH₂), 61.47 (d, 1C, CH-NHCO), 61.37 (t, 1C, N-CH₂), 47.81 (t, 1C, NH-CH₂), 33.05 (t, 1C, N-CH₂-CH₂), 19.08 (t, 1C, N-(CH₂)₂-CH₂), 12.46 (q, 1C, N-(CH₂)₃-CH₃).

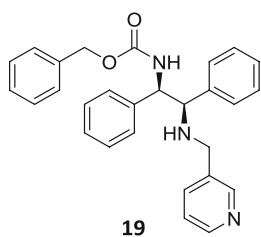
II.12. Benzyl ((1*R*,2*R*)-2-amino-1,2-diphenylethyl)carbamate (**18**)



Compound **18** was prepared following literature procedure.^{iv}

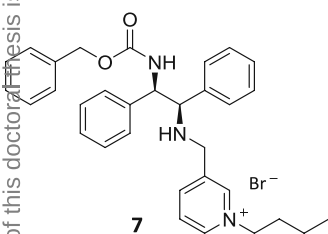
(*R,R*)-DPEN (2.36 mmol, 500 mg) was dissolved 10 mL anhydrous EtOH, and benzyl-phenyl-carbonate (2.36 mmol, 540 mg) was added. The reaction mixture was stirred at room temperature for 24 hours and the EtOH was removed *in vacuo*. 10 M HCl (567 μL) was added, the formed precipitate was filtered off, and successively washed with diethyl-ether and H₂O. Then, it was treated with a solution of NaOH (210 mg) in H₂O (1.42 mL). In a few minutes, the precipitate was filtered off, and it was washed with H₂O (3 x 10 mL) to yield **18** as a pale white solid (530 mg, 65 %). The compound is known in literature.⁴ **M.p.**: 93-94 °C; [α]_D²⁰ : + 3.4 (c 1.0, CHCl₃); **IR (ATR, cm⁻¹)** : 3356 (N-H v), 3026 (C-H v), 1688 (C=O v), 1498 (N-H δ), 1448 (C-H δ), 699 (C-H arom δ); **¹H NMR (400 MHz, CDCl₃) δ** : 7.31 - 7.17 (m, 15H, *H*-arom), 6.04 (d, *J* = 7.24 Hz, 1H, CH-NHCO), 4.92 (s, 2H, CH₂-arom), 4.83 (brs, 1H, NH), 4.30 (s, 1H, CH-NH₂), 1.33 (brs, 2H, NH₂); **¹³C NMR (100 MHz, CDCl₃) δ** : 157.1 (s, 1C, NH-CO), 141.4 (s, 1C, C-arom), 140.5 (s, 1C, C-arom), 136.9 (s, 1C, C-arom), 128.0 (d, 1C, C-arom), 127.8 (d, 2C, C-arom), 127.6 (d, 1C, C-arom), 127.4 (d, 1C, C-arom), 127.1 (d, 2C, C-arom), 127.1 (d, 2C, C-arom), 127.0 (d, 2C, C-arom), 126.9 (d, 2C, C-arom), 126.8 (d, 2C, C-arom), 66.2 (t, 1C, CH₂-arom), 62.2 (d, 1C, CH-NHCO), 60.2 (d, 1C, CH-NH₂).

II.13. Benzyl((1*R*,2*R*)-1,2-diphenyl-2-((pyridin-3-ylmethyl)amino)ethyl)carbamate (19)



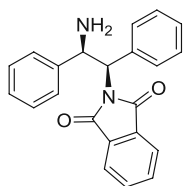
In accordance with the synthesis of compound **2**: substrate (**18**, 0.87 mmol, 300 mg), molecular sieve 4 Å (1.0 g), pyridine-3-carboxaldehyde (0.87 mmol, 81 μ L), then reduction with NABH_4 (1.31 mmol, 50 mg). Work up and isolation were according to the synthesis of compound **2**, obtaining the pure **19** as a white solid (223 mg, 59 %). **M.p.**: 85-86 °C; HRMS (ESI-TOF) m/z : $[\text{M} + \text{H}]^+$ Calculated for $\text{C}_{28}\text{H}_{28}\text{N}_3\text{O}_2$ 438.2182, Found 438.2184; $[\alpha]_{\text{D}}^{20}$: + 4.5 (c 1.0, CHCl_3); IR (ATR, cm^{-1}): 3262 (N-H ν), 3030 (C-H ν), 1722 (C=O ν), 1495 (N-H δ), 1445 (C-H δ), 752 (C-H arom δ), 697 (C-H arom δ); $^1\text{H NMR}$ (400 MHz, CDCl_3) δ : 8.40 (d, J = 4.72 Hz, 1.90 Hz 1H, H -pyridine), 8.26 (s, 1H, H -pyridine), 7.36 (d, J = 7.24 Hz, 1H, H -pyridine), 7.23 - 7.08 (m, 16H, H -pyridine, H -arom), 5.77 (d, J = 7.76 Hz, 1H, CH-NHCO), 4.94 (s, 2H, CH_2 -arom), 4.83 (brs, 1H, NH-CO), 3.89 (d, J = 3.72 Hz, 1H, CH-NH), 3.58 (d, J = 13.72 Hz, 1H, NH-CH_2), 3.34 (d, J = 13.76 Hz, 1H, NH-CH_2), 1.61 (brs, 1H, NH-CH_2); $^{13}\text{C NMR}$ (100 MHz, CDCl_3) δ : 156.03 (s, 1C, NH-CO), 149.55 (d, 1C, C -pyridine), 148.57 (d, 1C, C -pyridine), 139.34 (s, 1C, C -pyridine), 135.59 (d, 1C, C -pyridine), 135.11 (s, 3C, C -arom), 128.57 (d, 4C, C -arom), 127.82 (d, 2C, C -arom), 127.78 (d, 4C, C -arom), 127.54 (d, 1C, C -arom), 126.51 (d, 4C, C -arom), 123.37 (d, 1C, C -pyridine), 66.78 (t, 1C, CH_2 -arom), 66.43 (d, 1C, CH-NH_2), 60.35 (d, 1C, CH-NHCO), 48.47 (t, 1C, NH-CH_2).

II.14. 3-((((1*R*,2*R*)-2-(((Benzyloxy)carbonyl)amino)-1,2-diphenylethyl)amino)methyl)-1-butylpyridin-1-ium (7)



In accordance with the synthesis of chiral ligand **3**: compound **19** (0.34 mmol, 150 mg) and $n\text{BuBr}$ (0.41 mmol, 44.0 μ L). The mixture was stirred at 80°C for 20 hours. After concentration *in vacuo*, product **7** could be obtained as an orange foam (193 mg, 99 %). HRMS (ESI-TOF) m/z : $[\text{M}]^+$ Calculated for $\text{C}_{32}\text{H}_{36}\text{N}_3\text{O}_2$ 494.2806, Found 494.2830; $[\alpha]_{\text{D}}^{20}$: + 8.4 (c 1.0, CHCl_3); IR (ATR, cm^{-1}): 3230 (N-H ν), 3030 (C-H ν), 1701 (C=O ν), 1497 (N-H ν), 1453 (C-H δ), 750 (C-H arom δ), 699 (C-H arom δ); $^1\text{H NMR}$ (400 MHz, CDCl_3) δ : 9.15 (s, 1H, H -pyridine) 8.06 (d, J = 7.62 Hz, 1H, H -pyridine), 7.71 (t, J = 6.76 Hz, 1H, H -pyridine), 7.18 - 7.07 (m, 16H, H -arom), 4.92 (brs, 3H, CH-NHCO , CH_2 -arom), 4.66 (m, 2H, N-CH_2), 4.11 (d, J = 7.96 Hz, 1H, CH-NH), 3.76 (dd, J = 27.52 Hz, 15.0 Hz, 2H, NH-CH_2), 1.82 (qvin, J = 7.28 Hz, 2H, $\text{N-CH}_2\text{-CH}_2$), 1.26 (sex., J = 7.28 Hz, 2H, $\text{N-(CH}_2)_2\text{-CH}_2$), 0.86 (t, J = 7.26 Hz, 3H, $\text{N-(CH}_2)_3\text{-CH}_3$); $^{13}\text{C NMR}$ (100 MHz, MeOD) δ : 158.52 (s, 1C, NH-CO), 146.00 (d, 1C, C -pyridine), 144.95 (d, 1C, C -pyridine), 144.33 (s, 1C, C -pyridine), 141.84 (d, 1C, C -pyridine), 141.08 (s, 3C, C -arom), 129.52 (d, 4C, C -arom), 129.40 (d, 2C, C -arom), 129.18 (d, 2C, C -arom), 128.99 (d, 2C, C -arom), 128.70 (d, 1C, C -arom), 128.58 (d, 4C, C -arom), 128.25 (d, 1C, C -pyridine), 68.65 (d, 1C, CH-NH), 67.61 (t, 1C, CH_2 -arom), 62.74 (d, 1C, N-CH_2), 62.58 (d, 1C, CH-NHCO), 48.78 (t, 1C, NH-CH_2), 34.39 (t, 1C, $\text{N-CH}_2\text{-CH}_2$), 20.45 (t, 1C, $\text{N-(CH}_2)_2\text{-CH}_2$), 13.85 (q, 1C, $\text{N-(CH}_2)_3\text{-CH}_3$).

II.15. 2-[(1*R*,2*R*)-2-Amino-1,2-diphenylethyl]-1*H*-isoindole-1,3(2*H*)-dione (20)

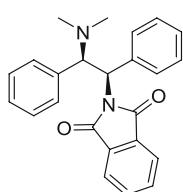


20

Compound **20** was prepared according to the literature procedure.^v

In a round bottom flask *p*-TsOH·H₂O (4.7 mmol, 891 mg) was dissolved in anhydrous toluene. Activated molecular sieve 4 Å (3.00 g), phthalic anhydride (5.2 mmol, 760 mg) and (1*R*,2*R*)-1,2-diphenyl-1,2-ethanediamine (4.7 mmol, 1.0 g) were added and the reaction mixture was refluxed overnight. The mixture was filtered over Celite, washed with CH₂Cl₂ and stirred with saturated Na₂CO₃ solution. The phases were separated and the organic phase was dried over Na₂SO₄. The solvent was removed under reduced pressure to yield **20** as pale yellow solid (1.17 g, 73%), which was used without further purification. ¹H NMR (200 MHz, CDCl₃) δ: 8.02 – 8.00 (m, 1H, *H*-arom), 7.85 – 7.82 (m, 1H, *H*-arom), 7.71 – 7.66 (m, 2H, *H*-arom), 7.40 – 7.29 (m, 7H, *H*-arom), 7.28– 7.15 (m, 3H, *H*-arom), 5.56 (d, *J* = 5.63 Hz, 1H, *CH*-NHCO), 5.02 (d, *J* = 5.63 Hz, 1H, *CH*-NH₂).

II.16. 2-[(1*R*,2*R*)-2-(Dimethylamino)-1,2-diphenylethyl]-1*H*-isoindole-1,3(2*H*)-dione (21)

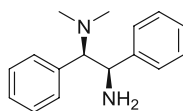


21

Compound **21** was prepared according to the literature procedure.⁵

Amine **20** (2.9 mmol, 990 mg) was dissolved in concentrated formic acid (98%, 14mL) and stirred for 30 minutes. Formaldehyde (37% in H₂O, 12 mL) was added and the mixture refluxed until TLC indicated complete conversion. Remaining formaldehyde was removed under reduced pressure and the reaction mixture was neutralized with 4M NaOH. After extraction with CH₂Cl₂ and drying over Na₂SO₄ the solvent was removed under reduced pressure to yield **21** as yellow solid (1.01 g, 94%). ¹H NMR (200 MHz, CDCl₃) δ: 7.80 – 7.69 (m, 2H, *H*-arom), 7.65 – 7.54 (m, 2H, *H*-arom), 7.49 – 7.40 (m, 2H, *H*-arom), 7.23 – 6.93 (m, 8H, *H*-arom), 5.90 (d, *J* = 12.46 Hz, 1H, *CH*-NHCO), 5.14 (d, *J* = 12.46 Hz, 1H, *CH*-N(CH₃)₂), 2.02 (s, 6H, 2 x CH₃).

II.17. (1*R*,2*R*)-*N*¹,*N*¹-Dimethyl-1,2-diphenyl-1,2-ethanediamine (22)

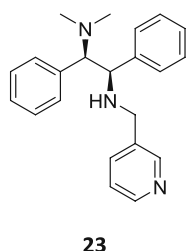


22

Procedure adapted from literature.⁵

Hydrazine hydrate (27.0 mmol, 1.68 mL 50% solution in H₂O) was added to a dispersion of **21** (2.7 mmol, 990 mg) in 35 mL EtOH and the reaction mixture was refluxed for 2 hours. After cooling to room temperature, the mixture was diluted with Et₂O and the formed precipitate was removed via filtration. The organic phase was dried over Na₂SO₄ and the solvent removed under reduced pressure to yield **22** as yellow, viscous liquid (630 mg, 97%). ¹H NMR (200 MHz, CDCl₃) δ: 7.13 – 6.86 (m, 10H, *H*-arom), 4.31 (d, *J* = 10.50 Hz, 1H, *CH*-NH₂), 3.55 (d, *J* = 10.50 Hz, 1H, *CH*-N(CH₃)₂), 2.29 (brs, 2H, NH₂), 2.10 (s, 6H, 2 x (CH₃)₂).

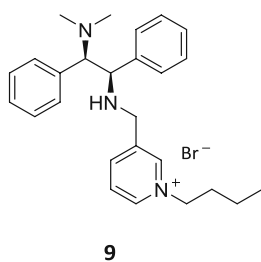
II.18. (1*R*,2*R*)-*N*¹,*N*¹-Dimethyl-1,2-diphenyl-*N*²-(pyridin-3-ylmethyl)ethane-1,2-diamine (**23**)



Procedure adapted from literature.²

Similarly to the synthesis of compound **2**: Substrate **22** (2.2 mmol, 535 mg), molecular sieve 4 Å (2.0 g), pyridine-3-carboxaldehyde (2.2 mmol, 0.2 mL) in anhydrous MeOH (20 mL), then, NaBH₄ (3.3 mmol, 126 mg) for the reduction. The work-up was in accordance with those for compound **2**. After purification via chromatography (45 g silica, CH₂Cl₂ : MeOH 40:1 + Et₃N) product **23** could be obtained as yellow solid (648 mg, 88%). **M.p.**: 85-88 °C; **HRMS (ESI-TOF) m/z**: [M + H]⁺ Calculated for C₂₂H₂₅N₃ 332.2121; Found 332.2129; **α_D²⁰**: -12.4 (c 1.05, MeOH); **IR (ν_{max}/cm⁻¹)**: 3379 (N-H v), 2935 (C-H v), 1574 (C-C v), 1491 (N-H δ), 1451 (C=C v), 1133 (C-N v), 755 (C-H pyridine δ), 696 (C-H arom δ); **¹H NMR (400 MHz, CDCl₃) δ**: 8.44 (d, *J* = 1.98, 1H, *H*-pyridine), 8.42 (dd, *J*₁ = 1.61 Hz, *J*₂ = 4.65 Hz, 1H, *H*-pyridine), 7.56 – 7.52 (m, 1H, *H*-pyridine), 7.18 – 7.13 (m, 3H, *H*-pyridine, *H*-arom), 7.08 – 6.93 (m, 6H, *H*-arom), 6.88 – 6.84 (m, 2H, *H*-arom), 3.96 (d, *J* = 10.74 Hz, 1H, CH-NH), 3.67 – 3.60 (m, 2H, CH-N(CH₃)₂, NH-CH₂), 3.46 (d, *J* = 13.64 Hz, 1H, NH-CH₂), 3.28 (brs, 1H, NH), 2.01 (s, 6H, N-(CH₃)₂); **¹³C NMR (100 MHz, CDCl₃) δ**: 149.9 (d, 1C, C-pyridine), 148.3 (d, 1C, C-pyridine), 141.1 (s, 1C, C-pyridine), 136.2 (s, 1C, C-arom), 136.0 (d, 1C, C-pyridine), 132.9 (s, 1C, C-arom), 129.9 (d, 2C, C-arom), 128.9 (d, 2C, C-arom), 127.9 (d, 2C, C-arom), 127.3 (d, 2C, C-arom), 127.0 (d, 2C, C-arom), 123.3 (d, 1C, C-pyridine), 74.3 (d, 1C, CH-N(CH₃)₂), 61.6 (d, 1C, CH-NH), 48.5 (t, 1C, NH-CH₂), 40.6 (q, 2C, N-(CH₃)₂).

II.19. 1-Butyl-3-((((1*R*,2*R*)-2-(dimethylamino)-1,2-diphenylethyl)amino)methyl)pyridin-1-ium bromide (**9**)

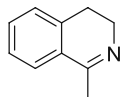


According to the synthesis of chiral ligand **2**: Compound **23** (0.9 mmol, 300 mg), *n*-butylbromide (1.1 mmol, 0.11 mL). The mixture was stirred at 80 °C for 20 h. After concentration *in vacuo*, product **9** was obtained as an orange foam (373 mg, 88%), which was used without further purification. For analytical purpose the product was purified via preparative HPLC. **HRMS (ESI-TOF) m/z**: [M]⁺ Calculated for C₂₆H₃₄N₃ 388.2747, Found 388.2750; **α_D²⁰**: +24.9 (c 0.95, MeOH); **IR (ν_{max}/cm⁻¹)**: 3406 (N-H v), 2944 (C-H v), 1633 (C-C v), 1498 (N-H δ), 1454 (C=C v), 1156 (C-N v), 765 (C-H pyridine δ), 703 (C-H arom δ); **¹H NMR (400 MHz, CDCl₃) δ**: 9.66 (s, 1H, *H*-pyridine), 8.84 (d, *J* = 5.60 Hz, 1H, *H*-pyridine), 8.35 (d, *J* = 7.83 Hz, 1H, *H*-pyridine), 7.95 – 7.85 (m, 1H, *H*-pyridine), 7.48 (m, 4H, *H*-arom), 7.25 – 7.16 (m, 3H, *H*-arom), 7.10 – 6.95 (m, 3H, *H*-arom), 5.09 (d, *J* = 11.64 Hz, 1H, CH-NH), 4.99 (d, *J* = 11.64 Hz, 1H, CH-(CH₃)₂), 4.78 (t, *J* = 7.16 Hz, 2H, N-CH₂), 4.27 (d, *J* = 15.44 Hz, 1H, NH-CH₂), 3.88 (d, *J* = 15.44 Hz, 1H, NH-CH₂), 2.90 (s, 6H, N-(CH₃)₂), 2.05 – 1.96 (m, 2H, N-CH₂-CH₂), 1.41 – 1.28 (m, 2H, N-(CH₂)₂-CH₂), 0.89 (t, *J* = 7.21 Hz, 3H, N-(CH₂)₃-CH₃); **¹³C NMR (100 MHz, CDCl₃) δ**: 144.7 (d, 1C, C-pyridine), 144.4 (d, 1C, C-pyridine), 142.3 (d, 1C, C-pyridine), 141.7 (s, 1C, C-pyridine), 138.0 (s, 1C, C-arom), 131.7 (d, 1C, C-arom), 130.2 (d, 1C, C-arom), 128.9 (d, 2C, C-arom), 128.7 (d, 2C, C-arom), 128.3 (d, 2C, C-arom), 127.9 (d, 1C, C-arom), 127.5 (d, 2C, C-arom), 127.5 (s, 1C, C-pyridine),

72.7 (d, 1C, CH-NH), 61.6 (t, 1C, N-CH₂), 60.8 (d, 1C, CH-N(CH₃)₂), 47.7 (t, 1C, NH-CH₂), 33.5 (t, 1C, N-CH₂-CH₂), 19.4 (t, 1C, N-(CH₂)₂-CH₂), 13.6 (q, 1C, N-(CH₂)₃-CH₃).

III. Synthesis of imine substrates for ATH reactions

III.1. 1-Methyl-3,4-dihydroisoquinoline (12)



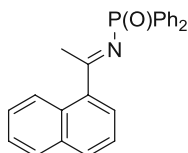
12

Reaction protocol adapted from literature.^{vi}

Phenylethylamine (24.80 mmol, 3.0 g) was dissolved in anhydrous DCM (80 mL) and Et₃N (30.0 mmol, 4.19 mL) was added in one portion. The reaction mixture was cooled to 0°C, and acetyl-chloride (29.51 mmol, 2.10 mL) was added dropwisely. The temperature of the reaction mixture was gradually increased to 40°C, and the mixture was stirred for 15 minutes. The organic phase was separated, and it was washed with 5% aqueous Na₂CO₃-solution, 5% aqueous HCl-solution, again with 5% aqueous Na₂CO₃-solution and finally with H₂O. The organic layer was dried on Na₂SO₄, and the solvent was removed *in vacuo*. *N*-phenethylacetamide was obtained in quantitative yield (4.05 g), and it was used without further purifications.

N-phenethylacetamide (24.80 mmol, 4.05 g), P₂O₅ (31.00 mmol, 4.40 g) and POCl₃ (93.0 mmol, 8.72 mL) were mixed together in *ortho*-xylene (100 mL), and the reaction mixture was refluxed for 14 hours. The cooled mixture was slowly hydrolyzed with warm H₂O, and the phases were separated. 5.4 mL concentrated HCl was added to the aqueous phase, and it was washed with toluene. The combined organic phases were extracted with 3.6 w% HCl-solution. The aqueous phases were combined, cooled in ice bath, and basified with c.c. NaOH-solution (87 mL) under vigorous stirring. After cooling down, it was extracted with toluene, dried on Na₂SO₄, and concentrated *in vacuo*. The crude product was purified by *Kugelrohr*-distillation (0.4 mBar, 50°C to 100°C) to obtain imine **12** as a colorless liquid (2.25 g, 62 %). ¹H NMR (400 MHz, CDCl₃) δ : 7.39 (d, *J* = 7.28 Hz, 1H, *H*-arom), 7.28-7.20 (m, 2H, *H*-arom), 7.10 (d, *J* = 6.92 Hz, 1H, *H*-arom), 3.58 (t, *J* = 7.28 Hz, 2H, N-CH₂), 2.61 (t, *J* = 7.64 Hz, 2H, CH₂-arom), 2.31 (s, 3H, CCH₃); ¹³C NMR (100 MHz, CDCl₃) δ : 164.2 (s, 1C, CCH₃), 137.4 (s, 1C, C-arom), 130.6 (s, 1C, C-arom), 129.6 (d, 1C, C-arom), 127.4 (d, 1C, C-arom), 126.9 (d, 1C, C-arom), 125.3 (d, 1C, C-arom), 47.0 (t, 1C, N-CH₂), 26.0 (t, 1C, CH₂-arom), 23.3 (q, 1C, CCH₃).

III.2. *N*-(1-(Naphthalen-1-yl)ethylidene)-*P,P*-diphenylphosphinic amide (13)



13

Imine **13** was prepared according to literature procedure.^{vii}

To a stirred solution of NH₂OH·HCl (15.1 mmol, 1.05 g) and NaOAc (15.1 mmol, 1.24 g) in EtOH/H₂O mixture (V/V = 1/1, 10 mL) 1-acetylnaphthalene (10.5 mmol, 1.57 mL) was added, and the mixture was

refluxed until total conversion. The mixture was cooled down to room temperature, and allowed to lay in the fridge for 24 hours. The precipitate formed was filtered off and washed with H₂O. The oxime intermediate was obtained in a quantitative yield (1.94 g), and it was used without further purification. The oxime (10.5 mmol, 1.94 g) was dissolved in a light petrol/CH₂Cl₂ mixture (V/V = 1/1, 33 mL) and triethylamine (10.5 mmol, 1.46 mL) was added. The mixture was cooled to -45°C, and chlorodiphenylphosphine (11.0 mmol, 1.97 mL) in CH₂Cl₂ (10 mL) was dropwisely added. After total conversion, the cooling bath was removed, and the mixture was allowed to warm up to room temperature. The solvent was evaporated, the residue was dissolved in CH₂Cl₂, and it was washed with saturated NaHCO₃-solution and brine. The organic phase was dried on Na₂SO₄, and the solvent was removed under reduced pressure. The crude product was purified by column chromatography (200 g silica, light petrol: ethyl acetate 1:3 + Et₃N), yielding imine **13** as a light yellow solid (2.49 g, 65 %). **¹H NMR (400 MHz, CDCl₃) δ** : 8.05 (d, *J* = 8.02 Hz, 1H, *H*-arom), 7.90-7.80 (m, 5H, *H*-arom), 7.51 (d, *J* = 6.80 Hz, 1H, *H*-arom), 7.43 – 7.31 (m, 10H, *H*-arom), 2.94 (d, *J* = 1.80 Hz, 3H, CCH₃); **³¹P NMR (100 MHz, CDCl₃) δ** : 18.8; **¹³C NMR (100 MHz, CDCl₃) δ** : 135.4 (s, 1C, CCH₃), 133.8 (s, 1C, C-arom), 132.9 (s, 1C, C-arom), 131.7 (d, 4C, C-arom), 131.5 (d, 4C, C-arom), 130.6 (d, 1C, C-arom), 128.5 (d, 4C, C-arom), 128.3 (d, 4C, C-arom), 126.8 (d, 1C, C-arom), 126.2 (d, 1C, C-arom), 124.8 (d, 1C, C-arom), 28.7 (q, 1C, CCH₃).

IV. General procedure for the asymmetric transfer hydrogenation

General remarks

Asymmetric transfer hydrogenations were carried out in flame-dried flasks using standard Schlenk techniques. Before the reactions, a 20 mg/mL stock solution of Ru[(*p*-cymene)₂Cl₂]₂ in anhydrous acetonitrile was freshly prepared in a glovebox. All liquids involved in the reactions were freshly degassed by using the *freeze-dry-thaw* method, and they were subsequently purged with argon for 30 minutes prior to use.

Asymmetric transfer hydrogenation of ketones

An aliquot of a freshly prepared stock solution of Ru[(*p*-cymene)₂Cl₂]₂ (0.01 mmol, 306 μL) was transferred into a Schlenk-flask, and the solvent was removed under vacuum. Chiral ligand **3-9** (0.021 mmol) was dissolved in 4 mL H₂O. This solution was added to the catalyst precursor in the Schlenk-flask under argon atmosphere and stirred at 40 °C for 30 min to form the active catalyst. Sodium formate (10.0 mmol, 680 mg) was added, followed by the addition of ketone (2.0 mmol). The reaction mixture was stirred at given temperature for 24 h. Then, the aqueous phase was extracted with diethyl ether and the combined organic phases were dried over Na₂SO₄, and concentrated *in vacuo*. The product was isolated *via* column chromatography (light petrol: ethyl acetate 10:1). Remaining solvents were removed under vacuum to yield the pure secondary alcohols.

Asymmetric transfer hydrogenation of imines

An aliquot of a freshly prepared stock solution of Ru[(*p*-cymene)₂Cl₂]₂ (0.005 mmol, 153 μL) was transferred into a Schlenk-flask, and the solvent was removed under vacuum. Chiral ligand **3-9** (0.0105 mmol) was dissolved in 1.5 mL H₂O/MeOH mixture (V/V = 1/1 or 1/2). This solution was added to the catalyst precursor in the Schlenk-flask under argon atmosphere, and stirred at 40 °C for 30 min to form the active catalyst. Formic acid/triethylamine mixture (n/n = 1.1/1, 0.5 mL) was added, followed by the imine (1.0 mmol). The reaction mixture was stirred at 40 °C for 24 h. Then, the methanol was removed under reduced pressure, and the aqueous phase was basified with 0.5 M Na₂CO₃ solution. The aqueous layer was extracted with dichloromethane. The combined organic phases were dried on Na₂SO₄ and concentrated *in vacuo*. The product was isolated *via* column chromatography to afford the pure secondary amine products.

General procedure for the chiral derivatization

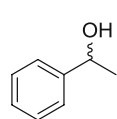
In a flame-dried Schlenk-flask, the alcohol/amine (0.1 mmol) was dissolved in anhydrous dichloromethane (1 mL). Triethylamine (21 μ L, 0.15 mmol) and (*S*)-Mosher's acid chloride (22 μ L, 0.12 mmol) were added and the reaction mixture was stirred at 25°C. After completion, 5 mL of dichloromethane was added, and the organic phase was successively washed with 0.5 M Na₂CO₃ and water, dried over Na₂SO₄, and concentrated *in vacuo*. The enantiomeric composition was analysed by ¹⁹F NMR measurement.

Reusability experiment

An aliquot of a freshly prepared stock solution of Ru[(*p*-cymene)₂Cl₂]₂ (306 μ L, 0.01 mmol) was transferred into a Schlenk-flask, and the solvent was removed under vacuum. Chiral ligand **3** (0.021 mmol) was dissolved in 4 mL H₂O. This solution was added to the catalyst precursor in the Schlenk-flask under argon atmosphere and stirred at 40 °C for 30 min to form the active catalyst. Sodium formate (680 mg, 10.0 mmol) was added, followed by the addition of acetophenon (2 mmol) The reaction mixture was stirred at 60 °C. In every hour, a sample was taken, and another batch of acetophenone (233 μ L, 2.0 mmol) and sodium formate (136 mg, 2.0 mmol) were added. The conversion was measured every time *via* ¹H NMR measurement, while chiral HPLC was used to determine the enantiomeric excess.

V. Analytical data of ATH products

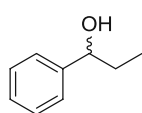
V.1. 1-Phenylethan-1-ol (11a)^{viii}



11a

By using chiral ligand 3: column chromatography (light petrol: ethyl acetate 10:1); 92 % yield; 91 % ee; α_D^{20} : + 51.1 (*c* 1.1, CHCl₃); ¹H NMR (200 MHz, CDCl₃) δ : 7.34 – 7.13 (m, 5H, *H*-arom), 4.81 (q, *J* = 6.42 Hz, 1H, CH-OH), 1.82 (s, 1H, CH-OH), 1.42 (d, *J* = 6.45 Hz, 3H, CH-CH₃).^{Chiral HPLC analysis:} (chiracel diacel IB column, ⁿhexane : 2-propanol 98.5:1.5 V/V, 1.0 mL/min, 25°C, UV 254 nm): *t*_R (major) = 13.4 min (*R*-enantiomer), *t*_R (minor) = 15.5 min (*S*-enantiomer).

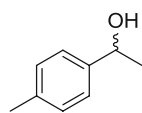
V.2. 1-Phenylpropan-1-ol (11b)^{ix}



11b

By using chiral ligand 3: column chromatography (light petrol: ethyl acetate 10:1); 68 % yield; 82 % ee; α_D^{20} : + 36.2 (*c* 1.2, CHCl₃); ¹H NMR (200 MHz, CDCl₃) δ : 7.24 – 7.07 (m, 5H, *H*-arom), 4.37 (t, *J* = 6.67 Hz, 1H, CH-OH), 2.61 (brs, 1H, CH-OH), 1.75 – 1.46 (m, 2H, CH₂-CH₃), 0.76 (t, *J* = 7.41 Hz, 3H, CH₂-CH₃).^{Chiral HPLC analysis:} (chiracel diacel IB column, ⁿhexane : 2-propanol 98.5:1.5 V/V, 1.0 mL/min, 25°C, UV 254 nm): *t*_R (major) = 11.6 min (*R*-enantiomer), *t*_R (major) = 12.7 min (*S*-enantiomer).

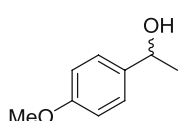
V.3 1-(4-Methylphenyl)ethanol (11c)^x



11c

By using chiral ligand 3: column chromatography (light petrol: ethyl acetate 10:1); 82 % yield; 97 % ee; α_D^{20} : + 43.1 (*c* 1.05, CHCl₃); ¹H NMR (200 MHz, CDCl₃) δ : 7.24 – 7.15 (m, 2H, *H*-arom), 7.12 – 7.04 (m, 2H, *H*-arom), 4.79 (q, *J* = 6.39 Hz, 1H, CH-OH), 2.27 (s, 3H, CH₃-arom), 1.73 (brs, 1H, CH-OH), 1.41 (d, *J* = 6.42 Hz, 3H, CH-CH₃).^{Chiral HPLC analysis:} (chiracel diacel AS-H column, ⁿheptane : 2-propanol 98.0:2.0 V/V, 0.7 mL/min, 25°C, UV 254 nm): *t*_R (minor) = 16.3 min (*S*-enantiomer), *t*_R (major) = 18.4 min (*R*-enantiomer).

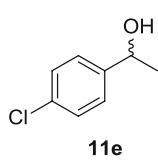
V.4. 1-(4-Methoxyphenyl)ethanol (11d)¹⁰



11d

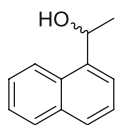
By using chiral ligand 3: column chromatography (light petrol: ethyl acetate 10:1); 74 % yield; 83 % ee; α_D^{20} : + 20.0 (*c* 1.05, CHCl₃); ¹H NMR (200 MHz, CDCl₃) δ : 7.26 – 7.17 (m, 2H, *H*-arom), 6.85 – 6.75 (m, 2H, *H*-arom), 4.78 (q, *J* = 6.54 Hz, 1H, CH-OH), 3.72 (s, 3H, OCH₃), 1.73 (brs, 1H, CH-OH), 1.40 (t, *J* = 6.63 Hz, 3H, CH-CH₃).^{Chiral HPLC analysis:} (chiracel diacel IB column, ⁿhexane : 2-propanol 98.5:1.5 V/V, 1.0 mL/min, 25°C, UV 254 nm): *t*_R (major) = 21.0 min (*R*-enantiomer), *t*_R (minor) = 22.6 min (*S*-enantiomer).

V.5. 1-(4-Chlorophenyl)ethanol (11e)⁸



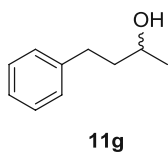
By using chiral ligand **3**: column chromatography (light petrol: ethyl acetate 10:1); 76 % yield; 81 % ee; α_D^{20} : + 40.9 (*c* 1.0, CHCl₃); ¹H NMR (200 MHz, CDCl₃) δ : 7.26 – 7.15 (m, 4H, *H*-arom), 4.76 (q, *J* = 6.44 Hz, 1H, *CH*-OH), 2.13 (brs, 1H, *CH*-OH), 1.36 (d, *J* = 6.40 Hz, 3H, *CH*-CH₃). Chiral HPLC analysis: (chiracel diacel IB column, ⁿhexane : 2-propanol 98.5:1.5 V/V, 1.0 mL/min, 25°C, UV 254 nm) *t*_R (minor) = 14.3 min (*S*-enantiomer), *t*_R (major) = 15.0 min (*R*-enantiomer).

V.6. 1-(1-Naphtyl)ethanol (11f)^{xi}



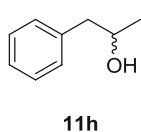
By using chiral ligand **3**: column chromatography (light petrol: ethyl acetate 10:1); 73 % yield; 93 % ee; α_D^{20} : + 54.7 (*c* 1.0, CHCl₃); ¹H NMR (200 MHz, CDCl₃) δ : 8.14 – 7.41 (m, 7H, *H*-arom), 5.56 (q, *J* = 6.44 Hz, 1H, *CH*-OH), 3.35 (brs, 1H, *CH*-OH), 1.66 (d, *J* = 6.71 Hz, 3H, *CH*-CH₃). Chiral HPLC analysis: (chiracel diacel IB column, ⁿheptane : 2-propanol 93.0:7.0 V/V, 1.0 mL/min, 25°C, UV 254 nm): *t*_R (minor) = 9.3 min (*S*-enantiomer), *t*_R (major) = 12.1 min (*R*-enantiomer).

V.7. 4-Phenyl-2-butanol (11g)^{xii}



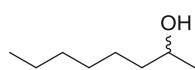
By using chiral ligand **4**: column chromatography (light petrol: ethyl acetate 10:1); 86 % yield; 17 % ee; α_D^{20} : + 0.7 (*c* 1.03, CHCl₃); ¹H NMR (200 MHz, CDCl₃) δ : 7.25 – 7.15 (m, 2H, *H*-arom), 7.14 – 7.08 (m, 3H, *H*-arom), 3.75 (sex, *J* = 6.35 Hz, 1H, *CH*-OH), 2.73 – 2.55 (m, 2H, arom-CH₂), 1.77 – 1.63 (m, 2H, CH₂-CH), 1.38 (brs, 1H, *CH*-OH), 1.15 (d, *J* = 6.07 Hz, 3H, *CH*-CH₃); Chiral HPLC analysis: (chiracel diacel IB column, ⁿhexane : 2-propanol 99.3:0.7 V/V, 1.0 mL/min, 25°C, UV 254 nm): *t*_R (major) = 26.3 min (*S*-enantiomer), *t*_R (minor) = 39.3 min (*R*-enantiomer).

V.8. 1-Phenylpropan-2-ol (11h)^{xiii}



By using chiral ligand **3**: column chromatography (light petrol: ethyl acetate 10:1); 86 % yield; 26 % ee; α_D^{20} : + 5.8 (*c* 1.08, CHCl₃); ¹H NMR (200 MHz, CDCl₃) δ : 7.27 – 7.08 (m, 5H, *H*-arom), 3.89 (q, *J* = 5.51 Hz, 1H, *CH*-OH), 2.66 (dd, *J* = 13.46 Hz, 5.85 Hz, 1H, CH_{2a}-CH), 2.59 (dd, *J* = 13.46 Hz, 5.85 Hz, 1H, CH_{2b}-CH), 1.82 (brs, 1H, *CH*-OH), 1.13 (d, *J* = 6.05 Hz, 3H, *CH*-CH₃); Chiral HPLC analysis: (chiracel diacel IB column, ⁿhexane : 2-propanol 99.3:0.7 V/V, 1.0 mL/min, 25°C, UV 254 nm): *t*_R (major) = 15.6 min (*S*-enantiomer), *t*_R (minor) = 16.8 min (*R*-enantiomer).

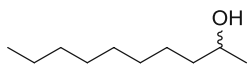
V.9. 2-Octanol (11i)^{xiv}



11i

By using chiral ligand **4**: column chromatography (light petrol: ethyl acetate 10:1) 86 % yield; 92 % ee; α_D^{20} : - 0.5 (c 1.09, CHCl₃); ¹H NMR (200 MHz, CDCl₃) δ : 3.75 (sex, J = 5.92 Hz, 1H, CH-OH), 2.13 (brs, 1H, CH-OH), 1.50 – 1.23 (m, 10H, 5 x CH₂), 1.15 (d, J = 6.26 Hz, 3H, CH-CH₃), 0.86 (t, J = 6.70 Hz, 3H, CH₃-CH₂); ¹⁹F NMR for determining the ee (100 MHz, CDCl₃) δ : - 69.9, (minor diastereomer), - 71.5 (major diastereomer).

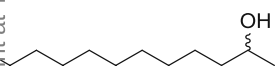
V.10. 2-Decanol (11j)¹⁴



11j

By using chiral ligand **4**: column chromatography (light petrol: ethyl acetate 10:1); 37 % yield; 90 % ee; α_D^{20} : - 2.5 (c 0.75, EtOH); ¹H NMR (200 MHz, CDCl₃) δ : 3.77 (sex, J = 5.72 Hz, 1H, CH-OH), 1.66 (brs, 1H, CH-OH), 1.50-1.20 (m, 14H, 7 x CH₂), 1.17 (d, J = 6.28 Hz, 3H, CH-CH₃), 0.87 (t, J = 5.85 Hz, 3H, CH₃-CH₂); ¹⁹F NMR for determining the ee (100 MHz, CDCl₃) δ : - 70.9, (major diastereomer), - 71.7 (minor diastereomer).

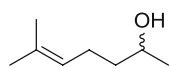
V.11. 2-Dodecanol (11k)^{xv}



11k

By using chiral ligand **4**: column chromatography (light petrol: ethyl acetate 10:1); 44 % yield; 78 % ee; α_D^{20} : - 1.2 (c 0.5, CHCl₃); ¹H NMR (200 MHz, CDCl₃) δ : 3.79 (sex, J = 5.42 Hz, 1H, CH-OH), 1.56 – 1.22 (m, 19H, 9 x CH₂, CH-OH), 1.18 (d, J = 6.17 Hz, 3H, CH-CH₃), 0.88 (t, J = 5.87 Hz, 3H, CH₃-CH₂); ¹⁹F NMR for determining the ee (100 MHz, CDCl₃) δ : - 70.9, (minor diastereomer), - 71.9 (major diastereomer).

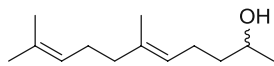
V.12. 6-Methyl-5-hepten-2-ol (11l)¹⁴



11l

By using chiral ligand **4**: column chromatography (light petrol: ethyl acetate 10:1); 67 % yield; 78 % ee; α_D^{20} : + 0.8 (c 1.03, CHCl₃); ¹H NMR (200 MHz, CDCl₃) δ : 5.16 – 5.08 (m, 1H, CH-C(CH₃)₂), 3.80 (sex, J = 6.24 Hz, 1H, CH-OH), 2.14 – 1.98 (m, 2H, CH₂-CH-C(CH₃)₂), 1.65 (d, J = 13.26 Hz, 6H, CH-C(CH₃)₂), 1.55 – 1.41 (m, 2H, CH₂-CH-OH), 1.24 (brs, 1H, CH-OH), 1.18 (d, J = 6.25 Hz, 3H, CH-CH₃); Chiral GC analysis (90°C to 150 °C, 1.5 °C/min.): t_R (major) = 5.65 min (S-enantiomer), t_R (minor) = 5.96 min (R-enantiomer).

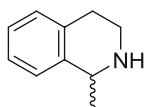
V.13. 6,10-Dimethyl-5,9-undecadien-2-ol (11m)^{xvi}



11m

By using chiral ligand **4**: column chromatography (light petrol: ethyl acetate 10:1); 28 % yield; 24 % ee; α_D^{20} : + 1.1 (c 5.0, CHCl₃); ¹H NMR (200 MHz, CDCl₃) δ : 5.14 – 4.95 (m, 2H, 2 x CH-C(CH₃)₂), 3.74 (sex, J = 6.20 Hz, 1H, CH-OH), 2.10 – 1.87 (m, 6H, CH₂-CH-C(CH₃)₂, CH₂-CH₂-CH-C(CH₃)₂, CH₂-CH₂-CH-OH), 1.61 (s, 3H, CH₃-C), 1.57 – 1.49 (d, J = 13.26 Hz, 6H, CH-C(CH₃)₂), 1.48 – 1.34 (m, 3H, CH₂-CH-OH, OH), 1.12 (d, J = 6.29 Hz, 3H, CH-CH₃); Chiral GC analysis (90°C to 150 °C, 1.5 °C/min.): t_R (minor) = 6.19 min (R-enantiomer), t_R (major) = 6.58 min (S-enantiomer).

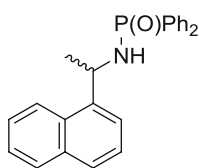
V.14. 1-Methyl-1,2,3,4-tetrahydroisoquinoline (24)^{xvii}



24

By using the chiral ligand **3**: column chromatography (DCM: MeOH 10:1 + Et₃N); 94% yield, 87 % ee; $[\alpha]_D^{20}$: + 59.9 (c 1.0, CHCl₃); ¹H NMR (200 MHz, CDCl₃) δ : 7.05 – 6.97 (m, 4H, *H*-arom), 4.78 (q, *J* = 6.60 Hz, 1H, *CH*-NH), 3.17 – 3.16 (m, 1H, *CH*_{2a}-NH), 2.77-2.70 (m, 3H, *CH*_{2b}-NH, *CH*₂-arom) 1.71 (br s, 1H, *CH*-NH), 1.37 (d, *J* = 6.60 Hz, 3H, *CH*-CH₃); ¹⁹F NMR for determining the ee (100 MHz, CDCl₃) δ : = - 69.74, (minor diastereomer), - 71.30 (major diastereomer).

V.15. *N*-(1-(Naphthalen-1-yl)ethyl)-*P,P*-diphenylphosphinic amide (25)^{xviii}



25

By using the chiral ligand **3**: column chromatography (light petrol: ethyl acetate:1:3 + Et₃N); 60% yield, 86 % ee; $[\alpha]_D^{20}$: - 53.1 (c 1.0, CHCl₃); ¹H NMR (200 MHz, CDCl₃) δ : 7.90 – 7.63 (m, 7H, *H*-arom), 7.56 (d, *J* = 8.20 Hz, 1H, *H*-arom), 7.49 – 7.14 (m, 9H, *H*-arom), 5.16 (qvin., *J* = 6.74 Hz, 1H, *CH*-NH), 3.35-3.28 (m, 1H, NH), 1.62 (d, *J* = 6.32 Hz, 3H, *CH*-CH₃); ³¹P NMR (100 MHz, CDCl₃) δ : 23.11; Chiral HPLC analysis (chiracel diacel AS-H column, ⁿheptane : EtOH 95:5 V/V, 1.0 mL/min, 25°C, UV 254 nm): *t*_R (minor) = 29.7 min, *t*_R (major) = 32.9 min.

VI. Reference

- i Lee, D.W.; Ha, H.; Lee, W.K. Selective Mono-BOC Protection of Diamines. *Synth. Commun.*, **2007**, *37*, 252-255. DOI: 10.1080/00397910601131403
- ii Vasiloiu, M.; Gaertner, P.; Zirbs, R.; Bica, K. Coordinating Chiral Ionic Liquids: Design, Synthesis, and Application in Asymmetric Transfer Hydrogenation under Aqueous Conditions. *Eur. J. Org. Chem.*, **2015**, *11*, 2374-2381. DOI: 10.1002/ejoc.201403555
- iii Tiffner, M.; Novacek, J.; Busillo, A.; Gratzner, K.; Massa, A.; Waser, M. Design of chiral urea-quaternary ammonium salt hybrid catalysts for asymmetric reactions of glycine Schiff bases. *RSC Adv.*, **2015**, *5*, 78941–78949. DOI: 10.1039/C5RA14466C
- iv Kucherenko, A.S.; Siyutkin, D.E.; Nigmatov, S.G.; Chizhov, A.O.; Zlotin, S.G. Chiral Primary Amine Tagged to Ionic Group as Reusable Organocatalyst for Asymmetric Michael Reactions of C-Nucleophiles with α,β -Unsaturated Ketones. *Adv.Synth. Catal.*, **2012**, *16*, 3078-3086. DOI: 10.1002/adsc.201200338
- v Guduguntla, S.; Hornillos, V.; Tessier, R.; Fañanás-Mastral, M.; Feringa, B. L. Chiral Diarylmethanes via Copper-Catalyzed Asymmetric Allylic Arylation with Organolithium Compounds. *Org. Lett.*, **2016**, *18*, 252–255. DOI: 10.1021/acs.orglett.5b03396
- vi Pecháček, J.; Václavík, J.; Přeck, J.; Šot, P.; Januščák, J.; Vilhanová, B.; Vavřík, J.; Kuzma, M.; Kačer, P. Asymmetric Transfer Hydrogenation of Imines Catalyzed by a Noyori-Type Ru(II) Complex – A Parametric Study. *Tetrahedron: Asymmetr.*, **2013**, *24*, 233–239. DOI: 10.1016/j.tetasy.2013.01.010
- vii Huang, J.; Liu, X.; Wen, Y.; Qin, B.; Feng, X. Enantioselective Strecker Reaction of

Phosphinoyl Ketoimines Catalyzed by in Situ Prepared Chiral N,N'-Dioxides. *J. Org. Chem.*, **2007**, *72*, 204-208. DOI: 10.1021/jo062006y

- viii Kagohara, E.; Pellizari, V. H.; Comasseto, J. V.; Andrade, L. H.; Porto, A. L. M. Bio-transformations of substituted phenylethanols and acetophenones by environmental bacteria. *Food Technol. Biotechnol.*, **2008**, *46*, 381–387. ISSN: 1330-9862
- ix Hayes, A. M.; Morris, D. J.; Clarkson, G. J.; Wills, M. A class of ruthenium(II) catalyst for asymmetric transfer hydrogenations of ketones. *J. Am. Chem. Soc.*, **2005**, *127*, 7318–7319. DOI: 10.1021/ja051486s
- x Swizdor, A.; Janeczko, T.; Dmochowska-Gladysz, J. *Didymosphaeria igniaria*: A new microorganism useful for the enantioselective reduction of aryl-aliphatic ketones. *J. Ind. Microbiol. Biotechnol.*, **2010**, *37*, 1121–1130. DOI: 10.1007/s10295-010-0759-9
- xi Ito, J.; Teshima, T.; Nishiyama, H. Enhancement of enantioselectivity by alcohol additives in symmetric hydrogenation with bis(oxazolinyl)phenyl ruthenium catalysts. *Chem. Commun.*, **2012**, *48*, 1105–1107. DOI: 10.1039/C1CC16057E
- xii Inagaki, T., Ito, A., Ito, J.-i. and Nishiyama, H., Asymmetric Iron-Catalyzed Hydrosilane Reduction of Ketones: Effect of Zinc Metal upon the Absolute Configuration. *Angew. Chem Int. Ed.*, **2010**, *49* 9384–9387. DOI: 10.1002/anie.201005363
- xiii Mourad, B.; Saoussen, Z.; Jacqueline, C.; Jean-Claude, F.; Louisa, A.Z. Screening method for the evaluation of asymmetric catalysts for the reduction of aliphatic ketones. *Tetrahedron Lett.*, **2011**, *52*, 1485-1489. DOI: 10.1016/j.tetlet.2011.01.112
- xiv Nakamura, K.; Matsuda, T. Asymmetric Reduction of Ketones by the Acetone Powder of *Geotrichum candidum*. *J. Org. Chem.*, **1998**, *63* (24), 8957–8964.
DOI: 10.1021/jo9812779
- xv Wen-Xu, H.; Kent A., B.; Xingquan, M.; Raymond, C.S.; Mark, Y. Design, Synthesis, and Properties of Branch-Chained Maltoside Detergents for Stabilization and Crystallization

of Integral Membrane Proteins:Human Connexin 26. *Langmuir*, **2010**, *26* (11), 8690-8696. **DOI:** 10.1021/la904893d

xvi Vidal, D. M.; Fonseca, M. G.; Zarbin, P. H. G. Enantioselective synthesis and absolute configuration of the sex pheromone of *Hedypathes betulinus* (Coleoptera: Cerambycidae). *Tetrahedron Lett.*, **2010**, *51* 6704-6706.

DOI: 10.1016/j.tetlet.2010.10.024

xvii Pedrosa, R.; Andrés, C.; Iglesias, J.M. A Novel Straightforward Synthesis of Enantiopure Tetrahydroisoquinoline Alkaloids. *J. Org. Chem.*, **2001**, *66*, 243-250.

DOI: 10.1021/jo001397s

xviii Graves, C.R.; Scheidt, K.A.; Nguyen, S.T. Enantioselective MSPV Reduction of Ketimines Using 2-Propanol and (BINOL)Al^{III}. *Org. Lett.*, **2006**, *8*, 1229-1232.

DOI: 10.1021/ol060110w

Appendix B

Supporting information:

Asymmetric transfer hydrogenation in thermomorphic microemulsions based on ionic liquids

Supporting Information

Asymmetric transfer hydrogenation in thermomorphic microemulsions based on ionic liquids

Mahtab Hejazifar^a, Ádám Márk Pálvölgyi^a, Jacqueline Bitai^a, and Katharina Bica-Schröder^{a}*

^a Institute of Applied Synthetic Chemistry, Vienna University of Technology, Getreidemarkt 9/163, 1060 Vienna, Austria.

* Corresponding author Katharina Bica-Schröder. Email: katharina.schroeder@tuwien.ac.at, Tel: +43 1 58801 163601.

| | | |
|-----|-----------------------|-----|
| I. | Phase diagrams | 143 |
| II. | Kinetic studies | 146 |

I. Phase diagrams

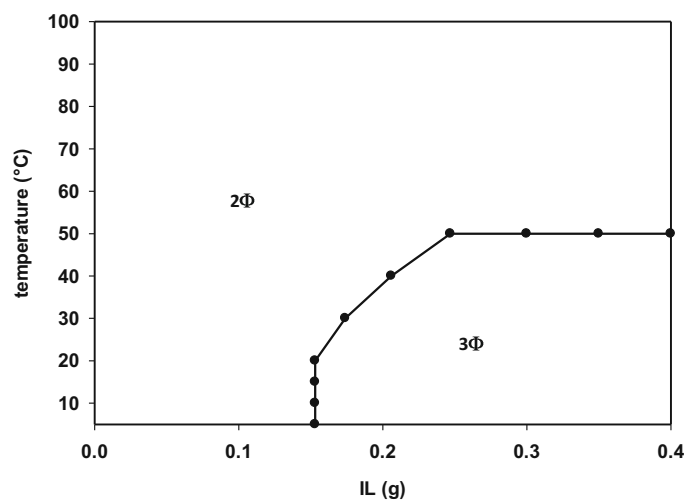


Figure S1: Phase diagram of HCOONa (2 mmol), acetophenone (0.25 mmol), 1-phenylethanol (0.25 mmol), at mass fraction of water/*n*-heptane 2/1 (g), ($\alpha = 0.33$).

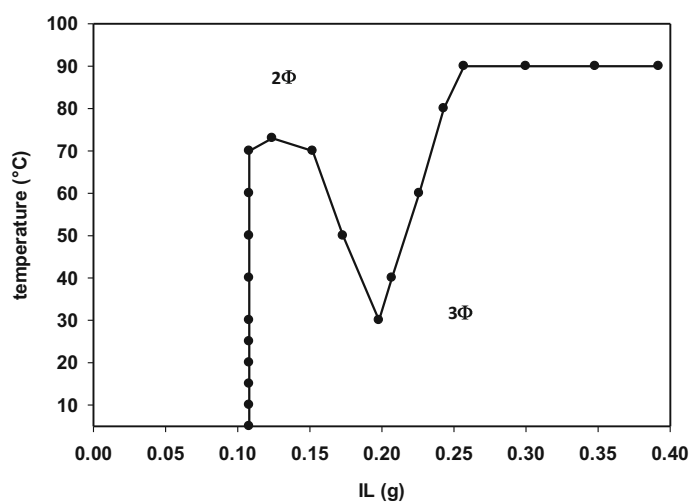


Figure S2: Phase diagram of HCOONa (2 mmol), acetophenone (0.25 mmol), 1-phenylethanol (0.25 mmol), at equal mass fraction of water/*n*-heptane 2/2 (g), ($\alpha = 0.5$).

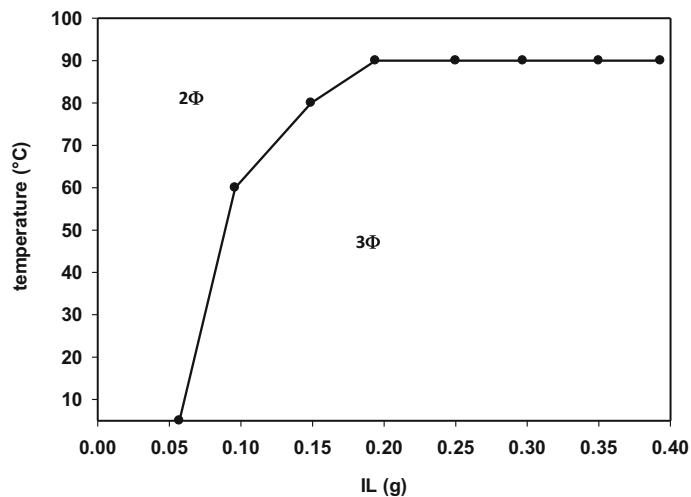


Figure S3: Phase diagram of HCOONa (2 mmol), acetophenone (0.25 mmol), 1-phenylethanol (0.25 mmol), at mass fraction of water/*n*-heptane 2/3 (g), ($\alpha = 0.6$).

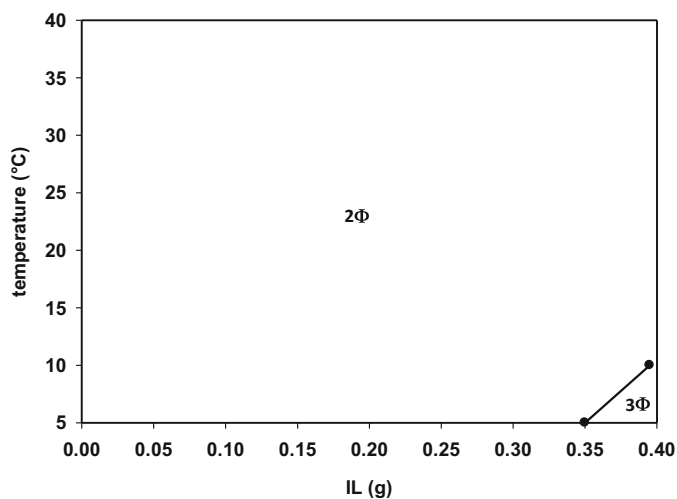


Figure S4: Phase diagram of HCOONa (2 mmol), 1-phenylethanol (0.5 mmol), at mass fraction of water/*n*-heptane 2/1 (g), ($\alpha = 0.33$).

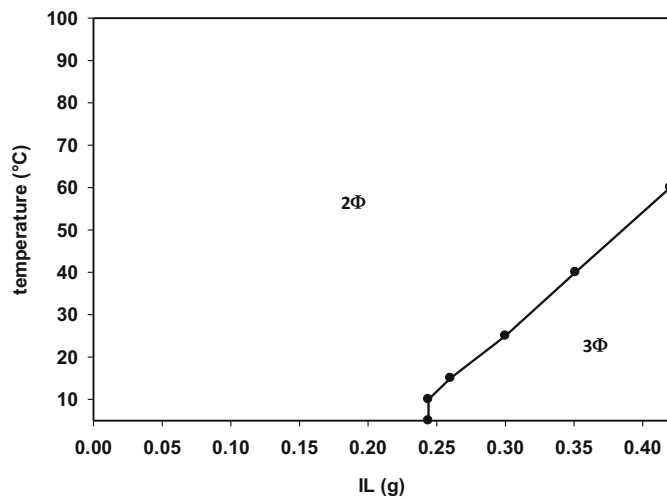


Figure S5: Phase diagram of HCOONa (2 mmol), 1-phenylethanol (0.5 mmol), at equal mass fraction of water/*n*-heptane 2/2 (g), ($\alpha = 0.5$).

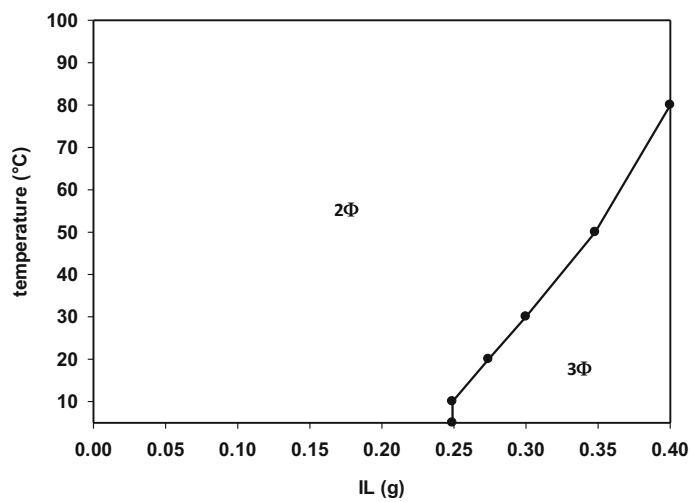


Figure S6: Phase diagram of HCOONa (2 mmol), 1-phenylethanol (0.5 mmol), at mass fraction of water/*n*-heptane 2:3 (g), ($\alpha = 0.6$).

II. Kinetic studies

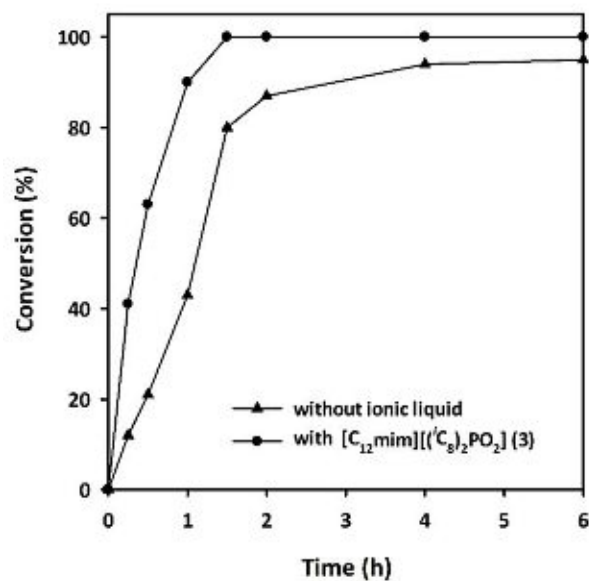


Figure S7: Kinetic studies for the ATH of acetophenone at different systems by using ionic liquid 3/*n*-heptane/water 0.3/0.5/2 g, 0.5 mmol acetophenone, 2 mmol HCOONa, 0.005 mmol (0.5 mol%) catalyst, 60 °C.

Appendix C

Supporting information:

Counterion enhanced organocatalysis: A novel approach for the asymmetric transfer hydrogenation of enones

Supporting Information

Counterion enhanced organocatalysis: A novel approach for the asymmetric transfer hydrogenation of enones

Fabian Scharinger,^[a] † Ádám Márk Pálvölgyi,^[a] † Veronika Zeindlhofer,^[b] Michael Schnürch,^[a] Christian Schröder,^[b] and Katharina Bica-Schröder*^[a]

^[a] Institute of Applied Synthetic Chemistry, TU Wien, Getreidemarkt 9/163, A-1060 Vienna, Austria.

^[b] Department of Computational Biological Chemistry, University of Vienna, Währinger Str. 17, 1090 Vienna, Austria.

† These authors contributed equally to this manuscript.

e-mail: katharina.schroeder@tuwien.ac.at

1

| | | |
|----|--|-----|
| 1. | General remarks..... | 150 |
| 2. | Synthesis of L-amino acid derivatives | 151 |
| 3. | General synthesis of the phosphoric acids | 157 |
| 4. | Synthesis of the Hantzsch ester | 161 |
| 5. | Synthesis of ATH substrates..... | 162 |
| 6. | General procedure and optimization of the ATH reactions..... | 165 |
| 7. | Computational studies..... | 179 |

1. General remarks

All purchased chemicals from commercial suppliers were used without further purification. Dry solvents were pre-distilled and desiccated on aluminium oxide columns (PURESOLV, Innovative Technology).

Column chromatography was performed on standard manual glass columns using Merck (40-60 μm) silica gel with pre-distilled solvents (PE : petrolether, EtOAc : ethyl acetate, Et₂O : diethyl ether). For TLC analysis, precoated aluminium-backed plates were purchased from Merck (silica gel 60 F₂₅₄). UV active compounds were detected at 254 nm. Non-UV active compounds have been detected using vanillin staining solution (5% vanillin in EtOH + H₂SO₄).

¹H, ¹³C, and ³¹P NMR spectra were recorded on a Bruker Advance UltraShield 200 MHz or 400 MHz spectrometer and chemical shifts are reported in ppm using TMS (tetramethylsilane) as internal standard. Coupling constants (*J*) are given in Hz. For NMR purpose, the following abbreviations are used: s (singlet), d (doublet), t (triplet), q (quartet), m (multiplet), brs (broad singlet), dd (doublet of doublets), ddd (doublets of doublet of doublets), td (triplet of doublets), dt (doublet of triplets).

GC analysis have been performed on a Thermo Scientific Focus on BGB5 column by using FID detector. Chiral GC measurements were performed on chiral BGB columns (BGB173 or BGB175) by using FID detector.

Chiral HPLC measurements were carried out on a DIONEX UPLC equipped with a photodiode array (PDA) plus detector (190–360 nm), using a Diacel Chiralcel AS-H column (250×4.60 mm, 5 μm).

Optical rotation was measured on an Anton Paar MCP500 polarimeter at the specific conditions and the results have been compared to literature values. Concentrations are given in g / 100 ml.

HR-MS analysis was performed using HTC PAL system auto sampler, an Agilent 1100/1200 HPLC and Agilent 6230 AJS ESI-TOF mass spectrometer.

Microwave reactions were performed on a Biotage Initiator Classic in 20 ml pressure tight glass vials.

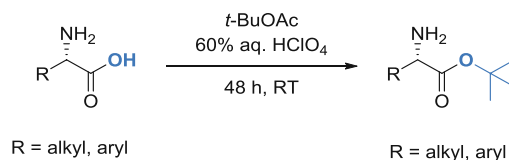
Melting points above room temperature were measured on an automated melting point system OPTI MELT of Stanford Research Systems and are uncorrected.

Infrared spectra were recorded on a Perkin-Elmer Spectrum 65 FT IR spectrometer equipped with a specac MK II Golden Gate Single Reflection ATR unit.

2. Synthesis of L-amino acid derivatives

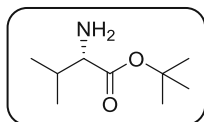
2.1 General procedure for the synthesis of L-amino acid *tert*-butyl esters

Compound have been prepared by the following literature procedure: ²



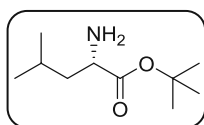
To a solution of the corresponding L-amino acid (1.0 equiv.) in *tert*-butyl acetate (18.0 equiv.), HClO₄ (60 % aqueous solution, 1.5 equiv.) was added dropwise at 0°C. The reaction mixture was stirred 18 h at room temperature. Distilled H₂O was added, and the reaction mixture was extracted with distilled H₂O (2×) and 1 N HCl (3×). The combined aqueous phases were then adjusted to pH 10 with a saturated Na₂CO₃ solution. The resulting solution was then extracted with CH₂Cl₂. The combined organic phases were dried over anhydrous Na₂SO₄ and concentrated under reduced pressure to give the L-amino acid *tert*-butyl esters, which were found to be pure without further purifications.

tert-Butyl L-valinate ²



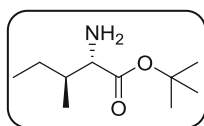
Light yellow oil (67% yield). ¹H NMR (400 MHz, CDCl₃) δ 3.17 (d, *J* = 4.8 Hz, 1H, CH-NH₂), 2.03 – 1.97 (m, 1H, CH-(CH₃)₂), 1.57 (s, 2H, NH₂), 1.46 (s, 9H, 3 × CH₃-C), 0.97 (d, *J* = 6.9 Hz, 3H, CH₃-CH), 0.89 (d, *J* = 6.9 Hz, 3H, CH₃-CH).

tert-Butyl L-leucinate ²



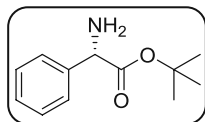
Light yellow oil (69% yield). ¹H NMR (400 MHz, CDCl₃) δ 3.26 (t, *J* = 8.0 Hz, 1H, CH-NH₂), 1.74 – 1.67 (m, 1H, CH-(CH₃)₂), 1.48 – 1.37 (m, 12H, CH_{2a}-CH-NH₂, NH₂, 3 × CH₃-C), 1.33 – 1.27 (m, 1H, CH_{2b}-CH-NH₂), 0.86 (t, *J* = 9.0 Hz, 6H, 2 × CH₃-CH).

tert-Butyl L-isoleucinate ³



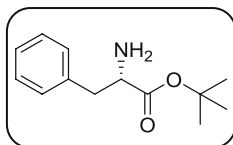
Light yellow oil (36% yield). ¹H NMR (400 MHz, CDCl₃) δ 3.22 (d, *J* = 4.8 Hz, 1H, CH-NH₂), 1.73 – 1.67 (m, 1H, CH-CH₃), 1.48 (s, 2H, NH₂), 1.46 (s, 9H, 3 × CH₃-C), 1.12 – 1.23 (m, 2H, CH₂-CH₃), 1.12 – 0.70 (m, 6H, 2 × CH₃).

tert-Butyl-(S)-2-amino-2-phenylacetate³



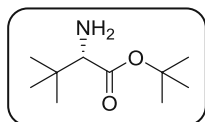
Light yellow solid (61% yield). ¹H NMR (400 MHz, CDCl₃) δ 7.30 – 7.16 (m, 5H, *H*-arom), 4.39 (s, 1H, *CH*-NH₂), 1.99 (s, 2H, NH₂), 1.30 (s, 9H, 3 × CH₃-C).

tert-Butyl L-phenylalaninate³



Light yellow oil (65% yield). ¹H NMR (400 MHz, CDCl₃) δ 7.23 – 7.14 (m, 5H, *H*-arom), 3.54 (t, *J* = 7.8 Hz, 1H, *CH*-NH₂), 2.97 (dd, *J* = 16.0 Hz, 8.0 Hz, 1H, CH_{2a}-CH-NH₂), 2.77 (dd, *J* = 16.0 Hz, 8.0 Hz, 1H, CH_{2b}-CH-NH₂), 1.40 (s, 2H, NH₂), 1.35 (s, 9H, 3 × CH₃-C).

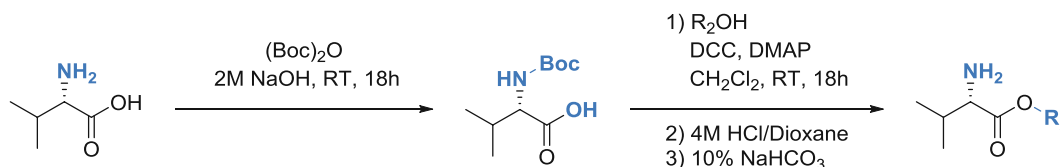
tert-Butyl (S)-2-amino-3,3-dimethylbutanoate²



Light yellow oil (72% yield). ¹H NMR (400 MHz, CDCl₃) δ 2.95 (s, 1H, *CH*-NH₂), 1.41 (s, 11H, NH₂, 3 × CH₃-C), 0.90 (s, 9H, 3 × CH₃-C).

2.2 General procedure for the synthesis of L-amino acid esters via DCC/DMAP coupling

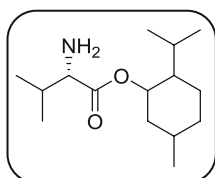
L-Valine menthyl esters (all three diastereomers), L-valine cyclohexyl ester and L-valine 4-(*tert*-butyl)cyclohexyl ester have been prepared by the following two step general procedure: ⁴



A solution of L-valine (5.0 g, 43 mmol, 1.0 equiv.) in 2 N NaOH (43 mL) was cooled to 0°C and Boc_2O (11.3 g, 51.6 mmol, 1.2 equiv.) was added slowly *via* syringe. The ice bath was removed and the reaction mixture stirred for 18 h at room temperature. The mixture was acidified (pH = 2) by using a 4 N HCl and extracted with EtOAc (3 × 50 mL). The combined organic phases were dried over anhydrous Na_2SO_4 and concentrated to give (*tert*-butoxycarbonyl)-L-valine as a colorless oil (8.3 g, 90%).

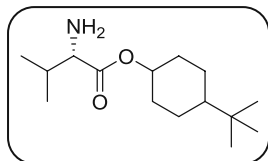
To a solution of (*tert*-butoxycarbonyl)-L-valine (1.0 equiv.) in dry CH_2Cl_2 , DCC (1.1 equiv.) was added at room temperature. The suspension was cooled to 0°C followed by the addition of the corresponding alcohol (1.0 equiv.) and DMAP (0.1 equiv.). The reaction mixture was stirred for 18 h at room temperature followed by the addition of EtOAc. After 10 min of stirring, the dicyclohexyl urea was filtered off, rinsed with EtOAc and the filtrate was successively washed with 1 N HCl solution, saturated NaHCO_3 solution, dried over anhydrous Na_2SO_4 and concentrated under reduced pressure. 4 N HCl in dioxane was added and the resulting mixture was stirred for 3 h at room temperature. The solvent was removed, Et_2O was added and stirred for 10 min. The amino acid HCl salt was filtered off, washed with Et_2O (3×) and dried in vacuo. The salt was suspended in CH_2Cl_2 , saturated NaHCO_3 was added and stirred for 2 h at room temperature. The organic phase was separated, washed with saturated NaHCO_3 (3×) and concentrated under reduced pressure to yield the corresponding esters.

Menthyl valinates (all diastereomers)



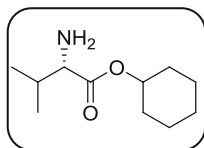
Colorless oil (DL: 58% yield, D: 55% yield, L: 58% yield). $^1\text{H NMR}$ (400 MHz, CDCl_3) δ 4.73 (td, $J = 10.9, 4.4$ Hz, 1H, CH-O), 3.29 (d, $J = 4.8$ Hz, 1H, CH-NH_2), 2.15 – 2.01 (m, 1H, $\text{CH-(CH}_3)_2$), 2.00 – 1.01 (m, 10H, NH_2 , *H*-menthol), 0.99 (d, $J = 6.9$ Hz, 3H, $\text{CH}_3\text{-CH}$), 0.90 (m, 9H, 2 × $\text{CH}_3\text{-CH}$, $\text{CH}_3\text{-CH-menthol}$), 0.76 (d, $J = 7.0$ Hz, 3H, $\text{CH}_3\text{-menthol}$); $^{13}\text{C NMR}$ (100 MHz, CDCl_3) δ 175.30, 74.88, 60.40, 47.08, 41.01, 34.37, 31.90, 31.53, 26.11, 23.09, 22.15, 21.01, 19.79, 16.65, 15.89.

4-(tert-Butyl)cyclohexyl-L-valinate



Colorless oil (18% yield). $^1\text{H NMR}$ (400 MHz, CDCl_3) δ 4.73 – 4.66 (m, 1H, CH-O), 3.30 (d, J = 4.8 Hz, 1H, CH-NH₂), 2.25 (s, 2H, NH₂), 2.12 – 1.94 (m, 3H, CH-(CH₃)₂, CH₂-CH-O), 1.85 – 1.75 (m, 2H, CH₂-CH-O), 1.41 – 1.22 (m, 2H, CH₂-CH-C-tbu), 1.18 – 1.00 (m, 2H, CH₂-CH-C-tbu), 0.99 (d, J = 6.9 Hz, 3H, CH₃-CH), 0.92 (d, J = 6.9 Hz, 3H, CH₃-CH), 0.85 (s, 9H, 3 × CH₃-C).

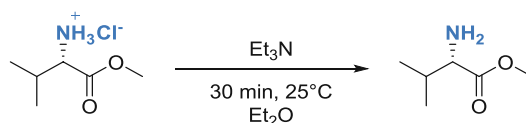
Cyclohexyl L-valinate⁵



Colorless oil (49% yield). $^1\text{H NMR}$ (400 MHz, CDCl_3) δ 4.93 – 4.64 (m, 1H, CH-O), 3.24 (d, J = 4.9 Hz, 1H, CH-NH₂), 2.05 – 1.97 (m, 1H, CH-(CH₃)₂), 1.81 (bs, 2H, NH₂), 1.74 – 1.00 (m, 10H, CH-cyclohexyl), 0.96 (d, J = 6.9 Hz, 3H, CH₃-CH), 0.88 (d, J = 6.9 Hz, 3H, CH₃-CH).

2.3 Synthesis of other L-amino acid esters

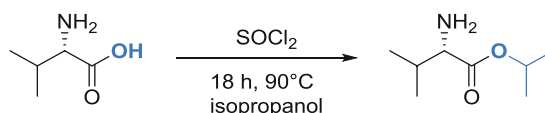
Methyl L-valinate⁶



To a slurry of L-valine methyl-ester hydrochloride (1.27 g, 7.6 mmol, 1.0 equiv.) in dry MeOH (1 mL), Et₃N (1.6 mL, 12 mmol, 1.6 equiv.) was added. After 10 min of stirring, dry Et₂O (30 mL) was added, the solution was cooled to 0°C and it was stirred for another 30 min. The triethylamine hydrochloride salt was filtered off and the filtrate was concentrated to yield the product as a colorless oil (800 mg, 81%).

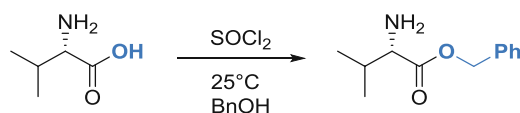
¹H NMR (400 MHz, CDCl₃) δ 3.70 (s, 3H, CH₃-O), 3.28 (d, *J* = 5.1 Hz, 1H, CH-NH₂), 2.11 – 1.93 (m, 1H, CH-(CH₃)₂), 1.45 (s, 2H, NH₂), 0.95 (d, *J* = 6.9 Hz, 3H, CH₃-CH), 0.88 (d, *J* = 6.9 Hz, 3H, CH₃-CH).

Isopropyl L-valinate⁷



To a solution of L-valine (1.0 g, 8.5 mmol, 1.0 equiv.) in isopropanol (26 mL, 341 mmol, 40 equiv.) was added thionyl chloride (3.1 mL, 43 mmol, 5.0 equiv.) at 0°C. The reaction mixture was then refluxed for 18 h. After cooling to room temperature, the solvent was evaporated, Et₂O (50 mL) was added and the amino acid hydrochloride salt was filtered off. CH₂Cl₂ (50 mL) was added, followed by the addition of sat. NaHCO₃ (50 mL) and the two phases were stirred for 30 min. The organic phase was washed several times with sat. NaHCO₃ (3 × 25 mL), dried over anhydrous Na₂SO₄ and concentrated to give the product as a colorless liquid (380 mg, 23%). **¹H NMR (400 MHz, CDCl₃)** δ 5.09 – 5.02 (m, 1H, CH-O), 3.26 (d, *J* = 4.9 Hz, 1H, CH-NH₂), 2.07 – 1.99 (m, 1H, CH-(CH₃)₂), 1.82 (s, 2H, NH₂), 1.42 – 1.16 (m, 6H, 2 × CH₃-CH-O), 0.98 (d, *J* = 6.9 Hz, 3H, CH₃-CH), 0.91 (d, *J* = 6.9 Hz, 3H, CH₃-CH).

Benzyl L-valinate⁸



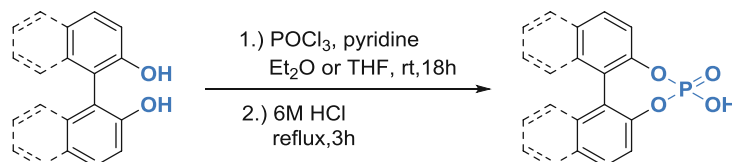
To a solution of L-valine (1.0 g, 8.5 mmol, 1.0 equiv.) in benzyl alcohol (26 mL, 341 mmol, 40 equiv.) was added thionyl chloride (3.1 mL, 43 mmol, 5.0 equiv.) at 0°C. The reaction mixture was then stirred for 18 hours at room temperature. Et₂O (50 mL) was added and the amino acid hydrochloride salt was

filtered off. CH_2Cl_2 (50 mL) was added, followed by the addition of sat. NaHCO_3 (50 mL) and the two phases were stirred for 30 min. The organic phase was washed several times with sat. NaHCO_3 (3×25 mL), dried over anhydrous Na_2SO_4 and concentrated under reduced pressure to give the product as a colorless liquid (1.12 g, 62%). $^1\text{H NMR}$ (400 MHz, CDCl_3) δ 7.37 – 7.32 (m, 5H, *H*-arom), 5.15 (dd, $J = 12.0$ Hz, 16.0 Hz, 1H, CH_2 -arom), 3.34 (d, $J = 4.0$ Hz, 1H, CH-NH_2), 2.08 – 2.01 (m, 1H, $\text{CH-(CH}_3)_2$), 1.68 (s, 2H, NH_2), 0.96 (d, $J = 6.9$ Hz, 3H, CH_3 -CH), 0.88 (d, $J = 6.9$ Hz, 3H, CH_3 -CH).

3. General synthesis of the phosphoric acids

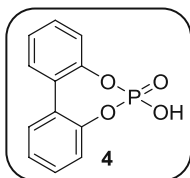
The phosphoric acids have been prepared following either a one or a two-step reaction pathway:

1.) One step procedure:⁹



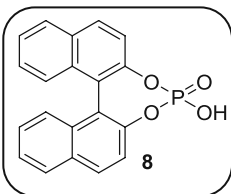
To a solution of the corresponding diol (1.0 equiv.) in dry Et₂O or THF pyridine (2.0 equiv.) was added. The reaction mixture was cooled to 0°C and POCl₃ (1.4 equiv.) was added slowly *via* syringe. The resulting reaction mixture was stirred for 18 h at room temperature. The pyridinium hydrochloride was filtered off and it was rinsed several times with Et₂O. The filtrate was concentrated and recrystallized from *n*-heptane. The white solid was filtered off, washed with *n*-heptane (3×) and hydrolyzed with 6 N HCl for 3 h at reflux temperature. Filtration gave the products as a white solid.

6-Hydroxydibenzo[*d,f*][1,3,2]dioxaphosphepine 6-oxide⁹



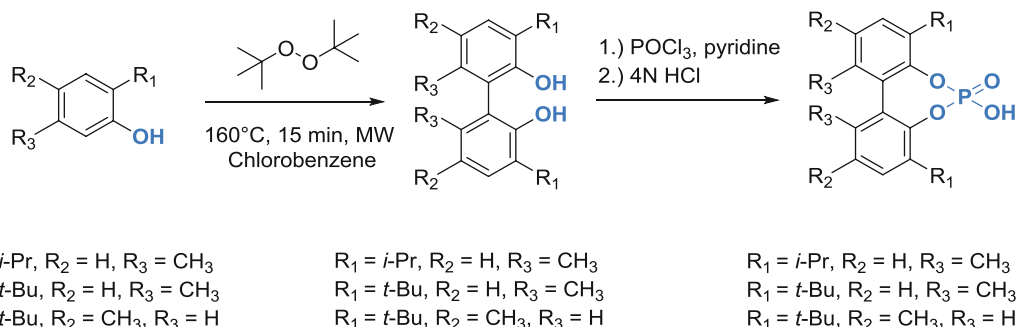
White solid (81% yield). ¹H NMR (400 MHz, DMSO-*d*₆) δ 7.63 (dd, *J* = 7.6, 1.7 Hz, 2H, *H*-arom), 7.50 (td, *J* = 7.8, 1.7 Hz, 2H, *H*-arom), 7.39 (tt, *J* = 7.5, 1.3 Hz, 2H, *H*-arom), 7.32 – 7.21 (m, 2H, *H*-arom); ³¹P NMR (162 MHz, DMSO-*d*₆) 1.72. Analytical data were in accordance with the literature.⁸

4-Hydroxydinaphtho[2,1-*d*:1',2'-*f*][1,3,2]dioxaphosphepine 4-oxide



White solid ((*S,R*): 89% yield, (*R*): 93% yield, (*S*): 94% yield). ¹H NMR (400 MHz, DMSO-*d*₆) δ 8.18 (d, *J* = 8.9 Hz, 2H, *H*-arom), 8.08 (d, *J* = 1.3 Hz, 2H, *H*-arom), 7.57 (dd, *J* = 8.8, 0.9 Hz, 2H, *H*-arom), 7.52 (ddd, *J* = 8.1, 6.7, 1.2 Hz, 2H, *H*-arom), 7.37 (ddd, *J* = 8.3, 6.8, 1.4 Hz, 2H, *H*-arom), 7.23 (dd, *J* = 8.5, 1.1 Hz, 2H, *H*-arom); ³¹P NMR (162 MHz, DMSO-*d*₆) 2.66. Analytical data were in accordance with the literature.⁸

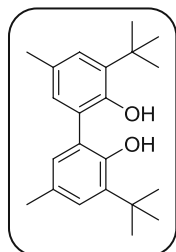
2.) Two step procedure: ^{10, 11}



In a 20 mL microwave vial equipped with a stir bar, the corresponding phenol (1.0 equiv.) was dissolved in chlorobenzene (1.66 M). Di-*tert*-butyl peroxide (1.05 equiv.) was then added *via* syringe. The vial was capped and the reaction mixture was stirred for 15 min at room temperature. The vial was then placed in the microwave reactor and heated to 160°C (high absorption setting) and stirred for 15 min. The reaction mixture was allowed to cool down and volatiles have been removed under reduced pressure. The resulting crude mixture was purified by column chromatography (EtOAc: PE, UV visualization) to afford the desired 2,2'-diols (**Step A**).

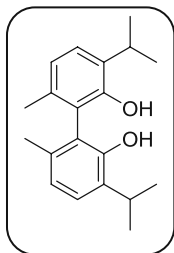
To a solution of the corresponding 2,2'-diol (1.0 equiv.) in pyridine, POCl₃ (2.0 equiv.) was added slowly *via* syringe at 0°C. After stirring the reaction mixture for 24 h at 95°C, it was cooled to room temperature and distilled H₂O was added slowly. The resulting clear solution was stirred for another 18 h at 95 °C. After cooling down to room temperature, 4 N HCl was added slowly. The precipitate of the product was filtered off and washed with 4 N HCl. The solid product was further hydrolyzed by re-dissolving it in CH₂Cl₂ and washing several times with 4 N HCl (3-4×) After being dried over anhydrous Na₂SO₄, removal of the solvent gave the phosphoric acids (**Step B**).

3,3'-Di-*tert*-butyl-5,5'-dimethyl-[1,1'-biphenyl]-2,2'-diol (STEP A) ¹²



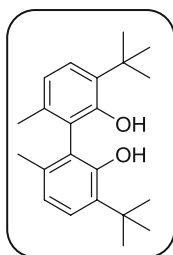
Column chromatography (1.5% EtOAc in light petrol) afforded the product as pale yellow solid (53% yield). ¹H NMR (400 MHz, CDCl₃) δ 7.20 (d, *J* = 2.1 Hz, 2H, *H*-arom), 6.94 (d, *J* = 2.1 Hz, 2H, *H*-arom), 5.24 (s, 2H, 2 × OH), 2,36 (s, 6H, 2 × CH₃), 1.48 (s, 18H, 6 × CH₃-C).

3,3'-Diisopropyl-6,6'-dimethyl-[1,1'-biphenyl]-2,2'-diol (STEP A)¹³



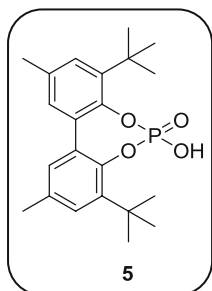
Column chromatography (2% EtOAc in light petrol) afforded the product as light yellow oil (58% yield). ¹H NMR (400 MHz, CDCl₃) δ 7.19 (d, *J* = 7.7 Hz, 2H, *H*-arom), 6.89 (d, *J* = 7.8 Hz, 2H, *H*-arom), 4.76 (s, 2H, 2 × OH), 3.32 – 3.25 (m, 2H, 2 × CH-(CH₃)₂), 1.96 (s, 6H, 2 × CH₃), 1.26 (dd, *J* = 6.9, 2.7 Hz, 12H, 4 × CH₃-CH); ¹³C NMR (100 MHz, CDCl₃) δ 150.99, 135.67, 132.57, 126.75, 122.22, 119.38, 27.17, 22.64, 22.50, 19.26.

3,3'-Di-tert-butyl-6,6'-dimethyl-[1,1'-biphenyl]-2,2'-diol (STEP A)¹⁴



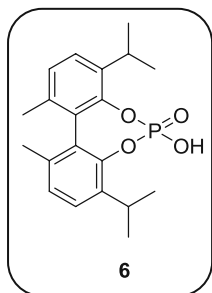
Column chromatography (1.5% EtOAc in light petrol) afforded the product as white solid (45% yield). ¹H NMR (400 MHz, CDCl₃) δ 7.27 (d, *J* = 8.0 Hz, 2H, *H*-arom), 6.87 (d, *J* = 8.0 Hz, 2H, *H*-arom), 5.01 (s, 2H, 2 × OH), 1.94 (s, 6H, 2 × CH₃), 1.42 (s, 18H, 6 × CH₃-C); ¹³C NMR (100 MHz, CDCl₃) δ 152.35, 134.08, 127.50, 121.97, 120.26, 34.79, 29.64, 19.28.

4,8-Di-tert-butyl-6-hydroxy-2,10-dimethyldibenzo[d,f][1,3,2]dioxaphosphepine 6-oxide (STEP B)¹⁵



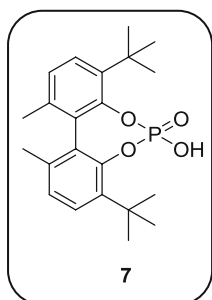
Grey solid (63% yield). ¹H NMR (400 MHz, CDCl₃) δ 7.26 (s, 2H, *H*-arom), 7.02 (s, 2H, *H*-arom), 2.36 (s, 6H, 2 × CH₃), 1.50 (s, 18H, 6 × CH₃-C); ³¹P NMR (162 MHz, CDCl₃) δ 0.48. Analytical data were in accordance with the literature.¹⁶

6-Hydroxy-4,8-diisopropyl-1,11-dimethyldibenzo[d,f][1,3,2]dioxaphosphepine-6-oxide (STEP B)



Brown solid (85% yield). ¹H NMR (400 MHz, CDCl₃) δ 7.27 (d, *J* = 8.0 Hz, 2H, *H*-arom), 7.15 (d, *J* = 8.0 Hz, 2H, *H*-arom), 3.49 – 3.45 (m, 2H, 2 × CH-(CH₃)₂), 2.14 (s, 6H, 2 × CH₃), 1.27 (dd, *J* = 25.5, 6.9 Hz, 12H, 4 × CH₃-CH); ³¹P NMR (162 MHz, CDCl₃) δ 2.40; ¹³C NMR (100 MHz, CDCl₃) δ 145.40, 137.74, 136.08, 128.02, 127.11, 126.31, 26.60, 24.10, 22.75, 19.67; IR ATR (ν_{max}/cm⁻¹) 2963 (O-H), 2872 (C-H), 1610 (C=C), 1204 (C-O), 967 (C-H), 818 (C-H arom); HRMS (ESI-TOF) [M + Na]⁺ calc. 383.1388, found 383.1389.

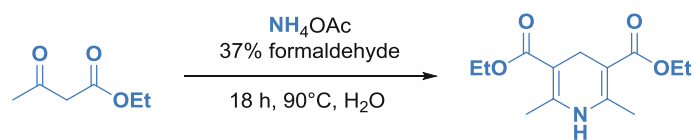
4,8-Di-tert-butyl-6-hydroxy-1,11-dimethyldibenzo[d,f][1,3,2]dioxaphosphepine 6-oxide (STEP B)



White solid (66% yield). $^1\text{H NMR}$ (400 MHz, CDCl_3) δ 7.38 (dd, $J = 8.0, 1.5$ Hz, 2H, H -arom), 7.11 (dd, $J = 11.8, 8.2$ Hz, 2H, H -arom), 2.01 (d, $J = 27.3$ Hz, 6H, $2 \times \text{CH}_3$), 1.48 (d, $J = 12.4$ Hz, 18H, $6 \times \text{CH}_3\text{-C}$); $^{31}\text{P NMR}$ (162 MHz, CDCl_3) δ 3.99; $^{13}\text{C NMR}$ (100 MHz, CDCl_3) δ 144.48, 144.31, 140.81, 140.72, 134.81, 130.10, 129.91, 128.89, 35.18, 31.26, 21.10; IR ATR ($\nu_{\text{max}}/\text{cm}^{-1}$) 2961 (O-H), 2872 (C-H), 1610 (C=C), 1308 (C-O), 1023 (C-H), 901 (C-H arom); HRMS (ESI-TOF) $[\text{M} + \text{Na}]^+$ calc. 411.1701, found 411.1732.

4. Synthesis of the Hantzsch ester

Diethyl 2,6-dimethyl-1,4-dihydropyridine-3,5-dicarboxylate¹⁷



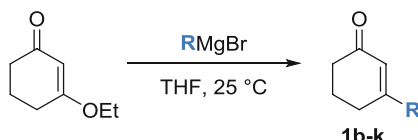
Compound was prepared by the following modified literature procedure.

A mixture of formaldehyde (37% aqueous solution, 4.0 g, 49 mmol, 1.0 equiv.), NH_4OAc (7.6 g, 99 mmol, 2.0 equiv.), ethyl acetoacetate (26 g, 0.2 mol, 4.0 equiv.) and distilled H_2O (100 mL) was refluxed at 90°C for 18 h. After cooling the reaction mixture to room temperature, cold distilled H_2O (100 mL) was added, the crude product was filtered off, washed with cold distilled H_2O (100 mL) and dried in vacuo. Recrystallization from MeOH gave the product as a yellow solid (7.5 g, 60%). $^1\text{H NMR}$ (400 MHz, CDCl_3) δ 5.19 (s, 1H, NH), 4.16 (q, $J = 7.1$ Hz, 4H, $2 \times \text{CH}_2\text{-O}$), 3.26 (s, 2H, CH_2), 2.19 (s, 6H, $2 \times \text{CH}_3$), 1.28 (t, $J = 7.1$ Hz, 6H, $2 \times \text{CH}_3\text{-CH}_2\text{-O}$).

5. Synthesis of ATH substrates

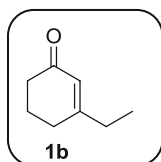
3-Methyl-2-cyclohexenone, 3-methyl-cyclopentenone and isophorone have been purchased from commercial supplier (*Sigma Aldrich*).

The remaining 3-alkylcyclohexenones and 3-arylcyclohexanones have been prepared by the following procedure, starting from 3-ethoxycyclohexenone (*Acros Organics*):¹⁸



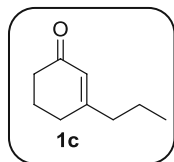
A 3 M solution of the Grignard reagent was prepared freshly from freshly ground Mg (1.0 equiv.), alkyl/aryl bromide (1.0 equiv.) in dry THF, and it was refluxed for 1 h. After being cooled to 0°C, 3-ethoxycyclohexenone (1.0 equiv.) was added slowly and the reaction mixture was stirred for 18 h at room temperature. The reaction was quenched with 1 N HCl solution (50 mL) at 0°C. Et₂O was added and the organic phase was washed with 1 N HCl solution (3 × 25 mL), sat. NaHCO₃ (3 × 25 mL), dried over anhydrous Na₂SO₄ and concentrated under reduced pressure. The crude products were purified by column chromatography (Et₂O: PE, UV TLC visualization) to provide the pure products.

3-Ethyl-2-cyclohexenone¹⁹



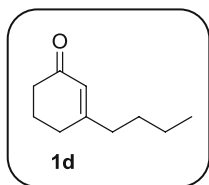
Column chromatography (25% Et₂O in PE) afforded the product as a yellow oil (67% yield). ¹H NMR (400 MHz, CDCl₃) δ 5.87 (s, 1H, CH), 2.45 – 2.11 (m, 6H, CH₂-CO, CH₂-CH₂-CO, CH₂-C-ethyl), 2.07 – 1.81 (m, 2H, CH₂-CH₃), 1.09 (t, J = 7.4 Hz, 3H, CH₃).

3-Propyl-2-cyclohexenone²⁰



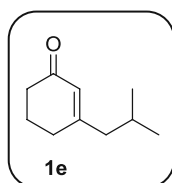
Column chromatography (25% Et₂O in PE) afforded the product as a yellow oil (60% yield). ¹H NMR (400 MHz, CDCl₃) δ 5.87 (s, 1H, CH), 2.53 – 2.07 (m, 6H, CH₂-CO, CH₂-CH₂-CO, CH₂-C-propyl), 2.07 – 1.73 (m, 2H, CH₂-CH₂-CH₃), 1.68 – 1.36 (m, 2H, CH₂-CH₃), 0.93 (t, J = 7.4 Hz, 3H, CH₃).

3-Butyl-2-cyclohexenone²¹



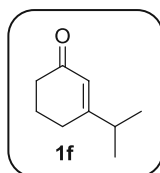
Column chromatography (30% Et₂O in PE) afforded the product as a yellow oil (74% yield). ¹H NMR (400 MHz, CDCl₃) δ 5.86 (s, 1H, CH), 2.48 – 2.09 (m, 6H, CH₂-CO, CH₂-CH₂-CO, CH₂-C-butyl), 2.06 – 1.79 (m, 2H, CH₂-CH₂-CH₂-CH₃), 1.61 – 1.15 (m, 4H, CH₂-CH₂-CH₃), 0.91 (t, *J* = 7.0 Hz, 3H, CH₃).

3-Isobutyl-2-cyclohexenone²²



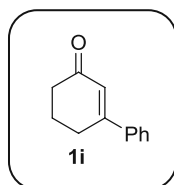
Column chromatography (25% Et₂O in PE) afforded the product as a yellow oil (69% yield). ¹H NMR (400 MHz, CDCl₃) δ 5.84 (s, 1H, CH), 2.54 – 2.17 (m, 4H, CH₂-CO, CH₂-CH₂-CO), 2.18 – 1.56 (m, 5H, CH₂-C-isobutyl, CH₂-CH(CH₃)₂, CH₂-CH(CH₃)₂), 0.90 (d, *J* = 6.5 Hz, 6H, 2 × CH₃-CH).

3-Isopropyl-2-cyclohexenone²³



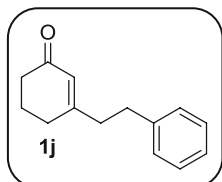
Column chromatography (25% Et₂O in PE) afforded the product as a yellow oil (10% yield). ¹H NMR (400 MHz, CDCl₃) δ 5.88 (s, 1H, CH), 2.61 – 2.17 (m, 5H, CH₂-CO, CH₂-CH₂-CO, CH-(CH₃)₂), 2.13 – 1.81 (m, 2H, CH₂-C-isopropyl), 1.10 (d, *J* = 6.9 Hz, 6H, 2 × CH₃-CH).

3-Phenyl-2-cyclohexenone²⁴



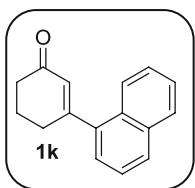
Column chromatography (30% Et₂O in PE) afforded the product as a white solid (88% yield). ¹H NMR (400 MHz, CDCl₃) δ 7.53 – 7.41 (m, 5H, *H*-arom), 6.42 (s, 1H, CH), 2.85 – 2.78 (m, 2H, CH₂-CO), 2.62 – 2.49 (m, 2H, CH₂-CH₂-CO), 2.18 – 2.14 (m, 2H, CH₂-C-phenyl).

3-Phenethyl-2-cyclohexenone²⁵



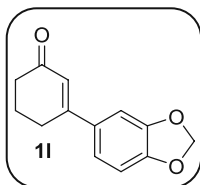
The formation of the grignard-reagent and the reaction have been carried out at 40°C. Column chromatography (30% Et₂O in PE) afforded the product as a light yellow oil (91% yield). ¹H NMR (200 MHz, CDCl₃) δ 7.34 – 7.15 (m, 5H, *H*-arom), 5.90 (s, 1H, CH), 2.89 – 2.76 (m, 2H, CH₂-CO), 2.58 – 2.47 (m, 2H, CH₂-CH₂-CO), 2.40 – 2.26 (m, 4H, phenyl-CH₂-CH₂) 2.05 – 1.92 (m, 2H, CH₂-C-phenyl).

3-(Naphthalen-1-yl)-2-cyclohexenone²⁶



Column chromatography (30% - 50% Et₂O in PE) afforded the product as a yellow oil (94% yield). ¹H NMR (200 MHz, CDCl₃) δ 7.92 – 7.82 (m, 3H, *H*-arom), 7.54 – 7.45 (m, 3H, *H*-arom), 7.35 – 7.28 (m, 1H, *H*-arom), 6.21 (s, 1H, CH), 2.82 – 2.74 (m, 2H, CH₂-CO), 2.64 – 2.56 (m, 2H, CH₂-CH₂-CO), 2.33 – 2.19 (m, 2H, CH₂-C-arom).

3-Piperonyl-2-cyclohexenone²⁷

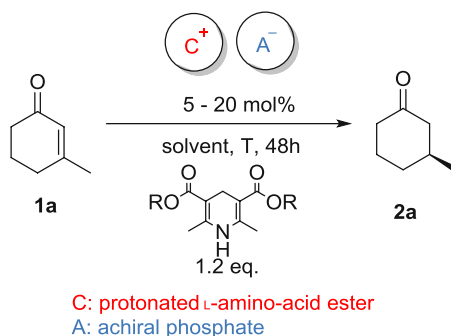


Column chromatography (30% Et₂O in PE) afforded the product as a yellow foam (90% yield). ¹H NMR (200 MHz, CDCl₃) δ 7.06 (ddd, *J* = 8.0 Hz, 4.0 Hz, 2.0 Hz, 2H, *H*-arom), 6.83 (d, *J* = 8.0 Hz, 1H, *H*-arom), 6.33 (s, 1H, CH), 6.01 (s, 2H, OCH₂), 2.76 – 2.67 (t, *J* = 6.0 Hz, 2H, CH₂-CO), 2.50 – 2.41 (t, *J* = 6.0 Hz, 2H, CH₂-CH₂-CO), 2.19 – 2.06 (m, 2H, CH₂-C-arom).

6. General procedure and optimization of the ATH reactions

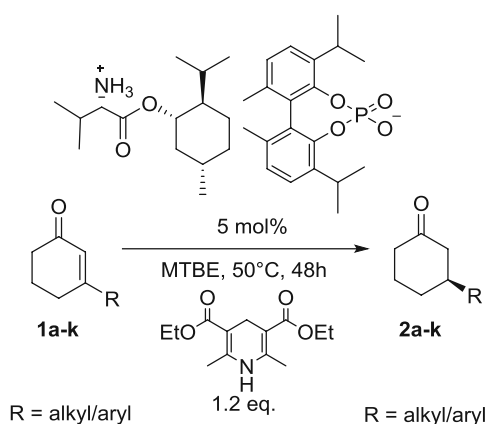
6.1 General procedures

General procedure for parameter optimization



An 8 mL screw cap vial equipped with a magnetic stir bar was charged with 3-methylcyclohexenone (0.18 mmol, 1.0 equiv.) in the appropriate solvent (0.55 mL, 0.33 M), followed by the addition of the catalyst (0.009 – 0.036 mmol, 5 mol% – 20 mol%) and the appropriate Hantzsch ester (0.22 mmol, 1.2 equiv.). The reaction mixture was stirred at the given temperature for 48 h. The conversion and yield have been determined by GC measurement by using *n*-dodecane as internal standard, while chiral GC have been used to determine the enantiomeric excess.

General procedure for scope and limitations

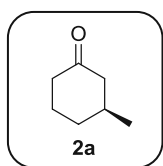


A 20 mL microwave vial equipped with a magnetic stir bar was charged with ketone (1.8 mmol, 1.0 equiv.) in MTBE (5.5 mL, 0.33 M), followed by the addition of the catalyst (55.4 mg, 0.09 mmol, 5 mol%) and Hantzsch ester (552 mg, 2.2 mmol, 1.2 equiv.). The reaction mixture was stirred at 50°C for 48 h. After cooling to room temperature, Et₂O (5 mL) and 4 M HCl (10 mL) was added and the mixture was stirred until the phases were transparent (30 min). The phases were separated and the organic phase

was washed with 4 M HCl (3 × 20 mL). The organic phase was dried over Na₂SO₄ and concentrated under reduced pressure. Purification by column chromatography (Et₂O: PE, vanillin staining agent or UV visualization) gave the 3-substituted cyclohexanones.

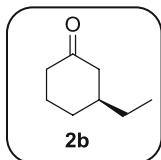
6.2 Analytical data of ATH products

(S)-3-Methylcyclohexanone



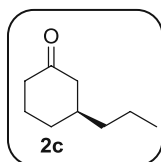
Column chromatography (25% Et₂O in PE) afforded the product as a colorless oil. GC yield: 98%, isolated yield: 72% due to high volatility, 95% ee. $[\alpha]_{\text{D}}^{20}$: -11.1 (c = 1.0, CHCl₃); ¹H NMR (400 MHz, CDCl₃) δ 2.41 – 2.21 (m, 3H), 2.09 – 1.82 (m, 4H), 1.76 – 1.57 (m, 1H), 1.42 – 1.24 (m, 1H), 1.02 (d, J = 6.4 Hz, 3H). **Determination of the enantiomeric excess** BGB175 column (85°C isotherm 20 min, 30°C/min to 220°C): t_R (S) = 9.0 min, t_R (R) = 9.6 min.

(S)-3-Ethylcyclohexanone



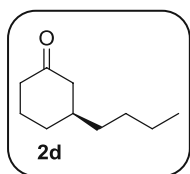
Column chromatography (25% Et₂O in light petrol) afforded the product as a colorless oil. GC yield: 85%, isolated yield: 76% due to high volatility, 92% ee. $[\alpha]_{\text{D}}^{20}$: -15.6 (c = 1.0, CHCl₃); ¹H NMR (400 MHz, CDCl₃) δ 2.45 – 2.23 (m, 3H), 2.09 – 1.87 (m, 3H), 1.76 – 1.63 (m, 2H), 1.41 – 1.28 (m, 3H), 0.91 (t, J = 7.5 Hz, 3H). **Determination of the enantiomeric excess** BGB173 column (52°C isotherm 110 min, 30°C/min to 220°C): t_R (R) = 51.0 min, t_R (S) = 54.9 min.

(S)-3-Propylcyclohexanone



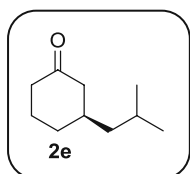
Column chromatography (25% Et₂O in PE) afforded the product as a colorless oil. GC yield: 70%, isolated yield: 55% due to high volatility, 91% ee. $[\alpha]_{\text{D}}^{20}$: -14.7 (c = 1.0, CHCl₃); ¹H NMR (400 MHz, CDCl₃) δ 2.42 – 2.22 (m, 3H), 2.06 – 1.86 (m, 3H), 1.80 – 1.74 (m, 1H), 1.67 – 1.59 (m, 1H), 1.35 – 1.26 (m, 5H), 0.92 – 0.86 (m, 3H). **Determination of the enantiomeric excess** BGB175 column (70°C isotherm 60 min, 1°C/min to 150 °C, 5 min at 150°C, 30°C/min to 220°C): t_R (S) = 50.6 min, t_R (R) = 53.1 min.

(S)-3-Butylcyclohexanone



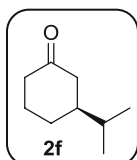
Column chromatography (25% Et₂O in PE) afforded the product as a colorless oil. GC yield: 91%, isolated yield: 87%, 93% ee. $[\alpha]_{\text{D}}^{20}$: -15.0 (c = 1.0, CHCl₃); ¹H NMR (400 MHz, CDCl₃) δ 2.44 – 1.56 (m, 7H), 1.40 – 1.09 (m, 7H), 0.91 – 0.82 (m, 4H). **Determination of the enantiomeric excess** BGB175 column (70 °C isotherm 60 min, 1°C/min to 150°C, 5 min at 150°C, 30 °C /min to 220°C): t_R (S) = 76.9 min, t_R (R) = 78.1 min.

(S)-3-Isobutylcyclohexanone



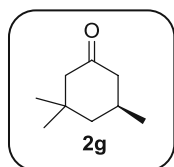
Column chromatography (25% Et₂O in PE) afforded the product as a colorless oil. GC yield: 85%, isolated yield: 60% due to high volatility, 86% ee. $[\alpha]_{\text{D}}^{20}$: -11.3 (c = 1.0, CHCl₃); ¹H NMR (400 MHz, CDCl₃) δ 2.42 – 2.21 (m, 2H), 2.03 – 1.61 (m, 4H), 1.66 – 1.41 (m, 2H), 1.33 – 1.10 (m, 3H), 0.89 – 0.84 (m, 6H). **Determination of the enantiomeric excess** BGB175 column (70 °C isotherm 5 min, 0.5 °C/min to 110°C, 5 min at 110°C, 30°C /min to 220°C): t_R (R) = 39.2 min, t_R (S) = 40.7 min.

(S)-3-Isopropylcyclohexanone



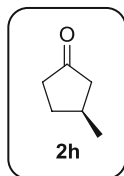
Column chromatography (25% Et₂O in PE) afforded the product as a colorless oil. GC yield: 75%, isolated yield: 68% due to high volatility, 88% ee. $[\alpha]_{\text{D}}^{20}$: -12.4 (c = 1.0, CHCl₃); ¹H NMR (400 MHz, CDCl₃) δ 2.44 – 1.23 (m, 10H), 0.92 (d, J = 6.0 Hz, 3H), 0.90 (d, J = 6.0 Hz, 3H). **Determination of the enantiomeric excess** BGB175 column (85°C isotherm 20 min, 30°C/min to 220°C): t_R (R) = 20.75 min, t_R (S) = 20.96 min.

(S)-3,5,5-Trimethylcyclohexanone



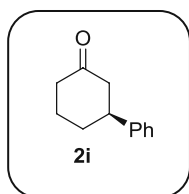
Column chromatography (25% Et₂O in PE) afforded the product as a colorless oil. GC yield: 66%, isolated yield: 60% due to high volatility, 92% ee. $[\alpha]_{\text{D}}^{20}$: -11.9 (c = 1.0, CHCl₃); ¹H NMR (400 MHz, CDCl₃) δ 2.33 – 2.14 (m, 2H), 1.92 – 1.83 (m, 3H), 1.60 – 1.56 (m, 1H), 1.38 – 1.25 (m, 2H), 1.05 – 1.01 (m, 5H), 0.88 (s, 3H). **Determination of the enantiomeric excess** BGB175 column (85°C isotherm 20 min, 30°C/min to 220°C): t_R (S) = 13.4 min, t_R (R) = 17.9 min.

(S)-3-Methylcyclopentanone



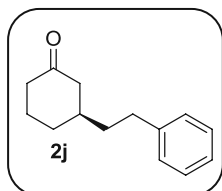
Column chromatography (25% Et₂O in PE) afforded the product as a colorless oil. GC yield: 94%, isolated yield: 80% due to high volatility, 89% ee. $[\alpha]_{\text{D}}^{20}$: -13.2 (c = 1.0, CHCl₃); ¹H NMR (200 MHz, CDCl₃) δ 3.22 – 2.70 (m, 1H), 2.51 – 1.81 (m, 5H), 1.32 – 1.29 (m, 1H), 1.11 – 1.02 (m, 3H). **Determination of enantiomeric excess** BGB175 column (85°C isotherm 20 min, 30°C/min to 220°C): t_R (S) = 8.1 min, t_R (R) = 8.5 min.

(S)-3-Phenylcyclohexanone



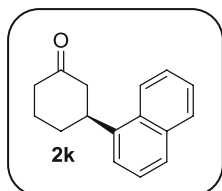
Column chromatography (25% Et₂O in light petrol) afforded the product as a colorless oil. GC yield: 86%, isolated yield: 84%, 82% ee. $[\alpha]_{\text{D}}^{20}$: -17.2 (c = 1.0, CHCl₃); ¹H NMR (200 MHz, CDCl₃) δ 7.39 – 7.37 (m, 2H), 7.32 – 7.27 (m, 3H), 3.11 – 3.00 (m, 1H), 2.68 – 2.44 (m, 4H), 2.23 – 2.15 (m, 2H), 1.93 – 1.81 (m, 2H). **Determination of the enantiomeric excess** BGB175 column (120°C isotherm 55 min, 30°C /min to 220°C): t_R (R) = 48.8 min, t_R (S) = 49.5 min.

(S)-3-Phenethylcyclohexanone



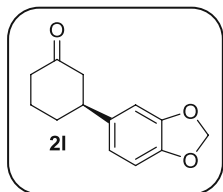
Column chromatography (25% Et₂O in light petrol) afforded the product as a colorless oil. GC yield: 94%, isolated yield: 91%, 90% ee. ¹H NMR (200 MHz, CDCl₃) δ 7.37 – 7.22 (m, 5H), 2.75 – 2.33 (m, 5H), 2.14 – 1.70 (m, 7H), 1.49 – 1.38 (m, 1H). **Determination of the enantiomeric excess** Chiralcel Diacel AS-H column (n-heptane/*i*-PrOH 97/3 V/V%, 1 mL/min, 25°C, λ = 220 nm): t_R (R) = 15.6 min, t_R (S) = 16.6 min.

(S)-3-(Naphthalen-1-yl)cyclohexanone



Column chromatography (25% Et₂O in light petrol) afforded the product as a colorless oil. GC yield: 65%, isolated yield: 62%, 94% ee. $[\alpha]_{\text{D}}^{20}$: -49.2 (c = 1.0, CHCl₃); ¹H NMR (200 MHz, CDCl₃) δ 8.05 – 7.75 (m, 3H), 7.54 – 7.38 (m, 4H), 3.92 – 3.82 (m, 1H), 2.75 – 1.94 (m, 8H). **Determination of the enantiomeric excess** Chiralcel Diacel AS-H column (n-heptane/*i*-PrOH 95/5 V/V%, 1mL/min, 25°C, λ = 220 nm): t_R (R) = 13.8 min, t_R (S) = 22.7 min.

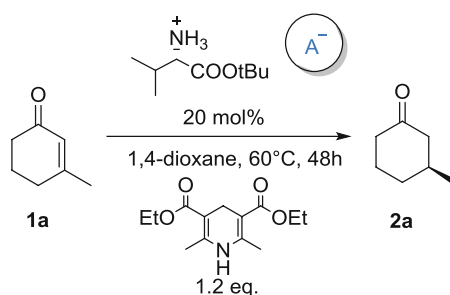
(S)-3-Piperonycyclohexanone



Column chromatography (25% Et₂O in light petrol) afforded the product as a colorless oil. GC yield: 65%, isolated yield: 62%, 94% ee. $[\alpha]_{\text{D}}^{20}$: -15.3 (c = 1, CHCl₃); ¹H NMR (200 MHz, CDCl₃) δ 6.74 – 6.63 (m, 3H), 5.93 (s, 2H), 2.98 – 2.87 (m, 2H), 2.54 – 2.39 (m, 4H), 2.17 – 2.02 (m, 2H), 1.83 – 1.73 (m, 2H). **Determination of enantiomeric excess** Chiralcel Diacel AS-H column (*n*-heptane/*i*-PrOH 85/15 V/V%, 1 mL/min, 25 °C, λ = 220 nm): t_R (S) = 23.5 min, t_R (R) = 28.0 min.

6.3 Optimization of reaction conditions

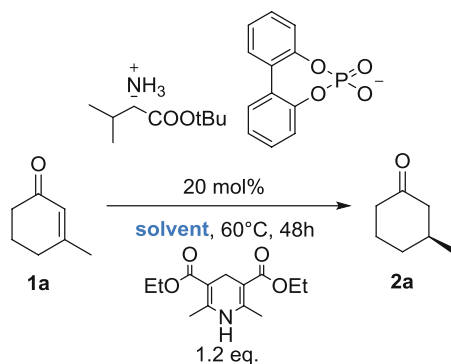
Table S1.: Proof of concept in 1,4-dioxane



| Entry ^a | Counteranion | Yield ^b [%] | ee ^c [%] | Δee ^d [%] |
|--------------------|--------------|------------------------|---------------------|----------------------|
| 1 | | 49 | 54 (S) | - |
| 2 | | 49 | 54 (S) | - |
| 3 | | 27 | 64 (S) | + 10 |
| 4 ^e | | 72 | 74 (S) | + 23 |
| 5 | | 13 | 54 (S) | 0 |
| 6 | | 13 | 54 (S) | 0 |
| 7 | | 15 | 54 (S) | 0 |

^a Performed with 0.18 mmol 3-methyl-2-cyclohexenone, 0.036 mmol catalyst, 0.22 mmol Hantzsch ethyl ester in 0.55 mL 1,4-dioxane at 60°C for 48 hours. ^b Determined by GC analysis using *n*-dodecane as internal standard. ^c Determined by chiral GC analysis using a BGB175 chiral capillary column. Absolute configurations have been determined by measuring the optical rotation and comparing with literature data. ^d ee difference compare to the reaction with TFA counteranion. ^e MTBE was used as solvent.

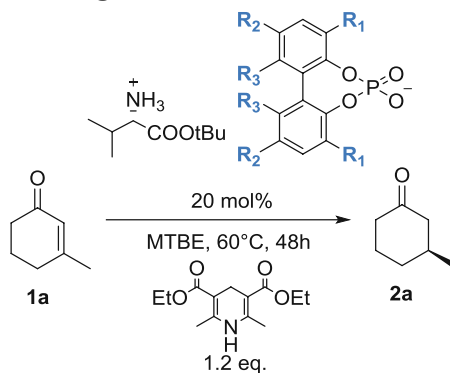
Table S2.: Solvent screening

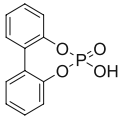
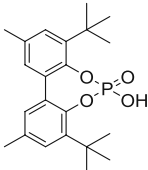
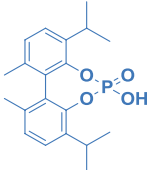
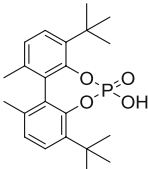


| Entry ^a | Solvent | Yield ^b [%] | ee ^c [%] |
|--------------------|-------------------|------------------------|---------------------|
| 1 | EtOAc | 48 | 67 (S) |
| 2 | BuOAc | 41 | 62 (S) |
| 3 | THF | 60 | 68 (S) |
| 4 | 1,4-Dioxane | 27 | 64 (S) |
| 5 | MTBE | 72 | 74 (S) |
| 6 | Bu ₂ O | 16 | 62 (S) |
| 7 | Toluene | 17 | 75 (S) |
| 8 | CHCl ₃ | 23 | 53 (S) |
| 9 | H ₂ O | 9 | 42 (S) |
| 10 | MeOH | 10 | 30 (S) |
| 11 | EtOH | 20 | 50 (S) |
| 12 | ⁱ PrOH | 26 | 57 (S) |
| 13 | ^t BuOH | 30 | 60 (S) |
| 14 | Acetonitrile | 17 | 37 (S) |

^a Performed with 0.18 mmol 3-methyl-2-cyclohexenone, 0.036 mmol catalyst, 0.22 mmol Hantzsch ethyl ester in 0.55 mL solvent at 60°C for 48 hours. ^b Determined by GC analysis using *n*-dodecane as internal standard. ^c Determined by chiral GC analysis using a BGB175 chiral capillary column. Absolute configurations have been determined by measuring the optical rotation and comparing with literature data.

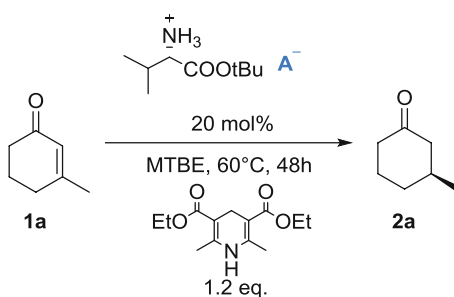
Table S3.: Phosphoric acid screening

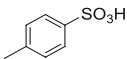
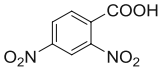
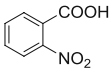
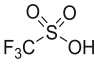
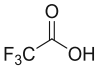
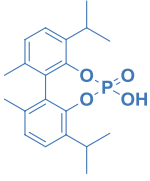


| Entry ^a | Phosphoric acid | Yield ^b [%] | ee ^c [%] |
|--------------------|---|------------------------|---------------------|
| 1 |  4 | 72 | 74 (<i>S</i>) |
| 2 |  5 | 70 | 77 (<i>S</i>) |
| 3 |  6 | 94 | 80 (<i>S</i>) |
| 4 |  7 | 43 | 76 (<i>S</i>) |

^a Performed with 0.18 mmol 3-methyl-2-cyclohexenone, 0.036 mmol catalyst, 0.22 mmol Hantzsch ethyl ester in 0.55 mL MTBE at 60°C for 48 hours. ^b Determined by GC analysis using *n*-dodecane as internal standard. ^c Determined by chiral GC analysis using a BGB175 chiral capillary column. Absolute configurations have been determined by measuring the optical rotation and comparing with literature data.

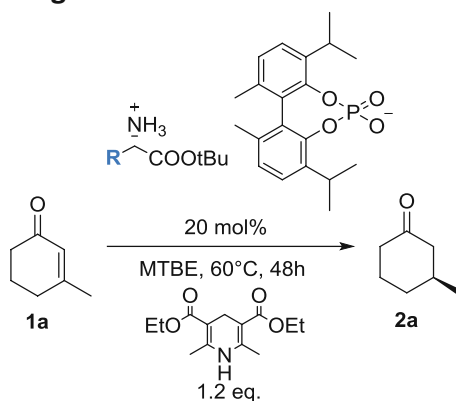
Table S4.: Comparison of selectivity by screening other acids



| Entry ^a | Acid | Yield ^b [%] | ee ^c [%] |
|--------------------|---|------------------------|---------------------|
| 1 |  | 34 | 58 (S) |
| 2 |  | 91 | 37 (S) |
| 3 |  | 93 | 45 (S) |
| 4 | HOOC-CH ₂ -COOH | 45 | 55 (S) |
| 5 |  | 40 | 52 (S) |
| 6 |  | 88 | 51 (S) |
| 7 |  | 94 | 80 (S) |

^a Performed with 0.18 mmol 3-methyl-2-cyclohexenone, 0.036 mmol catalyst, 0.22 mmol Hantzsch ethyl ester in 0.55 mL MTBE at 60°C for 48 hours. ^b Determined by GC analysis using *n*-dodecane as internal standard. ^c Determined by chiral GC analysis using a BGB175 chiral capillary column. Absolute configurations have been determined by measuring the optical rotation and comparing with literature data.

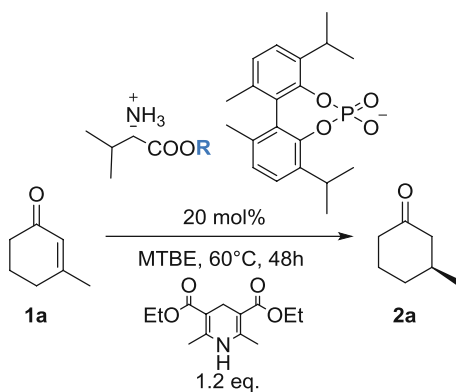
Table S5: L-Amino acid screening



| Entry ^a | L-amino acid | Yield ^b [%] | ee ^c [%] |
|--------------------|--------------|------------------------|---------------------|
| 1 | | 94 | 80 (S) |
| 2 | | 52 | 77 (S) |
| 3 | | 73 | 72 (S) |
| 4 | | 55 | 9 (S) |
| 5 | | 83 | 60 (S) |
| 6 | | 91 | 76 (S) |
| 7 | | 73 | 33 (S) |

^a Performed with 0.18 mmol 3-methyl-2-cyclohexenone, 0.036 mmol catalyst, 0.22 mmol Hantzsch ethyl ester in 0.55 mL MTBE at 60°C for 48 hours. ^b Determined by GC analysis using *n*-dodecane as internal standard. ^c Determined by chiral GC analysis using a BGB175 chiral capillary column. Absolute configurations have been determined by measuring the optical rotation and comparing with literature data.

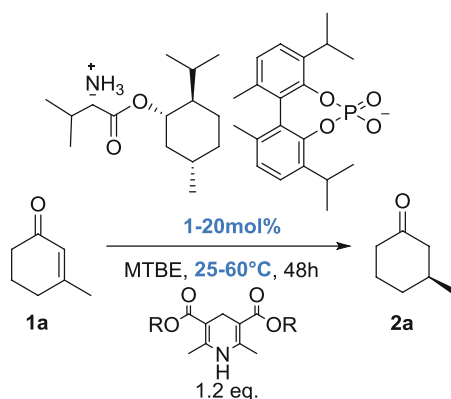
Table S6: Ester screening



| Entry ^a | L-valine ester | Yield ^b [%] | ee ^c [%] |
|--------------------|----------------|------------------------|---------------------|
| 1 | | 94 | 80 (S) |
| 2 | | 90 | 76 (S) |
| 3 | | 70 | 57 (S) |
| 4 | | 95 | 50 (S) |
| 5 | | 92 | 74 (S) |
| 6 | | 94 | 73 (S) |
| 7 | | 98 | 85 (S) |
| 8 | | 98 | 93 (S) |
| 9 | | 98 | 82 (S) |

^a Performed with 0.18 mmol 3-methyl-2-cyclohexenone, 0.036 mmol catalyst, 0.22 mmol Hantzsch ethyl ester in 0.55 mL MTBE at 60°C for 48 hours. ^b Determined by GC analysis using *n*-dodecane as internal standard. ^c Determined by chiral GC using a BGB175 chiral capillary column. Absolute configurations have been determined by measuring the optical rotation and comparing with literature data.

Table S7: Screening of catalyst loading and temperature

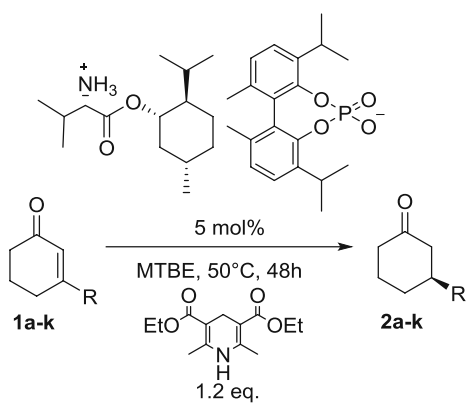


| Entry ^a | Temperature | Catalyst loading [mol%] | Hantzsch ester | Yield ^b [%] | ee ^c [%] |
|--------------------|-------------|-------------------------|------------------|------------------------|---------------------|
| 1 | 60 | 20 | ethyl | 98 | 93 (S) |
| 2 | 50 | 20 | ethyl | 98 | 95 (S) |
| 3 | 40 | 20 | ethyl | 96 | 95 (S) |
| 4 | 25 | 20 | ethyl | 59 | 96 (S) |
| 5 | 25 | 10 | ethyl | 43 | 96 (S) |
| 6 | 25 | 5 | ethyl | 29 | 96 (S) |
| 7 | 25 | 1 | ethyl | 11 | 96 (S) |
| 8 | 50 | 10 | ethyl | 99 | 94 (S) |
| 9 | 50 | 5 | ethyl | 98 | 95 (S) |
| 10 | 50 | 1 | ethyl | 68 | 93 (S) |
| 11 ^d | 25 | 20 | methyl | 14 | 83 (S) |
| 12 ^d | 25 | 20 | ethyl | 17 | 88 (S) |
| 13 ^d | 25 | 20 | <i>i</i> -propyl | 58 | 69 (S) |
| 14 ^d | 25 | 20 | <i>t</i> -butyl | 58 | 67 (S) |

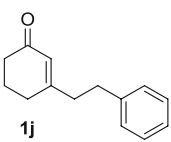
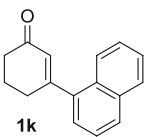
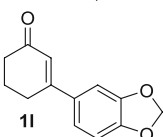
^a Performed with 0.18 mmol 3-methyl-2-cyclohexenone, 0.009-0.036 mmol catalyst, 0.22 mmol Hantzsch ester in 0.55 mL MTBE at the given temperature for 48 hours. ^b Determined by GC analysis using *n*-dodecane as internal standard. ^c Determined by chiral GC analysis using a BGB175 chiral capillary column. Absolute configurations have been determined by measuring the optical rotation and comparing with literature data.

^d Performed with (L)-valine *t*-butyl ester instead of (L)-valine (+)-(-1*R*,3*R*,4*S*) menthyl ester.

6.4 Reaction scope and limitations



| Entry ^a | Substrate | Yield ^d [%] | ee ^e [%] |
|--------------------|-----------|------------------------|---------------------|
| 1 | | 98 (72) ^f | 95 (S) |
| 2 | | 85 (76) ^f | 92 (S) |
| 3 | | 70 (55) ^f | 91 (S) |
| 4 | | 91 (87) | 93 (S) |
| 5 | | 85 (60) ^f | 86 (S) |
| 6 | | 75 (68) ^f | 88 (S) |
| 7 ^b | | 66 (60) | 92 (S) |
| 8 ^c | | 94 (80) ^f | 89 (S) |
| 9 | | 86 (84) | 82 (S) |

| | | | |
|----|---|---------|--------|
| 10 |  | 94 (91) | 90 (S) |
| 11 |  | 65 (62) | 94 (S) |
| 12 |  | 89 (86) | 70 (S) |

^a Performed with 1.8 mmol ketone, 5 mol% catalyst and 2.2 mmol Hantzsch ethyl ester in 5.5 mL MTBE at 50°C for 48 h. ^b 20 mol% catalyst. ^c 10 mol% catalyst. ^d Determined by GC or GC-MS analysis. Isolated yields after flash column chromatography are given in parenthesis. ^e Determined by chiral GC analysis using a BGB175 or BGB173 chiral capillary column, or by chiral HPLC analysis using a Diacel Chiralcel AS-H column. Absolute configurations have been determined by measuring the optical rotation and comparing with literature data. ^f Lower isolated yield because of high volatility of the product.

7. Computational studies

7.1 Quantummechanical calculation of rotational barriers

7.1.1 Choice of method and basis set

Although several studies on the calculation of rotational barriers in substituted biphenyls have been published^{28,29,30}, the only systematic protocol so far has been established by Masson.³¹ A key finding of Masson's study is that for accurate barrier energies, inclusion of vibrational corrections is crucial. Since frequency computations as well as transition state optimizations for molecules as large as the substituted phosphoric acids can become quite expensive, a compromise between accuracy and efficiency is necessary in terms of the method.

The popular as well as efficient B3LYP functional³² has been shown to perform well for the estimation of rotational barriers for unsubstituted and substituted biphenyls^{29,30,33}. However, as also noted by Masson, empirical dispersion correction terms such as Grimme's DFT-D or DFT-D3^{34,35} are necessary to obtain accurate energies with B3LYP, so we chose B3LYP-D3 as a functional. The correlation of the uniform electron gas in the B3LYP functional was modeled according to the Vosko-Wilk-Nusair VWN5 formalism.³⁶

Since Masson achieved good results with DFT/def2-TZVPP³⁷, we tested both the single-polarized def2-TZVP and double-polarized def2-TZVPP set for compound **4**. Since energies on the B3LYP-D3 level of theory differed only by 0.07 kcal/mol between both basis sets, we chose the computationally cheaper def2-TZVP basis set. Summarizing, all geometry optimizations, energy evaluations and frequency calculations (at 333.15K) were performed on the B3LYP-D3/def2-TZVP level of theory. All computations were performed with ORCA.³⁸ For further validation of the method, we compared the B3LYP-D3/def2-TZVP electronic barrier energies of phosphoric acid **4** against single point electronic energies on the same geometry computed on the benchmark DLPNO-CCSD(T)/def2-QZVP^{36,39} level of theory. Only a small energy difference of 0.28 kcal/mol could be observed.

Masson also addresses the role of solvent when computing rotational barriers. In all studies on the computation of biphenyl racemization barriers published so far, good agreement with experiment is achieved without the consideration of solvent effects. Possible justification can be found in a study by Graybill and Leffler⁴⁰, who found a compensation of enthalpy and entropy in different solvents. For a more detailed discussion, see References 30 and 39.

However, Masson emphasizes that solvent effects cannot be confidently neglected for negatively charged biphenyls. Since solvent effects and likely specific interactions with both solvent and cation

need to be considered when computing rotational barriers of the anionic forms of phosphoric acids **4**-**7**, the barrier of the corresponding anions will be the topic of more detailed future work.

7.1.2 Optimization of transition states

The systematic search for rotational transition states is not straightforward. Usually, fixing the torsional dihedral angle around the aryl-aryl bond to 0 degrees and optimizing this constrained structure yields good guesses for rotational transition states of substituted biphenyl.³⁰ The situation is trickier when the planar transition state is hindered by bulky ortho-substituents such as the isopropyl and tert-butyl groups in phosphoric acids **6** and **7**. For all phosphoric acids, we optimized the structure while fixing one of the dihedral angles to 0° and used the result as guesses for the transition state optimizations. In addition, for phosphoric acid **6** we performed a systematic transition state search with the nudged elastic band (NEB) method implemented in ORCA.^{41,42} We also used the result of this NEB calculation to construct another transition state guess for phosphoric acid **7**. The imaginary frequencies of all transition states corresponded to an out-of-plane torsion of the phenyl rings.

For phosphoric acids **4** and **5**, fully planar transition states as depicted in Figure S1 are obtained when using the constrained structures as transition state guesses.



Figure S1: Rotational transition states for phosphoric acids **4** and **5**.

As already mentioned, compounds **6** and **7** have methyl groups in the 6,6'-position, which hinder the planar transition state. Instead, they adopt a conformation in which the aryl-aryl-bond is out-of-plane and the two rings roughly coplanar. This peculiar transition state geometry for ortho-substituted biphenyls has been anticipated by Baddeley as early as 1946.⁴³ Ling and Harris proposed the associated mechanism in 1964.⁴⁴ They suggested an asynchronous nature of the racemization, with 6,6'-groups passing over each other subsequently instead of synchronously, minimizing the barrier energy. The out-of-plane transition states as well as the asynchronous nature of the racemization has been confirmed by Masson's calculation.³⁰ The asynchronous mechanism is also visible in the case of both phosphoric acids **6** and **7**. By constraining different dihedral angles during pre-optimization, two different transition states can be obtained. The first transition state corresponds to passing of the methyl groups prior to

reaching the transition state, in the second transition state the ester oxygens of the phosphate groups have passed instead (Figure S2 and S3, left and right). No pathway is favored over the other, the electronic barriers of the two transition states for both phosphoric acid **6** and **7** only differ by 0.01 kcal/mol.

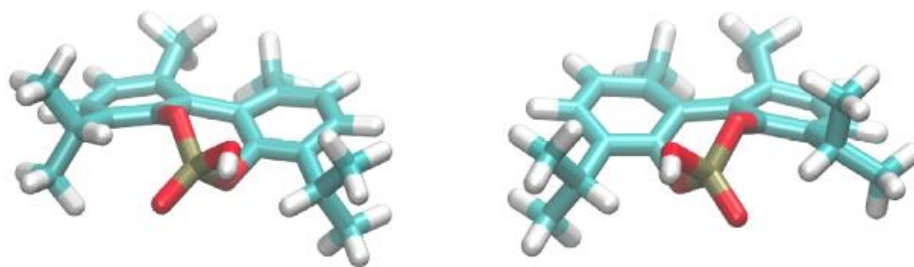


Figure S2: Asynchronous transition states for phosphoric acid **6**.

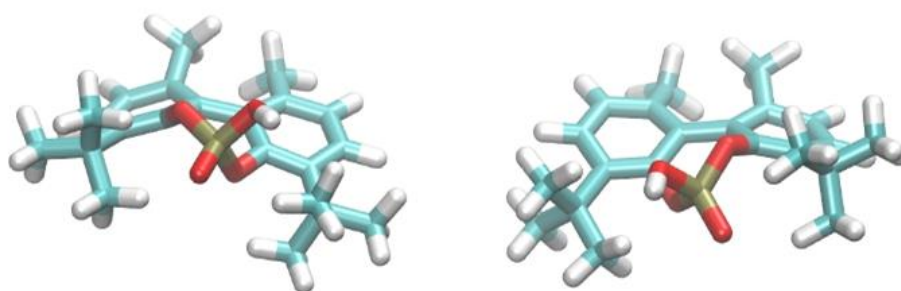


Figure S3: Asynchronous transition states for phosphoric acid **7**.

7.2 Molecular Dynamics Simulations

7.2.1 Simulation setup

Force fields for the anionic form of anion **6** and the iminium intermediate evolving from the L-valine (+)-(1*S*,2*R*,5*S*)-menthyl-cation were obtained from PARAMCHEM^{45,46} without further modification. Since no force field for MTBE was available, we chose n-methylbutylether as a solvent. The solvent parameters were taken from the CGenFF force field⁴⁷. Simulation boxes contained a single ion pair and 216 molecules of n-methylbutylether. To consider all possible isomers and stereoisomers, both the (*E*)- and (*Z*)-form of the cation as well as both anion enantiomers were considered, yielding four different systems (see Table S8.). 10 replica simulations of every system were conducted under the following conditions: All simulations were performed with the program package CHARMM.⁴⁸ Initial configurations were created with PACKMOL.⁴⁹ All simulations were conducted in the NpT ensemble

and employed the CHARMM CPT algorithm, the leapfrog integrator and the Hoover thermostat. A temperature of 330 K, a pressure of 1 atm and a non-bonded cutoff of 11 Å were used. Electrostatics were treated using the Particle Mesh Ewald method, with a grid size of approximately 1 Å, cubic splines of order 6 and a K of 0.41 Å⁻¹. The SHAKE algorithm was employed to fix the length of bonds to hydrogens.

Boxes were first equilibrated for 2 ns using a timestep of 1 fs, followed by production simulations of at least 38 ns (see Table S8 for system details) under the same conditions. Coordinates were written to disk every 250 steps.

Table S8: Overview over all four simulated systems.

| System number | Cation-Isomer | Anion-Isomer | Average boxsize [Å] | Number of replica | Simulation time per replica [ns] |
|---------------|---------------|--------------|---------------------|-------------------|----------------------------------|
| 1 | Z | R | 36.1 | 10 | 38 |
| 2 | Z | S | 36.1 | 10 | 58 |
| 3 | E | R | 36.1 | 10 | 38 |
| 4 | E | S | 36.1 | 10 | 78 |

For trajectory analysis, the MDAnalysis library⁵⁰ as well as self-written python code was used. Plots were created with R (ggplot).⁵¹ Hydrogen bonds were analyzed using CHARMM and a cutoff distance of 2.4 Å and a cutoff angle of 135°. Every 10th step of the trajectory was considered in the analysis.

7.2.2 Statistical considerations

To ensure statistical convergence of the simulations, several measures were taken. For both cation isomers (E and Z) 10 different conformers optimized for RMSD diversity were generated using a genetic algorithm implemented in OpenBabel.⁵² Sampling of anion conformations was not done due to the structural rigidity of the anion. For each of the 10 replica/systems, a different cation conformer was used to create an initial configuration. Since we were especially interested in ion-ion-interactions, we monitored the distribution of several atom-atom interionic distances to assess sampling. Every system was simulated until the distributions reached convergence, the respective times for every system are listed in Table S8. These converged distributions are depicted in Figure S4 and show that especially the N23-O48 and N23-O49 distance distributions show full overlap.

To illustrate the distribution prior to convergence, the distributions of the E/S system after 38 ns and the full simulation time of 78 ns are depicted in Figure S5. It can be clearly seen that the N23-O48 and

N23-O49 distance distributions are different at 38 ns, but after a simulation time of 78 ns the distributions have equalized.

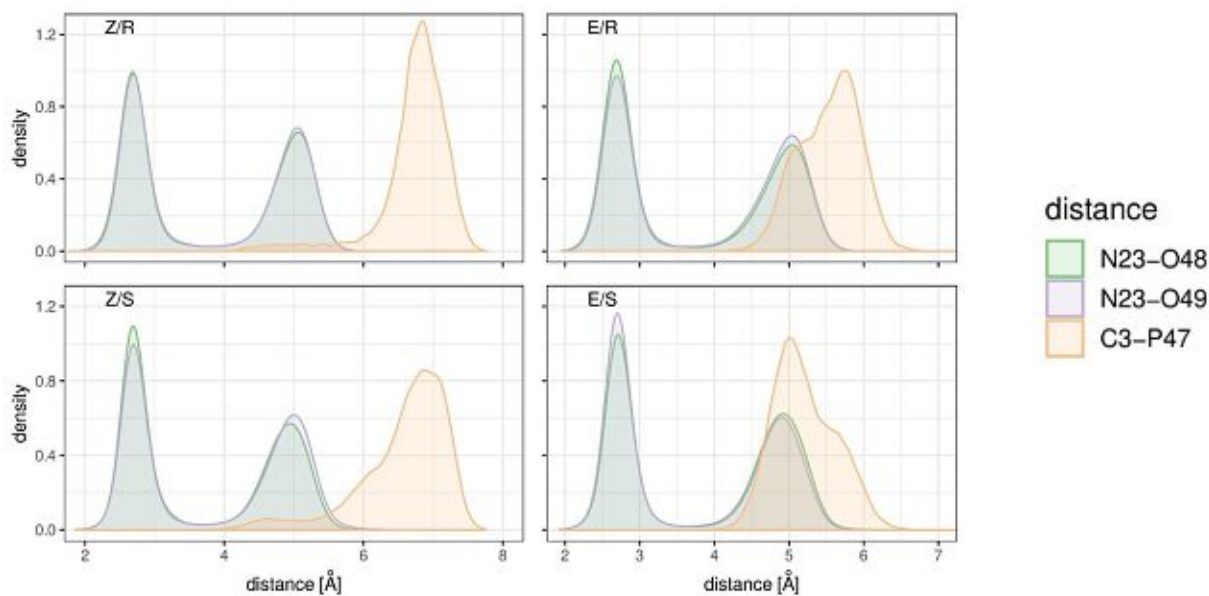
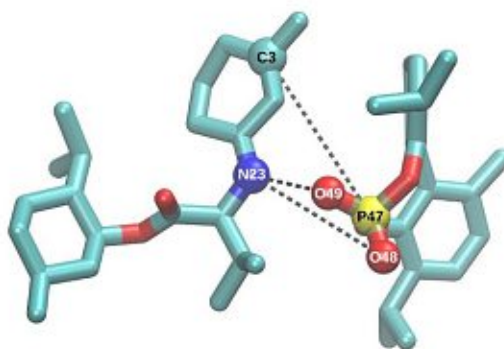


Figure S4. Interionic distances illustrated for the E-cation/S-anion pair (top) and the distributions after the full simulation time (bottom). Simulation times for the different systems are listed in Table S8.

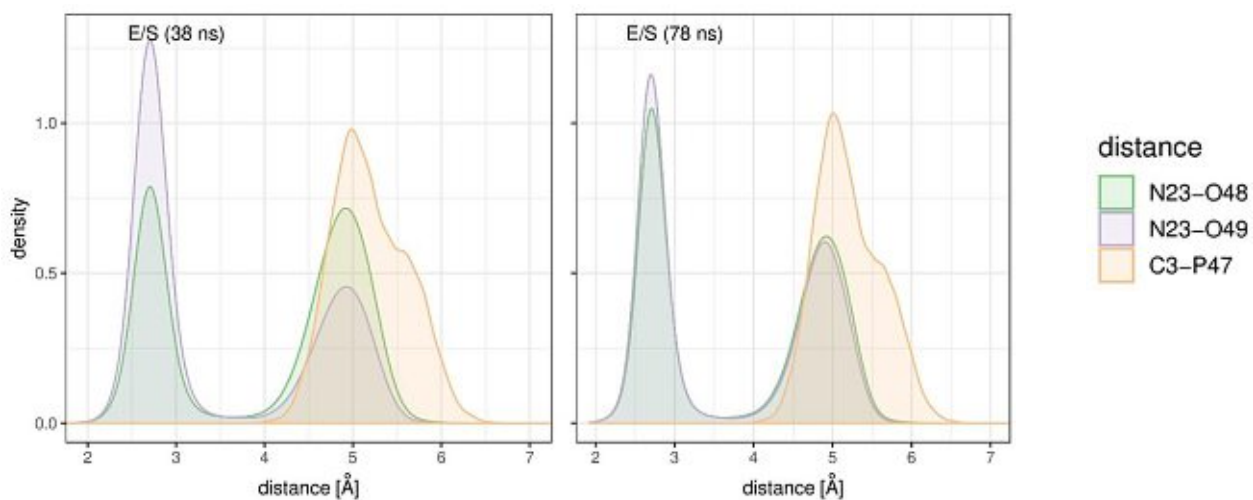


Figure S5. Distribution of interionic distances for the E-cation/S-anion pair after 38 ns (left) and 78 ns (right) simulation time. It is clearly visible that 78 ns are necessary to converge the distributions.

-
- 1
2 H. Chen, Y. Feng, Z. Xu, T. Ye, *Tetrahedron* **2005**, *61*, 11132–11140.
- 3 J. Han, J. Lian, X. Tian, S. Zhou, X. Zhen, S. Liu, *Eur. J. Org. Chem.* **2014**, *32*, 7232–7238.
- 4 T. Akama et al. *Bioorg. Med. Chem. Lett.* **2018**, *28*, 6–10.
- 5 S. Kandil, J. Balzarini, S. Rat, A. Brancale, A. D. Westwell, C. McGuigan, *Bioorg. Med. Chem. Lett.* **2016**, *26*, 5618–5623.
- 6 S. Thétiot-Laurent et al. *ChemBioChem.* **2017**, *18*, 300–315.
- 7 T. J. Trivedi, K. S. Rao, T. Singh, S. K. Mandal, N. Sutradhar, A. B. Panda, A. Kumar, *ChemSusChem.* **2011**, *4*, 604–608.
- 8 J. You, B. Liu, Y. Wang, *J. Chin. Chem. Soc.-Taip.* **2009**, *56*, 1010–1017.
- 9 W. Kuchen, H. F. *Phosphorus Sulfur.* **1980**, *8*, 139–145.
- 10 S. Grant-Overton, J. A. Buss, E. H. Smith, E. G. Gutierrez, E. J. Moorhead, V. S. Lin, A. G. Wenzel, *Synth. Commun.* **2015**, *45*, 331–337.
- 11 E. G. Gutierrez, E. J. Moorhead, E. H. Smith, V. S. Lin, L. K. G. Ackerman, C. E. Knezevic, V. Sun, S. Grant, A. G. Wenzel, *Eur. J. Org. Chem.* **2010**, *16*, 3027–3031.
- 12 L. lu, J. A. Fuentes, M. E. Janka, K. J. Fontenot, M. L. Clarke, *Angew. Chem. Int. Ed.* **2019**, *58*, 2120–2124.
- 13 D. R. Armstrong, C. Cameron, D. C. Nonhebel, P. G. Perkins, *J. Chem. Soc.* **1983**, *5*, 587–589.
- 14 R. Singh, C. Czekelius, R. R. Schrock, P. Müller, A. H. Hoveyda, *Organometallics* **2007**, *26*, 2528–2539.
- 15 T. Wenliang, CAN149:307958, **2008**.
- 16 Wenliang, T. *Production of Substituted Biphenyl Acid-Form Phosphate Ammonium Salt.* CAN149:307958, **2008**.
- 17 L. M. Schneider, V. M. Schmiedel, T. Pecchioli, D. Lentz, C. Merten, M. Christmann, *Org. Lett.* **2017**, *19*, 2310–2313.
- 18 N. J. A. Martin, B. List, *J. Am. Chem. Soc.* **2006**, *128*, 13368–13369.
- 19 B.-D. Chong, Y.-I. Ji, S.-S. Oh, J.-D. Yang, W. Baik, S. Koo, *J. Org. Chem.* **2002**, *62*, 9323–9325..
- 20 E. Brenna, M. Crotti, M. De Pieri, F. G. Gatti, G. Manenti, D. Monti, *Adv. Synth. Catal.* **2018**, *360*, 3677–3686.
- 21 S. T. Cohen-Anisfeld, P. T. Lansbury, *J. Am. Chem. Soc.* **1993**, *115*, 10531–10537.
- 22 M. D’Augustin, L. Palais, A. Alexakis, *Angew. Chem.* **2005**, *117*, 1400–1402.
- 23 J.-G. Jun, T. H. Ha, B. P. Mundy, K. E. Bartelt, R. S. Bain, J. H. Cardellina, *J. Chem. Soc. Perkin Trans. 1* **1994**, *18*, 2643.
- 24 E. D. Scott, N. Amishiro, S. E. Denmark, N. Amishiro, *J. Org. Chem.* **2003**, *68* (18), 6997–7003.

- 25 V. Jurkauskas, J. P. Sadighi, S. L. Buchwald, *Org. Lett.* **2003**, *5*, 2417-2420.
- 26 Y. Fall, H. Doucet, M. Santelli, *Tetrahedron* **2009**, *2*, 489-495.
- 27 M. K. Das, S. De, Shubhashish; A. Bisai, *Org. Biomol. Chem.* **2015**, *13*, 3585-3588.
- 28 F. Cecacci, G. Mancini, P. Mencarelli, C. Villani, *Tetrahedron: Asymmetry* **2003**, *14*, 3117-3122.
- 29 L. Luzzani, M. Mancinelli, A. Mazzanti, S. Lepri, R. Ruzziconi, M. Schlosser, *Org. Biomol. Chem.* **2012**, *10*, 1847-1855.
- 30 R. Sahnoun, S. Koseki, Y. Fujimura, *J. Phys. Chem. A* **2006**, *110*, 2440-2447.
- 31 E. Masson, *Org. Biomol. Chem.* **2013**, *11*, 2859.
- 32 A. D. Becke, *J. Chem. Phys.* **1993**, *98*, 5648-5652.
- 33 M. P. Johansson, J. Olsen, *J. Chem. Theory Comput.* **2008**, *4*, 1460-1471.
- 34 S. Grimme, J. Antony, S. Ehrlich, H. Krieg, *J. Chem. Phys.* **2010**, *132*, 154104.
- 35 S. Grimme, S. Erlich, L. Georigk, *J. Comput. Chem* **2011**, *32*, 1456-1465.
- 36 S. H. Vosko, L. Wilk, M. Nusair, *Can. J. Phys.* **1980**, *58*, 1200-1211.
- 37 F. Weigend, R. Ahlrichs, *Phys. Chem. Chem. Phys.* **2005**, *7*, 3297-3305.
- 38 F. Neese, *Wiley Interdisciplinary Reviews: Computational Molecular Science* **2012**, *2*, 73-78.
- 39 C. Riplinger, F. Neese, *J. Chem. Phys.* **2013**, *138*, 034106.
- 40 J. E. Leffler, B. M. Graybill, *J. Phys. Chem.* **1959**, *63*, 1457-1460.
- 41 G. Henkelman, B. P. Uberuaga, H. J. Jónsson, *Chem. Phys.* **2000**, *113*, 9901-9904.
- 42 D. Sheppard, R. Terrell, G. Henkelman, *J. Chem. Phys.* **2008**, *128*, 134106.
- 43 G. Baddeley, *Nature* **1946**, *157*, 694-695.
- 44 C. C. K. Ling, M. M. Harris, *J. Chem. Soc.* **1964**, *0*, 1825-1835.
- 45 K. Vanommeslaeghe, A. D. MacKerell, *J. Chem. Inf. Model.* **2012**, *52*, 3144-3154.
- 46 K. Vanommeslaeghe, E. P. Raman, A. D. MacKerell, *J. Chem. Inf. Model* **2012**, *52*, 3155-3168.
- 47 K. Vanommeslaeghe, E. Hatcher, C. Acharya, S. Kundu, S. Zhong, J. Shim, E. Darian, O. Guvench, P. Lopes, I. Vorobyov et al., *J. Comput. Chem* **2010**, *31*, 671-690.
- 48 B. R. Brooks, C. L. Brooks, A. D. Mackerell, L. Nilsson, R. J. Petrella, B. Roux, Y. Won, G. Archontis, C. Bartels, S. Boresch et al., *J. Comput. Chem* **2009**, *30*, 1545-1614.
- 49 L. Martínez, R. Andrade, G. Birgin, J. M. Martínez, *J. Comput. Chem.* **2009**, *30*, 2157-2164.
- 50 N. Michaud-Agrawal, E. J. Denning, T. B. Woolf, O. Beckstein, *J. Comput. Chem* **2011**, *32*, 2319-2327.
- 51 H. Wickham. ggplot2: Elegant Graphics for Data Analysis. Springer-Verlag New York, 2016.
- 52 The Open Babel Package, version 2.4.1
<https://openbabel.readthedocs.io/en/latest/3DStructureGen/multipleconformers.html>

Appendix D

Supporting information:

Counterion-Enhanced Pd/Enamine Catalysis: Direct Asymmetric α -Allylation of Aldehydes with Allylic Alcohols by Chiral Amines and Achiral or Racemic Phosphoric Acids.

Supporting Information

Counterion Enhanced Pd/Enamine Catalysis: Direct Asymmetric α -Allylation of Aldehydes with Allylic Alcohols by Chiral Amines and Achiral or Racemic Phosphoric Acids

Ádám Márk Pálvölgyi^a, Jakob Smith^a, Michael Schnürch^a and Katharina Bica-Schröder^{a*}

^a Institute of Applied Synthetic Chemistry, TU Wien, Getreidemarkt 9/163, A-1060 Vienna, Austria

* Corresponding author. e-mail: katharina.schroeder@tuwien.ac.at

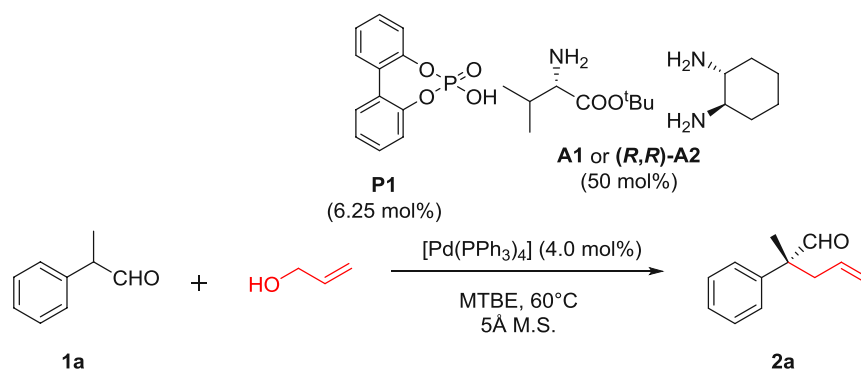
| | | |
|----|--|-----|
| 1. | Optimization of the reaction conditions | 190 |
| 2. | Analysis of intermediates for the plausible reaction mechanism | 198 |
| 3. | NMR studies to investigate the atropisomerism of the phosphoric acids..... | 202 |

1. Optimization of the reaction conditions

1.1 Representative procedure for the parameter optimization

All reactions were carried out in flame-dried Schlenk tubes (25 mL, VWR) by using standard Schlenk technique. A flame-dried Schlenk tube was charged with finely ground and freshly activated 5 Å molecular sieves (190 mg), [Pd(PPh₃)₄] (17.3 mg, 0.015 mmol, 4.0 mol%), amine or amino-acid ester (50 mol%), phosphoric acid (6.25 mol%), and solvent (0.75 mL). Allyl alcohol (50 μL, 0.75 mmol, 2.0 equiv.) and 2-phenylpropanal (50 μL, 0.375 mmol, 1.0 equiv.) were added and the reaction mixture was stirred at the specific temperature for 16 hours. Upon completion, Et₂O (3 mL) and 2N HCl (5 mL) were added, and the reaction mixture was vigorously stirred 30 minutes. A sample for GC and chiral HPLC analysis was taken to determine the yield and the enantioselectivity.

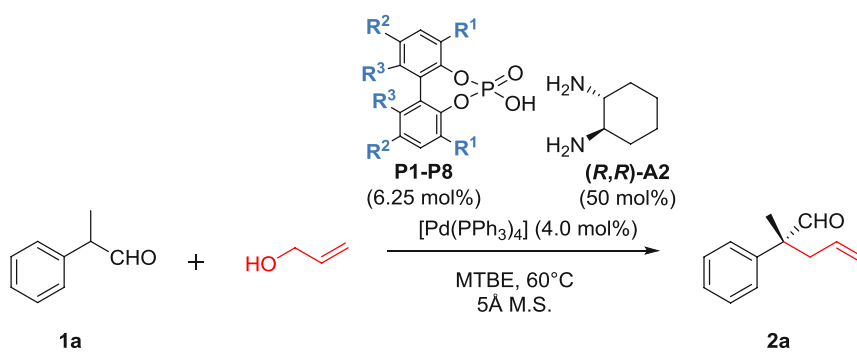
Table S1: Initial results and proof of concept

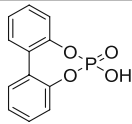
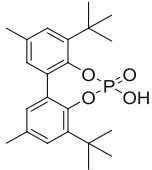
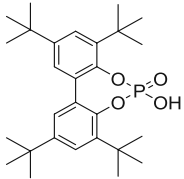
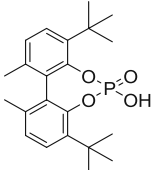
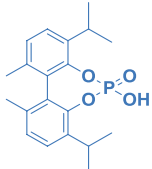


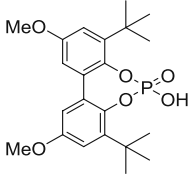
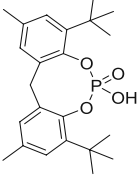
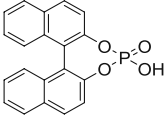
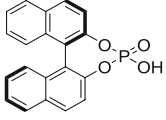
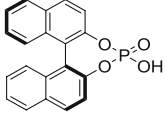
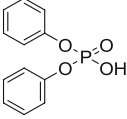
| Entry ^a | [Pd(PPh ₃) ₄] (mol%) | Amine (mol%) | Phosphoric acid (mol%) | Yield ^b (%) | ee ^c (%) |
|--------------------|--|--------------|------------------------|------------------------|----------------------|
| 1 ^d | 4.0 | 50 | 6.25 | 82 | 31 (<i>S</i>) |
| 2 | 4.0 | 50 | 6.25 | 87 | 78 (<i>R</i>) |
| 3 | 0 | 50 | 6.25 | <1 | n.d. |
| 4 | 4.0 | 50 | 0 | 37 | 35 (<i>R</i>) |
| 5 | 4.0 | 0 | 6.25 | 81 | 1 (<i>R</i>) |

^a Performed with 0.375 mmol 2-phenylpropanal using 0 or 4.0 mol% [Pd(PPh₃)₄], 0 or 50 mol% (*1R,2R*)-diaminocyclohexane ((*R,R*)-**A2**), 0 or 6.25 mol% phosphoric acid **P1**, 190 mg 5 Å molecular sieve, and 0.75 mmol allyl alcohol in 0.75 mL MTBE at 60°C for 16 hours. ^b Determined by GC analysis. ^c Determined by chiral HPLC analysis using a DIACEL Chiralcel AS-H column. Absolute configurations were determined by measuring the optical rotation and comparing with literature data. ^d L-valine *tert*-butyl ester (**A1**) instead of (*R,R*)-**A2**.

Table S2: Screening of different phosphoric acids

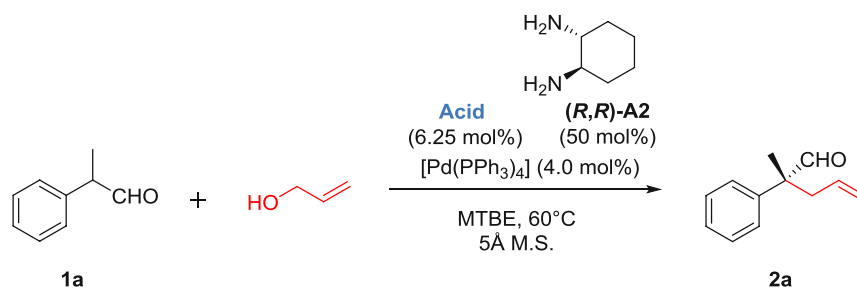


| Entry ^a | Phosphoric acid | Yield ^b (%) | ee ^{c,d} (%) |
|--------------------|--|------------------------|-----------------------|
| 1 |  P1 | 87 | 78 (<i>R</i>) |
| 2 |  P2 | 87 | 84 (<i>R</i>) |
| 3 |  P3 | 93 | 85 (<i>R</i>) |
| 4 |  P4 | 92 | 85 (<i>R</i>) |
| 5 |  P5 | 98 | 94 (<i>R</i>) |

| | | | |
|----|--|----|-----------------|
| 6 |  <p>P6</p> | 90 | 82 (<i>R</i>) |
| 7 |  <p>P7</p> | 91 | 85 (<i>R</i>) |
| 8 |  <p>(±)-P8</p> | 88 | 73 (<i>R</i>) |
| 9 |  <p>(R)-P8</p> | 90 | 72 (<i>R</i>) |
| 10 |  <p>(S)-P8</p> | 90 | 72 (<i>R</i>) |
| 11 |  | 84 | 70 (<i>R</i>) |

^a Performed with 0.375 mmol 2-phenylpropanal using 4.0 mol% [Pd(PPh₃)₄], 50 mol% amine (*R,R*)-**A2**, 6.25 mol% phosphoric acid **P1-P8** or diphenyl phosphate, 190 mg 5Å molecular sieves and 0.75 mmol allyl alcohol in 0.75 mL MTBE at 60°C for 16 hours. ^b Determined by GC analysis. ^c Determined by chiral HPLC analysis using a DIACEL Chiralcel AS-H column. Absolute configurations were determined by measuring the optical rotation and comparing with literature data.

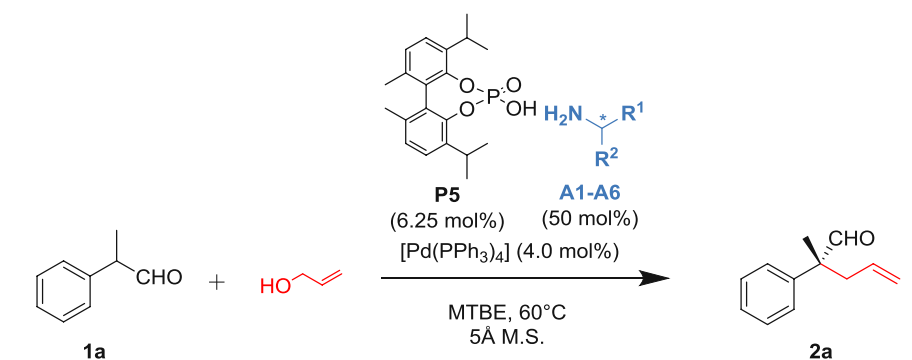
Table S3: Screening of other acids

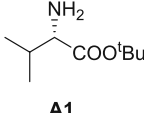
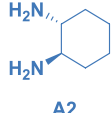
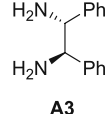
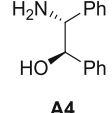
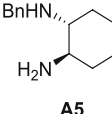
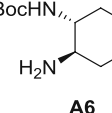


| Entry ^a | Acid | Yield ^b (%) | ee ^{c,d} (%) |
|--------------------|---|------------------------|-----------------------|
| 1 | | 92 | 14 (<i>R</i>) |
| 2 | | 90 | 7 (<i>R</i>) |
| 3 | | 83 | 55 (<i>R</i>) |
| 4 | CF ₃ COOH | 92 | 75 (<i>R</i>) |
| 5 | FeCl ₃ | 25 | 40 (<i>R</i>) |
| 6 | TiCl ₄ | 27 | 65 (<i>R</i>) |
| 7 | Al(O ^{<i>i</i>} Pr) ₃ | n.r. | n.d. |

^a Performed with 0.375 mmol 2-phenylpropanal using 4.0 mol% $[Pd(PPh_3)_4]$, 50 mol% amine **(R,R)-A2**, 6.25 mol% acid, 190 mg 5Å molecular sieves and 0.75 mmol allyl alcohol in 0.75 mL MTBE at 60°C for 16 hours. ^b Determined by GC analysis. ^c Determined by chiral HPLC analysis using a DIACEL Chiralcel AS-H column. Absolute configurations were determined by measuring the optical rotation and comparing with literature data.

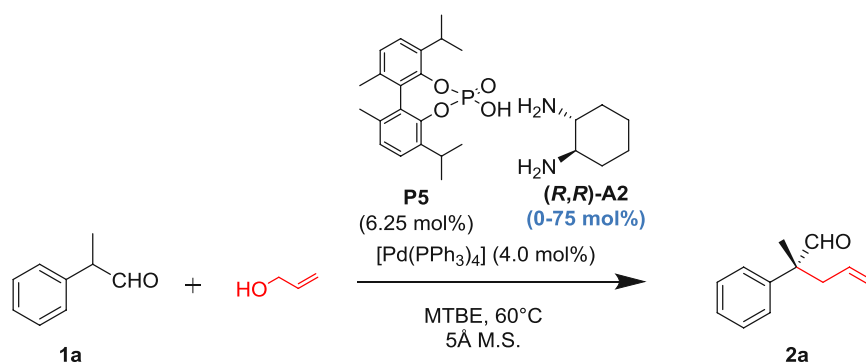
Table S4: Screening of amine sources



| Entry ^a | Amine source | Yield ^b (%) | ee ^c (%) |
|--------------------|--|----------------------------------|----------------------------------|
| 1 |  A1 | 89 | 31 (<i>S</i>) |
| 2 |  A2 | 98 (<i>R</i>) | 94 (<i>R</i>) |
| | | 97 (<i>S</i>)^d | 94 (<i>S</i>)^d |
| 3 |  A3 | 89 | 37 (<i>R</i>) |
| 4 |  A4 | 89 | 21 (<i>S</i>) |
| 5 |  A5 | 90 | 60 (<i>R</i>) |
| 6 |  A6 | 97 | 44 (<i>R</i>) |

^a Performed with 0.375 mmol 2-phenylpropanal using 4.0 mol% $[\text{Pd}(\text{PPh}_3)_4]$, 50 mol% chiral amine or amino acid ester (**A1-A6**), 6.25 mol% phosphoric acid **P5**, 190 mg 5Å molecular sieves and 0.75 mmol allyl alcohol in 0.75 mL MTBE at 60°C for 16 hours. ^b Determined by GC analysis. ^c Determined by chiral HPLC analysis using a DIACEL Chiralcel AS-H column. Absolute configurations were determined by measuring the optical rotation and comparing with literature data. ^d (*S,S*)-**A2** instead of the (*R,R*)-**A2** was used.

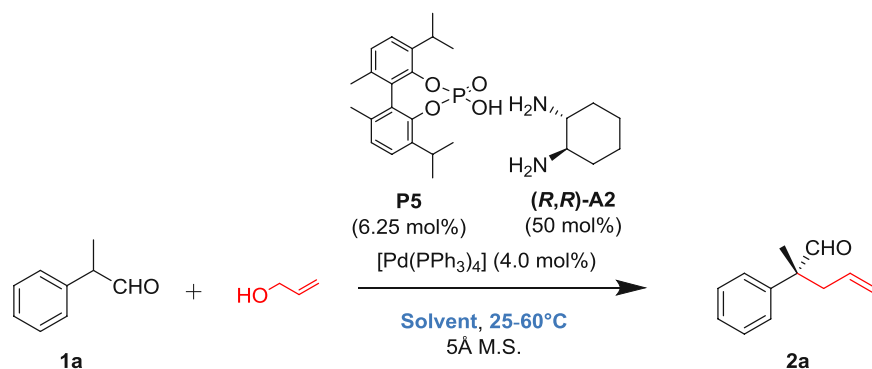
Table S5: Screening of different amine-to-phosphoric acid ratios



| Entry ^a | Amine/acid ratio | Yield ^b (%) | ee ^c (%) |
|--------------------|------------------|------------------------|----------------------|
| 1 | 0/1 | 83 | 1 (<i>R</i>) |
| 2 | 1/1 | 76 | 4 (<i>R</i>) |
| 3 | 2/1 | 80 | 10 (<i>R</i>) |
| 4 | 4/1 | 84 | 40 (<i>R</i>) |
| 5 | 6/1 | 90 | 75 (<i>R</i>) |
| 6 | 8/1 | 98 | 94 (<i>R</i>) |
| 7 | 10/1 | 97 | 85 (<i>R</i>) |
| 8 | 12/1 | 95 | 80 (<i>R</i>) |

^a Performed with 0.375 mmol 2-phenylpropanal using 4.0 mol% $[Pd(PPh_3)_4]$, 0-75.0 mol% amine (*R,R*)-**A2**, 6.25 mol% phosphoric acid **P5**, 190 mg 5Å molecular sieves and 0.75 mmol allyl alcohol in 0.75 mL MTBE at 60°C for 16 hours. ^b Determined by GC analysis. ^c Determined by chiral HPLC analysis using a DIACEL Chiralcel AS-H column. Absolute configurations were determined by measuring the optical rotation and comparing with literature data.

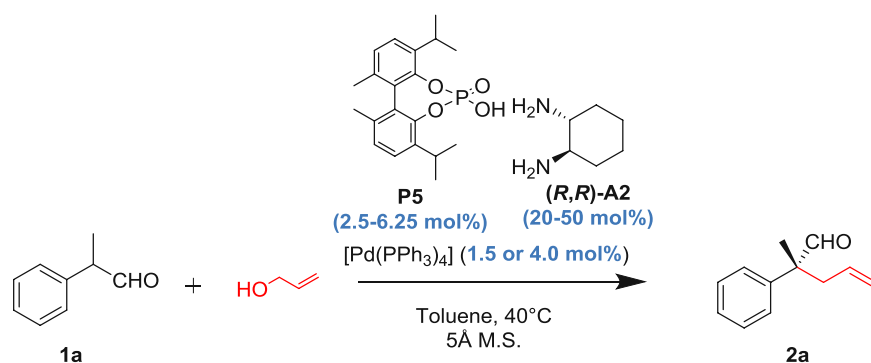
Table S6: Solvent and temperature screening



| Entry ^a | Solvent | Yield ^b (%) | ee ^c (%) |
|-----------------------|--------------------------------|------------------------|----------------------|
| 1 | CHCl ₃ | 25 | 50 (<i>R</i>) |
| 2 | 2-Me-THF | 97 | 87 (<i>R</i>) |
| 3 | ⁱ Pr ₂ O | 97 | 94 (<i>R</i>) |
| 4 | ⁿ Bu ₂ O | 96 | 92 (<i>R</i>) |
| 6 | 2-MeTHF | 97 | 87 (<i>R</i>) |
| 9 | ^t BuOAc | 94 | 90 (<i>R</i>) |
| 10 | Isoamyl acetate | 90 | 80 (<i>R</i>) |
| 11 | MTBE | 98 | 94 (<i>R</i>) |
| 12 ^d | MTBE | 97 | 89 (<i>R</i>) |
| 13 | Toluene | 97 | 94 (<i>R</i>) |
| 15^d | Toluene | 96 | 94 (<i>R</i>) |
| 16 ^e | Toluene | 83 | 85 (<i>R</i>) |

^a Performed with 0.375 mmol 2-phenylpropanal using 4.0 mol% $[Pd(PPh_3)_4]$, 50 mol% amine **(R,R)-A2**, 6.25 mol% phosphoric acid **P5**, 190 mg 5Å molecular sieve and 0.75 mmol allyl alcohol in 0.75 mL solvent at 60°C for 16 hours. ^b Determined by GC analysis. ^c Determined by chiral HPLC analysis using a DIACEL Chiralcel AS-H column. Absolute configurations were determined by measuring the optical rotation and comparing with literature data. ^d Reaction was performed at 40°C. ^e Reaction was performed at 25°C.

Table S7: Optimization of catalyst loading



| Entry ^a | $[Pd(PPh_3)_4]$ (mol %) | Amine (mol %) | Phosphoric acid (mol %) | Yield ^b (%) | ee ^c (%) |
|--------------------|----------------------------|------------------|----------------------------|------------------------|----------------------|
| 1 | 4.0 | 50 | 6.25 | 96 | 94 (<i>R</i>) |
| 2 | 4.0 | 40 | 5.0 | 96 | 94 (<i>R</i>) |
| 3 | 1.5 | 40 | 5.0 | 95 | 94 (<i>R</i>) |
| 4 | 1.5 | 30 | 3.75 | 86 | 83 (<i>R</i>) |
| 5 | 1.5 | 20 | 2.5 | 67 | 72 (<i>R</i>) |

^a Performed with 0.375 mmol 2-phenylpropanal using 1.5 or 4.0 mol% $[Pd(PPh_3)_4]$, 20-50 mol% amine **(R,R)-A2**, 2.5-6.25 mol% phosphoric acid **P5**, 190 mg 5Å molecular sieves and 0.75 mmol allyl alcohol in 0.75 mL toluene at 40°C for 16 hours. ^b Determined by GC analysis. ^c Determined by chiral HPLC analysis using a DIACEL Chiralcel AS-H column. Absolute configurations were determined by measuring the optical rotation and comparing with literature data.

2. Analysis of intermediates for the plausible reaction mechanism

The plausible reaction mechanism was investigated by analytical studies, using *L*-valine *tert*-butyl ester (**A1**) and (*R,R*)-diaminocyclohexane (*R,R*-**A2**) as amine source, respectively.

Plausible catalytic cycle with (*R,R*)-diaminocyclohexane (*R,R*-**A2**) as amine source:

The reaction mechanism by using (*R,R*)-diaminocyclohexane (*R,R*-**A2**) was investigated *via* ESI-MS analysis (*Shimadzu*). In the ESI-MS spectra, the corresponding enamine (**I**, *m/z*: 229), imine (**IV**, *m/z*: 270), the product ((*R*)-**2a**, *m/z*: 174), the activated allylic alcohol (**V**, *m/z*: 418), the phosphoric acid (**P5**, *m/z*: 359 and 361) and the allylpalladium- π complex (*m/z*: 671) could be all detected after 5 minutes reaction time in toluene at 40 °C (Figure S1).

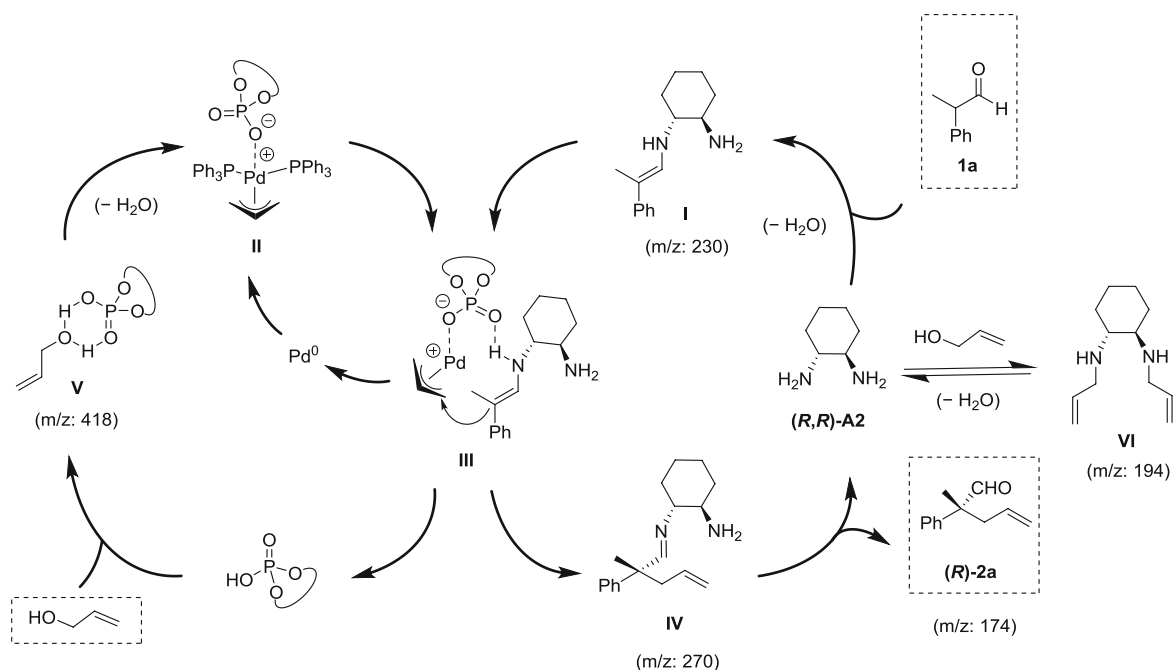
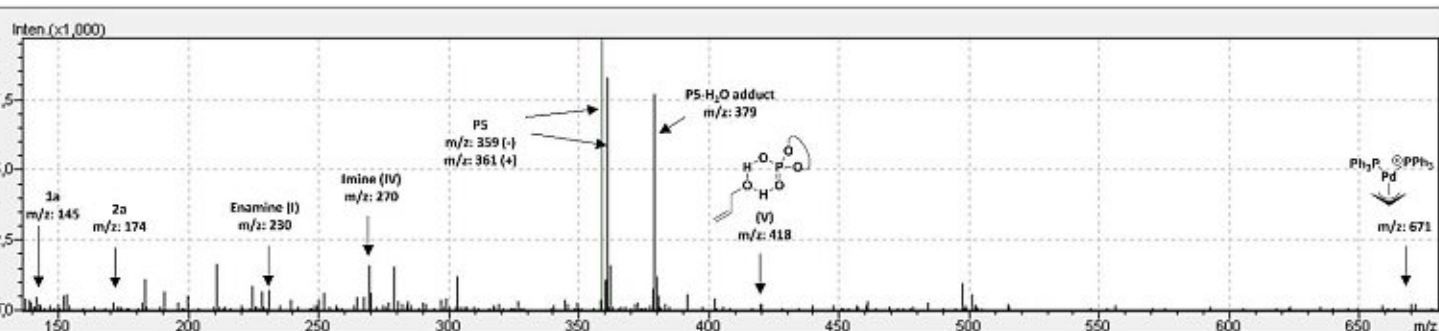


Figure S1. ESI-MS and the plausible reaction mechanism by using amine (*R,R*-**A2**), phosphoric acid **P5** and Pd(PPh₃)₄. The reaction procedure is in accordance to Table S7, entry 3 (page S10). The reaction time was 5 minutes. The product enantiomer generated in excess [(*R*)-**2a**] is illustrated in the cycle for clarity.

Plausible catalytic cycle by using L-valine *tert*-butyl ester (**A1**) as amine source:

The corresponding enamine (**I***), the imine (**IV***), the product ((*S*)-**2a**) and the *N*-allylated amino-acid ester (**VI***) could be detected by GC-MS (*Thermo Scientific DSQ II, quadrupole, BGB5 column*), after 5 minutes reaction time in toluene at 40 °C, as depicted on the next pages (189-190). Based on these proofs, the catalytic cycle is as follows:

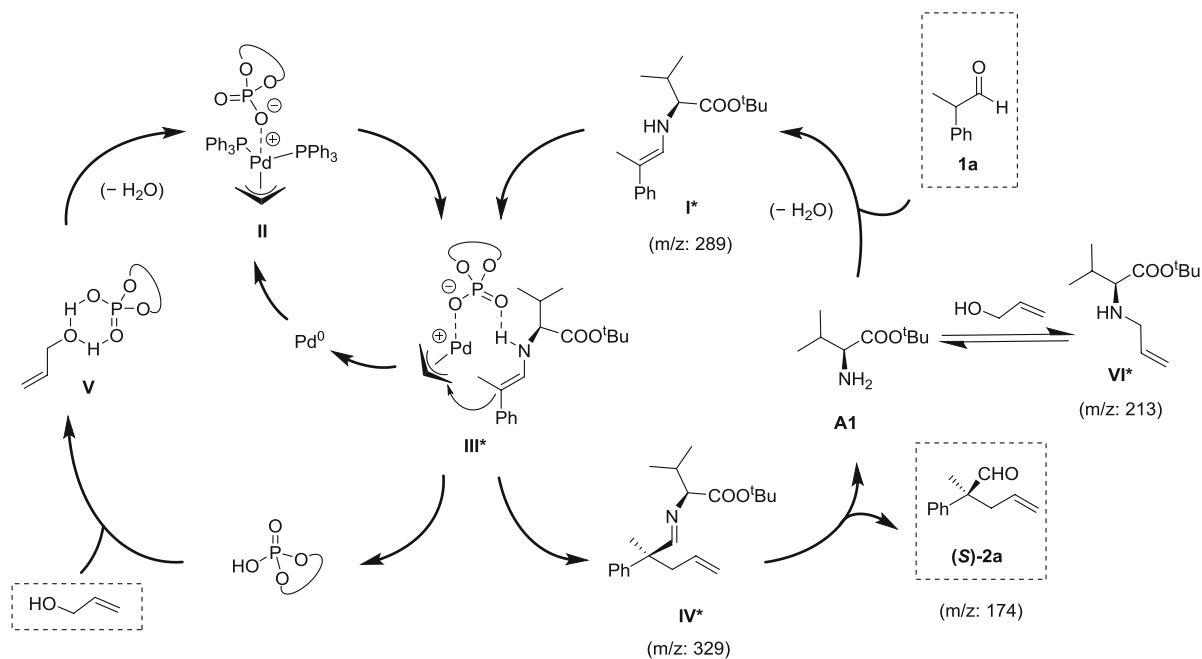


Figure S2. ESI-MS and the plausible reaction mechanism by using amine **A1**, phosphoric acid **P5** and Pd(PPh₃)₄. The reaction procedure is in accordance to Table S7, entry 3 (page S10). The reaction time was 5 minutes. The product enantiomer generated in excess ((*S*)-**2a**) is illustrated in the cycle for clarity.

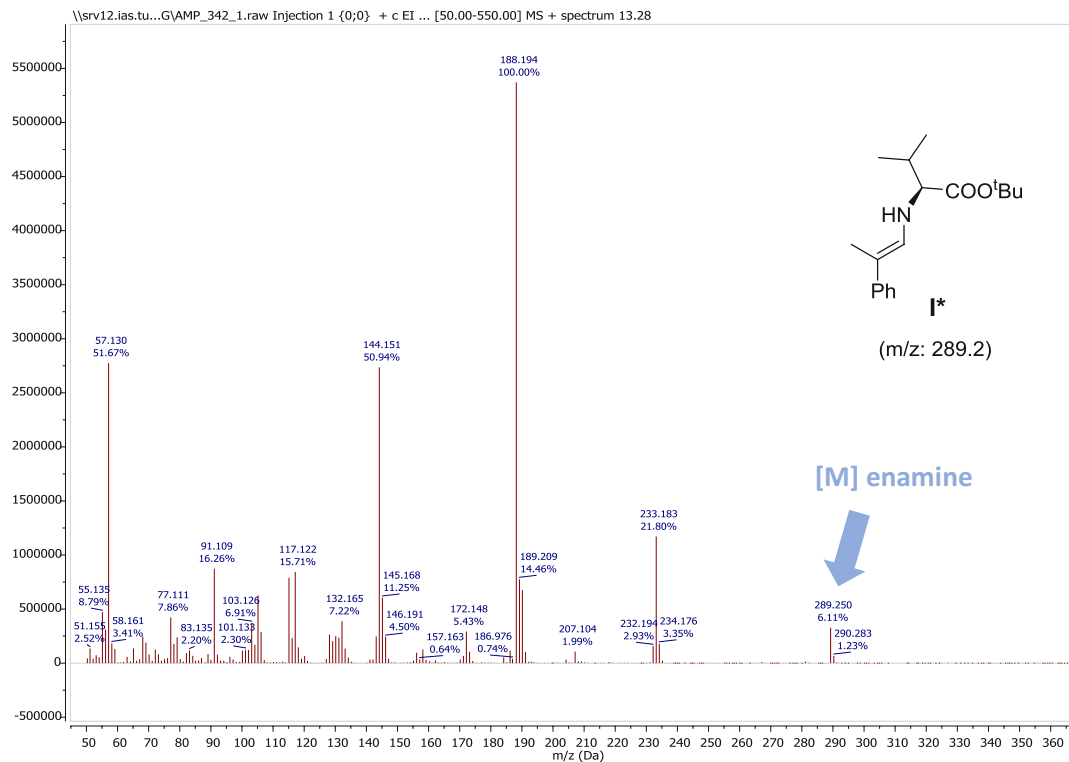


Figure S3. MS spectra of the enamine (**I***)

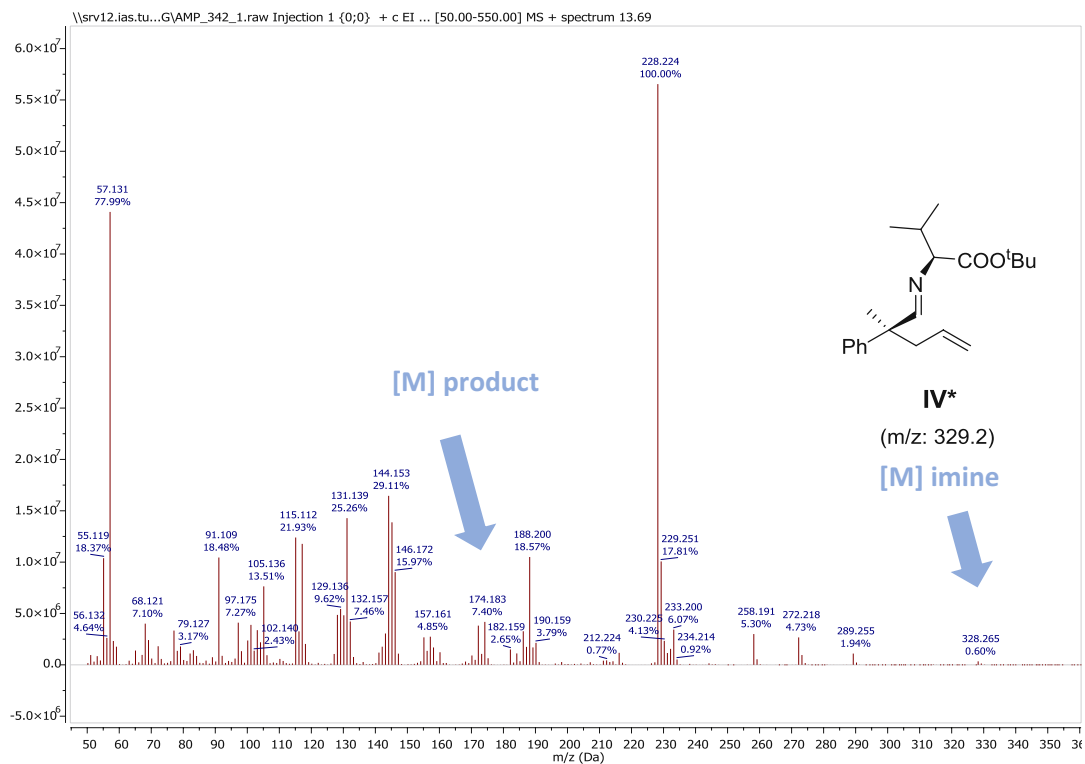


Figure S4. MS spectra of the imine (**IV***)

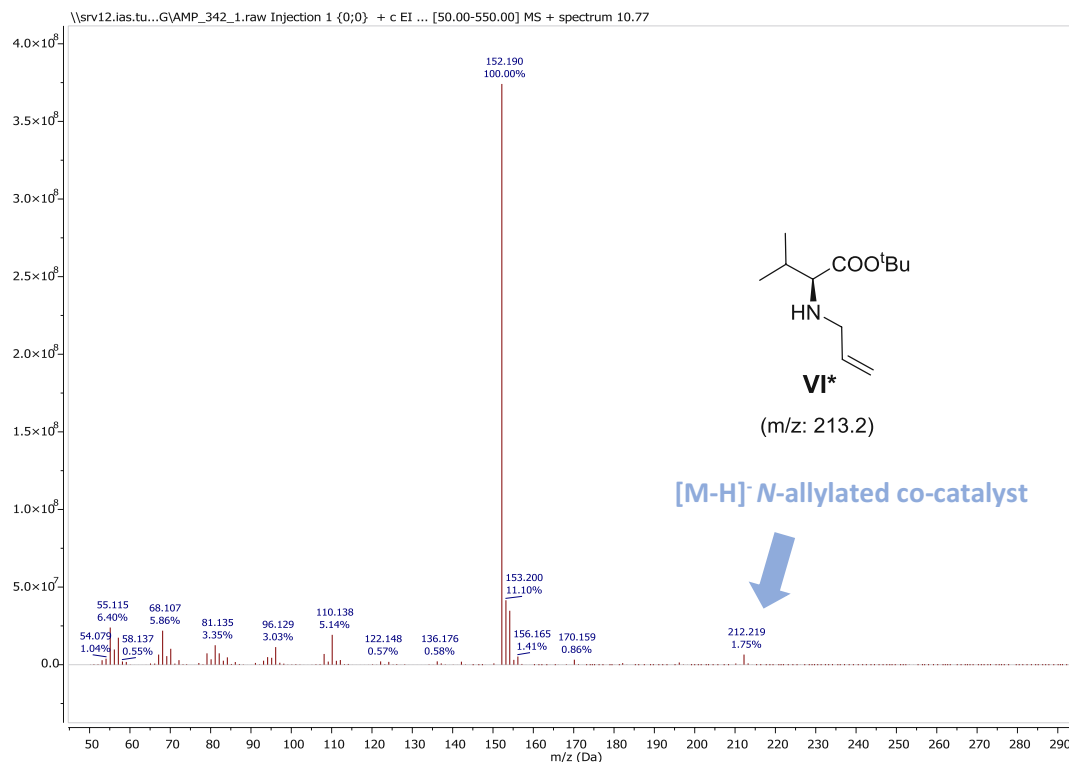


Figure S5. MS spectra of the *N*-allylated L-valine *tert*-butyl ester (**VI***)

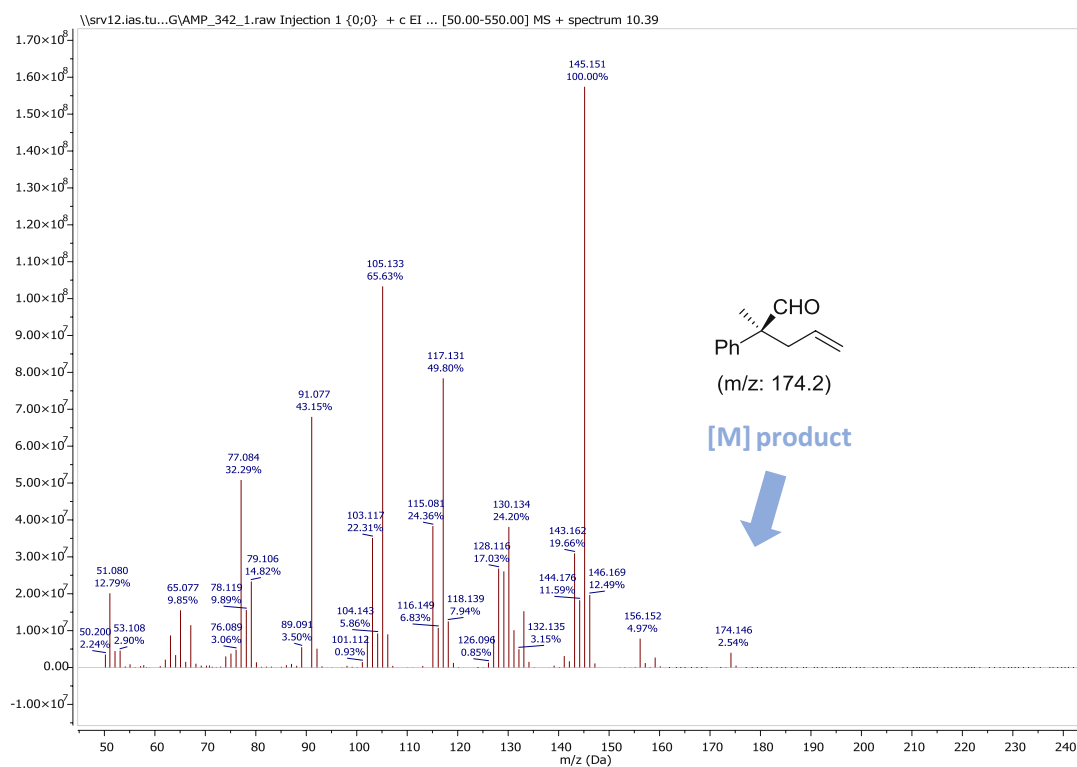


Figure S6. MS spectra of the product (*S*)-**2a**

3. NMR studies to investigate the atropisomerism of the phosphoric acids

In order to investigate whether the phosphoric acids **P1-P8** might form stable atropisomers at room temperature, NMR studies on the ion-aggregation of *L*-valine-*tert*-butyl ester with the phosphoric acids were carried out. Compounds **P3** and **P5** were chosen as representative examples for biphenyl-phosphoric acid derivatives without and with methyl groups in the *ortho* positions.

In case of the salt of **P5** with *L*-valine-*tert*-butyl ester, the ^{31}P NMR spectra showed the complete disappearance of the phosphoric acid peak and 2 new peaks with same integrals corresponding to the (*R,S*) and the (*S,S*)-diastereomeric salts appeared. Together with our previous MD-simulations for the rotation barrier of acid **P5** being ca. 172 kJ/mol, (Scharinger, F.; Pálvölgyi, Á. M.; Zeindlhofer, V.; Schnürch, M.; Schröder, C.; Bica-Schröder, K. Counterion Enhanced Organocatalysis: A Novel Approach for the Asymmetric Transfer Hydrogenation of Enones. *ChemCatChem* **2020**, *12*, 3776-3782.) compounds having 6,6'-methyl substituents like **P4** and **P5** should exist as stable atropisomers at room temperature. On the other hand, no such phenomenon was observed in case of the salt of **P3**, as the ^{31}P NMR spectrum showed only one single peak after derivatization with *L*-valine-*tert*-butyl ester. As the rotation barriers for such biphenyl derivatives without substituents in the 6,6'-positions are in the range of 42-50 kJ/mol, the phosphoric acids **P1-P3** and **P6-P7** should be simple achiral compounds.

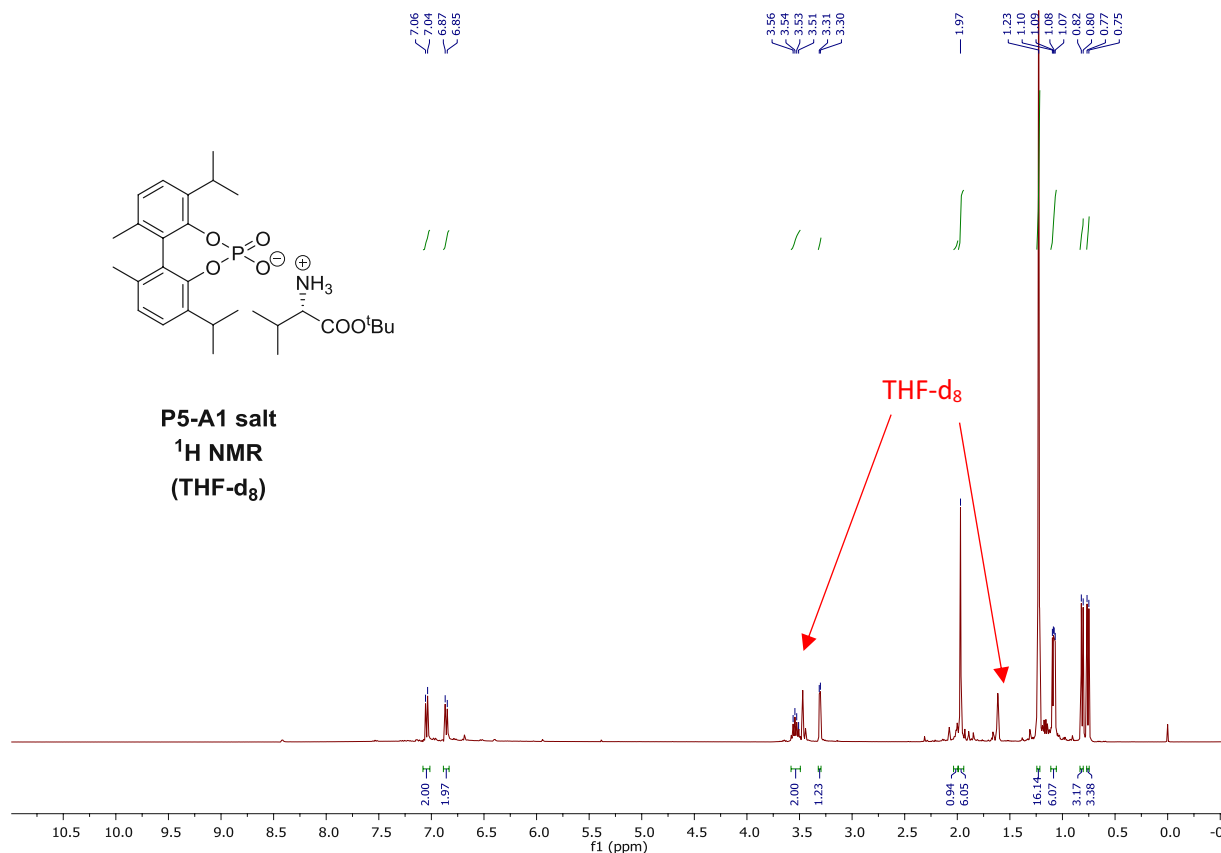
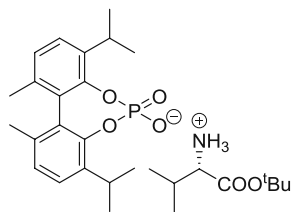


Figure S7. ^1H NMR spectrum of **P5-A1** salt (400 MHz, THF- d_8)



P5-A1 salt
³¹P NMR
(THF-d₈)

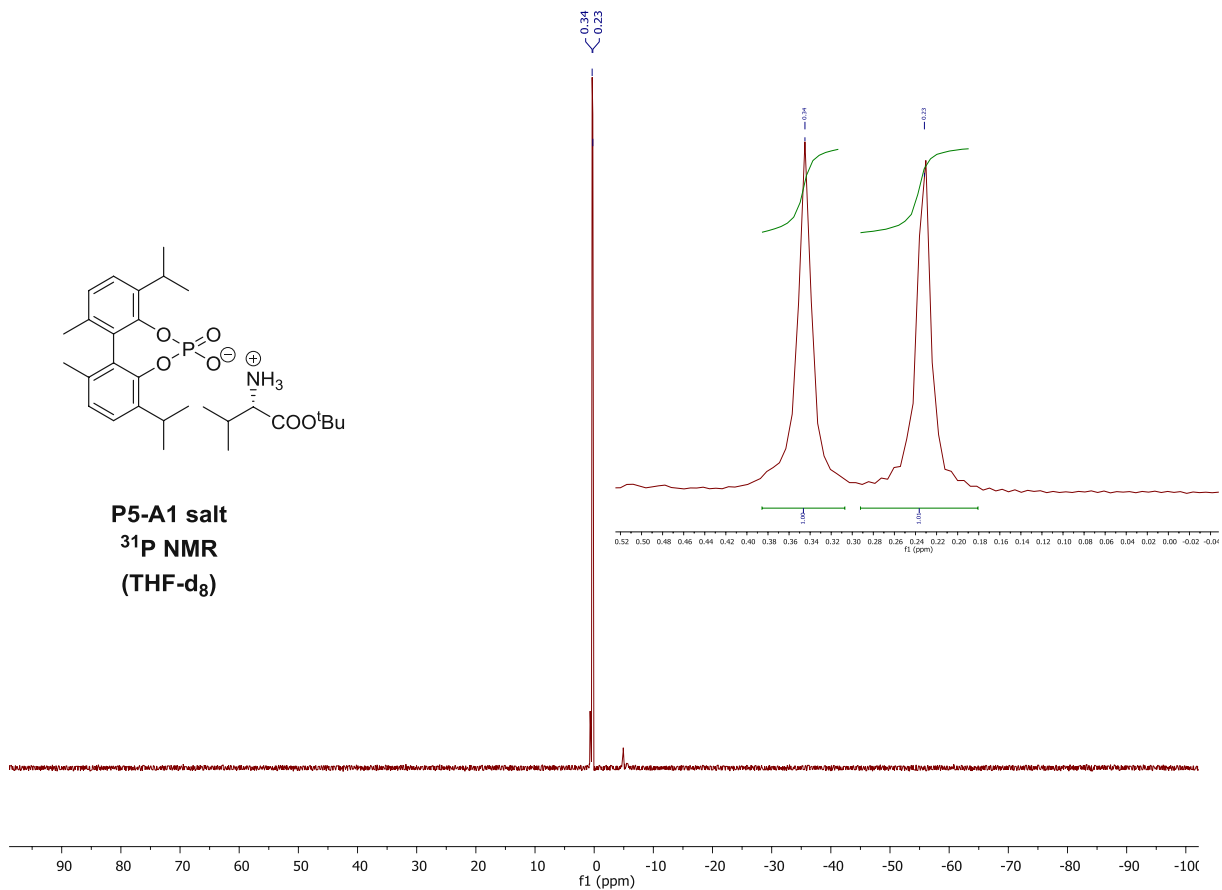
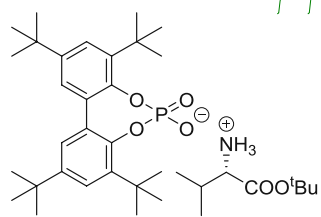


Figure S8. ³¹P NMR spectrum of **P5-A1** salt (162 MHz, THF-d₈)



P3-A1 salt
¹H NMR
(THF-d₈)

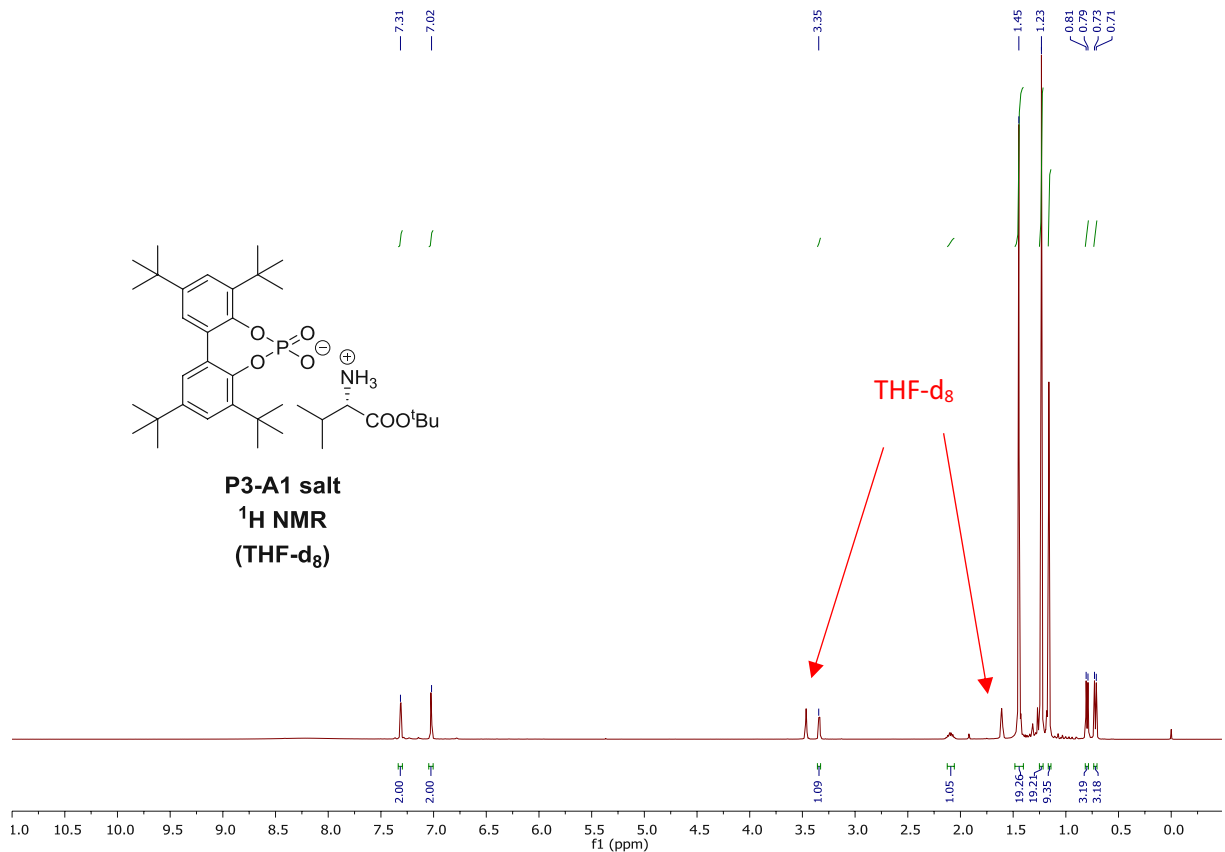


Figure S9. ¹H NMR spectrum of **P3-A1** salt (400 MHz, THF-d₈)

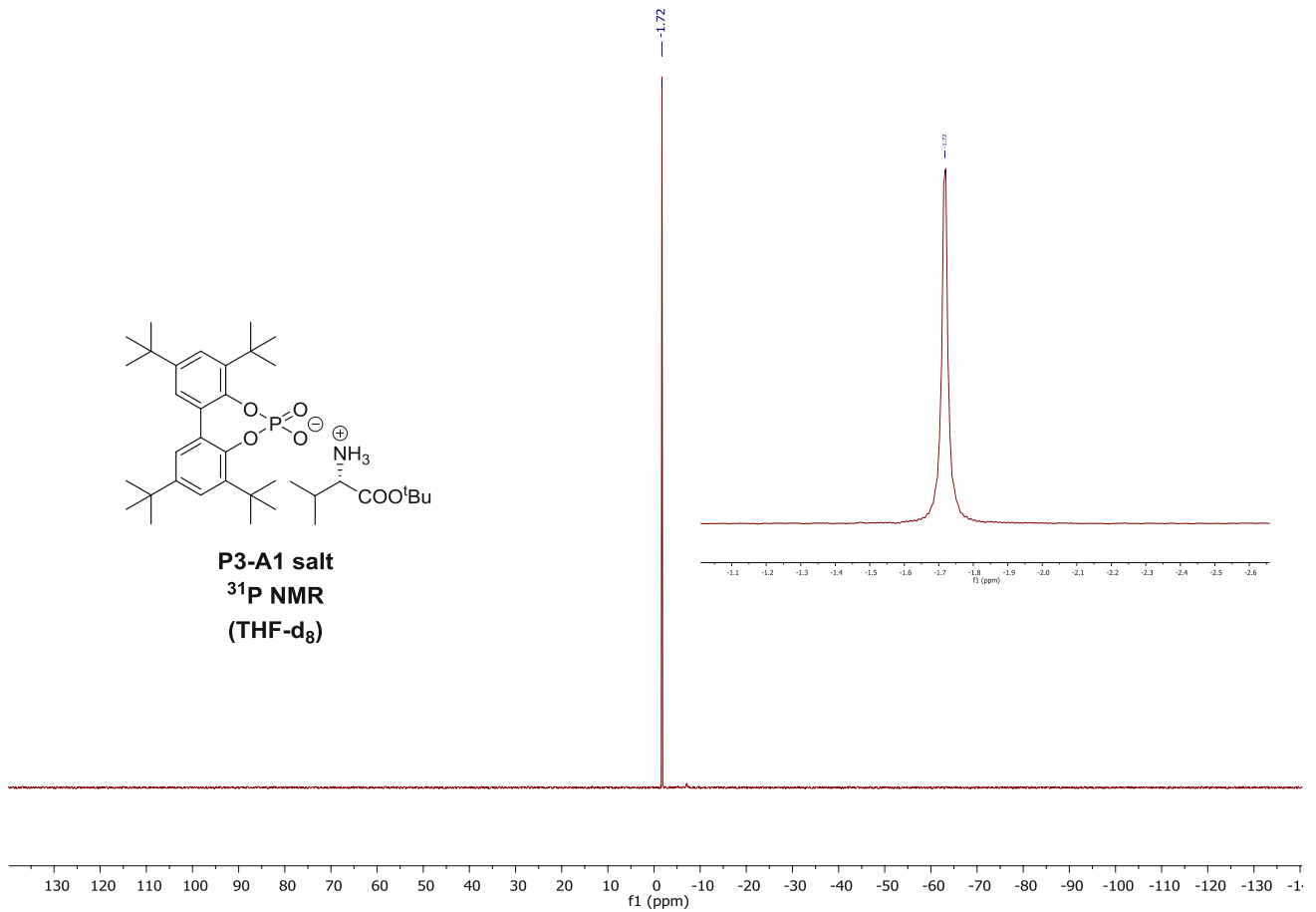
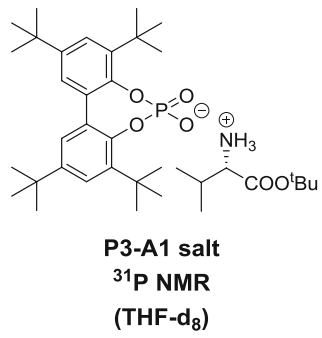


Figure S10. ³¹P NMR spectrum of **P3-A1** salt (162 MHz, THF-d₈)